The University Of Sheffield.

Quantitative Investigation on the Transient Evaporation of Fuel Droplet Using High Speed Imaging and Digital Image Processing

By:

Ahmad Fuad Bin Abdul Rasid

A thesis submitted in partial fulfilment of the requirements for the degree of Doctor of Philosophy

The University of Sheffield

Faculty of Engineering

Department of Mechanical Engineering

September 2019

Table of Contents

Declaration

"I hereby to declare that the work is my own except for summaries and quotations which have been duly acknowledged. No portion of the work referred to in the thesis has been submitted in support of an application for another degree or qualification of this or any or the university or institute of learning"

Ahmad Fuad Bin Abdul Rasid

10 August 2019

Publications

Journal Papers

Rasid, A. F. A., & Zhang, Y. (2019). Combustion characteristics and liquid-phase visualisation of single isolated diesel droplet with surface contaminated by soot particles. Proceedings of the Combustion Institute, 37(3), 3401–3408. https://doi.org/10.1016/j.proci.2018.08.023

Rasid, A. F. A., & Zhang, Y. Effect of Droplet Heating and Fuel Vapour Accumulation to the Quasi-Steadiness Evaporation of Single Isolated Diesel and Ethanol Under Normal Gravity. – (Under Preparation)

Rasid, A. F. A., & Zhang, Y. Detailed Process of Droplet Breakup and Transient Evaporation of Ethanol and Water Emulsion Fuel Droplets – (Under Preparation)

Rasid, A. F. A., & Zhang, Y. Insight on Microexplosion Process of Emulsion Fuel Droplets – (Under Preparation)

Rasid, A. F. A., & Zhang, Y. Combustion Characteristics of Single Isolated Diesel Droplet with a Stable Suspension of Soot Particles – (Under Preparation)

Conference Proceedings

Rasid, A. F. A., Hanriot, S., & Zhang, Y. (2019). Combustion Instability of Closely Packed Diesel Droplets Caused by Soot Contamination. 27th ICDERS, Beijing, paper 194

Acknowledgements

I am grateful to the God for the good health and wellbeing that were direly needed in order to complete this thesis.

I am also grateful to Professor Yang Zhang, Dr. Ahmad Faik, Dr. Francisco Javier Carranza Chavez, Dr. Halleh Mortazavi, Dr. Yiran Wang, Dr. Lukai Zheng, Mr. Shuaida Ji and all the other members of group. I am extremely thankful and indebted them for sharing their expertise and valuable guidance and encouragement extended to me.

Also, not forgetting my scholarship sponsors Universiti Teknikal Malaysia Melaka and Minister of Higher Education Malaysia for their continuous moral and financial support throughout my study in the University of Sheffield.

Finally, I take this opportunity to express gratitude to all of the department and faculty members for their help and support. I also thank my parents for the unceasing encouragement, support and attention. I am also grateful to my wife Dr. Afida binti Jemat who supported me throughout this venture. Last but not least, my gratitude to all my children; Alma Safiyyah, Ammar Safiy and Aydin Safiy for always cheering and accompanying me throughout this study.

Abstract

Evaporation, flame formation and liquid-phase dynamics of isolated fuel droplet shares similar characteristics with the droplets within fuel spray. Hence, isolated droplet studies which involves simple mass and energy transport are relevance to the complex spray environment in combustion. Motivations in the present work evolves around the evaluation of disruptive, transient liquid and gas phase of evaporating liquid fuel between analytical and experimental method. These disruptive and transient effects were analysed by several droplet conditions and arrangements including the experimentation on neat fuel with large difference in volatility and sooting propensities, stable and unstable emulsion droplets, soot contaminated diesel and multi-droplet combustion. Fuel droplets experimented in present work were suspended on 100 μm silicon carbide fibre and ignited in normal gravity, atmospheric pressure and ambient air. Backlighting was utilised to image the droplet and the flame was imaged directly by high speed cameras. The discrepancies between experimental and analytical works were divided into two conditions. Prolonged droplet heating affected the prediction accuracy of burning rate whilst prolonged fuel vapour accumulation affected the prediction accuracy of flame stand-off ratio. Higher amount liquid mass was ejected from water emulsion compared to ethanol emulsion droplet resulting 100% higher burning rate in each additive loading. It was found that microexplosion only occurs once all three conditions are present; the droplet temperature reaches the superheat limit of its lower boiling point component, a complete phase separation of emulsion components and the location of dispersed phase near the centre of the droplet. Compared to the unchanged reduction in burning rate of surface-contaminated droplet, the burning rate of volume-contaminated droplet was further reduced when the particle loading was higher. The difference was determined to be factored by the agglomeration rate of particles. Surface-contaminated droplet had a complete particle agglomeration upon ignition whilst volume-contaminated droplet had gradual agglomeration of particles, with faster particle agglomeration in higher loadings. In both contamination conditions, the droplet heating effect was longer due to high particle absorbance and the accumulated fuel vapour is found to be reduced due to the supressed evaporation rate. During the combustion of closely packed fuel droplets, the critical distance is found to be longer for lower volatility fuel factored by its tendency to have fuel vapour accumulation effect which enlarges the flame size when there is a starvation of oxygen. Transient droplet heating during multi-droplet combustion was found to be affected by the availability of oxidiser and heat transfer from the flame of nearby droplets. On the other hand, the combustion stability depended on the inter-droplet distance between neighbouring droplet. Overall, it is found that during transient droplet heating, longer duration taken for a fuel droplet to reach its boiling point would prolong its effect whilst the effect of fuel vapour accumulation is highly depended on the evaporation rate and volatility of fuel.

List of Figures

List of Tables

Nomenclature

Symbol	Description
B	Spalding transfer number
C_p	Specific heat (kJ/kg.K)
D	Diameter (mm)
D^2	Squared droplet diameter (mm^2)
g	Gravity (m/s^2)
h_c	Heat of combustion (kJ/kg)
h_{fg}	Latent heat of vaporisation (kJ/Kg)
k	Thermal conductivity (W/m.K)
L	Separation distance (m)
M_E	Instantaneous evaporation (kg/s)
M_R	Instantaneous consumption (kg/s)
$\dot{m}''_f$	Mass flux (kg/m^2s)
$\dot{m}_f$	Mass consumption (kg/s)
Q	Heat per unit mass (kJ/kg)
r	Radius (mm)
R, θ	Polar unit vectors (mm, °)
T	Temperature (K)
t	Time (s)
u	Velocity (m/s)
x	Distance/size (mm)

Greek Symbol	Description
ρ	Density (kg/m^3)
σ	Surface tension (mN/m)
ν	Stoichiometric air/fuel ratio
η	Burning rate correction factor

Subscript	Description
a	Ambient
f	Flame
g	Gas-phase
i-I	Interior of the droplet
o	initial
rel	Relative (ambient gas - droplet surface)
s	surface

Abbreviation	Description
CO	Carbon monoxide
DE	Diesel-in-ethanol
DW	Diesel-in-water
ED	Ethanol-in-diesel
EDns	Ethanol-in-diesel (no surfactant added)
FSR	Flame stand-off ratio
fps	Frame per second
GNP	Graphene nanoplatelet
HLB	Hydrophile-Lipophile Balance number
MWNT	Multi-Walled Carbon Nanotubes
MWNT-OH	Hydroxide-functionalized Multi-Walled Carbon Nanotubes
NO_x	Nitrogen oxide
OW	Oil-in-water
PAHs	Polycyclic aromatic hydrocarbons
QS	Quasi-steady
RCCI	Reactivity controlled compression ignition
SCD	Surface-contaminated droplet
SiC	Silicon carbide
TEM	Transmission electron microscope
TIFF	Tag image file format
UHC	Unburned hydrocarbon
VCD	Volume-contaminated droplet
WD	Water-in-diesel
WDns	Water-in-diesel (no surfactant added)

We	Weber number
WO	Water-in-oil

Chapter 1

Introduction

1.1 Research background

Current research direction in transportation energy focuses on either alternative sustainable source of energy or the optimisation of conventional combustion of heat engine. Although there is a promising development in green approach in the near future, high dependence on internal combustion engine is present in most of heat engine, particularly for transportation. Therefore, it is crucial to enhance the capability of the engine to operate with higher efficiency and lower emission, specifically diesel engine [1]. In order to further improve current efficiency of a diesel engine, the ignition and combustion mechanism of diesel fuel spray need to be examined at a basic level, which is the fuel droplet study [2-6].

Understanding droplet combustion characteristics is beneficial as it is a component of stratification via liquid fuel sprays. Therefore, a deeper understanding of fuel droplet ignition and combustion characteristics would provide a relative insight of spray combustions [7]. Scaling approach towards the relativity of isolated droplet and spray combustion would serve as a meaningful data for numerical and modelling study; since the size of a liquid fuel spray is sufficiently smaller [2]. Furthermore, it was observed that the combustion behaviour of a single isolated droplet and droplets within fuel sprays shares the same similarities in terms of droplet evaporation, ignition mechanism and droplet evolution dynamics [3, 4]. Hence, isolated droplets studies which involve simple mass and energy transport are relevance to the complex spray environment in combustion.

Classical quasi-steady model first proposed by Godsave [8] and Spalding [9] predicted that a liquid fuel droplet undergoess steady gasification process throughout its lifetime. The assumption made on the model prediction involves the droplet to be spherically symmetric with a uniform and constant droplet temperature. The effect of droplet heating and fuel vapour accumulation were neglected [10, 11]; making mass and energy transport during the evaporation process to be one-dimensional [12]. However, in the actual evaporation process, liquid fuel droplet undergoes few transient evaporation processes which involves droplet

heating, fuel vapour accumulation and disruptive dynamics in liquid-phase evolution [13], [14]. As a result, the experimental results are found to be non-one-dimensional especially during the evaporation of a fuel droplet in normal gravity. Such discrepancies have motivated several researchers to modify the quasi-steady model analytically to improve the prediction accuracies [7-13].

There are several focuses on quantitative measurements of isolated and grouped droplet combustion studies including detailed dynamics throughout droplet lifetime in high speed imaging [15, 16], ignition and combustion behaviour of binary mixtures [17, 18], group interactions of droplet combustion [19-21] and droplet flame spread mechanism [22-24]. These type of research approaches are highly beneficial to support the analytical analyses of several papers [19, 25], to precisely models the actual combustion of fuel. It has taken over years of quantitative and analytical study to reduce the deviation and error between the calculated and measured results. Further researching these areas with more detailed measurement technique will provide more comprehensive details on the fuel evaporation processes.

This study aims on examining the behaviour of droplet combustion in various type of condition and fuel types quantitatively; focusing to summarise the results on detailed droplet evolution dynamics, flame structure and the phases of disruptive burning periods. High repetitive measurements acquired from the present work allows the identification of transient combustion processes involved during fuel droplet combustion to be possible. In the present work, literature study on all objective included in Chapter 2. Chapter 3 explains the general experimental setups and result analysis in the present work. Chapter 4 discusses the transient combustion processes of neat fuel droplet associated with the discrepancies between classical quasi-steady model and experimental results. Chapter 5 analyses the disruptive processes during evaporation of emulsion fuels; including the main cause of the droplet to microexplode. Chapter 6 explains the effect of soot contamination to a diesel droplet during combustion. Chapter 7 explores the unsteady effects during the combustion of closely packed interacting droplet. Chapter 8 concludes major findings in each research objective and suggestions on future works based on the research questions that emerged from the present work.

1.2 Problem Statements

The classical quasi-steady model predicts one-dimensional process of mass and heat transfer during evaporation of liquid fuel droplets. Because of this, several studies of droplet evaporation were conducted in a microgravity to reduce the discrepancies between experimental and quasi-steady model by making the droplet to assume spherically symmetric shape resulting one-dimensional heat and mass transfer processes [16, 18, 20, 22, 26-29]. Such effort managed to prove the prediction accuracy of the quasi-steady model. However, actual fuel spray combustion process undergoes more complex heat and mass transfer processes resulting unsteady evaporation process. Some studies discussed the transient processes involved during the droplet evaporation which involves droplet heating [13, 30, 31] and fuel vapour accumulation effects [11, 14, 32]. However, a detailed correlation between the quantitative measurements on the droplet surface regressions, flame formation and liquid-phase dynamics were not presented to specify the unsteady effect throughout the lifetime of evaporating fuel droplet. Under these reasons, investigation on the cause of discrepancies between the experimental results and analytical model need to be conducted to specify the unsteady behaviours. With high measurement repeatability, such processes can be categorised by correlating the characteristics between surface regression, flame formation and liquid-phase dynamics.

The disruptive burning behaviour during the combustion of emulsion fuel is well documented by study conducted by several researchers [33-35]. Faik [36] concluded that a water emulsion has higher burning rate than an ethanol emulsion resulted by the more active process of puffing and sub-droplet ejections. However, The surfactant holding strength of a water emulsion is stronger than an ethanol in combustion condition [35]. This finding shows that an ethanol emulsion should have a higher sub-droplet ejection rate than a water emulsion which in turn would result higher burning rate due to a larger amount of mass loss. On the other hand, the main cause of an emulsion droplet to microexplode is unclear. Some theorised that a microexplosion will definitely occur when the lower boiling point component has reached its superheat limit [1, 37-39], while some theorised when it is shortly after the formation of phase separation within the droplet [34, 40], and some others theorised it is the combination of both phase separation and exceeding the superheat limit of the more volatile component [29, 33, 41]. Under these reasons, a clear visualisation and more precise quantitative measurements are needed to determine the cause of elevated burning rate of a water emulsion despite its stronger surfactant strength. Moreover, the microexplosion

mechanics are needed to be studied in detail by considering all factors involved including the superheat limit temperature and liquid phase separation condition.

The combustion characteristics of a fuel droplet is found to be enhanced when an energetic nanoparticle is suspended inside a base fuel [42, 43]. Beneficial properties of nanofluid includes the enhancement of combustion heat, increase in radiative absorption by the particle and improve mixing by a secondary atomisation [44-46]. Their results show that there is a critical nanoparticle loading that would optimise the combustion characteristics. Within the combustion of energetic nanofluid studies, such enhancement is well established. On the other hand, a soot that forms within the hot combustion gas is a nano-sized particle with a size ranging from 10 to 50 nm [47-50]. During continuous combustion process in a compression ignition engine, there is a possibility of soot to contaminate the fuel droplet contained in the spray [43, 51-55]. However, an experimental analysis on combustion behaviour of continuous, random and non-stabilised contamination of soot particles on a fuel droplet surface and within the droplet volume are not present. There is a high possibility of soot to contaminate the droplet in actual spray due to their larger surface to volume ratio compared to a single droplet having the same mass. Because of these reasons, the combustion characteristics of isolated diesel droplets contaminated with solid soot particles need to be examined.

Interacting combustion between a multiple fuel droplet is known to reduce the burning rate thus deviates the regression of squared droplet diameter from linear as predicted by D^2-law [21, 56-58]. Significant increase in the deviation is found on a higher number of droplet or closer interaction (high density number). This is due to the increase competition of available oxidiser as the density number increases [25]. On the other hand, the combustion of fuel with a high carbon number (high sooting propensity) releases high amount of soot particles in the fuel rich region [59, 60]. Within certain inter-droplet distance, there is a possibility of soot formed by the burning of the nearby droplets to contaminate each other. Within this scope, no literature describes the cause of disruptive burning during a multi-droplet combustion; and its effect to the burning characteristics. Because of this, an investigation on the transient burning of multiple droplets need to be conducted by considering all transient burning processes involved and quantitatively categorising them by their effects during combustion.

1.3 Research Objectives

In general, the aim of the study focuses on the quantitative investigation during the combustion of a liquid fuel droplet through high speed imaging techniques. Specifically, the aim of the research can be achieved by:

1. Determining transient liquid-phase and gas-phase combustion of neat diesel and ethanol droplet that would deviates the experimental results from the classical quasi-steady prediction.
2. Evaluating the disruptive burning of an emulsion fuel droplets. The aim is to identify the differences in the droplet breakup and secondary atomisation processes between a flammable and incombustible property of additives with a lower boiling point compared to the base fuel.
3. Identifying the main cause of emulsion droplet to microexplode in terms of activation temperature, liquid coagulations and the location of dispersed liquid upon complete droplet breakup.
4. Analysing the effect of soot contamination to the combustion characteristics of diesel fuel droplet. Comparisons are made between surface-contaminated and volume-contaminated diesel droplet to visualise and analyse their differences in liquid-phase dynamics.
5. Evaluating the effect of gas-phase interactions on droplet heating, fuel vapour accumulation and disruptive surface regression during multi-droplet combustion.

1.4 Research Scopes

The scope of the study is to evaluate and develop a strong theory on transient characteristics of evaporating droplet through high speed imaging. Specifically, they are:

1. Investigations on droplet evaporation and burning are measured quantitatively using high-speed imaging techniques
2. Tests are done under normal gravity and atmospheric pressure in ambient air
3. Droplets are ignited by a thermal heating wire to ensure neat ignition except during specific objectives such as heightening the effect of fuel vapour accumulation and soot contamination processes.
4. Droplets are suspended on 100 μm Silicon Carbide (SiC) fibre

5. Droplet and flame images are processed using image processing algorithm in Matlab
6. The fuel mixing processes are assumed reliable when the repeatability of measured results is high

1.5 Summary

The experimental analysis done in the present work focuses on the practicality of selected fuel and evaporating conditions during actual fuel spray combustion. Diesel is widely used in compression ignition engine and with the recent development in alternative fuel, ethanol is introduced. Comprehensive study on the evaporating behaviour of both fuels would provide beneficial insight towards combustion optimisation by identifying the variation of their transient evaporation processes as well as reducing the discrepancies between experimental and predicted calculations.

Also, results from the analysis of emulsion fuel combustion conducted in this study would provide clearer identification of microexplosion processes. This would lead to a more comprehensive understanding towards improving fuel mixing during combustion process of fuel spray. Furthermore, clearer combustion characteristics of ethanol and water emulsion are described which would provide definitive guideline during fuel selection processes.

The contamination processes and effects during fuel spray combustion are unclear. The analysis on the effect of soot contamination to the droplet evaporation experimented in the present work would clearly demonstrate its influence towards combustion stability and transient behaviour at fundamental level. This would help to provide useful data towards optimising the efficiency of the combustion during actual fuel sprays which focuses on minimising the soot contamination within the cylinder.

Lastly, experimentation on multi-droplet combustion in the present work demonstrates the correlation between the fuel properties and their effect to the transient evaporation behaviour during interacting droplet within fuel spray. This would provide a definitive description towards the optimisation of fuel spray which focuses on injection parameters such as spray angle, pressure and timing which would vary the separation distance, droplet size and fuel type.

Chapter 2

Literature Review

2.1 Introduction to combustion

Combustion process involves high temperature with extremely fast exothermic reactions between fuel and oxidiser that produces oxidised and gaseous products. The physical and chemical process from combustion releases heat as a form of energy that propagates outwards from the reaction in the form of flame when interacted with fire [61]. Process of combustion involves fuel and oxidiser mixing, flame propagation through ignition and termination when the fuel is depleted. The highest temperature within combustion region is the flame, where the fuel and oxidiser react, and the heat ensures a self-sustaining combustion process. Present study focuses on the combustion of organic fuel which is always exothermic due to the weaker double bond in oxygen compared to the combustion products carbon dioxide and water. Since the energy released by the products (new bonds) is greater than the energy needed to break the former bonds, heat is always produced [62].

When the combustion is complete, the reactant is thoroughly burned producing possible maximum heat release with minimum amount of oxidiser and this process always referred as stoichiometric air. In case of hydrocarbon fuels, the primary yields of reaction are carbon dioxide and water. Combustion in stoichiometric air is not possible since the liquid droplets dispersed in actual process are not fine enough for fast evaporation with some location within the spray is inaccessible for oxidiser to penetrate. However, calculation of stoichiometric air is used as a reference for theoretical predictions of combustion efficiency in actual combustors [63]. When there is insufficient oxidiser to completely react with the fuel for primarily producing carbon dioxide and water, incomplete combustion occurs. Product of pyrolysis that occurred before combustion remains unburned and contaminate the emission with particulate matter and smoke such as carbon (soot and dust) and carbon monoxide. Incomplete combustion process is typical in every combustor and contributes in the factor of discrepancies between experimental and theoretical predictions in combustion studies.

There are two common physical states of reactant in combustion. When the physical state of the reactant is the same with the oxidiser such as gaseous fuel and oxygen, the term homogeneous combustion is referred. Combustion of fuel and reactant with different initial physical phases such as liquid fuel in air, heterogeneous combustion is referred [64]. Applications in combustion is majorly heterogeneous combustion involving vaporised liquid fuel or pulverised coal particle with air. This process involves multiphase transitions of reactant and complicates the theoretical prediction. Hence more comprehensive experimental study is needed to develop firm understanding on the physical and chemical processes involved.

Flame produced from combustion is divided into two type of formations, within two type of flows. On the formations, when the fuel and oxidiser separately enter the combustion zone for reaction, diffusion flame will occur. Due to the slow diffusion process between the fuel and oxidiser, higher rate of incomplete combustion occurred and observable by its bright yellow flame formation which indicates the oxidation of soot. When the oxidiser and fuel is well-mixed prior to ignition, premixed flames will take place. This type of flame has higher combustion efficiency with lower harmful emission due to higher portion of the fuel being completely burned. This formation is observable with its blue coloured flame [65]. When the flame formations produced in laminar flow, it is termed laminar flames whereas in turbulent flow, it is termed turbulent flames [66].

The present experimental work involves examination on the combustion of liquid fuel droplet suspended on fibre. Therefore, the scope focuses on heterogeneous combustion of fuel with laminar diffusion flame based on the aforementioned combustion and flame types.

2.2 Liquid Fuel Spray

The first self-running compression ignition engine was designed by Hans Linder and Rudolf Diesel in 1894 who used air-blast injection to supply diesel fuel into the cylinder [67]. The injection system was later upgraded by James McKechnie in 1910 to a poppet-type airless injection system which became the origin of injection system in diesel engine [68]. Diesel spray is characterised by the high-momentum dispersions of liquid diesel fuel in high surrounding pressure for well-mixed spray-air mixture within the combustion chamber [69]. Injector is mounted on the cylinder head, which delivers the fuel via sprays between the piston face and upper portion of the cylinder head (also called combustion chamber). As a result, variable sized droplets is formed with random directions and velocities developing a

poorly defined combustion zone [66]. The breakup and formation of fuel spray is depicted in Fig. 2.1.

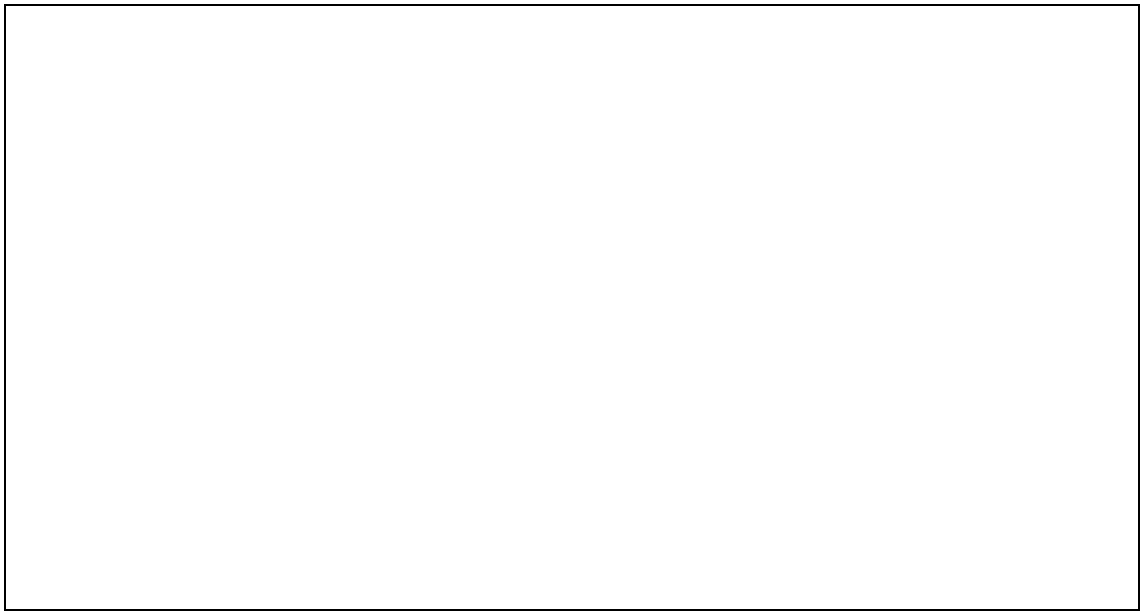

Fig. 2.1 Breakup and formation of liquid fuel spray (taken from [66])

There are several parameters that characterises fuel spray namely; (1) The degree of spray angle, (2) The breakup length referring to the length of the non-disintegrated liquid core within the spray, (3) The length of sprayed liquid phase region to a point where the fuel injection rate becomes equal to the fuel evaporation rate, (4) Size distribution of droplets in spray, (5) Sauter mean diameter which represents the equivalent diameter to surface area of spray, (6) Spatial distribution of spray and (7) Intensities of turbulence [69].

Once injected, the liquid spray is subjected to a turbulence and further breakup into a dense cloud of variable droplet size and penetrate the combustion zone with a process called atomisation. Atomisation is defined by the disintegration of sprayed liquid into smaller sized fuel droplets that is dispersed into a gaseous environment [70]. There are two atomisation processes involved termed primary and secondary atomisation process explains by illustration in Fig. 2.2. The velocity profile in the centre of the spray is the highest and gradually decreases to zero towards the edge of the disintegration zone. During primary atomisation, the continuous phase of liquid (liquid core) near the injector with the highest velocity profile disintegrates into filament and eventually collapses into droplets due to the interaction between the liquid spray and the gas inside the cylinder [71]. Typical fuel droplet size in sprays during primary atomisation varies between 50-150 μm [72].

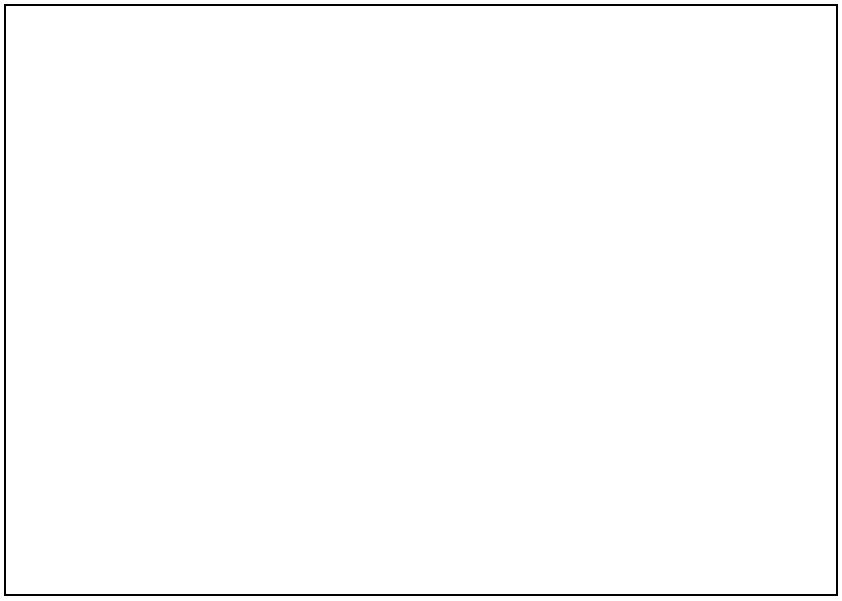

Fig. 2.2 Schematic of liquid fuel spray [71]

As the primary droplets penetrate to the surrounding air, the secondary atomisation is initiated where the primary droplets further break into smaller droplets due to aerodynamic forces of velocity gradient. With the combination of evaporation, the droplets continue to move along x-axis with reducing size. Secondary atomisation process numerically represented by Weber number (We) defined by the ratio between inertia and surface tension in equation 2.1

$$We = \frac{D\rho_a u_{rel}^2}{\sigma_s} \qquad \text{Equation 2.1}$$

Due to the atomisation process, fuel sprays consist multiple small sized droplet dispersed in ambient air. Hence, studies on isolated droplet evaporation and burning is one of the alternative approach of simplifying the evaporation process of droplets in spray [73]. Although the size of suspending droplet study is sufficiently larger than those sprayed inside a diesel engine, such quantitative data is meaningful in term of various sizing and arrays mechanism for scaling studies.

2.3 Quasi-Steady Theory in Droplet Evaporation and Combustion

Combustion of isolated fuel droplet is important as it relates to the theoretical study of liquid spray combustion which assumes dispersed droplets to be spherical symmetric [12]. To

model the evaporation of droplets in simplified manner, D^2-law was first proposed by Godsave [8] and Spalding [9] to model the evaporation of fuel droplet which predicts the linear reduction of droplet squared diameter with time as the droplet evaporates. The basic assumptions made for this model is the droplet being spherically symmetric, uniform and constant droplet temperature by neglecting the effect of droplet heating and fuel vapor accumulation [10, 11]. In both cases of vaporisation and combustion, D^2-law predicts a constant gasification rate [74]. The combustion model of isolated droplet evaporating in stagnant oxidising environment is shown in Fig. 2.3. The oxidiser radially diffuses inward from the ambient to the flame interface while the fuel vapour from the droplet surface diffuses outward towards the flame interface [75]. Three processes are involved in bringing the liquid element to the surface of the droplet for evaporation. The first one includes mass diffusion of species in fuel. The second is convection that produced by internal circulation of the droplet; induced by the shear stress exerted by external gas flow on the droplet surface. The third is the regression of the droplet surface through evaporation, which eventually exposes the interior liquid [76]. The flame envelopes the droplet and characterised as diffusion-controlled combustion. Fuel evaporates and transported to the flame front for the combustion process [77]. Heat transfer within liquid droplet is a result of conduction and convection from internal circulation of the liquid droplet caused by friction of flowing gas to the surface of the droplet. For gas-phase, the heat transfer to the surface of the droplet dominated by convection induced by thermophoretic force and radiation from the flame [78].

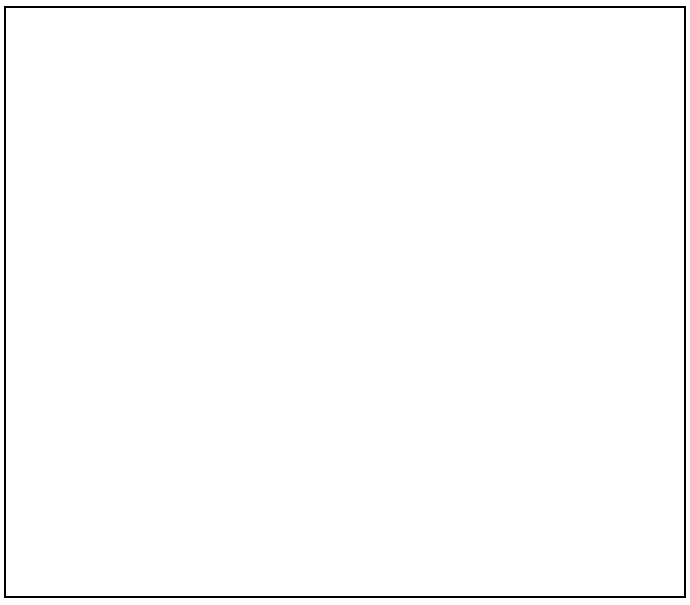

Fig. 2.3 isolated droplet evaporating in stagnant oxidising environment (taken from [66])

Droplet evaporation principles involved on the assumption made with control mechanism of mass and heat transfer rate from ambient to droplet surface. Evaporating droplet have its surface temperature to be near the boiling point and modelled with a simple mathematical expression. Also, this theory is practically useful for droplet burning model, considering the surrounding flame as the ambient temperature interacting with the droplet itself. Apart from the aforementioned assumptions, there are several other assumptions made for this model [79]:

a) The evaporation process is in steady state which eliminates the partial differential equations expressions.
b) Single-component liquid fuel is assumed.
c) Uniform droplet temperature of near boiling point and the transient heating behaviour of the droplet is neglected.
d) Constant thermal conductivity, density and specific heat.
e) Non-sooting combustion with negligible radiation.

Several main combustion characteristics of droplet combustion can be predicted in quasi-steady theory. With constant value throughout the droplet lifetime, the mass burning rate is evaluated as:

$$\dot{m}_f = \frac{4\pi k_g r_s}{c_{pg}} ln[1 + B] \qquad \text{Equation 2.2}$$

With constant gasification and stoichiometric air fuel ratio, flame temperature is expressed as:

$$T_f = T_s + \frac{q_{i-l} + h_{fg}}{c_{pg}(1 + v)}(vB - 1) \qquad \text{Equation 2.3}$$

With Spalding transfer number, B for both evaporating and burning droplet expressed by:

$$B = \frac{\Delta h_c / v + c_{pg}(T_a - T_s)}{q_{i-l} + h_{fg}} \qquad \text{Equation 2.4}$$

Due to the constant gasification, flame stand-off ratio is predicted to be constant at all time during the combustion of droplet and expressed as:

$$\frac{r_f}{r_s} = \frac{ln(1+B)}{ln[(v+1)/v]} \qquad \text{Equation 2.5}$$

And the burning rate constant which is also assumed to be constant in quasi-steady assumption:

$$K = \frac{8k_g}{\rho_l c_{pg}} ln(B+1) \qquad \text{Equation 2.6}$$

Hence, linear correlation between squared droplet diameter and droplet lifetime is assumed with $D^2(t) = Do^2 - Kt$. This expression is valid for all droplet within stated assumptions and generally referred as D^2-law; and it is shown in Fig. 2.4.

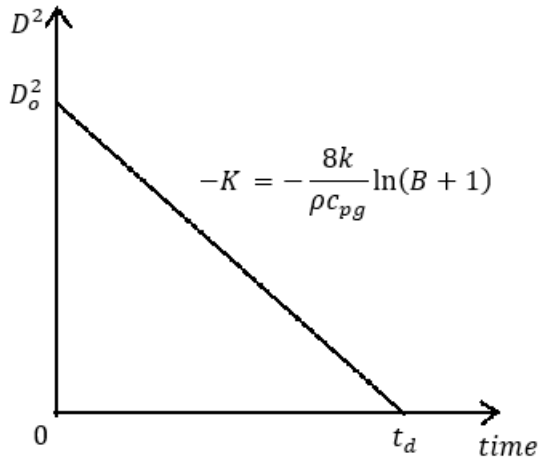

Fig. 2.4 D^2-law for droplet evaporation in quasi-steady assumptions (Reproduced from [79])

In general, the square of droplet diameter is linearly decreased by time; as dictated by D^2-law. However, in certain cases, the conformation of the law is more profound in later stage of droplet burning compared to initial stage of ignition [4]. The differences in the combustion stages are due to the limited parameter of the assumptions and subjected to various reasons. For instance, first stage of droplet ignition shown an increase in droplet size due to volumetric expansion thus swelling the droplet. Furthermore, the burning behaviour is subjected to the initial droplet and ambient temperature; on high initial temperature of a droplet, the burning duration of the droplet is shorter as the droplet size reduces. It is because the droplet heating time becomes shorter thus the combustion energy is used most on the evaporation of the droplet rather than to heat the droplet for evaporation

temperature [6]. Transient behaviour presented during droplet burning is subjected to their multiple combustion stages. According to Okai et. Al [20], the burning stages can be divided into four (4) types. The first stage is called droplet heating; when there is a small swelling and oscillation in the droplet due to the thermal expansion of droplet. Also, fuel vapour formed in the centre of the droplet is unable to escape through the surface, thus nucleate and swell the droplet [18]. Second stage is determined as puffing; with sudden emission of air, vapour or smoke. Higher amount of bubble nucleation oscillates the droplet even more. As the temperature distribution gets more constant throughout the droplet, the small amount of gas trapped inside will be able to escape through the surface due to reduced surface tension; creating a behaviour of puffing. Third stage mentioned is boiling; having high droplet oscillation but with no puffing or disruptive burning. In this stage, the measurement of the burning rate constant confirms with the quasi-steady assumptions of D^2-law. The fourth stage is disruptive burning. The puffing and oscillation of droplet is profound in this stage, deviating the measurement of burning rate from constant D^2 regression. As observed by Wang et. Al. [1], as the combustion progresses, more viscous droplet surface will form as a result of fuel decomposition. This will trap more gas inside the droplet and the only way of the inner vapour to escape through the droplet surface is by rupturing the surface of the droplet.

In other words, classical quasi-steady theory is reliable to predict the combustion parameter gained from experimental study but limited to fuel droplet that evaporates with steady heating phase and low boiling point [73]. Results from experimental studies may deviates from quasi-steady assumption by up to 20% uncertainties [31]. Therefore, several studies have been done to numerically modify the quasi-steady assumptions as well as determining the effect of transient and unsteady phase of combustion experimentally.

2.4 Transient Droplet Combustion Process

There are two transient processes, namely droplet heating and fuel vapour accumulation effect which deviates the gasification rate and flame stand-off ratio of experimental droplet combustion from the quasi-steady assumption. The transient effect is profound in high boiling point and low volatility fuel [73]. In this section, droplet heating is considered as transient liquid-phase process whereas fuel vapour accumulation is considered the transient gas-phase process [11].

2.4.1 Transient Liquid-Phase Combustion

Droplet heating assumes liquid-phase transient process and generally neglected in quasi-steady assumptions based on the argument of insignificant duration of such process within droplet lifetime. However, the effect of droplet heating actually occupies a portion of droplet lifetime and the effect is more significant during multicomponent and multi-droplet combustion [14]. During the transient heating period, the surface regression rate is much slower than the internal heat conduction rate and clearly observable in experimental study for a short period of time upon ignition with a non-linear regression of D^2 [13]. The manifestation of non-linear burning mechanism is when the burning rate increases with time [80], shown by the gradual increase of instantaneous burning rate in the early lifetime of droplet in Fig. 2.5. Furthermore, Deprédurand et al. [81] stated that droplet heating is less important for droplet with high volatility. They calculated that the heat flux entering the droplet is low (indicates low heat flux needed for droplet heating) when heat flux due to evaporation is high (higher evaporation rate of high volatility fuel).

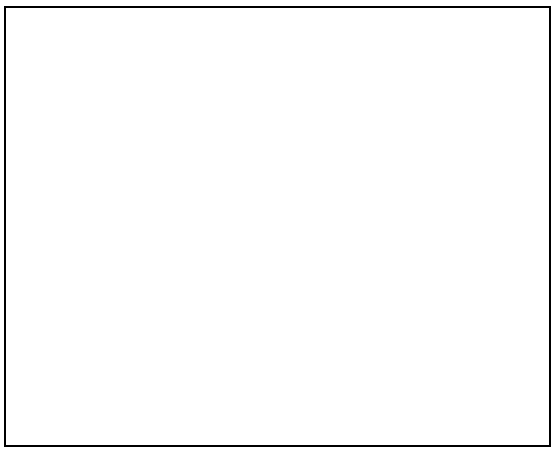

Fig. 2.5 Instantaneous burning rate of nonane/hexanol mixture droplets [80]

For a droplet with low boiling point, the surface regression of droplet assumes linear in shorter period of time even though the droplet heating is still progressing. As long as the surface layer is heated to a boiling at high rate, the subsequent heating of droplet interior required less heating for gasification thus satisfies the requirement of D^2 law [82]. Droplet heating phase is estimated between 10-20% of droplet lifetime. However, the heating lifetime highly dependent on the boiling point and volatility of the fuel droplet [83]. Law et al. [11] concluded the unsteady effects constitutes between 20-25% for benzene and Sirignano and

Law [13] found it constitutes 20% of octane droplet lifetime. The differences between the unsteady lifetime shows that the effect of droplet heating to the surface regression is physical and chemical dependent.

2.4.2 Transient Gas-Phase Combustion

In gas-phase transient process, quasi-steady theory assumes the consumption rate of gas at the flame is equal to the evaporation rate since the smaller density of gas is assumed to move faster towards the flame compared to the regression of liquid surface. However, in actual observations, there is a fuel vapour accumulation inside the gas film surrounding the droplet due to the steep increase and infinity value of flame stand-off ratio upon ignition and toward the flame extinction respectively. This implies that the rate of evaporation is faster than the fuel consumption [14]. Fuel accumulation effect is low during droplet heating and gradually increases over time. This in turn pushes the flame front further from the droplet surface and believed to be the main reason of increasing flame stand-of ratio. Law et. al [11] simulated the droplet by three conditions shown in Fig. 2.6 and they have found that the fuel vapour accumulation dominates the regression of FSR even with added droplet heating effect. Towards the end of droplet lifetime, the rate of vapour consumption is higher compared to evaporation rate due to the burnout of accumulated vapour in the gas film. Their analysis proves to have discrepancies with the D^2-law model which assumes instantaneous consumption of vapour at the droplet surface by the flame [14].

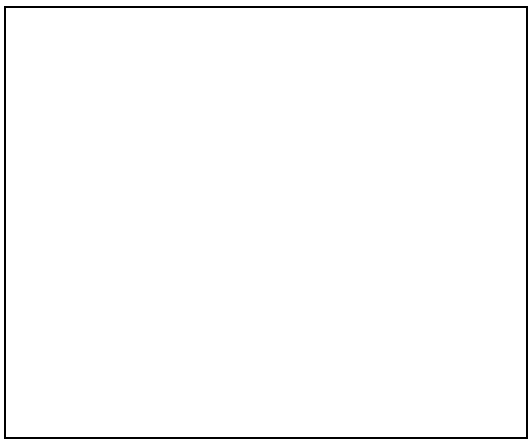

Fig. 2.6 Variations of FSR with the effect of droplet heating, fuel vapour accumulation and both transient conditions [11]

Awasthi et al. [32] formulated the relative delay between vapour consumption and gasification implies that instantaneous mass evaporation rate from the droplet surface is given by:

$$\dot{m}_E(t) = \int_{\theta=0}^{\pi} \dot{m}''_{f,\theta}.2\pi R^2.sin\theta d\theta \qquad \text{Equation 2.7}$$

And instantaneous vapour consumption is given by:

$$\dot{m}_R(t) = \int_{r=R}^{r=r_\infty}.\int_{\theta=0}^{\pi} \dot{m}_f\ .2\pi r^2.sin\theta d\theta dr \qquad \text{Equation 2.8}$$

Accumulation dominates when $\dot{m}_R < \dot{m}_E$ whilst vapour consumption dominates when $\dot{m}_R > \dot{m}_E$. It is expected that $\dot{m}_E$ is higher during the early stage of combustion and $\dot{m}_R$ is higher towards the end of the droplet lifetime. In case of quasi-steady assumption, $\dot{m}_R$ is equal to $\dot{m}_E$ which justifies the constant gasification and vapour consumption rate resulting constant flame stand-off ratio [79].

2.5 Droplet Flame Formation

In normal gravity, flame flow is buoyancy induced [22]. Shown in Fig. 2.7(a), the flame of burning fuel droplet is elongated to the opposite direction of the gravity due to natural convection [77]. Also, the faint part at the top of the flame is because of buoyancy [82]. In buoyant flame, the temperature contours are widely and closely spaced near the droplet surface and continues to converge as the flame moves upward. The highest temperature is recorded at the distance of twice the droplet diameter above the burning droplet [84]. The dynamic behaviour of flame structure in droplet burning relates closely with the droplet evaporation mechanism. Larger initial droplet diameter burns with larger flame formation which in turn increases the radiative heat loss from the flame for droplet heating [28] thus reduces the evaporation rate. This shows that with a slight change in evaporation rate, droplet excitation or flame intensities tend to influence each other.

(a) (b)

Fig. 2.7 Flame structure of suspended diesel droplet showing; (a) diffusion flame and (b) premixed flame formation upon ignition

In the early lifetime of droplet combustion, the flame height and width recorded the highest before sharply reduced in size. The combustion is enhanced by the fuel vapour accumulation from droplet heating and evaporation resulting higher flame size [7]. Miyasaka and Law [82] observed similar trend in their experimental work stated that the flame length is considerably long during ignition due to the effect of fuel vapour accumulation. The flame then settled to a lower size and begins to increase by time. Umemura [72] observed that there is a faint premixed zone around the droplet before thin layer of diffusion flame appears, shown in Fig. 2.7(b). Oxidiser originally exists around the droplet that would mix with an amount of concentrated vapour prior to ignition. The amount of vapour burned in premixed flame is much smaller than the diffusion flame and would make the lifetime of premixed-mode flame significantly shorter within the droplet lifetime. Small sized premixed flame formation slightly improves the droplet heating due to the closer flame position to the droplet surface which enhances the radiative heat transfer [85] which in turn, increases the evaporation rate [86]. However, the transition to a large diffusion flame counter-effects the enhancement of heat transfer during heating period because the temperature in larger flame formation is lower due to higher amount of radiative heat loss [59]. Since the lifetime of large diffusion flame is substantially longer than the premixed flame formation, the effect on radiative heat transfer to the surface of the droplet is detrimental.

Higher ignition temperature reduces the heating time which prevents the droplet surrounding to have denser fuel vapour prior to ignition [24] but tends to increase the burning velocity of fuel, suggesting that flame front velocity is strongly dependant on the ignition temperature [87]. Although the heat transfer rate is low in early stage of combustion,

higher ignition temperature provides beneficial mechanism for flame spread mechanism in case of fuel sprays. In relation with droplet mass burning rate, higher rate is theoretically causes the flame temperature to be high due to a higher mass of energy consumption rate [4]. In this case, the flame intensities of burning droplet is dependence of the boiling point of the fuel, with higher flash point of the fuel results lower intensity of flame during combustion [16].

Flame size of an isolated droplet increases upon ignition and almost constant to the middle of its lifetime and it begins to drop [25]. In latter state of combustion, the flame temperature and size sharply reduce due to the diffusion-controlled combustion, where the evaporation of the fuel is continuously consumed by flame in steady manner; steady enveloped flame. During the lower flame size period, the combustion is steadier due to the controlled mixing of fuel vapour by diffusion flame [4]. This indicate that droplet combustion process involved two phases, ambient and diffusion-controlled conditions.

Consistent discrepancies were found on the flame stand-off ratio, FSR which is the ratio of instantaneous flame radius, r_f to the droplet radius, r_d when comparing results obtained from quasi-steady model and experimental works. Theoretical prediction shows that the FSR remains constant [75, 12] throughout the combustion based on steady gasification rate of droplet [80] with negligible effect of droplet heating and fuel vapour accumulation [32]. FSR increases sharply upon ignition, reduced to a steady increase and rises sharply again towards the end of the droplet lifetime in experimental observations [88]. The increase of FSR with time is attributed to fuel vapour accumulation between the flame and the droplet surface [89], making FSR a time dependent ratio throughout the lifetime of a burning droplet. Continuous accumulation of fuel vapour upon ignition pushes the flame front further from the droplet surface. Towards the end of droplet lifetime, the rate of vapour consumption is higher compared to evaporation rate due to the burnout of accumulated vapour in the gas film [14]. With higher amount of fuel vapour supplied to the flame front, the flame size enlarges. In microgravity experiment done by Fahd [16], FSR tends to increase throughout droplet lifetime due to better heat containment of flame structure. This was possible due to the thermal buffering on the far field of the combustion which in turn reduces the heat loss generated from the combustion of the droplet. This suggests that in lower flame size period, there is a slight increase in flame temperature. However, thermal buffering effects only presence in microgravity experiments, with spherically symmetric flame formation. In normal gravity, the effect of thermal buffering diminished due to the buoyancy that tends to push the flame upwards.

It is worth mentioning that the transient effect of droplet heating and vapour accumulation does deviates the experimental result from the theoretical prediction of quasi steady model especially during the early and towards the end of the droplet lifetime. The unsteady heating phase significantly effects the droplet surface regressions and the fuel vapour accumulation effects is more profound on the flame formation; which relevant to their terms as transient liquid-phase and transient gas-phase respectively. Conclusively, detailed experimental study to quantitatively measure these effects on several fuel types and arrangements would provide valuable insights to the unsteady burning of liquid fuel droplets.

2.6 Droplet suspension method

In droplet evaporation and burning study, droplet surface regressions as well as flame formations are mostly analysed through images acquired from visualisation technique via digital image recordings and some, film photograph during early experimental developments. In order to fulfil the requirements of imaging capabilities in term of spatial and temporal resolutions, the droplet suspension method plays an important role. The dynamics, positioning and conditions of the droplet needs to be acceptable for minimal errors. Among them, there are three suspension method considered to be most reliable in term of accuracy and repeatability; free-falling, fibre suspended and porous sphere droplet combustion. Fig. 2.8 illustrates typical suspension methods. All suspension technique has their advantages and drawbacks, which will be further explained in this section.

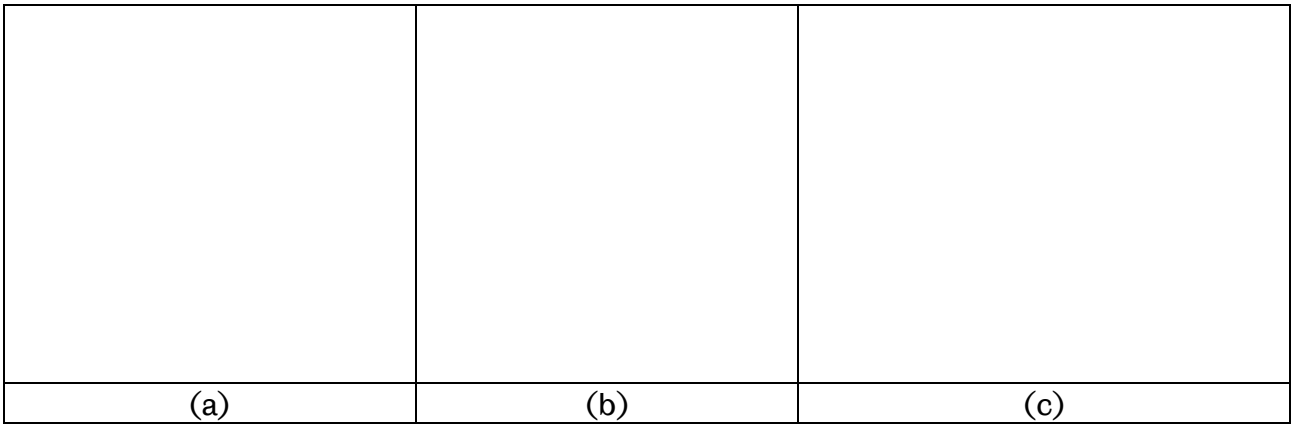

Fig. 2.8 Droplet suspension method in laboratory-controlled droplet combustion experiment; (a) Free-falling method (b) fibre suspended droplet and (c) Porous sphere method. [66]

2.6.1 Free-falling droplet technique.

In this technique, droplet is dispersed through imaging field of view with preferable velocity and direction of trajectories. Most popular method is by releasing the droplet to fall due to the force of gravity done by several researchers [42, 44, 90, 91] and some with multiple droplet dispersions with different angle for collision merged multicomponent droplet [37, 38, 92]. Typical arrangements of free-falling technique in droplet experiment is shown in Fig. 2.9.

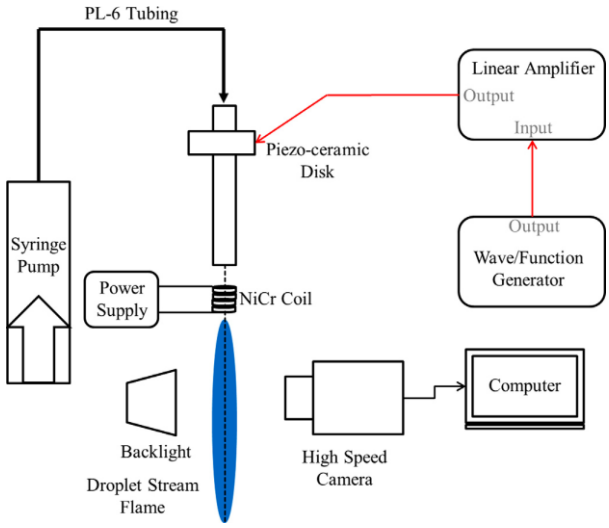

Fig. 2.9 Schematic of the droplet steam combustion experiment (taken from [42] with a permission from the publisher).

Droplet is generated mainly by liquid jet disintegration through vibrations from piezoceramic [42, 78, 81], modified ink-jet printing injector [60, 93], mechanical squeeze on fine nozzle [38, 94] and rapid retraction and jerking of small sized needle [12]. There are several advantages of employing free falling technique in droplet combustion study. The size of generated droplet can be as small as 0.1 mm [94] which is very close to the typical size of droplet in fuel spray of 0.1 mm or less [12]. This in turn minimises the measurement error in combustion characteristics between different sized droplets. The other advantage is instantaneous fuel mixing prior to ignition. Free falling droplet provides enough space for mixing a fuel in case of merge collision experiment done by [37]. Due to the inability to perform stable mixture of methanol/alkane, they performed experiment to collide water/oil emulsion fuel prior to auto-ignition in a heated environment. Results obtained was treated as emulsion fuel study. Visualising flame streak is one of the benefits of free-falling droplet experiment as shown in Fig. 2.10. Conducted by Botero et al. [95], the streak of flame images indicates the change in flame intensities and sooting propensities of burning droplet. The lifetime of the droplet is also well defined with the extinction of flame or via microexplosions.

Also, Guerieri et al. [44] conducted free-falling nanofluid droplet suspended with oxide compound able to determine the combustion phase change during the evaporation of the base fuel, mixture of base fuel, nanoparticle and disruptive secondary atomisation in flame streak visualisation. The condition of actual fuel spray can also be physically simulated. Wave function generator able to disturb to the free-falling fluid jet thus breaks up the stream to form a uniform and equal-sized droplet. This is practical to be applied in uniform droplet stream study experimented by Tanvir and Qiao [42].

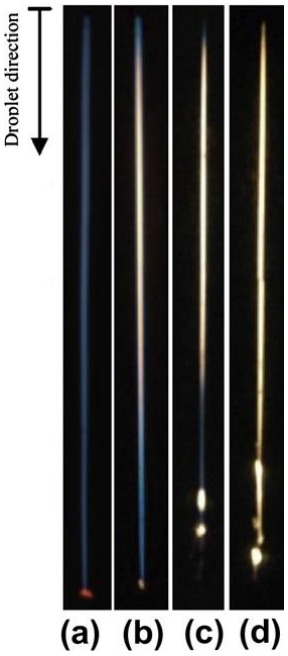

Fig. 2.10 Flame streak images for: (a) castor oil biodiesel, (b) biodiesel used in [9], (c) castor oil biodiesel and 30% toluene and (d) castor oil biodiesel and 30% tetralin. (taken from [95] with a permission from the publisher)

Despite of all those advantages, there are some drawbacks to this technique. The trajectories of the generated droplet cannot be maintained in a straight line, especially in a condition of disruptive burning and forced convective flow. This will complicate the experimental procedure especially with small field of view or when experimenting on multi-droplet interaction due to the dependence of droplet separation with time. Also, the effect of convection increases due to forced convection thus complicates further modelling work based on experimental technique. In case of visualising or quantitatively measure the effect of soot shell formed in radial position of the droplet, free falling droplet shows less occurrence due to the sweeping of soot particles in slip-velocity of co-flow on the droplet [90]. Buoyancy and slip effects on droplet eventually change the droplet shape to a non-spherical symmetry.

Furthermore, the magnification on the droplet is limited, depending on the initial droplet diameter in the expense of visualisation field of view. For instance, high magnification would limit the maximum droplet size to significantly small due to the moving and evaporating droplet that might be out of visualisation field of view before completely evaporates. Nevertheless, this technique has proven to have reliable outcome with acceptable repeatability as conducted by several researchers on multiple scope of analysis including the combustion of multicomponent droplet, burning rate, phase changes in flame streak, microgravity and multi-droplet interactions.

2.6.2 Fibre-Suspended Droplet Technique

Suspending the droplet on fibre is widely used in droplet combustion studies. Fig. 2.11 shows a typical fuel droplet suspension on a single thin fibre. Method of droplet suspension on a small sized fibre provide high controllability on experimented droplet with acceptable accuracy [39]. In general, the effect of heat transfer is negligible for a very small suspending fibre diameter which has almost no impact on the droplet evaporation rate [10]. Heat transfer through the fibre is proportional to the cross-sectional area of fairly thin diameter is negligible [82, 96]. Analysis by Jackson et al. [60] shows that the heat transferred to the fibre is less than 1% of total heat transfer to the droplet during evaporation and burning.

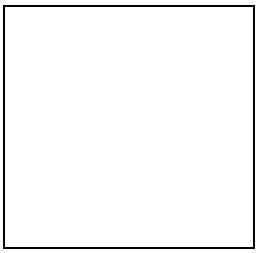

Fig. 2.11 Droplet suspended on a 100 μm SiC fibre [36]

There several common materials of suspending fibre used with various sizes and application. Table 2.1 shows some type of suspension fibres used by several researchers. Although there are many more varieties of suspending fibre used, all of them having diameter of 0.5 mm for a droplet of 2 mm in size at most. Suspension of droplet on fibre has several advantages in experimental study. One of them is the ability to ensure precise initial droplet diameter prior to ignition. Suspended droplet in ambient temperature have a brief moment of stagnant droplet condition which enable some adjustments to be made before proceeding

for ignition. For instance, droplet suspension method done by Faik and Zhang [36] and Rasid and Zhang [97] able to ensure the suspended droplet to have similar-sized droplet on each sample. Prior to ignition, they measured the suspended droplet using the live imaging software to measure and manually adjust the initial size to be 1 mm $\pm$ 0.05 mm. This ensures repeatability of experimental results as initial droplet size influences the combustion behaviour of droplet. Larger droplet diameter has lower burning rate due to larger flame size which increases radiative thermal loss thus reduces the evaporation [98]. By ensuring the repeatability of initial droplet size, comparisons of similar sized fuel droplet can be done on variety of fuel type, arrangements and burning conditions.

Table 2.1 Examples of several suspending fibre used in experimental work

Researcher(s)	Material	Size, mm	Droplet size, mm
Tsue et al. [33][99]	quartz	0.25	1.0
Rao et al. [100] Antaki and Williams [101]	quartz	0.2	1.2 to 1.8
Xu et al. [102][103]	quartz	0.5	0.6 to 1.8
Watanabe [34] Suzuki et al. [104] Kim et al. [105]	Thermocouple bead	0.05	0.85 to 1.0
Mohan et al. [106]	Thermocouple bead	0.075	1.4
Gan and Qiao [107]	Silicon Carbide	0.078	1 to 1.3
Nishiyama et al. [108]	Silicon Carbide	4 x 0.014	1
Faik and Zhang [36] Rasid and Zhang [97] Kim et al. [96]	Silicon Carbide	0.1	1
Park and Choi [109] Manzello et al. [89] Yozgatligil et al. [110] Avedisian and Calahhan [80]	Silicon Carbide	2 x 0.015	1 to 2
Nagata et al. [88]	glass	0.5	1
Chao et al. [29] Pan and Chiu [39]	Ceramic	2 x 0.015	0.5

Also, suspension of droplet on fibre ensures fixed position of droplet during combustion. Suspension technique is essential during experimentation of droplet burning in groups. The centre to centre droplet distance would vary without fixed suspension and the result from the combustion is inconclusive due to inconsistent physical parameters [111]. Furthermore, fibre is used to prevent the droplet to move out of field of view during combustion visualisation period [50, 59]. Because of the stationary condition of the droplet, very high imaging magnification can be conducted thus providing the ability for liquid-phase visualisation to be done [112]. Burning droplet would never move out of the field of view throughout its lifetime with sharp imaging focus on the interior of the droplet.

There are some drawbacks of using fibre suspension technique. The droplet shape is observed to be slightly deformed from spherical shape [113]. Droplet suspended on fibre is spheroidal with an elongation in the direction of fibre axis [22]. By assuming volume equivalence between ellipsoidal and spherical droplet, an equivalent spherical diameter is calculated. Hence, the equivalent diameter is calculated by the cubic root from the product of squared minor diameter times major diameter [111]. This calculation subjected to a fairly small error due to the effect of shape on combustion behaviour although the volume is equivalent. Throughout combustion, the fibre would promote heterogeneous nucleation around the fibre-droplet interface [39]. Also, stated by Okai et al. [20], fibre support promotes heterogeneous nucleation due to higher surface area with more violent disruption compared to homogeneous nucleation of free falling droplets. Using fibre with diameter larger than 150 μm transfers heat through it which would heat the centre of the droplet during combustion [82]. Enhanced heat transfer to the droplet would increase the evaporation rate thus renders the result incomparable to actual burning rate. For a fibre with diameter equal or less than one tenth of the droplet diameter [29], the measured burning rate is comparable to that of free-falling droplet technique. However, the fibre do perturbed the soot formation and cause some of unoxidised soot to be deposited on the fibre [114].

2.6.3 Porous sphere Technique

Early investigations of fuel droplet combustion in sprays leads to a study of isolated fuel droplet in convective flow [2]. Spalding [9] and Gollahalli & Brzustowski [115] observed differences in flame structures between a stationary and a droplet subjected to a convective flow. The droplet burns with an envelope flame (Fig. 2.12a) at a low relative speed and a wake flame (Fig. 2.12b) at high relative speed thus lead to the earliest establishment of porous-

sphere experimental method. This method allows the control of several parameters in study; including varying sphere diameter, fuel type and convective air velocity.

Fig. 2.12 Flame photographs of (a) enveloped flame and (b) Wake flame (taken from [116] with a permission from the publisher)

Fig. 2.13 shows typical experimental setup for porous sphere combustion method. The alundum sphere is supported by a 1.2 mm hypodermic needle. A radial hole of 0.4 mm is drilled at the end of the hypodermic needle to ensure uniform fuel distribution inside the sphere. Fuel is supplied by an infusion pump which pushed the glass syringe plunger at any speed for desirable volumetric flow rate of fuel. Airflow system is directly installed below the sphere consist of wind tunnel with a settling chamber [117-119]

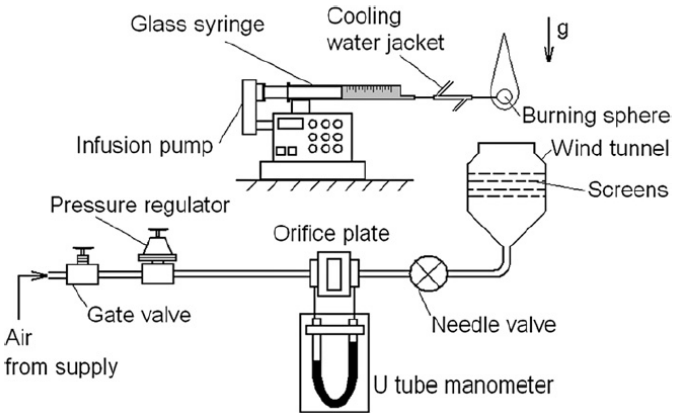

Fig. 2.13 Schematic diagram of porous sphere experimental setup (taken from [116] with a permission from the publisher)

Nevertheless, there are several limitations of this method on fuel droplet studies. The diameter of the sphere which is considerably large is assumed to be the size of the droplet. Large droplet size in high evaporation rate would have a high temperature gradient across the droplet. This in turn would make the droplet to have uneven evaporation around the sphere. Secondly, it is impossible to visualise the liquid phase of the fuel droplet during combustion due to the fuel being inside the porous sphere. Any instabilities of liquid phase would be left unnoticed. Lastly, the heat loss from the combustion is more complex as it involves conduction within the sphere as well as the hypodermic needle with considerably large surface areas.

2.7 Droplet Combustion in Microgravity

2.7.1 Microgravity Conditions

Microgravity environment is described as an environment which changes the apparent weight of a system to be smaller than the actual weight in normal gravity. Within the influenced of earth's gravity (ground and airspace), microgravity is created by putting any object in a state of free-fall [120]. There are two common method of creating microgravity for droplet combustion experimentation within earth's atmosphere and they are through the use of drop tower facilities and parabolic flight technique.

2.7.2 Drop Tower Facility

Experimentation using drop tower facilities involves the use of drop chamber consists of experimentation apparatus. Considering air resistance which would deaccelerate any falling object near the surface of the earth, a drag shield is utilised to minimise the effects air resistance during free-fall period [27]. Typical experimental apparatus of droplet combustion in microgravity is described by Segawa et al. [112]. Before the release of the capsule in the drop shaft, fuel was supply by a remote-controlled system of hypodermic needle, stepping motors and syringe. When the capsule is dropped, the electric current was supplied to the heating coil and translated towards the droplet for ignition. The coil then removed quickly upon ignition to prevent perturbation of flame. Electronic signal is sent to release the entire package that is hung by an electromagnet to initiate the free-fall sequence [39]. Experimental apparatus is enclosed in the drag shield that would fall relatively to each other. The

experimental apparatus made contact with the bottom of the drag shield at the moment when the entire package impacts the air bag. Fig. 2.14 depicts the drop tower facility in NASA Lewis Research Centre.

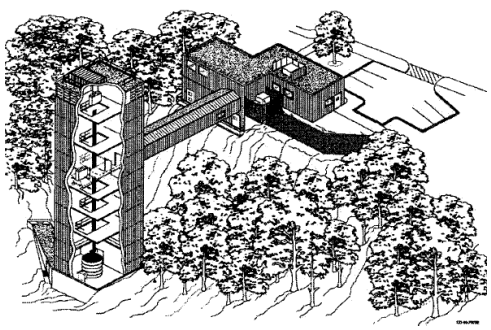

Fig. 2.14 Schematic of the NASA Lewis Research Center 2.2 Second Drop Tower [120].

2.7.3 Parabolic Flight Technique

Another method of creating microgravity is through the parabolic flight technique. Fig. 2.15 shows the schematic of parabolic flight path. When the plane flies on a parabolic path, microgravity environment is created. Typical parabolic flight lasts two to three hours. The process involves three flight manoeuvres starting from a rapid 45-47 degree climb angle, parabolic trace, and 43-45 degree descend angle. During parabolic trace, the gravity is approximately 10^{-2}g with 15 seconds of microgravity condition [121].

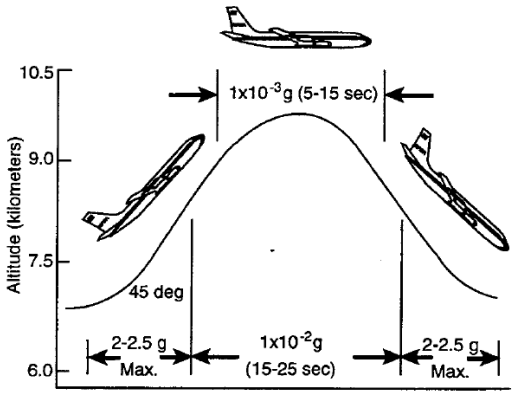

Fig. 2.15 Parabolic Flight Characteristics [120]

2.7.4 Fuel Droplet Experimentation in Microgravity

The first droplet combustion in microgravity was developed by Kumagai and Isoda [122]. Motivation for microgravity experiment came from the idea of creating a spherically

symmetric shape of liquid droplet for a comparable analysis against established numerical models in detailed chemical kinetics and transport derived from the classical quasi-steady assumptions [74]. Furthermore, microgravity further simplify the complex system of liquid combustion including droplet heat-up, phase change, chemical reactions and diffusion processes because of the spherical symmetry of the droplet [75]. This in turn reduces the computational cost especially in complex chemical kinetic study [123].

Table 2.2 Microgravity facilities used for fuel droplet combustion

Researchers	Facility	Tower height, m	Gravity condition, m/s^2	Microgravity duration, s
Tsue et al [33] Nakaya et al [28]	Microgravity lab in University of Tokyo	5	10-5	1
Mikami et al [111] Nakaya et al [98]	Drop tower in University of Tokyo	10	10-4	1.4
Nagata et al. [88] Struk et al. [25] Ikegami et al. [18]	Japan Microgravity centre, JAMIC	500	10-4	10
Nishiyama et al [108]	Micro-Gravity laboratory of Japan, MGLAB	100	10-4	4.5
Park and Choi [109] Manzello et al [89] Struk et al. [25] Yozgatligil et al. [26] Urban et al. [124]	NASA Glenn Research Centre (NASA-GRC)	24	10-4	2.2
Chao et al [29] Pan and Chiu [39]	No mention	3.5	10-4	0.68

The effect of buoyancy is mitigated in microgravity experiment which in turn forms a spherically symmetric flame shape [39, 80, 98]. Liquid and gas phase transport is symmetric around the droplet thus enables a one-dimensional analysis to be conducted [28]. Also, the burning process excludes convection which is considered one of the unknowns in burning conditions [50]. Investigation of sooting propensity of various type of fuel is possible with

microgravity experiment since diffusion, convection and thermophoresis are subjected to one-dimensional transport which is radial direction. Such one-dimensional characteristic creates a measurable ring of soot shell around the burning droplet [109]. Table 2.2 shows some of the facilities used by several researchers working on droplet combustion in microgravity.

2.8 Multicomponent Liquid Fuel Droplet Combustion

2.8.1 Evaporation Characteristics of multicomponent Fuel Droplet

In practical combustors, fuels are typically utilised in the form of multicomponent mixture either premixed as a stable fuel mixture such as Jet A, diesel and petrol or to be mix prior to utilisation. Combination of different fuel component varies depending on the specific requirement based on their advantages of drawbacks. There are few types of multicomponent fuel mixture that are widely used in modern combustors. They are in the form of blends (combination of miscible fuel) or emulsions (immiscible fuel mixture with addition of surfactant) [66]. The utilisation of multicomponent fuel is beneficial in enhancing the heating value, promotes atomisation and reduce the harmful emission by the base fuel. However, D2-law is not adequate to model the droplet size regression of a multicomponent fuel due to their much lower mass diffusion rate compared with thermal diffusion rate [125]. Most combustion characteristics of these fuel is explored in experimental study [29, 33, 36, 38, 41, 99, 100, 106, 126] and some with numerical study of improved model of quasi-steady assumption [10, 30, 34, 76, 92].

According to Wang et al. [3], there are three period of gasification in multicomponent droplet combustion. First, more volatile component envelopes the droplet with a thin layer of mass at the surface, thus dominate the gasification characteristic of the mixture. During this period, the boiling point of higher volatility component controls the droplet temperature, which has a lower temperature value between the boiling point of both components. Once the concentration of more volatile mixture reduced, this period ends. Second, as the concentration of more volatile component depleting at the surface, more of less volatile component resides on the surface and increases the droplet temperature to be near the boiling point of the less volatile component. During this stage, the gasification of the droplet is steady with fractional rate of gasification for both components is almost equivalence according to their initial mass fraction in the mixture. Lastly, as more volatile component

completely absents at the droplet surface, less volatile combustion behaviour is present. Similar conclusion was made by Ikegami et al. [18], stating that the multicomponent fuel mixture tend to vaporize according to the order of their volatility; which most of higher volatility component will vaporize first and followed by next lower volatility; shown by four stage of droplet surface regressions based on temperature variation in Fig. 2.16. This behaviour is also termed with *selective* or *preferential* evaporation. Because of the temperature is controlled by the order of volatility, the final surface temperature of droplet blends before extinction is the highest since it assumes the boiling temperature of lower volatile droplet which evaporates the last [92].

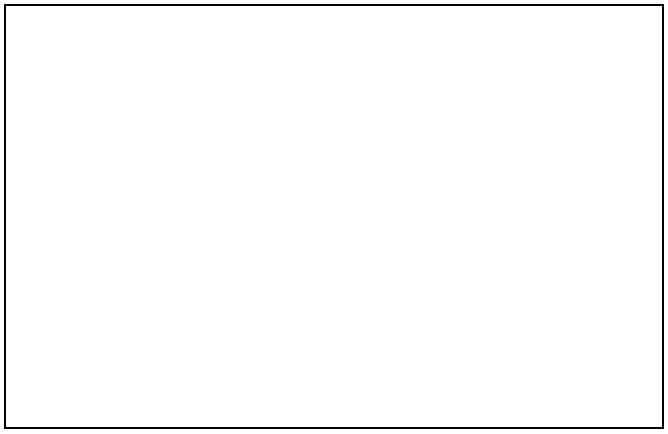

Fig. 2.16 Variation of surface temperature and surface regressions during the evaporation of heavy oil [18]

Droplet expansion is observed to occur multiple times during combustion especially during the transition of preferential evaporation [20]. Droplet size evolution during ignition for blends experiences higher fluctuation behaviour compared to their individual neat conditions. This transient behaviour represents the transition phase of burning behaviour; from volatile stage to less volatile stage combustion behaviour. In early stage of the combustion, the droplet temperature is limited to the boiling point of the more volatile component thus exhibit the less volatile component to be fully expanded. As soon as the intensity of more volatile component at the surface of the droplet is fairly reduced, the droplet temperature will increase to reach to boiling point of the less volatile component. This will allow the less volatile component to fully expand before transitioning to steady evaporation phase [7]. These behaviours are clearly observable during the combustion of multicomponent droplet with large volatility difference between individual component and in agreement with observation made by Sirignano [19]. On top of transient evaporation behaviour, sufficiently large volatility

difference would lead to disruptive effects on both liquid and gas phase of evaporating droplet.

2.8.2 Disruptive Burning of Multicomponent Fuel Droplet

Disruptive effects during combustion of fuel droplet mainly caused by a homogeneous bubble nucleation, expansion and eventually explosion that took place inside the droplet [127]. These processes are widely known by two phenomenon; puffing and microexplosion [36]. Puffing is described as a process of liquid or vapour ejection from a portion of a droplet that disintegrates into a smaller sized droplet. Microexplosion is a disintegration process of the whole droplet to a fragment of smaller sized droplets [106]. Landis and Mills [128] stated that the occurrence of microexplosion is possible since in certain region of the droplet interior, the equilibrium vapour pressure of the more volatile component exceeds the ambient pressure. Puffing and microexplosion constitutes secondary atomisation that improves fuel mixing with oxidiser which in turn enhances evaporation. Droplet satellites ejected from the parent droplet combusts quickly and adds an additional surface area to be exposed towards the flame for evaporation thus increases the burning rate [44]. As a result, NO_x formation and soot formations are retarded [95, 129]. Mohan et al. [106] conducted combustion of ternary emulsion droplet suspended on thin fibre discussed that the ejected sub-droplet is observed to have experienced puffing and microexplosion with similar breakup mechanism as their parent droplet despite their differences between suspended and free falling.

Although the evaporation of multicomponent fuel starts with the evaporation of the most volatile component that reside on the surface of the droplet, a portion of the more volatile component is still trapped inside the droplet. Without complete depletion of the more volatile component, the evaporation proceeds with higher surface temperature equivalent to the boiling temperature of the less volatile component, hence superheating the trapped volatile fuel [1, 10, 92, 129]. This leads to a homogeneous nucleation of multiple bubble forming inside the droplet [73]. Nucleation of trapped volatile component in a form of bubble near the core of the droplet tends to rupture the surface of the droplet as a mean of escaping [76, 95, 126]. On the bubble dynamics, Faik [66] stated that bubble growth inside a higher density component is slower with fewer number of nucleation bubble due to the increased resistance for expansion. On the other hand, bubble growth inside a lower density component would have higher bubble growth rate with a greater number of bubble nucleation and easily released or ejected through the surface. In addition, merging of multiple

vapour bubble inside the droplet would produce more effective atomisation process during surface rupture compared to multiple smaller bubble burst.

Typically, the bubble breakup undergoes multiple stage, mainly the development of liquid ligament, fragmentation of ligament and formation of small sub-droplet. The ejected droplet may be transported towards the flame for evaporation or explodes which in turn disturbs the flame formation [100]. It was observed repeatedly through shadowgraph [36] that a gush of vapour always occurs shortly before either sub-droplet ejection or ligament protruding at the same spot on the droplet surface. Release of vapour through the droplet surface created a low-pressure spot that pulls liquid toward the region. The internal pressure and velocity of the flowing fluid rushes toward this spot thus pushing the ruptured surface outward [126]. This observation is in agreement with modelling works of Shinjo et al. [130] who stated that the surface tension quickly shrinks the periphery of the ruptured hole followed by a flow of fluid to the bottom hole of the rupture which pushes the bottom part upward, known as *recoiling*; shown in Fig. 2.17. With the combination of repelling motion (pushing the droplet backward), wall is detached in a form of ligament.

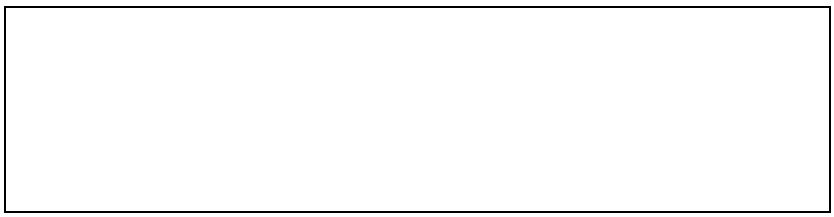

Fig. 2.17 Typical sub-droplet ejection processes [130]

Puffing of dispersed phase component inside the droplet typically ejects fuel vapour and sometimes together with small sub-droplet. On the other hand, puffing of continuous phase ejects the component in the form of ligaments which eventually detaches small sub-droplet due to the pinching process of surrounding pressure [131]. Rao et al. [100] categorised four bubble breakup mechanism as follows; low-intensities breakup, intermediate breakup, high-intensities breakup and microexplosion. Low-intensities breakup involves rupturing of small sized bubble with slight surface distortion whereas high-intensities breakup involves rupturing of large bubble with substantial droplet surface distortion. Two parameters determine the shape and stability of ligament evolution. Viscosity stabilises the evolution while surface tension inhibits the stretching of ligament and at the same time reduce the neck radius along the circumference to pinch-off the sub-droplet. The bubble size upon breakup is

smaller for mixture that has lower volume of more volatile component. The ligament exerted by smaller bubble detaches the sub-droplet faster in this condition.

According to Mohan et al [106], microexplosion strength categorised into two types; strong and weak disintegration shown in Fig. 2.18(a) and 2.18 (b) respectively. Strong microexplosion initiated by a protrusion on the droplet surface, expelling high pressure vapour expulsion with a fast speed sub-droplet ejection velocity. This type of microexplosion occurs every time a phase separation is observed. Weak disintegration initiated by a bulging on the surface with relatively small droplet ejection before complete disintegration, with larger and slower velocity of expelled sub-droplets. For both case, the microexplosion mechanism of droplet are as follows: protrusion/bulging on the surface prior to sub droplet ejection, rapid internal vapour expansion deforms the droplet into a shape of half cup with void space in the centre, expansion of liquid sheet, perforation of liquid sheet, extruded ligaments and breakup to small droplets.

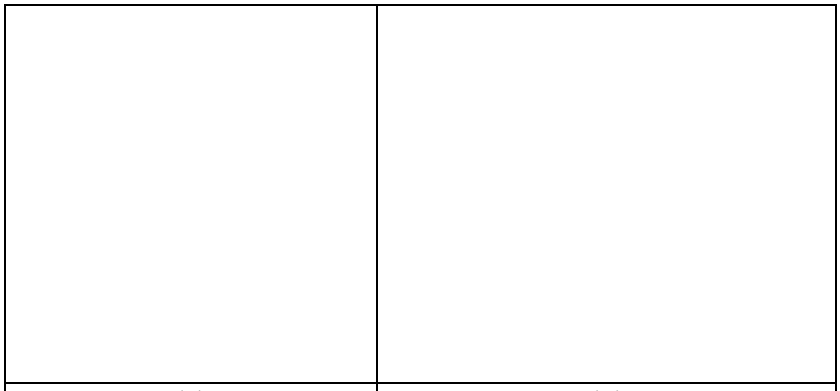

Fig. 2.18 Microexplosion with (a) weak disintegration and (b) strong disintegration [106]

Several conclusions on the mechanism that causes the droplet disruption to be transitioned from puffing to microexplosion were made by various studies on multicomponent droplet combustion. First argument focuses on the strength of pressure build-up inside the vapour bubble. Higher pressure will rupture the droplet with microexplosion whilst lower pressure bubble escapes through puffing, mainly contributed by the viscosity of the mixture [18, 126]. Hoxie et al. [129] explains higher tendency of droplet to microexplode when the transition from high volatility to low volatility-controlled diffusion is earlier within the droplet lifetime. This points out to the droplet with lower volumetric composition of high volatility fuel in the mixture. Most popular theories on the onset of microexplosion are either; as long as the more volatile component is heated up to its

superheat limit [1, 37-39], or shortly after the formation of phase separation within the droplet [34, 40], or combination of both phase separation and exceeding the superheat limit of the more volatile component [29, 33, 41]. Nevertheless, all probability contributed to their analysis came with strong experimental and numerical evidences. hence it is crucial to determine the main cause of microexplosion to be induced in multicomponent fuel droplet combustion by varying the mixture composition, stability and volatilities.

Although this phenomenon is usually described on the experimentation of single isolated droplet combustion study, these effects are reported during combustion of liquid fuel spray. Watanabe and Okazaki [132] observed the occurrence of puffing from the droplet size as small as 30-50 μm in actual sprays and observed to be more dominant than microexplosion. Furthermore, according to Shinjo et al. [133], the gas flow in a spray induces internal liquid circulation which produces a non-uniform liquid temperature that promotes local puffing rather than the microexplosion of the entire droplet. On the other hand, Zhang et al. [134] experimented diesel-ethanol emulsion spray in constant volume engine and observed the occurrences of microexplosion at 900 K and 4MPa ambient temperature and pressure respectively. Also, Wang et al. [135] experimented water-diesel emulsion spray with the same engine and ambient conditions observed microexplosions phenomena which increases the relative volume of spray by five times compared to neat diesel. Hence, the analysis of puffing and microexplosion of single isolated droplet is relevant and could provide useful insight in multicomponent fuel combustion characteristics.

2.9 Emulsion Fuel

Multicomponent alternative fuel provides better in-cylinder mixing during evaporation and spray breakup process due to puffing and microexplosion. Specifically, this phenomenon applies to a mixture of emulsion with large differences in their boiling point. Superheating, drastic heat-up and phase separation are promoted by utilising them in practical combustor. Emulsion fuel has the capability to microexplode or puff, which initiates the secondary atomisation caused by explosive boiling of dispersed phase droplets that ruptures the droplet [126]. Commonly known emulsion fuel that have a potential of such advantage are water-oil and ethanol-oil mixture [33-35].

Emulsion is a blend of fuel of between immiscible components such as water and oil or alcohol and oil [126]. To stabilise the emulsion, a surfactant need to be added and accumulated between the interface of the two liquids [35]. Addition of emulsifier forms an

elastic protective layer which would prevent early phase separation [36]. Adding lipophilic emulsifier with hydrophile-lipophile balance (0<HLB<9) forms water-in-oil emulsion (WO) with a structure consist of tiny water droplet dispersed in the base fuel whereas hydrophilic emulsifier with (11<HLB<20) forms oil-in-water (OW) emulsion consist of water dispersed in continuous phase throughout the droplet [105, 136, 137]. The solution is stirred vigorously to agitate the emulsion with very low amount of surfactant in volume (maximum 2%) and would interfere with the base fuel properties when added excessively [91]. For instance, the addition of 2% span 80 increases the boiling temperature of the emulsion by 2°C [105]. Also, higher surfactant concentration reduces the potential of a droplet to puffing and microexplode [138].

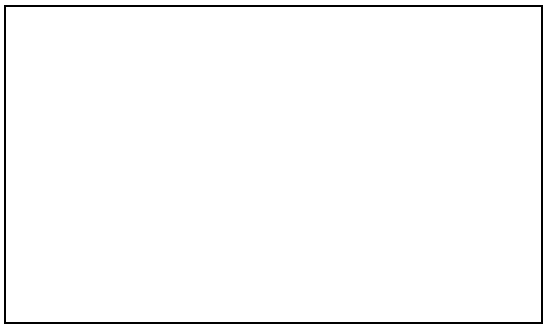

Fig. 2.19 Water-in-diesel and diesel-in-water emulsions in 10%, 20%, and 30% concentrations [66]

Water emulsion fuel droplet is opaque with a uniform colour of milky white prior to heating due to the immiscible nature between water and diesel [34, 36, 40]; shown in Fig. 2.19. Ethanol emulsion is observed to have tiny droplets of dispersed ethanol throughout the base fuel without noticeable change of respective colour. The addition of surfactant increases the surface tension of emulsion fuel. In low temperature condition, the surface tension is higher because the temperature is inversely proportional to the surface tension of the droplet. Higher surface tension in low temperature would hinder the water/ethanol vapour to blast through the droplet surface which in turn leads to a larger expansion of the droplet before rupturing [105]. Furthermore, surfactant has a high boiling point of 853 K at normal atmospheric pressure. Due to its high boiling point, evaporation of droplet containing a surfactant leads to a preferential evaporation of the base fuel since there is some concentration of the surfactant in the layer near the droplet surface [84, 104]. Additionally, surfactant at the interface of the water and oil destabilises above 350K-370K which aggregates the disperse water [33]. Consequently, droplet that burns with such behaviour tends to nucleate bubbles of vapour internally leading to sudden surface rupture by bursting

vapour in puffing process as explained in previous section. Due to their advantages in practical combustor, emulsion of diesel-ethanol and diesel-water is focused in present study.

2.9.1 Diesel – Ethanol Emulsion

Adding oxygenates into a diesel fuel has the capability to reduce particulate emissions in internal combustion engine. Strong candidate of oxygenated fuel is ethanol which has lower tendency to produce soot when compared to diesel [77, 38]. Ethanol is produced via a fermentation process of glucose which is derived from starch, sugar and cellulose [139]. Under normal atmospheric pressure, ethanol is known to have a non-sooting characteristics [28, 39]. For justification, visual observation of ethanol diffusion flame in atmospheric pressure was made by Urban et al. [124] further proves that there is no noticeable amount of soot is present. With the availability of oxygen atom to combine with oxygen molecule in air, more complete combustion can be achieved [95, 140] thus reduces the amount of unburned hydrocarbon (UHC), carbon monoxide (CO), particulates and Nitrogen oxide (NO_x) [109]. On the other hand, some traces of soot formation was reported by Urban et al. [124] on the combustion of ethanol droplet. Prior to ignition, a region of stratified fuel vapour and surrounding air is formed during deployment and growth. Some soot particulate was observed to be formed during this period but eventually burned during the transition to diffusive burning. Energy source added from the igniter to the rich stratified gas-phase of fuel and oxidiser mixture rapidly accelerates fuel pyrolysis which briefly forms soot.

(a)	(b)	(c)

Fig. 2.20 Backlit view of burning ethanol droplet in (a) 1.8 atm, 21% oxygen (b) 2 atm, 25% oxygen and (c) 2 atm, 30% oxygen [124]

In high ambient pressure and oxygen concentration, ethanol burns with luminous flame with observable amount of soot formation [110]. Major decomposition channel of ethanol produces mainly molecular products consist of C_2H_4 and H_2O. H abstraction from C_2H_4

further decomposes forming acetylene which is considered one of the key species of soot formation process. Decomposition process of ethylene however considered to be very low in normal atmospheric pressure but increased by more than threefold if the ambient pressure is doubled, which explain the low sooting and high sooting propensities of ethanol at normal and high atmospheric pressure respectively [26, 27]. Figure 2.20 shows the increasing density of soot ring from the combustion of ethanol droplet in elevated ambient pressures and oxygen concentrations. For instance, 10% addition of ethanol provides 3% oxygen addition to the ethanol-diesel emulsion and promotes better soot oxidation. Although more soot is generated, the rate of oxidation is higher leading to a reduced amount of soot emission at the end of the combustion [35].

Furthermore, ethanol addition promotes air-fuel mixing due to their tendency to microexplode, enhance combustion efficiency and lower the peak combustion temperature which in turn lowers exhaust emissions [73]. In addition, the heat up period of burning and evaporation of ethanol is observed to be short [28]. Hence, adding ethanol to the base fuel increases the burning rate due to the reduced heating time and enhanced evaporation characteristics of ethanol [95, 29]. Ethanol-diesel mixture is considered to be emulsion due to the immiscibility and the need for surfactant to stabilised the mixture [38]. Without the aid of stabilising surfactant, mixture of diesel-ethanol is found to be unstable and phase separation occurs especially for mixture with more than 10% volume of ethanol [133]. Surfactant serves as an interface within the mixture for homogeneous dispersion of ethanol [39] and mainly used to prevent phase separation while stabilises the fuel mixture [30].

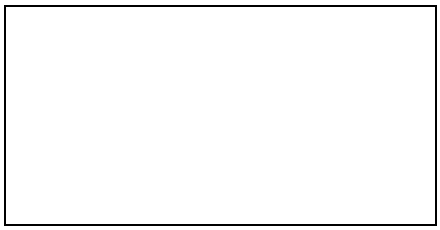

Fig. 2.21 Phase separation of ethanol in ethanol-biodiesel fuel mixture [29]

Combustion of diesel-ethanol assumes the characteristic burning of multicomponent fuel with high potential to behave in disruptive manner. Early droplet temperature of diesel-ethanol blend is lower due to the preferential evaporation of multicomponent fuel, which in this case ethanol with lower boiling point than diesel. As the concentration of ethanol get thinner, the droplet temperature suddenly increases and controlled by the less volatile fuel

component; diesel [30]. It is reported that the secondary atomisation took place at early as 10% of diesel-ethanol droplet lifetime [36]. Also, the occurrences of phase separation is reported by Chao et al. [29] shown in Fig. 2.21. Water could be absorbed by a droplet with alcohol mixture due to its hydrogen bond thus promotes immiscibility between the interface of ethanol and diesel. Formation of heterogeneous formation between diesel and ethanol blend is due to the hygroscopicity (capability of component to absorb or release water) of ethanol. High humidity and hygroscopicity of alcohol type would yield larger heterogeneous sites [29]. This suggests the capability of diesel-ethanol emulsion to microexplode due to the possibility of the mixture to have phase separation and ethanol having lower superheat limit than boiling point of diesel.

2.9.2 Diesel-Water Emulsion

In internal combustion engine particularly diesel engine, combustion process produced a very high range of operating temperature. This in turn results high emission of NO_x and particulates. In terms of controlling the combustion temperature so that the harmful emission can be reduced to a minimum, many studies have been conducted by means of using water as one of binary component fuel. As reported by Wang et al. [1], the emission of NO_x can be potentially reduced either by injecting water inside the chamber or through emulsification process first before injection. Addition of water increases the specific heat and latent heat of vaporisation of diesel which in turn reduced the peak combustion temperature and is known to reduce the generation of NO_x [34, 35, 91]. Increase in droplet temperature induces coalescence of water and drainage of water which in turn starts the phase separation [112]. This in turn would make the droplet to undergo significant growth during heating period by up to 20% of its initial size and attributes to the bubble nucleation and growth inside the droplet before puffing [141].

Water used as a component in fuel mixture have the capability to cause the fuel droplet to explode in microexplosion during combustion and have the potential to increase the burning rate and reduced particulate emissions [9, 142]. Reported by Kadota et al. [41], the probability of microexplosion to occur increases linearly with the water content, given the increased rate of water coalescence with larger diameter of phase separation [104]. Also, higher volume of water mixture in fuel will allow more surface of water to be exposed to the burning flame thus leads to a reduced flame temperature due to a higher expenditure of vaporization heat [1]. Microexplosion occurs when the water inside the emulsion droplet

coalescences into a complete phase separation within the droplet. However, a droplet size larger than 1 mm is needed to provide enough time for the phase separation before the droplet completely evaporated in normal gravity. On the other hand, the coalescence time of water is shorter in microgravity due to the absence of natural convection which promotes internal mixing. Without microexplosion, combustion proceeds with multiple occurrence of puffing [73].

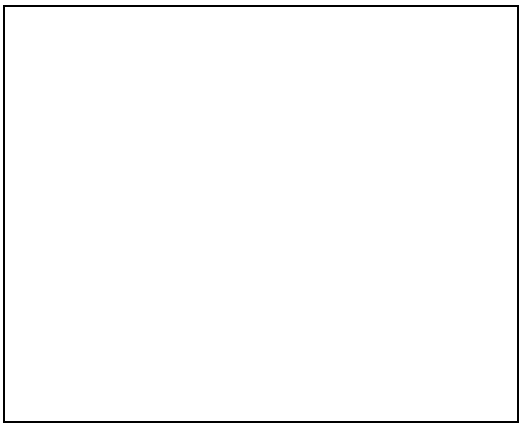

Fig. 2.22 D^2 regression of octane-water emulsion in distillation and frozen mode [76]

To further understand the evaporation characteristics of water emulsion, Law et al. [76] modelled the evaporation of octane-water with two case assumptions; distillation mode with active internal circulation, diffusing the lower boiling point component (water) towards the surface in early lifetime and the combustion transitions to the higher boiling point component as the water almost depleted. The other assumption is freezing mode, with no internal circulation but with only surface regression exposing the liquid for evaporation. Results from Fig. 2.22 shows that with distillation mode, the early droplet regression is low due to the evaporation being mostly water component. As soon as the water component fairly reduced, the surface regression transitioned to a higher regression rate indicating the starts of octane-dominated evaporation process. On the other hand, in freeze mode, the surface regression remains constant throughout the droplet lifetime with the value averaged between both regression in distillation mode due to the simultaneous evaporation of both components in regard to their initial volume composition. Both of these theories were compared with experimental observation done by the same authors. They found the evaporation behaviour of octane-water emulsion behaves exactly like the distillation mode, with distinct preferential evaporation sequence. It is concluded that the droplet would preferentially evaporates when the internal circulation is higher. If the droplet temperature does not reach the superheat

limit of water before the end of its lifetime, microexplosion would not occur. Droplet evaporation assumes distillation mode in normal atmospheric pressure whereas freeze mode can be experimented in fairly low ambient pressure between 0.1 and 0.15 atm with minimum effect of natural convection similar to microgravity. It is however, concluded by Tsue et al. [33] that microexplosion occurs earlier for droplet in normal gravity due to its higher heating rate in initial stage assisted by convection and water coagulation is accelerated due to internal circulation.

There are several differences in behaviour of combustion between oil-in-water (OW) and water-in-oil (WO) emulsions. For OW, When the temperature of the droplet elevated, the surfactant begins to destabilise resulting agglomeration of dispersed base oil in the continuous phase of water initiating phase separation. Complete phase separation is observed when there is an opaque formation of water droplet in the centre of the droplet surrounded by transparent layer of base fuel. The evaporation proceeds by distinct preferential evaporation with decreasing diesel mass layered on the surface of the droplet without any measured mass loss of water content [41]. Ejections of sub-droplet begins shortly after several occurrence of puffing for OW. The change from milky white droplet to a transparent with milky white droplet in the core of the droplet indicate its phase separation. For WO emulsions, the puffing continuously occurs throughout the lifetime with less sub-droplet ejection in average, but with more sub-droplet ejection at the end of its lifetime. Also, the droplet remains milky white without any phase separation [112]. OW has higher surface tension compared to WO emulsion. The dispersed water droplet of WO is dominant on the droplet surface with water having higher surface tension than oil [28]. Furthermore, Jang and Kim [91] found that WO has lower energy absorption compare to OW. This is explained by the position of dispersed water with milky white consistency that dominate the surface of the emulsified droplet with more light scattering intensities. Emulsification holds better in WO compared to OW emulsion which has water to be drained towards the centre. It is assumed that disruption of multiple sub-droplet ejection occurs because of the formation of water droplet internally by phase separation [112].

Despite similarities of combustion behaviour, there are few differences and drawbacks of using both ethanol and water emulsified fuel. The downside of water emulsion fuel is lower heating value, thermal efficiency and the water content in the emulsion potentially corrodes the metal parts in the combustor [105]. The combustion temperature of water emulsion is lower than ethanol emulsion. Furthermore, the oxygenated feature of water does not help with the soot oxidation due to water of being incombustible. The surfactant holding strength

of ethanol emulsion is stronger in evaporation condition while it is stronger for water emulsion in combustion condition. Because of that, microexplosion occurs at lower temperature for ethanol emulsion compared to water emulsion during combustion [35]. Finally, water is more abundance and easily acquired compared to ethanol which requires fermentation processes. To compare the combustion behaviour between ethanol and water emulsion especially during disruptive burning, isolated fuel droplet experiment would provide useful data on their respective differences.

2.10 Nanofluid Droplet Combustion

2.10.1 Introduction to Nanofluid

Dilution and suspension of nano-sized particle in fuel droplet studies were widely explored believed to emerged from work of Choi and Eastman [143] who proposed nanofluids concept. Within this field of study, stable form of agglomeration of nanofluid is formed by the addition of various type of energetic nanoparticles, surfactants, followed by rigorous stirrings and sonication [79, 96]. However, is it not absolute certain that the nanoparticles were evenly distributed inside the droplet during testing due to suspension process (injection or pressurised liquid flowing through a syringe), but with repeatable result, it is assumed to be evenly distributed [42]. Common nanofluid suspensions are either metallic typically boron, aluminium and titanium or non-metallic such as ceria, carbon and alumina. To aid with stabilisation, surfactants are added but, in some cases, none added because it would change the properties of the base fuel such as viscosity, boiling point and surface tension. Also, adding surfactant to a burning nanofluid produces a cross-linking structure by the decomposition of surfactant and would produce an impermeable shell of particles as a product of pyrolysis [107]. Without surfactant added to the nanofluid, the suspension was found to be stable for minimum of two hours [84].

2.10.2 Enhancement of Combustion Efficiency

Nanofluid is known to have enhanced ignition probability, shortened ignition delays, reduce the surface tension and in some cases, reduced combustion temperature [42]. Javed et. Al [43] conducted a study on various dilute concentrations of aluminium particles in kerosene and heptane droplet combustion concluded that metallized liquid fuels burns with higher

combustion energy due to higher gravimetric energy contents of metal compared with traditional liquid fuel. Positive attributes of nanoparticle suspension include high energy density [44], promotes complete combustion and high specific surface area [45]. Moreover, nanoparticle is known to become a secondary energy carrier that enhances the energy release during combustion [46]. Nanoparticles increases the thermal conductivity as well as thermal diffusivity which in turn improves the dispersion of energy conducted towards the centre of the droplet [144]. With size less than 10 nm, the cross-linking particles acted as a thermal bridge and improved thermal conductivity via Brownian motion [145, 146]. As the combustion progresses, the droplet temperature increase to a boiling and the nanoparticle acts as a heat source that continues to heat the droplet beyond the boiling temperature of the base fuel [96].

2.10.3 Combustion Phases of Nanofluid.

Nanofluid combustion involves multiphase, multicomponent and multiscale nature throughout the lifetime of the droplet due to their thermal conductivity, surface tension, radiative absorption and mass diffusivity which vary with time [96]. The combustion characteristics behaved differently in each combustion phases. Three typical combustion stages are observed in nanofluid combustion either in low or high loadings. They are defined with ignition and droplet heating, steady burning with multiple sub-droplet ejections and disruptive burning with higher frequency of puffing or microexplosion [84, 46]. During heating phase, nanofluid with the addition of surfactant burns with preferential combustion similar to multicomponent fuel droplet. Because of higher boiling point of surfactant, the base fuel vaporised first and leave a higher concentration of surfactant on the droplet surface as the burning progresses. Larger expansion of droplet was observed together with the occurrence of puffing that ejects nanoparticle to be burned [43]. During the steady combustion phase, some distortion on the droplet surface is observed. Particles inside the bubble heats up the droplet locally, initiating a heterogeneous nucleation which forms multiple small bubble that merged into one large bubble; with some puffed through the surface [147]. The steady stage ended when the bubble ruptured the droplet with stronger puff. In disruptive stage, more particles agglomerated, and puffing ejects some particles that burns inside the flame. This disturbs the formation of flame on the primary droplet. The particles agglomerated to a shell on the droplet surface, leading to a local heating on the surface that would superheat the

base fuel resulting stronger puffing and more frequent sub-droplet and particle ejection [107]. Fig. 2.23 illustrates the shell formation that leads to microexplosion in nanofluid combustion

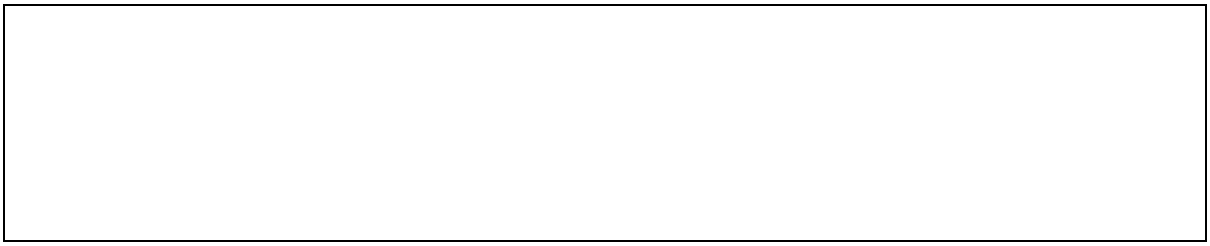

Fig. 2.23 Schematic illustrations of shell formation and liquid breakup during nanofluid combustion [46]

2.10.4 Aggregation of nanofluid.

Interparticle collisions causes the attachments between them is the main cause of particle aggregation, depending on the collision frequency and efficiency. Gan and Qiao [107] categorised the mechanism of particle aggregation with three major transport mechanism. (i) Brownian diffusion also known as perikinetic collision is a random movement of particles inside the droplet. (ii) Relative motion of particles which also known as orthokinetic aggregation due to fluid stirring, shear flow and turbulence. This is strongly affected by the natural convection which exerts shear stress on the surface of a droplet, causing internal circulation inside a burning droplet. Also, the surface of the droplet regresses as it evaporates, promoting collisions between particles concentrated on the surface of the droplet to move inward and collides with the particle contained inside. (iii) Differential settling is significant when the particle is denser and heavier than the base fuel. When particles settle during expansion, the settling particle collides with other particle and agglomerates. Once the particles aggregates through these means, it is less likely for the particles to be diffused back inward toward the centre of the droplet.

Tree parameter that can ensure a smooth regression of burning nanofluid droplet are the formation of porous spherical shell, delays of particle agglomeration and uniform distribution of particles [46]. Agglomeration of nanoparticle in high loading would be the main attribute for the reduction in the burning rate of droplet [148]. The surface energy of particle is reduced when they agglomerate, creating a larger restrictive force for the mass diffusion of the liquid fuel [84]. The formation of aggregate shell during the combustion not only depend on the size, but also on the morphology of the particle. It was observed by Ojha et al [46] that

stronger microexplosion occurs with crystalline boron that forms into an impermeable shell compared to amorphous boron which forms into a permeable shell. More evenly distributed particle inside the droplet would form a porous and permeable shell that allows nucleated vapour to escape easily. Typical nanoparticles has high specific surface area (5-50 m^2/g) [149] which forms a strong interaction between the particle and surrounding liquid. Repulsive force resulted from the absorption of ionic groups in a liquid to the surface of nanoparticles. This forces may reduce the agglomeration rate [107]. Further delaying the process of agglomeration, continuous diffusion near the surface ensures insufficient time for the nanoparticle to form large aggregates [42]. On the particle distribution, more evenly distributed particle inside the droplet would form a porous and permeable shell that allows nucleated vapour to escape easily. With higher particle loading, microexplosion is expected due to higher pressure resistive shell which leads to a higher pressure build up inside the droplet [46, 147].

2.10.5 Heat Transfer Mechanism in Nanofluid Combustion

Thermal conductivity in nanofluid is enhanced significantly [150] due to the aggregation of nanoparticles [151]. Nanofluid droplet is not entirely transparent compared to neat fuel and radiation emission from the flame significantly enhance the burning rate with higher radiation absorption. Larger surface area of nanofluid droplet enhances the radiation absorption which increases the evaporation rate [144]. Also, measurements done by Tanvir and Qiao [42] presented in Fig. 2.24 found that nanoparticles near the droplet surface absorbs most of radiation energy which leads to localised heating and boiling near the surface. This in turn promotes evaporation which found to be the main cause of enhanced burning rate of nanofluid. Even in low particle concentrations, the nanoparticle was found to absorb almost all the radiative energy. Higher concentration of nanoparticle does not affect the total radiative energy absorbed. However, as concluded by the authors, in high particle concentration, the photon does not penetrate deep enough and concentrated on the liquid/gas surface. Flame temperature is found to be constant throughout the combustion in each particle loading. Another possible change in the evaporation rate is due to the smaller size of flame. Smaller flame size improves heat conduction from the flame to the droplet surface due to its closer vicinity [84].

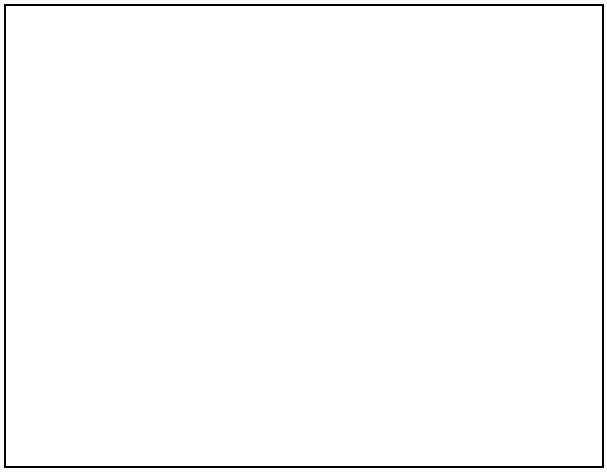

Fig. 2.24 The percentage of absorbed photons toward the surface of ethanol droplet suspended with graphite [42].

2.10.6 Differences Between Metal and Carbon-base Nanofluid Combustion

To investigate the differences of metal and carbon based nanofluids, Gan and Qiao [144] compared the burning characteristics and transmission spectrum between carbon and aluminium nanoparticles. The authors discovered that the metal particle in nanofluid absorbs the highest radiation energy but most of the energy was scattered away. On the other hand, carbon-based nanoparticles have higher absorption efficiency than the scattering efficiency which in turn produced higher evaporation rate. Yadav et al. [84] uses graphene nanoplatelet (GNP) in nanofluid shows that the burning rate is reduced in low amount of particle mass loading (below 0.2%) but enhanced to a maxima in 0.2% mass loading and begin to decline with additional loading due to their tendency to agglomerate. It is also found that the smaller specific surface area of GNP is, the more detrimental the effect to the burning rate in low particle loading. The results is in agreement with works done by Ghamari and Ratner [152] who determined the optimum mass loading for carbon-type nanoparticle is between 0.15% to 0.22% for GNP, Multi-Walled Carbon Nanotubes (MWNT) and OH functionalized Multi-Walled Carbon Nanotubes (MWNT-OH). On the other hand, higher loading causes more particles trapped near the surface of the droplet with little amount of the aggregation transported to the flame. Unburned carbon particles inside a droplet gradually extinguished the flame as more heat used to be absorbed rather than used to evaporate the fuel [152]. For metal-based nanofluid, the burning rate is found to continuously increased even after 1% mass loadings with shortened ignition delay [96][43][153]. It is also found that the burning rate is reduced in low amount of particle mass loading (below maxima of 1%) and the declining trend is more

profound when the ambient temperature gradually increased. Two important results worth to be mentioned here; carbon-based nanoparticle has very low optimum loading (0.2%) compared to metal-based nanoparticle (1%) and loadings lower than optimum for both cases are detrimental to the burning rate which is more profound when the ambient temperature is higher.

2.11 Soot Formation and Effect During Combustion

2.11.1 Introduction

Fuel is sprayed into a high temperature and pressure environment in diesel engine operation for a continuous combustion process. In practical combustor, it is not possible to achieve a complete combustion. As a result, hazardous air pollutants such as polycyclic aromatic hydrocarbons (PAHs) and carbon monoxide constitutes most of soot and gas phase produced during incomplete combustion [154][155][156]. In particulate emission, there are two categories of organic substances. Insoluble organic fraction consists of sulphate and soot while soluble organics fraction consists of low molecular weight substance mainly lubricants and unburned fuel [157]. PAHs and acetylene (C_2H_2) [77] are known as the soot precursor in hydrocarbon combustion that formed in the rich region of non-premixed flame due to high-temperature pyrolysis [110]. Formation of primary soot particle and precursors are located within the area between the flame front and the droplet surface. The equivalence ratio in this region is high and most of diffused oxygen from the ambient is consumed in the flame region [77]. Soot formation are greater than oxidation in fuel rich region and the opposite for lean zones. When the combustion temperature is higher, the rate of oxidation increases [158].

2.11.2 Soot Formation Process

Soot consist one-part hydrogen and eight parts of carbon with a density of 1.84 $\pm$ 0.1 g/cm^3 [158]. There are six process of solid soot formations by sequence involving pyrolysis, nucleation, coalescence, surface growth agglomeration and oxidation as shown by process flow in Fig. 2.25. During any point of these process, hydrocarbons converted to CO_2, CO, and H_2O through oxidation process [159]. Density of soot produced in combustion depend on the type and concentration of fuel. Diesel combustion with higher C/H ratio produced denser soot compared to butane which is in alkane group that considered to form very low soot

formation [52]. Also, higher number of carbon atoms in the fuel increases the mass of soot formed [89]

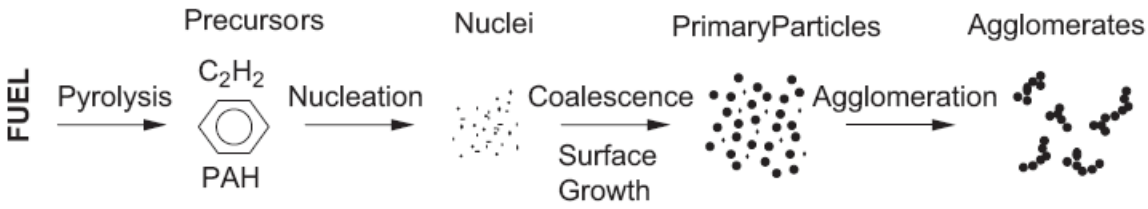

Fig. 2.25 Schematic diagram of the steps in the soot formation process from gas phase to solid agglomerated particles. (taken from [159] with a permission from the publisher)

2.11.3 Microstructure of Soot

Rohani and Bae [47] analysed the microstructure of soot particle taken from spray flame injected in ambient condition without external temperature and pressure rise. In their case, the soot collected is highly comparable to the soot formed by a droplet combustion. They observed the primary soot particle as an amorphous carbon which is surrounded by semi-graphitic shell. Particle sampled from spray is found to be less compact (larger primary particle of 25 nm) from the actual engine operation due to oxidation of lower combustion temperature with less aggregation (shorter fringe length, 0.796 nm) due to lower collision rate. However, the large-sized primary particle is not limited to combustion without external pressure and temperature elevation. Müller et al. [48] took a soot sample from raw exhaust of heavy duty diesel S2876 CR-engine and studied the microstructure and morphology of the soot particle with transmission electron microscope (TEM). They found a secondary chain-like structure of agglomerated particle which is a common morphology of soot shown in Fig. 2.26.

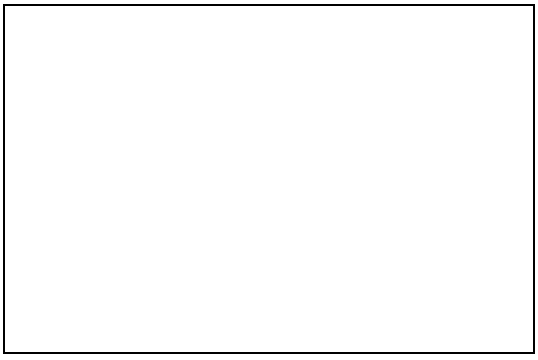

Fig. 2.26 TEM micrographs of soot [48]

The mean size of primary particle is about 25 nm and the built-up agglomerate has a size up to micrometres. The size of soot aggregate in spherically symmetric burning of droplet is found to be between 40-50 nm and consistent with other types of soot aggregate found in sooting flame. Temperature field and convection patterns influences the position of trapped aggregate but have no significant effect on the mean precursor size [108]. On the other hand, Tao et al. [49] predicted the size of soot through their soot prediction model stated that the diameter of primary soot particle is 10.28 nm with considerable amount of hydrogen contained in soot particle along with carbon atoms. Despite of slight differences of soot particle sizes in their measurements and modelling, it is reasonable to agree on the size to be within the range of 10 to 50 nm [50].

2.11.4 Morphology of soot.

Soot nuclei is formed when small sheet of graphene stacks on each other in circular fashion which grow in size by surface growth or collision, hence produces a soot primary particle [160][161] shown in Fig. 2.27. According to study on candle and natural gas soot performed by Su et. al [41], the number and size of soot particles varies between different type of fuel with definite presence of nanodiamond particles which began to nucleate inside the flame [162]. The aggregation of primary soot particle forms a chain-like agglomerates that is released through the exhaust [47]. Also mentioned by Omidvarborna et al. [163], rigid structure of graphitic crystallise surrounded a spherical nucleus that is structurally and chemically less stable. Majority constituent of soot particles are hydrophobic with the rest being hydrophilic and hygroscopic [156]. Soot particle is highly porous and results from [154] shows the existence of micropore structure of the soot particle and accounted for the specific surface area of the primary particle (1.9 m^2/g).

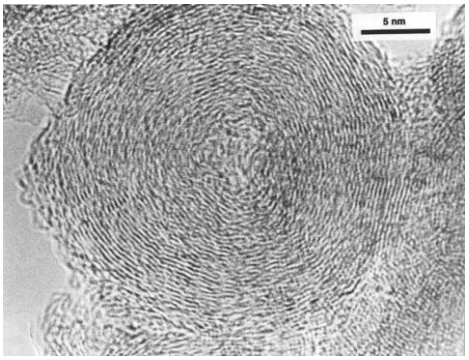

Fig. 2.27 Example of the well-known shell/core nanostructure of many primary soot particles. (Taken from [161] with a permission from the publisher)

2.11.5 Soot formation in droplet combustion.

Unburned fuel nucleates from vapour to solid phase at elevated temperature of fuel rich region and forms soot with higher propensity when the residence time of fuel molecule in burning environment is longer [59, 60]. On the other hand, soot formation from a smaller droplet is mitigated due to the shorter residence time of soot precursor [98, 164] in smaller flame size [52, 80]. The transport of soot particles is controlled by the temperature gradient of surrounding gas-phase that pushes the particle inward toward the surface of the droplet and viscous drag caused by the gasification of the droplet that pushed the particle outward towards the flame termed thermophoresis and Stefan Flux (diffusiophoretic force) respectively [28]. Stefan flow induced drag is influenced by the burning rate whilst thermophoresis highly effected by the flame radius and temperature. Higher burning rate produce high Stefan flux and the combination of high flame temperature and small flame stand-off ratio produce high thermophoresis [110]. Soot shell appears as a dark ring with porous structure surrounding the burning droplet and known to be trapped by the balance between inward force of thermophoresis and outward force of Stefan flux [90, 104, 165]. Visualisation of soot shell around a burning droplet between the droplet surface and flame microgravity experiments shown in Fig. 2.28 confirms the existence of these forces [89, 109, 110]. Burning of less volatile fuel tend to have soot shell to be formed closer to the droplet surface [60]. Once the Stefan Flux is lower than the thermophoresis, the soot particles is then pushed towards the flame to be oxidised. Larger flame has lower thermophoretic force due to the further vicinity of the heat source [59]. It was found that the burning rate becomes low whenever there's a formation of soot shell and jumps back to higher burning rate as the soot shell collapses [98]. On the other hand, soot particle from the combusted droplet in normal gravity is blown away by the buoyancy-induced convection; making it impossible to be measured quantitatively via visualisation method [39]. However, even in strong convection, soot precursor was found to be present and always trapped in the fuel-rich side between the droplet and the flame [50]. Convections slightly reduces the formation and agglomeration of soot particle in normal gravity as the flow carries the agglomerated particle towards the flame front without allowing thermophoresis to position the soot inside the flame for extended residence time for further soot accumulation [60].

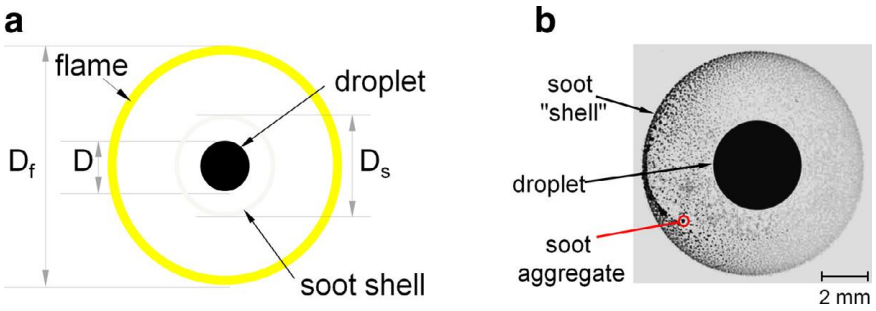

Fig 2.28 (a) Schematic of burning droplet with spherically symmetric flame formation and (b) formation of soot shell around droplet burns in microgravity. (taken from [12] with a permission from the publisher).

2.11.6 Effect of Soot Formation in Droplet Combustion.

The formation of soot results significant change in the heat transfer and evaporation characteristic of a burning droplet. Results of such effect in several literature focuses on the formation of soot away from the droplet, either forms as shape of shell (microgravity, balanced Stefan flux and thermophoresis) or flowing within the region between flame and the droplet surface due to the effect of imbalanced force of Stefan flow and thermophoresis or buoyancy (normal gravity). The soot shell formed around the burning droplet serves as a heat sink which reduces the radiation heat transferred to the droplet for evaporation [80]. Furthermore, soot shell acts as a physical barrier which reduces the mass diffusion of the vapour as well as hindering the oxidiser to reach the reaction zone [59, 60]. In different perspective, radiative heat transfer is enhanced by the presence of soot which acts as a heat sink, absorbing the radiative heat from the flame [109]. Because of that, the radiative heat transfer towards the droplet surface is enhanced in later period of droplet combustion because of the formation of soot shell. However, The radiative heat loss is also increased [85, 86] from the radiative emission of soot shell which in turn reduces the flame temperature and burning rate [89, 166]. Kittelson [167] used absorption spectroscopy to measure the visible light through diesel soot stated that the scattering of visible light is lower than absorbance for diesel soot particle regardless of size due to high carbon content of the particle. This justifies the soot as a high heat absorbing particle, which absorbs the heat, promotes heat loss from flame and acts as a physical barrier between the flame and the droplet that inhibit evaporation.

2.11.7 Soot Contamination in Fuel Droplet.

With turbulence flame, interacting burning droplet and buoyancy-driven soot particle transport, there is high possibility of soot contamination in droplet prior to ignition and during the combustion. Concluded by Kadota and Hiroyasu [51], the formation of soot is between the flame and droplet surface, considered to be in a thin layer region which partly pushed inward into the droplet while some of it oxidized [52]. When the thermophoretic force is higher than the Stefan flux, soot particles formed in the fuel-rich region would be pushed towards the droplet thus contaminating the surface. Under this possibility, Shaw and Williams [53] conducted numerical analysis on impure fuel droplets, suggesting fuel contamination with low volatility component from the product of combustion as they might have seeped into the droplet in gas phase during fuel pyrolysis. The author concluded as the impurity fraction increased, the evaporation rate became weaker as a result of flame contraction. Additionally, prior to ignition, Kittelson and Kraft [54] described the formation of soot cloud prior to ignition during the injection of fuel. These soot particles travelled in every direction in low temperature region and do not oxidized which gives the possibility to be absorbed as impurities in the droplet slightly before ignited, either from current or previous cycle. Moreover, soot is formed as a part of particulate matters circulated in the exhaust gas during combustion cycle, suggesting trapped aggregates within the cylinder and considered in soot modelling study of Mosbach et al. [55] as part of the combustion mixture. Some particles that re-enter the cylinder through engine gas recirculation (EGR) system survived the oxidation process upon entering and may act as a sponge and attach to other remaining fuel droplets, engine oil and soot particle [43]. Under these circumstances, it is possible to conduct an examination of fuel droplet contaminated with soot which would provide beneficial result on the contamination mechanisms and the effect to the burning behaviour.

2.12 Interaction of Multiple Fuel Droplet Combustion

An interaction between droplets must be taken into account in droplet combustion study rather than in isolation which in turn provides a better insight in the prediction of fuel spray behaviour [21, 25]. Vaporisation of droplets in spray behave differently from isolated fuel due to their interaction between each other [56]. Competition between droplets for available oxidizer inside the combustion chamber in spray combustion was concluded by Labowsky and Rosner [57] who stated that oxidizer is prevented to reach the spray core due to this

competition. This behaviour was confirmed by Chigier [58] who observed that the flame only surrounds the spray boundary without appearing in any location in the spray core which also in agreement with the findings of Sangiovanni [21]. The interactive combustion of fuel droplet mostly depends on the physical parameter during combustion, which is the separation distance, L. It is also reported by Miyasaka and Law [82] that buoyancy is enhanced during combustion of droplet in groups. This in turn enhances the oxygen supply to the droplet but closer distance below the effective critical distance of L/d = 10 starves the oxygen between interacting droplets [111]. Numerical analysis done by Marberry et al. [168] shows that the deviation of combustion characteristics of grouped droplet from single isolated droplet are significant for L/d < 20. Fig. 2.29 shows the diminishing effect of droplet interaction on to the surface regression when the separation distance is beyond 20.

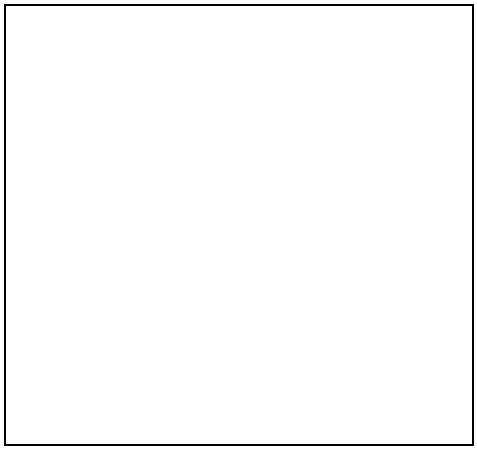

Fig. 2.29 Extinction droplet diameters as a function of pressure for a single droplet and binary droplet arrays in normal gravity [25]

Significant increase in the deviation is found for higher number of droplet or closer interaction (high density number). This is due to the increase competition of available oxidiser as the density number increases. Burning droplet would behaves comparable to an isolated droplet condition under certain separation distance, depending on the properties of the fuel droplet [25]. Fuel that burn with similar burning rate is expected to have the same interaction behaviour due to the same heating, heat flow and gasification rate [56]. In grouped droplet combustion, interaction between them is considered when there is a noticeable change in droplet surface regression, burning rate, droplet lifetime and flame formation of the fuel from droplet in isolation.

2.12.1 Combustion Stability of Interacting Droplet

Unsteady condition effects grouped droplet combustion, severely effecting centre-positioned droplet [82]. The flame region moves away from the droplet surface due to the search of diffused oxidiser and somewhat unsteady in shape and temperature. This would prevent the burning to settle down on quasi-steady condition [72]. According to Nagata et al. [88], unsteady behaviour dominates the dense cluster of small droplet due to fuel vapour accumulation effect. Flame formation in cluster of droplets is larger, and because of that the accumulated vapour took longer time to reach the enveloped flame, more fuel accumulated around the droplet rather than being consumed by the flame. Also, droplet heating duration becomes longer due to the radiative heat loss of larger flame formation. Upon ignition, early evaporation rate of droplet is higher than the vapour consumed by the flame and the flame front extends further as the field of vapour accumulation gets bigger. Eventually along the combustion lifetime, the vapour consumed by the flame is higher than the evaporation rate, similar to droplet heating and vapour accumulation effect of isolated droplet but with increased magnitude. Contradicting the result of previous authors, Okai et. Al. [20] stated that multidroplet burning stabilized the combustion irregularity and smoothen droplet liquid surface. Moreover, the onset of stability is earlier for multidroplet arrays compared to isolated droplet. Combustion stabilisation only apply when there is a strong interaction between a group of fuel droplets. Also, as mentioned by Mikami [24], It was observed that a group of droplets which burns in one enveloped flame is beneficial in flame stabilization mechanism in combustors especially on the flame spreading mechanism.

2.12.2 Effects of Droplet Interaction on Burning Rate and Lifetime

As stated by D^2-law, the surface area of an isolated droplet decreases linearly with time. The same trend should be imposed to the burning rate of an arrays of droplet if the multi-droplet position is geometrically constant throughout the droplet lifetime [21]. However, slight deviation from D^2-law is presented for less than 10 inter-droplet distances. Higher interaction between burning droplets increases the droplet lifetime; given with specific minimum spacing between them for each type of fuel. These interaction plays an important role in extending burning times of spray combustion. With more comprehensive details on the mechanism, one can control the burning duration and intensities to suit the optimum engine operation. Minimum lifetime of droplet (no inter-droplet reaction) in arrays can be achieved by a

specific inter-droplet distances, depending on the type of fuel used [20]. Strong interaction between the flow fields surrounding neighbouring droplets occurs when the droplet centres are less than two diameters apart [19]. Also, the lifetime of an isolated burning droplet is increased more than twice in droplet spacing that is less than 2 diameters [21] and these concluding remarks by Sirignano and Sangiovani respectively, applies to most type of fuel. It is again confirmed by Struk et al [25] that it is evidence that the burning rate is not significantly affected for the interaction with initial separation distance over initial droplet size (L/Do) above 5. Below normalised distance of 5, the burning rate reduces significantly. On the other hand, instantaneous burning rate of interacting droplets depends on the instantaneous droplet size, D and initial separation distance, L. Continuous increment of instantaneous separation distance is due to the reduction in droplet size as the combustion proceeds. This changes the intensity of droplet vaporisation with continuous change thus renders D^2-law non-existent [82, 56]. To analyse these changes, burning rate correction factor $\eta = K_{instant}/K_{isolated}$ was numerically introduced by Labowsky [169] to see the changes in burning rate that vary with time during interactions, with clearer differences of trend in the regression and implemented in experimental study by Miyasaka and Law (normal gravity) [82] and Mikami et al. (microgravity) [111]. With the correction factor, they determined that the effect of strong droplet interaction is indeed within the instantaneous separation distance below 5, with slight deviation from D^2-law above 5 shown in Fig. 2.30. Hence, the strength of the interaction mainly depended on the flash point, autoignition temperature and the chemical compound of the fuel itself and this is worth investigating thus providing a comprehensive datasheet of droplet interactions.

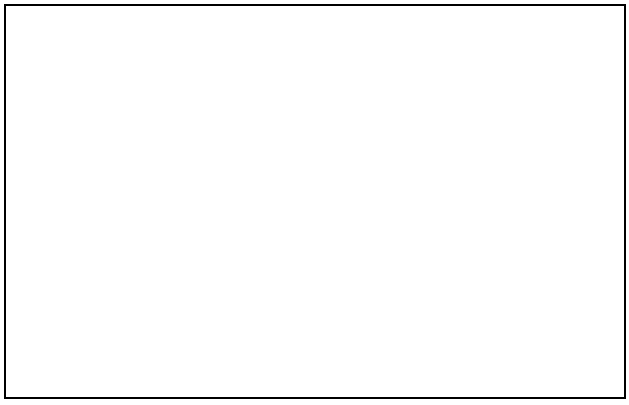

Fig. 2.30 Buoyancy-induced burning rate of multi-droplet combustion of decane droplet using burning rate correction factor [111]

2.12.3 Flame Structure and Heat Transfer of Interacting Droplet

Droplet interaction tends to change the combustion flame structure in term of size and shape. Group of droplet burns with two type of flame structure. The first would be individual combustion mode with separate flame that burns each droplet individually and the second would be an enveloped flame that engulf the entire group of droplets shown in Fig. 2.31. The flame mode depends on the chemical condition of the whole system and significantly affected by the vicinity of neighbouring droplets [72]. Overlapping flames and burning group of arrays is an evidence of a strong droplet interaction [21]. The oxygen depletion between the flame causes the flame to merge into one enveloped flame with larger flame size [23]. This in turn decreases the vaporisation rate, lower the temperature gradient within the group of flame thus prolong the combustion lifetime [170] due to further distance of flame front that reduces the heat transfer towards the surface of the droplet. Interaction between droplet still exist even without the overlapping of flame formation. Size and shape changes of the flame indicates the sign of droplet interaction and the effect is the strongest with merged flames [21].

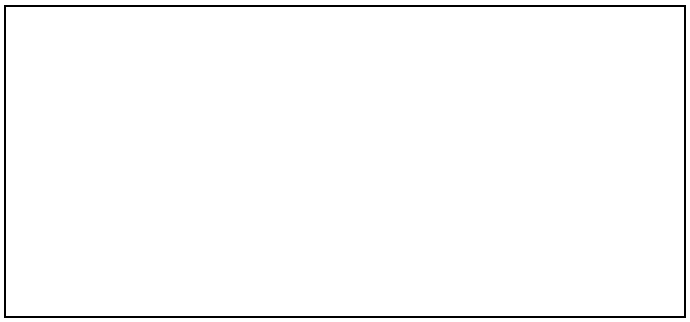

Fig. 2.31 Direct photographs of the flame for different flame shape modes [111]

During interaction of droplets, cooling effect is expected due to duplication of heat sink and evaporation of more vapour that cools the surrounding gas phase. Also, the supply of vapour is increased by multiple fuel source thus extending the lifetime of the burning droplet as well as increases the distance of flame front [108]. Closer spacing reduces the heat transfer from the flame to the surface of the droplet due to the increase of flame distance as well as radiation heat loss to the ambient [88]. Also, the Nusselt number based upon local ambient conditions will be less than the corresponding value for an isolated droplet and decreases as spacing decreases [19]. Referring to Okai [20], Heat loss is reduced between the droplets, but heat generation is retarded by their competition for available nearby oxidizer. For interacting

droplet that burns with individual flame, oxygen starvation considered not to be occurred. The radiative heat transfer is enhanced between the droplet, with the flame of neighbouring droplet increases the radiative heat transfer to the adjacent droplet [111]. Buoyancy is enhanced in close proximity of interacting droplet with better interior motion which in turn enhances the conductive heat transfer within the droplet. Although the effect of buoyancy is improved, close proximity still reduces the evaporation due to a higher decline in radiative heat transfer compared to little enhancement of conduction [82, 56]. Nevertheless, deeper analysis on droplet interaction is important to establish better understanding of fuel spray. Although a single isolated droplet study is beneficial in terms of combustion fundamental, it is restricted to isolation; without any interaction and instable burning behaviour.

2.13 Summary

Several hypotheses can be drawn from the transient behaviour of a burning droplet based on the extensive study made on the literature. Slight change made on a fuel droplet would vary their transient behaviour, especially during droplet heating and fuel vapour accumulation. These effects can be studied in detailed by various approaches.

Firstly, the transient burning of a fuel droplet highly depended on the properties of the fuel. Fuel with high boiling point would have significant droplet heating effect during the transient liquid-phase evaporation. Low volatility fuel would have significant fuel vapour accumulation effect as a result from lower fuel vapour consumption rate. However, such effects are only observable during experimental works. Classical quasi-steady analysis assumes constant gasification and equal evaporation-consumption during the evaporation of a fuel droplet. Since the droplet heating and fuel vapour accumulation constitutes a large portion of the droplet lifetime, high discrepancies between quasi-steady analysis and experimental result is expected when liquid and gas-phase transient effect are included into the quantitative measurement. Hence, comparison between a fuel with high and low boiling point with quasi-steady assumptions could demonstrate such transient effects.

Secondly, emulsion droplets have high potential to improve mixing during actual spray combustion as a result of more violent droplet breakup during their disruptive evaporation processes. From the literature, ethanol emulsion is expected to have a better breakup process compared to water emulsion due to its lower surface tension and flammable properties. However, adding a surfactant to stabilise the mixture would change the internal dispersion of lower boiling point component (ethanol and water). Higher holding strength of

surfactant would trap more volatile component within the droplet and initiates more violent droplet breakup process. Existing quantitative measurements between both emulsion fuels found that water emulsion has higher burning rate compared to ethanol emulsion. This must be contributed by the higher mass loss of liquid during the disruptive evaporation of water emulsion. It is believed that their distinct differences of droplet breakup can be identified by experimentally comparing them with a high repeatability measurement. Hence, more detailed measurement during their disruptive evaporation phases would provide an insight into their breakup processes.

Thirdly, an unstable emulsion fuel droplet has a high potential to microexplode. Mixroexplosion of an emulsion droplet are caused by a complete phase separation and upon reaching the superheat limit of the dispersed phase within the droplet. Three conclusions were drawn from various literatures. Firstly, it is theorised that an emulsion droplet will microexplode once the dispersed phase goes into a complete phase separation. Secondly, microexplosion will occur once the lower boiling point component has reached its superheat limit. Thirdly, microexplosion only occurs when both complete phase separation and when the superheat limit is reached. However, some literature reports that although both conditions are met, the emulsion droplet still able to completely evaporate without microexploding. It is believed that there must be another condition required to initiate a complete droplet breakup since the process is categorised into two exploding strength. One process involved nearly symmetrical expansion and one would undergo a strong gush of vapour jet prior to a complete breakup. Hence, detailed visualisation into the liquid-phase of emulsion droplet is needed to observe the dynamics of the dispersed liquid within emulsion fuel.

Fourth, the presence of nanoparticle within a fuel droplet significantly changes the burning behaviour. Nanoparticles has high heat absorbance which in turn would enhance the heat conduction within a fuel droplet, diminishing the droplet heating effect and improve mixing through particle oxidation. On the other hand, soot is a nano-sized particle produced within the rich fuel region of flame. The surface area of soot is measured to be much larger with smaller size of primary particle than the energetic nanoparticles used in nanofluid combustion. Furthermore, soot is hydrophobic and easily agglomerated due to its tendency to move towards the area with less liquid. With high potential of soot to contaminate the liquid droplet during turbulence mixing of fuel spray, the role of soot during the combustion of fuel droplet need to be taken into consideration. At a certain amount of nanoparticle suspended within a fuel droplet, a critical loading can be achieved with a significant

enhancement of combustion characteristics. Hence, the effect of soot contaminating a liquid fuel need to be studied and compared with existing nanofluid experimented by various studies.

Fifth, gas-phase interactions between multiple droplet combustion highly effect the transient evaporation process. Small spaces between burning droplet with larger flame starves the oxygen supply in the reaction zone. This in turn prolongs the droplet heating process. Also, higher density of multiple evaporating droplet increases the fuel vapour accumulated between the flame and the surface of the droplet. It is expected that within a certain critical droplet separation distance, the transient evaporation process would be affected significantly. On the other hand, Stefan flow is highly dependent on the mass consumption rate of a fuel droplet whereas the thermophoretic flux is highly dependent on the temperature gradient of gas in the hot region within the flame. The dynamic change of these parameters has the effect on the soot generation and position. Under a certain ratio of these flow, the soot generated would have the potential to either pushed toward the surface of the burning droplet or nearby droplet. Based on various literatures, the transient effect would behave differently between each type of fuel. Hence, meaningful comparisons can be made by experimenting on types of fuel with large differences in their volatility and sooting propensities.

Chapter 3

Research Methodology

3.1 Fuel Selection

Research advances in the combustion efficiency of compression ignition engine lead to a breakthrough in achieving a relatively high thermal efficiency. Recently, a study done by Splitter et al. [171] has achieved 60% thermal efficiency through reactivity controlled compression ignition (RCCI) system. Although diesel fuel considered to be more efficient combustion energy fuel compared to petrol in the recent study [172-176], diesel combustion posed a high risk to air pollution from its emission. Furthermore, additional problems raised by its price fluctuation, depletion and increasing energy demands. Researchers have been exploring an alternative source of energy to tackle these problems.

In order to meet the high energy demand and avoid price fluctuation, studies on diesel and bioethanol blending were conducted due to its renewable nature. Bioethanol is produced via a fermentation process of glucose which is derived from starch, sugar and cellulose [139]. Adding bioethanol into diesel fuel reduces the sooting propensity during combustion of the mixture [77, 38] because ethanol is an oxygenated fuel which in turn has the capability to promote more complete combustion [95, 140]. For instance, 10% addition of ethanol provides 3% oxygen addition to the ethanol-diesel emulsion and promotes better soot oxidation [35]. For this reason, it is worth to mix diesel and ethanol as subjects of study.

To further tackle high Nox emission from diesel combustion, water and diesel emulsion was introduced. Water addition into the combustion chamber reduced the operating temperature, thus reduces NO_x formation [177-179]. Also, reported by Faik [66], high excitation and explosion of diesel and water emulsion aided the combustion process, with higher burning rate constant and a number of secondary atomization. Also, higher water content has proven to further reduce the combustion temperature to a cold combustion region, with almost zero CO and NO_x emission. However, higher water content produced unstable combustion and posed a diminishing effect to higher operating load due to its nature

of microexploding. Closer study on diesel and water droplet emulsion would enable the categorisation of each mixture composition in term of its stability and reliability.

3.1.1 Neat Fuel

Neat fuels that were used in present work are diesel and ethanol. Diesel was treated as the base fuel for each blend and emulsion. The type of diesel fuel utilized in present work is a regular Shell Diesel Fuel. The type of ethanol fuel utilized in present work is a Biofuel-500 Gardeco, plant-based bioethanol produced from industrial distillation. The physical properties of diesel, ethanol and water used are depicted in table 3.1. These properties are used for the calculation of classical quasi-steady theory on neat fuel in the present work.

Table 3.1 Properties of neat fuel and water used in present work

Properties	Diesel	Ethanol	Water
Chemical composition	$C_{10}H_{22}$	C_2H_5OH	H_2O
Density @ 25 °C, kg/m^3	830	783.2	1000
Specific gravity @ 25 °C	0.83	0.79	1
Molecular weight, g/mol	148.6	46.07	18.02
Stoichiometric AF ratio	14.6	9	-
Thermal conductivity @ 25 °C, W/m.K	0.142	0.171	0.608
Kinematic Viscosity @ 40 °C, mm^2/s	3.05	1.08	0.892
Boiling point, °C	170-390	78	100
Flash point, °C	79	16.6	-
Specific heat @ 25 °C, kJ/kg.K	1.81	2.44	4.186
Latent Heat of Vaporization, kJ/kg	250	840	2257.7
Surface tension @ 25 °C, mN/m	28.2	22.1	72
Lower Heating Value, MJ/kg	43.2	26.8	-
Higher heating Value, MJ/kg	44.8	29.7	-

Diesel constitutes multiple component of volatile mixture within it, making the boiling point to be within the range of 170 to 390 °C. For the boiling point of diesel, 170 °C is used in the analytical study conducted in the present work; which considers the minimum temperature that is required for the onset of steady diesel evaporation. In analytical consideration, the fuel would only steadily evaporate when the boiling point is reached.

However, in the experimental observation, fuel starts to steadily evaporate even below the boiling point of a fuel. Hence, minimum boiling point of diesel was utilised in the calculation to avoid higher discrepancies between experimental and analytical analysis.

3.1.2 Emulsion Fuel

The diesel-ethanol and diesel-water fuel prepared in this experiment incorporated an emulsification method. This process was done to obtain a kinetically and thermodynamically stable solution for combustion purposes. The composition of emulsion fuel is depicted in Figure 3.1 [180]. Water-in-oil emulsion would have water-based liquid to be dispersed inside the continuous phase of oil whereas oil-in-water emulsion would have the oil to be dispersed inside the continuous phase of a water-based liquid. The emulsifying agent forms a protective layer between the boundary of the immiscible liquid which in turn prevents early coagulation and complete phase separation.

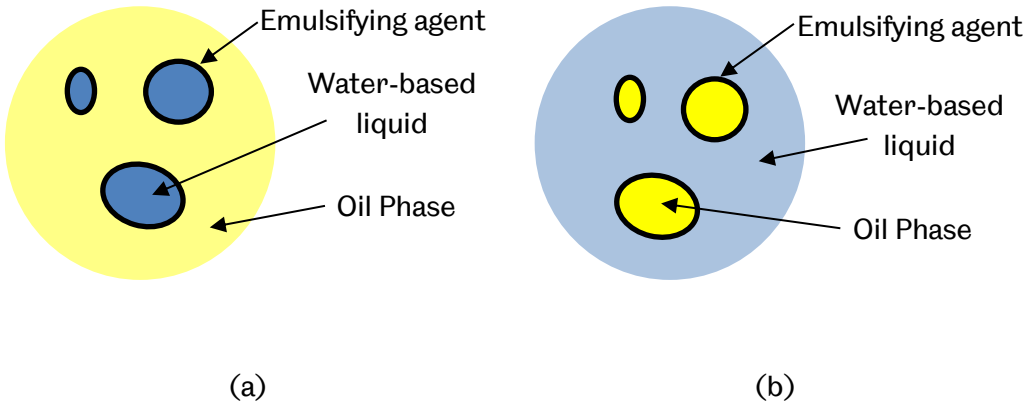

Figure 3.1 Illustration of (a) water-in-oil (WO) and (b) oil-in-water (OW) emulsion (reproduced from [180])

Generally, there are two types of emulsifier, which are hydrophilic and lipophilic emulsifiers. Hydrophilic emulsifier tends to form an oil-in-water emulsions whereas lipophilic emulsifiers produce a water-in-oil emulsion. These types of emulsifiers were scaled by a Hydrophile-Lipophile Balance number (HLB), from 0 to 20, having an equal emulsifier attraction to oil and water in the scale of 10 [181]. To simplify, the emulsifier characteristic based on their respective HLB is briefly described in table 3.2. To ensure the fuel prepared is water-in-oil emulsification, Sorbitan-mono-oleate with Hydrophile-Lipophile Balance number

(HLB) 4.3 was used. On the other hand, Polysorbate 80 with HLB =15 was used to produce oil-in-water emulsion fuel.

Table 3.2 Ranges of HLB number and characteristics

HLB Number	Type	Emulsion
0 < HLB < 9	Oil-soluble (Lipophilic)	Water-in-oil
10	hydrophilically-lipophilically balanced	N/A
11 < HLB < 20	Water-soluble (Hydrophilic)	Oil-in-water

The emulsifier (less than 2% of the total volume of solution) is added to the diesel (base fuel) and stirred by using a mechanical stirrer of 2000 rpm. Water or ethanol is added continuously to the base solution while under steady stirring. This method was similar to the preparation made by Califano [182], by ensuring the water or ethanol is added drop by drop to the base fuel while under continuous stirring. Specifically, experimental parameters of water composition in diesel were set at 10%, 20% and 30% for these sample preparations. Further increasing the water composition in the emulsion rendered the mixture incombustible. On the other hand, the volume loading of ethanol tested in this study is similar to water for the purpose of comparability.

3.1.3 Diesel fuel Contaminated by Soot Particles

The effect of soot particle contaminating a diesel fuel droplet is studied in present work. There were two contamination conditions in particular; surface contamination and volume contamination. These conditions were selected to simulate the instantaneous contamination process during fuel spray combustion.

Surface-contaminated diesel (SCD) droplets were prepared during the ignition process. The imaged neat diesel droplet was ignited by another diesel droplet positioned below it. The soot contained in the hot combustion gas flowed upward because of buoyancy and contacted the imaged droplet. At the same time, heat from the diesel flame positioned below ignited the imaged droplet. As a result, the imaged droplet was ignited while having its surface contaminated by soot particles. However, it is not possible to control the contamination density precisely due to the continuous process from the contamination to

droplet ignition. To minimise the measurement errors, this process was repeated by a significant amount of time to ensure each similar level of contamination can be repeated at least six times ranging from 30% to 100% of droplet surface coverage.

Volume-contaminated diesel (VCD) droplets were prepared before the droplet deployment. The diesel soot was collected from the particle's deposition during the burning of diesel fuel through a fibre glass-reinforced wick. A glass sheet was placed above the diesel flame for the soot deposition. The deposited particles are then scrapped by a spatula into a glass bottle and weighted. To ensure there was no moisture contained within the particles, drying process was done. The soot particle inside the glass bottle was placed inside a drying oven for over four hours to evaporate any moisture.

VCD droplet was prepared by adding the dried soot particles into a diesel fuel with 0.1% to 0.5% particle loadings by mass. It is stated from various studies on carbon-based nanofluid droplet combustion [42, 84, 144, 152] that the critical loading of nanoparticle for enhanced combustion characteristics is between 0.1 to 0.5%. Particle loading beyond the critical loading is found to detriment the burning rate and stabilities of a nanofluid droplet. Under these reasons, those particular mass loading of soot particles were investigated since the diesel soot is made up of mostly carbon-based particles. The collected soot particles were added to the diesel (base fuel) and stirred by using a mechanical stirrer of 2000 rpm. No surfactant was added to prevent significant change to the fuel properties of base fuel as well as the formation of a protective layer around the suspended soot particles. The suspended particles inside the base fuel is found to be evenly segregated from the visualisation on the droplet liquid-phase with good repeatability of measured results; further discussed in Chapter 6.

3.1.4 List of Fuels

Fig. 3.2 shows a complete list of fuels used in present work; categorised into each chapter. It is worth mentioning that the fuels were selected based on their respective objectives; mainly to evaluate the transient combustion processes of evaporating droplets.

In Chapter 4, neat diesel and ethanol were selected to analyse the transient burning of the fuel in neat condition respectively by comparing them based on their large differences in boiling point, volatility and sooting propensities. Diesel has high boiling point and low volatility which expected to have high droplet heating and fuel vapour accumulation effect. On the other hand, ethanol is expected to have minimum droplet heating and fuel vapour

accumulation effect due to its low boiling point and high volatility. With large differences in their properties, a significant difference in their transient behaviour could be observed. Hence, the identification of such transient effect can be made clearly by a comprehensive analysis that leads to a more detailed description.

In Chapter 5, two emulsion types with six mixture conditions were analysed. For a stable emulsion fuel of water-in-oil (water-in-diesel and ethanol-in-diesel), comparisons were made between them mainly to identify their disruptive burning behaviour. As a flammable component within emulsion fuel, ethanol is expected to enhance the evaporation rate of an emulsion fuel significantly compared to water. However, based on literature [66], water emulsion undergoes higher evaporation rate. Hence, a detailed liquid-phase visualisation is made to identify their characteristics during disruptive burning which influenced such enhancements. On the other hand, the main cause of emulsion droplet to microexplode is studied in detail by analysing the unstable emulsion of oil-in-water (diesel-in-ethanol, diesel-in-water and both emulsion without any surfactant added). By adjusting the heating, composition and dispersed condition within the unstable emulsions, the tendency of the droplet to micrexplode can be identified by looking into the effect of ambient temperature, phase separation and the location of dispersed phase.

Chapter 6 focuses on the effect of soot contamination onto the liquid fuel droplet. Diesel was selected to demonstrate such effect due to its practical use with high potential to be contaminated by soot during actual spray combustion. By igniting a diesel droplet positioned below the imaged diesel droplet, such effect can be simulated and analysed. To further analyse the role of soot as a nanoparticle that would potentially enhance the combustion, a uniform suspension of soot within a diesel droplet was studied. It is expected that uniform suspension of soot would enhance the combustion similar to nanofluid containing energetic nanoparticles.

Chapter 7 focuses on the effect of interaction during the combustion of multiple fuel droplet. This would simulate the liquid and gas phase behaviour of burning droplet during actual fuel spray in relative scales. Neat diesel and ethanol were selected based on their large differences in fuel properties. Larger flame formation and high sooting propensities of a burning diesel is expected to increase the effect of oxygen starvation and contaminate the nearby droplet respectively. The opposite effects are produced during the burning of ethanol. By comparing the multi-droplet combustion of both fuels, the effect of volatility and sooting propensity of a burning fuel to their transient evaporation behaviour is identified.

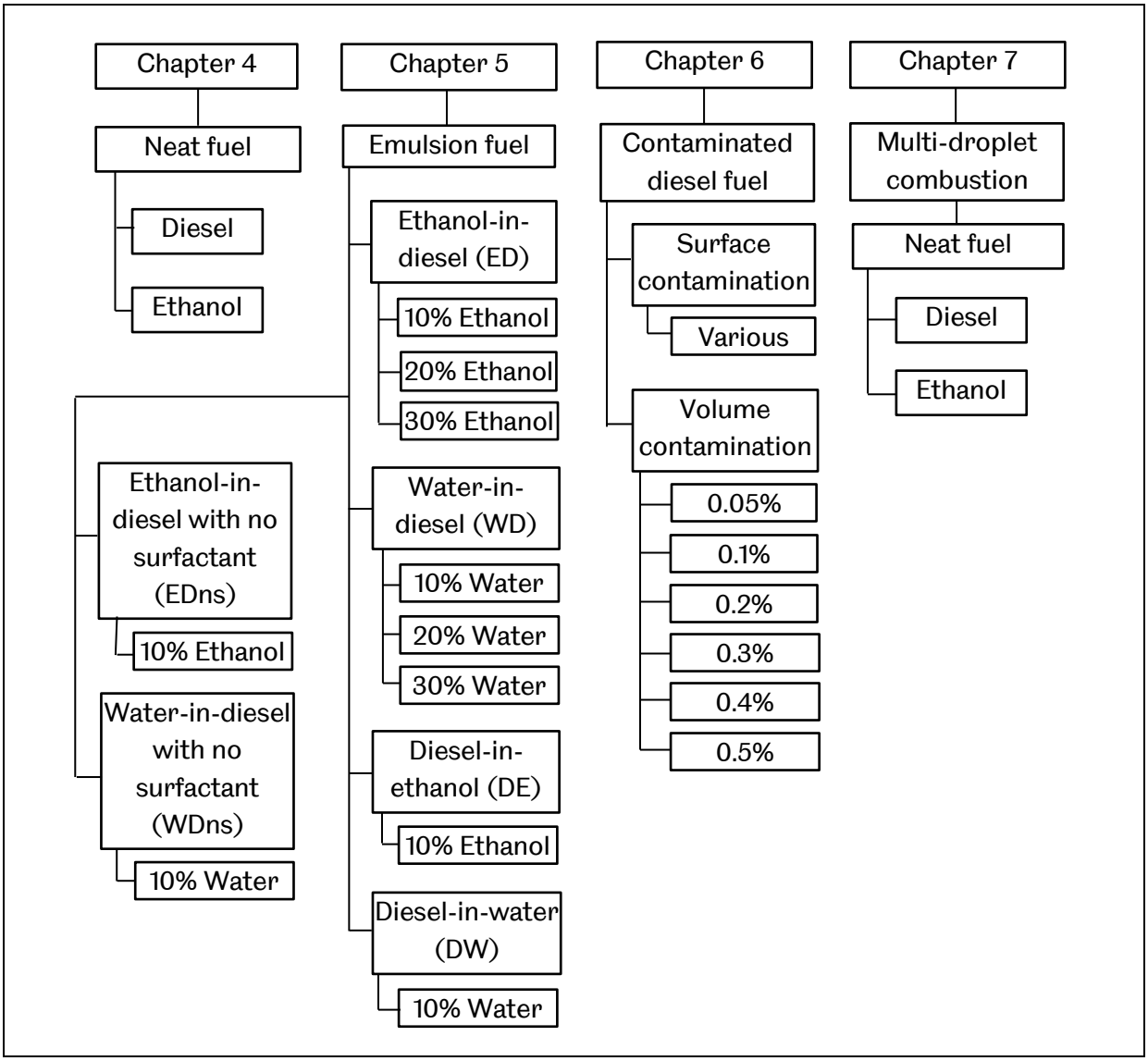

Fig. 3.2 Chart of fuels utilised in present work

3.2 Characterisation on Experimental Procedures

This section explains the characterisation of the experimental procedures, mainly focused on the droplet generation, suspension and ignition. Through the course of this research, similar characterisation approaches were implemented.

3.2.1 Droplet Generation and Suspension

Prior to suspending the fuel droplet, all neat fuel and emulsion were placed inside a chemical bottle and labelled. In present work, fuel droplets were suspended on a 95 μm Silicone Fibre enforced with 5 μm diameter tungsten core. According to trials done by Liu et al. [16], 14 μm fibre support enables the suspension of droplet less than 1 mm and 80 μm fibre support

could suspend a droplet higher than 1 mm. The main idea is to track the droplet dynamics and flame characteristics during droplet combustion. Therefore, the size of the fibre selected for testing is suitable for 1 mm fuel droplet size suspension in the purpose of observing clear nucleation inside the droplet and longer lifetime of combustion flame. For the purpose of liquid-phase visualisation, high magnification images on stationary droplet is required. Hence, fibre-suspension method was selected in the present work. Figure 3.3 shows the droplet suspension on the silicon carbide fibre prior to ignition.

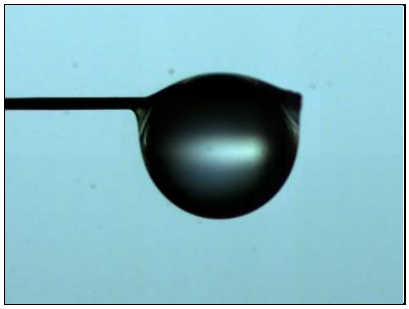

Figure 3.3 Suspended Diesel Droplet on 100 μm SiC Fibre

Droplets were suspended on the SiC fibre by transferring the fuel from the chemical bottle via micro-fine syringe with a hypodermic needle (0.33 mm diameter and 12.7 mm length). A relatively small amount of fuel then injected to the end of the fibre and measured to ensure the consistency of the transferred size.

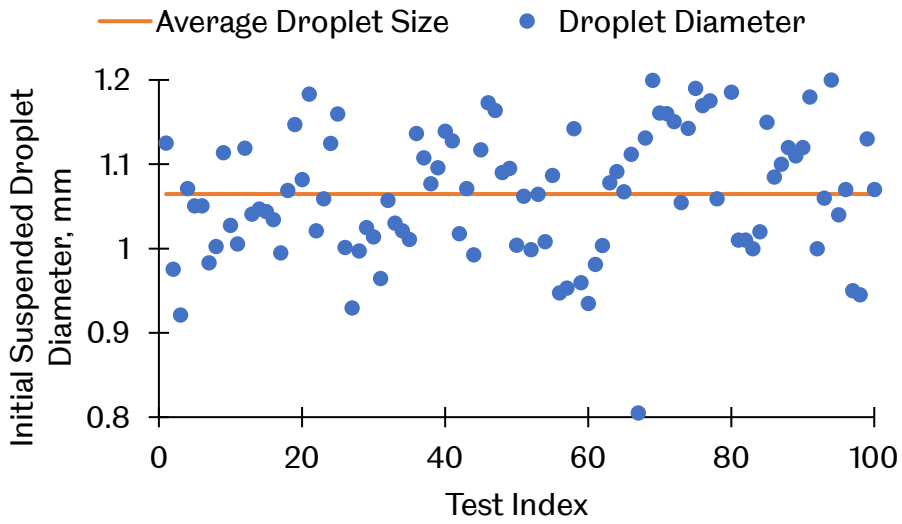

Figure 3.4 Initial Droplet size of suspended fuel droplet

As shown in Figure 3.4, the deviation in the initial droplet size was kept as minimum as possible to ensure the precision and repeatability of the experiment. Standard deviation was calculated to be as low as 0.075 mm whilst the average diameter is 1.064 mm. Hence, by manually injecting and measuring for each instance ensured the practicality of current method thus provided high reliability of analysed results.

3.2.2 Droplet Ignition

There were two methods of fuel droplet ignition used in the current study based on the specific scope of analyses. In general, two ignition devices involved with the various setup of heating approach.

Ignition with Butane Flame

After the suspension of the droplet, a butane lighter was ignited underneath the droplet and the flame edge was inserted to be at least 5 mm away from the droplet. This placement was made to ensure the ignited flame from the fuel droplet was free from disturbances from the butane flame; which might alter the actual size of the ignition flame. Ignition delays measured from this approach were neglected, due to its uncertainty of insertion speed, distance and flame intensity, which yielded between the range of 1 to 10 milliseconds. A study done by Faik [7, 36, 66] implemented this approach which focused on the burning rate constant, flame and droplet dynamics rather than the ignition characteristics. Figure 3.5 shows the timeframe between butane flame side heating insertion and ignition.

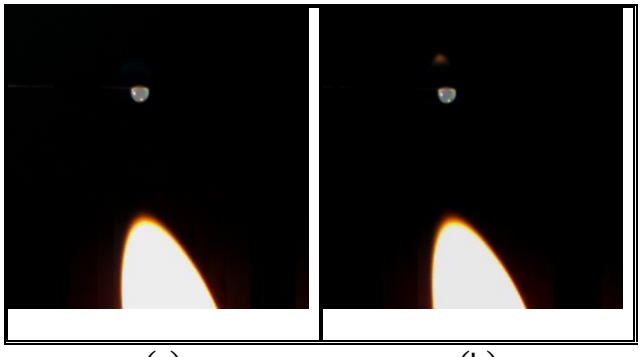

Figure 3.5 Butane flame side heating at (a) flame insertion at 0 ms (b) visible diffusion flame at 12 ms

Ignition with Thermal Wire Heater

The apparatus consists of the thermal wire heater (Smok Alien 220W) which able to vary the heating power output within range the of 6W to 220W. Wire setup on the atomizer varies, ranging from the type of wire, size, total resistance and shape. It was observed that the most stable configuration; which was used in this experiment is Kanthal A-1 wire, 6 number of coil round with 3 mm diameter. The resistance reading used is 0.82 ohm. From results obtained from the measurement of temperature responses in Chapter 4, it is confirmed that placing the thermal heating wire 1 mm away would provide a steady temperature distribution; similar to ignition method done by [18, 20, 22, 23]. However, ignition done by these researchers does not particularly controlling the ignition repeatability as the distances varied between 1 mm to 2 mm. Although the closer placement of the wire yielded higher precision, reducing the distance less than 1 mm would disturb the flame formation once the droplets were ignited. Hence, 1 mm was chosen to be the best suited for this experiment. To Precisely adjust the distance, a micrometer ratchet was used and the distance was measured using the Photron Fastcam Viewer Software on the image prior to recording. This ignition method was developed in the present work to ensure high repeatability of experimental measurement by providing neat ambient temperature elevation around the droplet without any external gas or vapour influence. With flexible adjustment of device wattage, the coil temperature can be controlled for any desired level. Furthermore, the small-sized heating device provides more compact arrangement of experimental apparatus thus simplifies the suspension and imaging method for more complicated arrangement such as soot contamination processes, multi-droplet arrays and repeatable disruptive processes in emulsion droplet.

The heating wire device actuated outside of the droplet range for at least 10 seconds to ensure the wire has reached a steady maximum temperature of given power settings. The device is then slid below the droplet with 1 mm distance and steadily heating until ignition. Preliminary measurement indicated that there was no reliable correlation between ignition delay and ignition temperature setting thus produced a negligible result (ranges between 10 to 100 ms). This is due to the low repeatability criteria of heating device insertion directly below the droplet. As soon as a visible flame is observed to form, the heating device was quickly retracted. This ignition method ensures neat combustion of each fuel droplet with only temperature elevation made to the ambient air. Figure 3.6 shows the device insertion sequence from reaching a steady maximum temperature to the ignition of the droplet

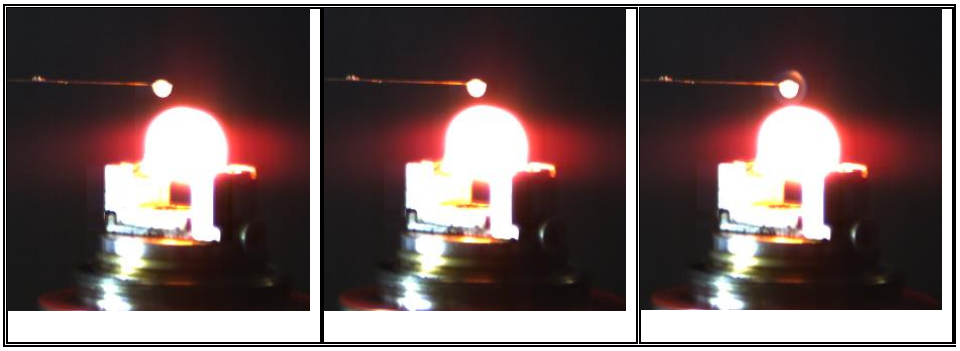

(a) (b) (c)

Figure 3.6 Thermal heating wire on steady maximum temperature at (a) away from the droplet (optical axis) (b) 1 mm away below the droplet (c) droplet ignition

3.3 Imaging Setup

In present work, two imaging setups were conducted, each with their specific purpose of image visualisation.

3.3.1 Backlighting and Direct Flame imaging

The imaging setup for all fuel droplet experiments conducted in the present work is shown in Fig. 3.7. For tracking droplet lifetime and droplet dynamics in high speed, HIG-HSV 1-High Speed Video 50k FPS-Phantom V210 camera was used. In the purpose of tracking droplet size and dynamics, a backlighting imaging was conducted by placing an IDT 19-LED high intensity illuminator with a diffuser behind the droplet which is opposite to the camera lens (Nikon AF Micro NIKKOR 60mm f/2.8D). Additionally, a direct flame imaging was conducted simultaneously with backlighting by positioning a Photron-SA4 high speed colour camera with its optical path in the perpendicular axis of droplet imaging with Nikon AF Nikkor 50 mm f/1.8D lens attached to it. This was done to acquire the flame formation of the combusted droplet, enabling real time tracking between droplet dynamic and flame characteristics.

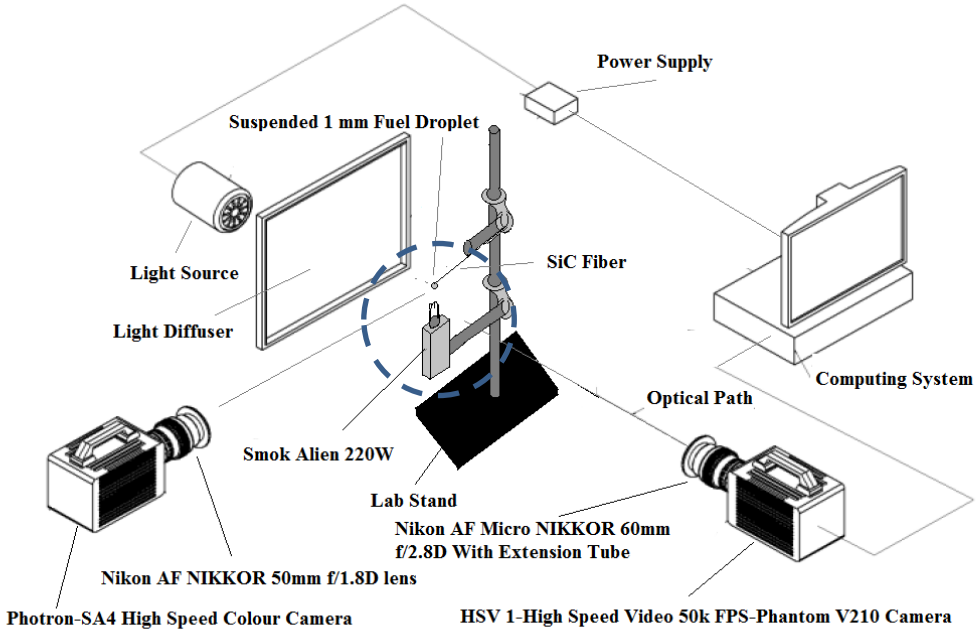

Figure 3.7 Backlit and Direct Flame Imaging Setup for Fuel Droplet Ignition

For droplet dynamics imaging, 10,000 to 20,000 frames per second was set. Direct flame imaging was done with 500 frames per second. Droplets initial diameters were kept constant at 1 $\pm$ 0.05 mm for each test. The recording of images was between the actuation of ignition devices to the flame extinction. The acquired images were stored as TIFF format and processed with each specific algorithm written in Matlab. Figure 3.8 shows an example of acquired images during the experiment. Table 3.3 summarises the visualisation parameters conducted in present work.

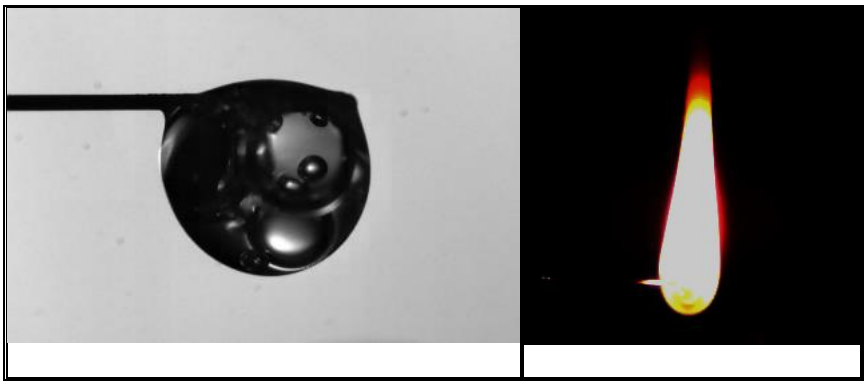

(a) (b)

Figure 3.8 Image of diesel fuel droplet at 0.53 s of combustion lifetime in (a) backlit imaging and (b) direct flame imaging

Table 3.3 Summary of visualisation parameters

Chapter	Resolution (pixels)	Backlighting		Direct flame visualisation	
		Spatial resolution (pixels/mm)	Temporal resolution (frames/second)	Spatial resolution (pixels/mm)	Temporal resolution (frames/second)
4	320 x 256	130	10,000	17.57	500
5	320 x 256	130	20,000	17.57	500
6	512 x 384	130	20,000	17.57	500
7	800 x 600	130	10,000	17.57	500

3.3.2 Arrangements of Suspended Droplet

The experimental work done in the present study implemented three arrangements of fuel droplets. In all arrangements, the initial droplet size was ensured to be 1 mm and suspended on 100 µm silicon carbide fibre. Because of a high spatial resolution of 130 pixel/mm and high temporal resolution between 10,000 to 20, 000 frames per second, only one droplet can be imaged in the field of view. The arrangements of the droplet are shown in Fig. 3.9, derived from the area circled in Fig. 3.7.

Visualisation on single isolated droplet is done by placing the kanthal wire 1 mm below the droplet after undergoes at least 10 seconds of preheating shown in Fig. 3.9 (a). In the droplet evaporation (non-burning) experiment, the position of heating wire remains 1 mm underneath the droplet until the droplet was fully evaporated. In droplet burning experiment, as soon as the first visible flame is formed, the kanthal wire was removed in quick succession. This arrangement was implemented during the experimental study of a single isolated neat fuel droplet in Chapter 4, single isolated emulsion fuel droplet in Chapter 5 and single isolated volume-contaminated diesel droplet in Chapter 6.

Fig. 3.9 (b) shows the droplet arrangement implemented during the combustion of surface-contaminated diesel droplet in Chapter 6. The imaged diesel droplet was ignited by another diesel droplet placed directly below it. The flame edge of the contaminating droplet was ensured to be at least 1 mm away from the imaged droplet. As soon as the imaged droplet was ignited, the burning contaminating droplet was removed in quick succession.

Fig. 3.9 (c) shows the arrangement during the experimentation of multi-droplet combustion in Chapter 7. The arrangement is either with two droplets or three fuel droplets. The distance between droplets was adjusted by turning the micrometre ratchet to the

desired position. The distance between droplets was checked again using the measurement tool inside Photron Fastcam Viewer to ensure precise inter-droplet distance prior to ignition. The droplets were positioned a bit further away from the light diffuser due to the space restriction of imaging equipment. As a result, the highest possible temporal resolution used to visualise the droplet was 10, 000 fps due to the lower intensity of light received by the camera's sensor.

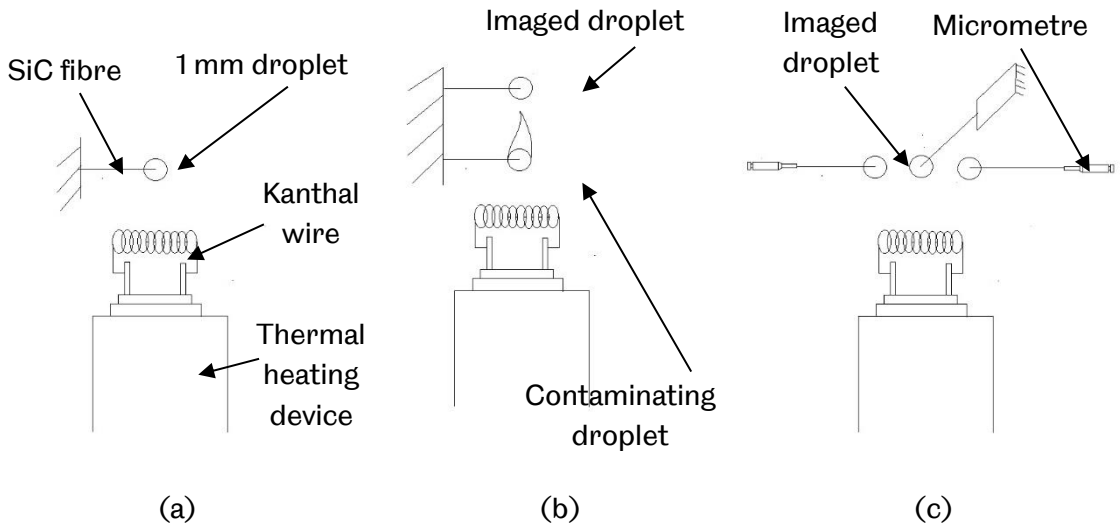

Fig. 3.9 Various arrangements of fuel droplet during the experimentation of (a) single isolated (b) soot contamination and (c) multi-droplet

3.4 Image Processing

Raw images from the experiment does not provide a complete quantitative data that were fully analysed and presentable. Therefore, processing the images were crucial for comprehensive analysis thus fulfilling the aim of the research. All images were processed using a Matlab software with an aid of image processing tools featured in the software. Figure 3.10 shows the processes done in the image processing section.

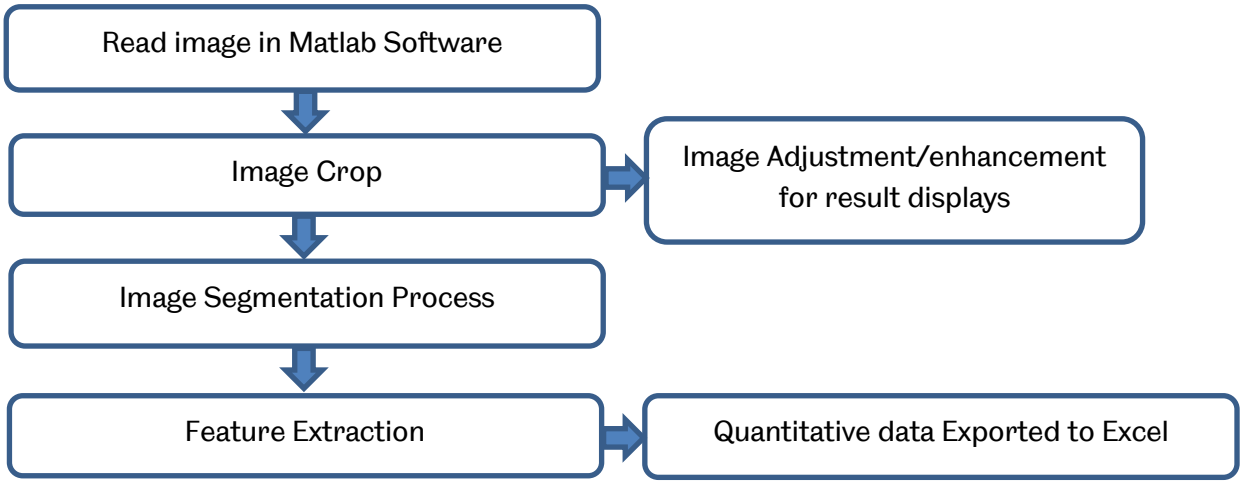

Figure 3.10 Flow chart of image processing sequence

3.4.1 Droplet and Flame Segmentation

In order to produce a suitable image for further processing, a segmentation process on acquired images of droplets and flames is needed. Is was proven that a well manipulated image served better measurement analysis in digital image processing [53]. Images captured from optical imaging were then processed in sequential order of segmentation and they are shown in Figure 3.11 for droplet image segmentation and Figure 3.12 for flame image segmentation

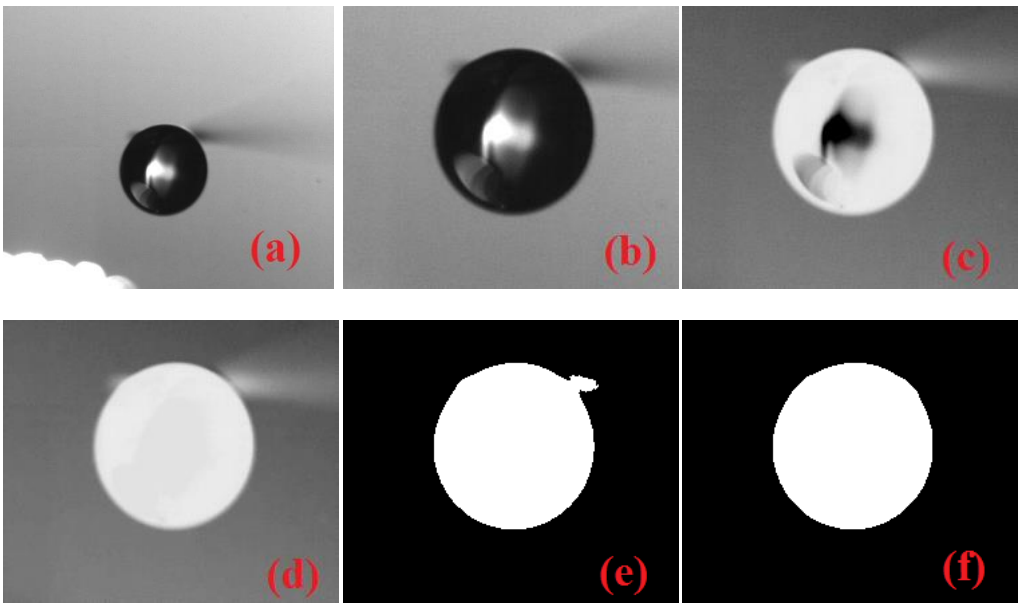

Figure 3.11 Digital Image Segmentation Processes on droplet image from (a) raw image, (b) cropped image, (c) complementation, (d) holes filling, (e) thresholding and (f) Noise filtering

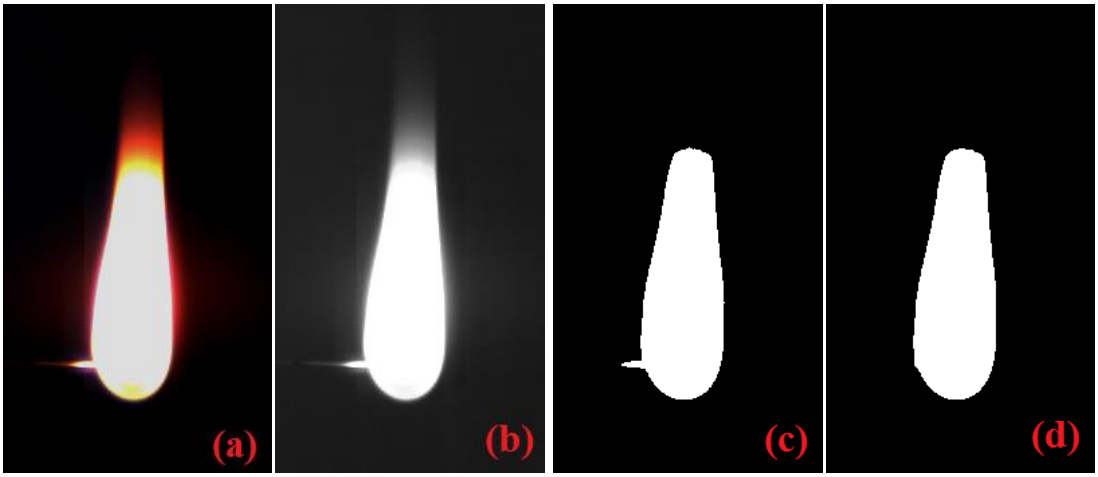

Figure 3.12 Digital Image Segmentation Processes on Droplet Flame from (a) Cropped image, (b) grayscale image, (c) thresholding and (d) noise filtering

The image was first cropped to isolate any unnecessary objects; in this case the image of the heating wire. For the morphological process later discussed in section 3.4.3, black and white images were needed to run the algorithm [54]. Droplet and flame segmentation processes were slightly different from each other due to the raw image types. Droplet images acquired by Phantom V210 camera were in grayscale whereas flame images from Photron-SA4 high speed colour camera were in red, green and blue format. In general, the result for segmentation processes were the same, which isolating the effective boundary of captured images in black and white format. This was done by a process of thresholding, which transformed the image into a white foreground and black background based on the specific value of thresholding. Pixel that has less value than the thresholding parameter was set in black background.

3.4.2 Actual Image Size Determination

To determine the actual size of the measured objects, a simple calibration was made on fixed magnification of the lenses. It was a crucial step in order to quantify the relationship of actual and image data which in general considered input and output data of measuring system [55]. This process was done based on the known actual size of the SiC fibre which is 100 μm. Figure 3.13 shows the actual size calibration method for this test.

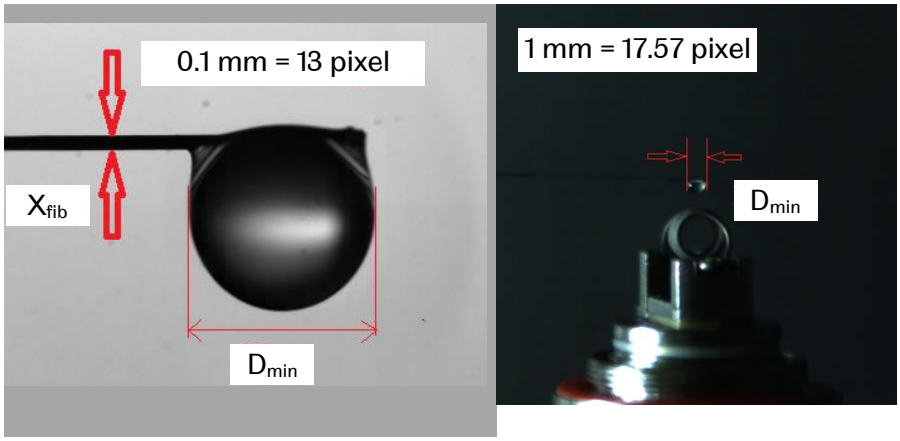

Figure 3.13 Image calibration parameters in (a) Nikon AF Micro Nikkor 60mm f/2.8D lens on droplet image and (b) Nikon AF Nikkor 50mm f/1.8D lens on flame image

The actual sizes of the droplet and flame formation were calibrated through two different magnification of lenses. The scales determination depicted in Figure 3.11 was acquired from using measurement tools in Photron Fastcam Viewer Software.

3.4.3 Feature Extraction

This step involved operations of Matlab algorithm run on segmented images. The main purpose is to extract the features from the images and convert them into a quantitative data for further analysis by transforming them into a presentable data. The process dealt with a morphological operation such as size, shape and quantity. Evaluation of the droplet diameter and flame length was then exported to excel in pixel values. With calibration parameters mentioned in Section 3.4.2, image coordinates in pixel were then converted into a measurable dimension; which in general expressed in mm.

In normal gravity, the shape of the suspended droplet is ellipsoid. The diameter measured by the feature extraction function in Matlab considers the minor and major diameter of the droplet. The equivalent volume is calculated from the product of squared minor diameter times major diameter. By assuming volume equivalence between ellipsoidal and spherical droplet, an equivalent spherical diameter D is calculated. The calculation of droplet diameter from the assumption of volume equivalence between ellipsoid and sphere was done by various researchers working on droplet combustion in normal gravity [77, 84, 107].

3.5 Combustion Phases

All analysis and discussions on combustion phases in this thesis will be referring to the diagram shown in Figure 3.14; taken from one regression of droplet squared diameter of burning diesel droplet processed in present work. Upon ignition, the droplet begins to swell and expand due to thermal expansion and denoted as Phase I. During this phase, the droplet undergoes droplet heating process with a gradual increase in temperature to its boiling point. Natural convection promotes internal circulation within the droplet, bringing the much higher temperature of liquid near the surface inward [50]. As a result, several high temperature spots exist within the droplet that initiates homogeneous nucleation of vapour bubble in small sizes. This bubble expands and escapes through the surface. These occurrences mildly distort the surface of the droplet and at the same time expands the diameter. The main characteristics of this phase are shown by the non-linear curve in the regression of D^2 which indicates the continuous process of both expansion and evaporation [4]. Hence, the measurement of droplet evaporation and the burning rate does not account the regression during this phase.

As soon as the droplet heating effect diminishes, the regression of D2 is shown to linearly reduce. According to Law and Sirignano [13], a high evaporation rate of the fairly large droplet (1 mm) would have a temperature gradient along the surface to the core of the droplet that varies with time. The unequal temperature across the droplet would initiate some puffing and mildly oscillates the droplet. During this phase, D2 reduces linearly with time and conforms with D^2-law [183]. During this period, it is theorised that the droplet surface is near its boiling point which in turn steadily evaporates the droplet. Hence, this phase is denoted as Phase II (boiling) and the measurement of evaporation and burning rate is made within the period of this phase.

Over time, the surface regressed disruptively as the droplet surface becomes more viscous resulted from fuel decomposition [1]. Also, some particle is observed to be trapped inside the droplet which in turn initiates heterogeneous nucleation of vapour bubble within the droplet. More bubbles try to escape through and upon the surface rupture, the liquid from the bottom of the bubble periphery pushed the liquid outside and ejects multiple sub-droplets. The sudden loss of liquid mass deviated the D^2 regression from D^2-law and the measurement of evaporation rate during this phase is unreliable [23, 152]. Disruptive burning causes the regression of D^2 during this phase to fluctuate and denoted as Phase III (disruptive)

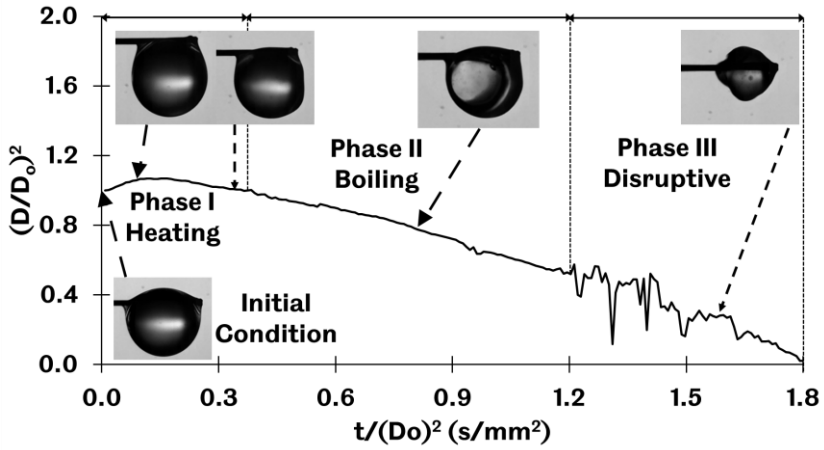

Fig. 3.14 Combustion phases throughout the lifetime of burning diesel droplet.

3.6 Experimental Challenges

Several challenges were faced throughout the entire scope of the present work. The first is to ensure the repeatability of the heating wire to exhibit constant temperature. The Kanthal wire would eventually oxidised after several use and decreases the temperature distribution around the droplet. A new coil of Kanthal need to be replaced after several use by ensuring the precise amount of resistance and coil structure. The temperature distribution needs to be check regularly to determine the condition of the coil for a new replacement.

Secondly, the dispersed droplet of ethanol and water has high tendency to separate even within the syringe. The mixtures need to be regularly stirred for each sample testing to ensure the homogeneity of the dispersed phase. It is found that without applying frequent stirring, the measurement repeatability was very poor.

Thirdly, similar separation conditions were observed during the suspension of soot particles. Without surfactant added to uniformly suspends the soot particles, the tendency of particle to agglomerate was high. Regular stirring was made to the mixture to ensure the soot particle to be evenly distributed within the diesel droplet in each sample. Also, the delay between soot quenching and the ignition of imaged droplet during SCD experiment varies with different density of contamination. Large amount of sample size was needed to analyse each respective contamination density so that a reliable conclusion can be drawn from the quantitative measurements.

Lastly, during the multi-droplet combustion, the dimension, orientation and position of each droplet in array need to be checked and manually adjusted to minimise the error

between them. It was observed that even with a slight difference in any of those parameters would deviate the results with poor repeatability. The SiC fibre was regularly replaced to ensure similar positioning of the droplets; preventing the imaged droplet to be out of the field of view.

Chapter 4

Evaporation Behaviour of Isolated Neat Fuel Droplet

4.1 Introduction

This chapter generally investigates the evaporation rate, flame formation and liquid-phase conditions of isolated fuel droplet subjected to elevated ambient temperature in pure evaporation and burning droplet. The results are then compared with the classical quasi-steady (QS) model for determining transient processes involved during droplet evaporation in detail. The focus mainly evolves around the theory of transient liquid-phase by analysing the droplet heating effect to the regression of squared droplet diameter, D^2 and the evaporation rates. Also, the effect of transient gas-phase by fuel vapour accumulation is demonstrated in detail by analysing the formation of flame during the combustion. Equation 2.3 to Equation 2.6 were used to calculate the evaporation characteristics and the sample calculation is shown in Appendix A.

Two type of fuel is selected to be tested due to their distinct evaporation characteristics. The first is a combustible fuel which is diesel; with high boiling point and sooting propensities. The second is a flammable fuel which is ethanol; with low boiling point and non-sooting fuel under atmospheric pressure [124]. Fuel with high flash and boiling point is expected to have a significant transient effect during droplet heating and fuel vapour accumulation period [72, 73, 81]. This would provide beneficial insight into the transient evaporation process of fuel droplet. Furthermore, the selection of both fuel for analysis and comparison is useful due to their practical use in fossil as well as renewable fuel operating engines.

Three types of droplet evaporating method are implemented in present work. The first is pure evaporation; by increasing the ambient temperature towards near ignition to evaluate the differences in evaporation behaviour between different ambient temperature. The second is by igniting the droplet with minimum ignition temperature to ensure diffusion-controlled evaporation of fuel droplet without external thermal influences. The third is by igniting the diesel droplet with a butane flame with butane lighter. Although the nature of this ignition method is unreliable, it was done to specifically elevate the droplet heating and fuel

vapour accumulation effect that can clearly demonstrate the transient effect which could be compared with diffusion-controlled evaporation and QS model.

4.2 Ambient Air Temperature Responses

Measurements were made on the air temperature 1 mm above the heating wire. An exposed type K thermocouple probe (nickel-chromium/nickel-alumel) with diameter of 0.315 mm was used to measure the ambient air temperature. For a real-time data collection and display, a thermocouple data logger TC-08 from Pico Technology paired with Picolog software was used. The temperatures value needed for the experiment were predetermined within the range of 250 °C to 400 °C by adjusting the wattage subjected to the atomiser of the thermal heating device. Fig. 4.1 shows the temperature responses of the ambient air 1 mm above the thermal wire upon initiation. The temperature increased to a steady state within 10 seconds with a slight fluctuation of $\pm$ 7 °C. The air temperature rose by the effect of thermal convection and radiation from the heated Kanthal wire. It has been taken into account that due to the effect of radiation, there are discrepancies between measured and actual air temperature 1 mm above the heating wire. The actual air temperature subjected to the surface of the droplet would differ from the reading of the thermocouple probe given their differences in emissivity under the effect of radiation. Nevertheless, this measurement was used as a reference point for the provisions of steady ambient temperature around the droplet with 50 °C increment during droplet evaporation experiments. The wire was heated outside the droplet area by up to 30 seconds to ensure the wire to have reached steady temperature before moving it 1 mm below the droplet centre. The wire position was kept in place during evaporation until the droplet was fully evaporated. The droplet evaporation tests were conducted within 250 °C to 350 °C as the suspended fuel droplet started to ignite when the temperature reading has reached 400 °C.

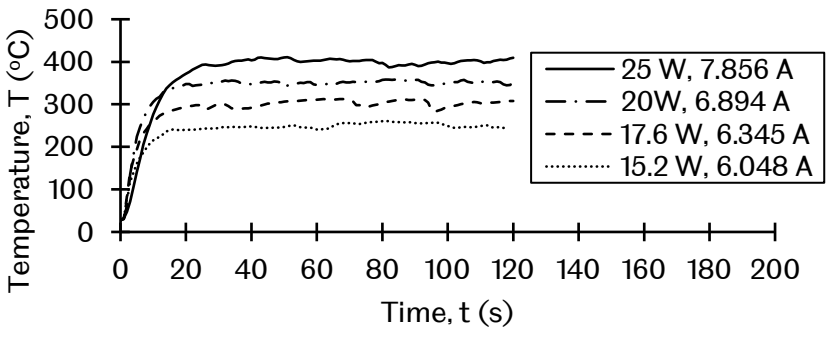

Fig. 4.1 Temperature response in an area of 1 mm above the thermal wire

For the droplet ignition part, the low ignition temperature of 400 °C was used to minimise the thermal effect from the Kanthal wire upon ignition. It is found that in the present work, all droplet started to ignite at this temperature thus selected to be used as the minimum ignition temperature. Excessive ignition temperature would shorten the lifetime of a burning droplet [6]. As soon as the droplet was ignited, the Kanthal wire positioned 1 mm below the centre of the droplet is removed. Droplet heating, steady evaporation and extinction were kept free from external thermal influence and the droplet evaporation during combustion was ensured to be affected only by the diffusion flame from the droplet. For both evaporation and burning tests, some errors in the measurement of droplet surface regression were considered for a short period of time during the initiation process; kanthal wire insertion in droplet evaporation and removal during ignition tests. The duration of evaporation and burning uncertainties during the early stages was short with the longest duration was determined to be 0.0907 seconds. Hence, no reliable visualisation and analysis such as bubble nucleation, surface distortion and evaporation rate are considered during this brief period.

4.3 Regressions of Squared Droplet Diameter, D^2

Quantitative measurements were made on the droplet surface regressions in each test and compared with the quasi-steady (QS) model. Fig. 4.2 shows an example of three repetitive measurements of droplet surface regression for diesel (Fig. 4.2-a) and ethanol (Fig. 4.2-b) in evaporation and burning processes. For experimental measurements, high repetitive measurements were achieved with slight discrepancies during initiation (evaporation) and ignition (burning) process due to the insertion processes. Droplet undergoes expansion during the heating period (PI) and transitioned to a steady reduction of squared droplet diameter (PII). In addition, a short duration of disruptive phase (PIII) towards the end of the droplet lifetime is shown in Fig. 4.2 (a) during droplet burning. As the ambient temperature increased, some surface distortions were observed especially in higher temperature exerted by diffusion flames. This is due to the occurrences of puffing caused by bubble rupture near the surface of the droplet [18]. For a fairly large droplet of 1 mm, temperature gradient exists across the droplet throughout the lifetime [13]. With internal circulation induced by natural convection, a liquid fuel that has reached to its boiling temperature would be circulated inside the droplet thus locally nucleates to a vapour bubble. In high ambient temperature,

more nucleation of vapour bubble appeared which in turn distorts the surface with higher frequency.

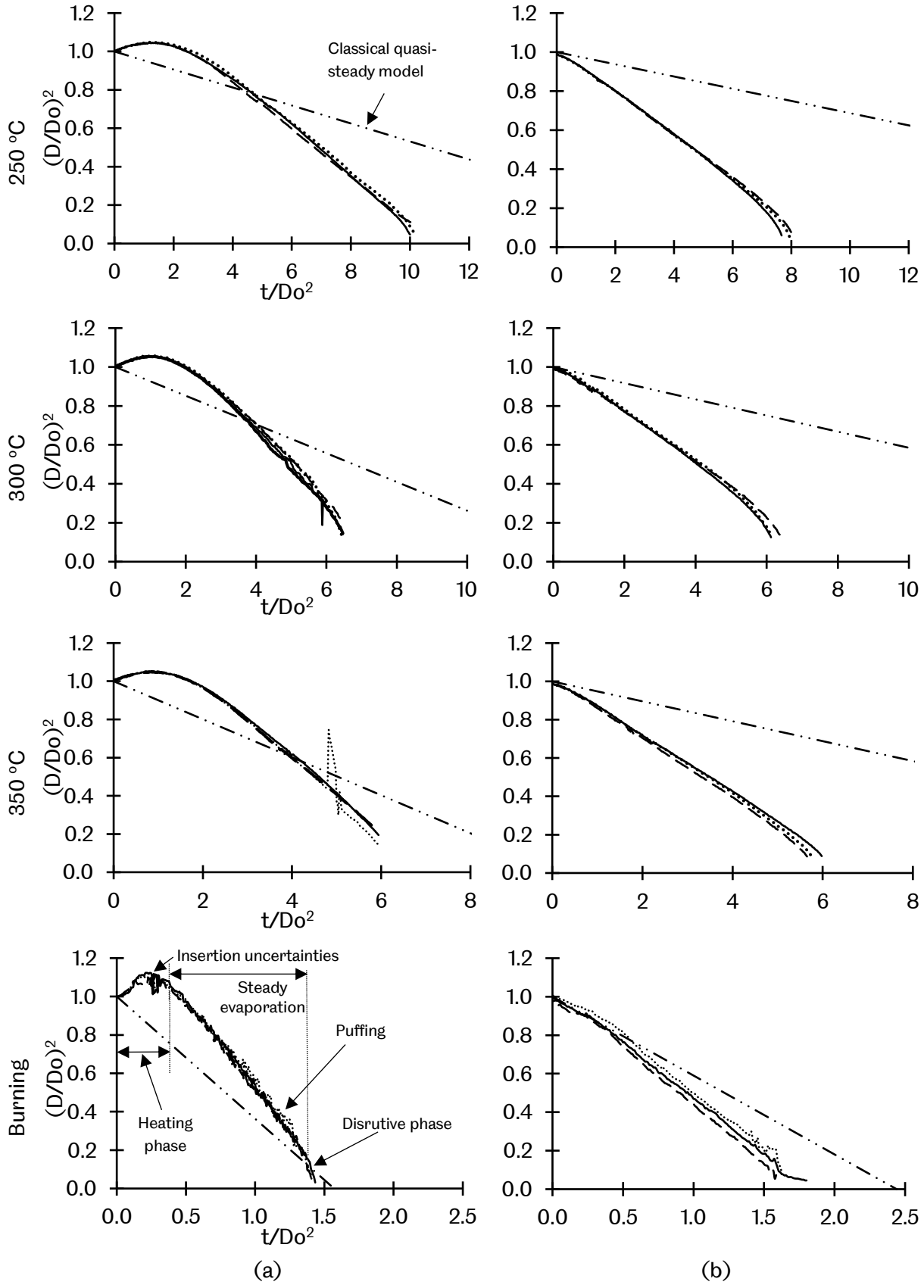

Fig. 4.2 Regression of squared droplet diameter in comparison with the classical quasi-steady model for (a) neat diesel and (b) neat ethanol

Significantly large differences between QS model and experimental results is shown in D^2 regressions. However, higher ambient temperature brought D^2 regression of QS model closer to the experimental measurements. Such discrepancies were based on several considerations that are absent in QS model. One of the reasons is due to the negligible effect of droplet heating in QS model [10, 11]. Higher ambient temperature shortened the droplet heating period thus brings the regression closer to the experimental measurement and such effect is shown in Fig. 4.2. Also, QS model neglects the effect of natural convection. Experiments were conducted in normal gravity which subjected to the effect of natural convection during droplet evaporation. Natural convection promotes internal circulation within the droplet thus enhances mass diffusion which in turn increases the evaporation rate [184]. This is evidenced by the steeper gradient of experimental D^2 regressions compared to the QS model in each case, indicating a higher evaporation rate of experimental results.

Fig. 4.3 shows the D^2 regressions of diesel droplet ignited by a butane flame. Five examples of the regressions are presented showing a low repetitive measurement of such ignition method. High butane flame temperature shortened the heating period (PI) but increased the duration of disruptive phase (PIII). The unburned butane gas supplied by the igniter mixes with the diesel fuel vapour surrounding the droplet and increases the total lifetime due to the addition of extra combustible gas on top of fuel vapour. Because of the inconsistencies in the mass of butane gas being released from the lighter, the effect varies between each repetitive measurement. Although it is possible to provide a consistent mass release of gas for high repetitive measurement, the gas accumulation effect is impossible to be eliminated. Distortions in the disruptive phase are more intense due to a higher occurrence of stronger puffing. Only one case of butane flame ignition is demonstrated in present work mainly to study the mechanism of droplet heating and fuel vapour accumulation effects despite of its unreliable evaporation rate and flame formations.

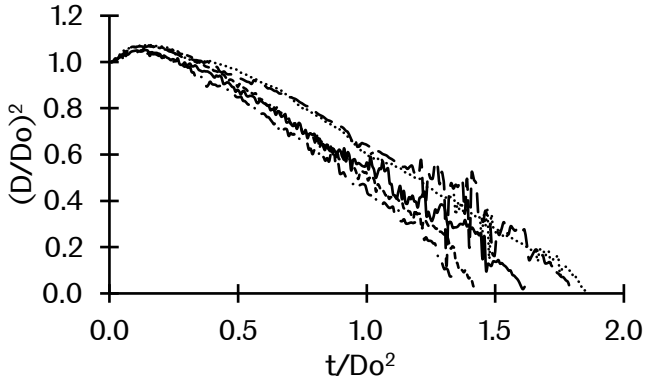

Fig. 4.3 D^2 regressions of diesel droplet ignition via butane flame

4.4 Evaporation Rate of Isolated Fuel Droplet

Quantitative measurements on the droplet evaporation rate were done during the steady evaporation phase (PII) with linear regression of D^2. During this phase, the droplet surface temperature is assumed to be near the boiling temperature of the fuel [79] with minimum disruptive evaporation and droplet heating effects [125]. Fig. 4.4 shows the evaporation rate of diesel and ethanol droplets subjected to elevated ambient temperature and diffusion flame. Diesel is found to have a higher evaporation rate compared to ethanol in each case. This can be explained by the higher temperature of diesel (170 °C) compared to ethanol (78 °C). When the surface of diesel droplet reaches the boiling point, higher heat is supplied to elevate the temperature of the liquid fuel inside the droplet, providing continuous evaporation process with a higher rate. Furthermore, diesel has lower heat of vaporisation (250 kJ/kg) compared to ethanol (840 kJ/kg) thus evaporates with higher rate. Such different in evaporation rate between diesel and ethanol satisfy the classical droplet combustion theory which states that the burning rate of fuel increases with an increase in flame temperature and a decrease in latent heat of vaporisation [77].

From the classical QS model, diesel flame temperature is calculated to be 1884.53 K and ethanol with 1484.66 K. It is mentioned by turns [79] that QS model underpredicts the flame temperature due to the absence of buoyancy and only taking into account that the fuel starts evaporating once the boiling temperature is reached. In actual condition, more fuel vapour is readily present around the droplet due to a lower flash point of fuel compared to its boiling temperature. Nevertheless, the approximation from QS proves that diesel flame provides higher heat transfer to the surface of the droplet thus increases the evaporation rate compared to ethanol. In the case of butane flame ignition, the evaporation rate measured to be less than thermal heating wire. This highlights the role of fuel vapour accumulation effect. Although the diesel droplet ignited with thermal heating wire undergoes fuel accumulation effect upon ignition, the effect is more profound in butane flame ignition. Combustion of accumulated vapor during heating process enlarges the flame formation [52]. Denser accumulation of fuel vapor with additional unburned butane gas pushes the flame front further away from the surface of the droplet. This in turn reduces the heat transfer from the hot combustion gas to the surface of the droplet thus reduces the evaporation rate [28, 59]. Once the accumulated butane gas completely consumed, the evaporation rate elevated with severe disruptive burning behaviour. Since the measurement of burning rate focuses on the

steady D^2 regression, the measured evaporation rate was done during the butane gas accumulation still present with lower evaporation rate.

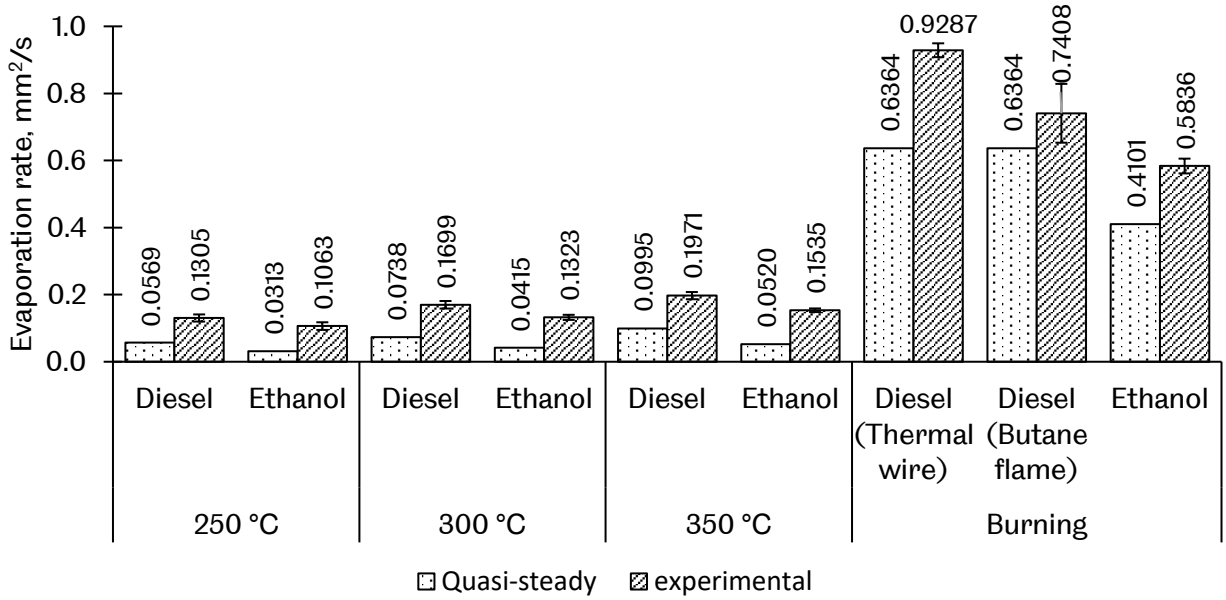

Fig. 4.4 Evaporation rate comparison between diesel and ethanol with their respective QS model

From the results obtained in the present work, classical QS model underpredicts the evaporation rate measured in the experimental study. The discrepancies between experimental and QS model prediction is shown in Fig. 4.5. For both cases, the differences are lower as the ambient temperature is increased. It is evidenced that the shorter duration of droplet heating reduces the deviated value, shown in Fig. 4.6. Butane flame provides high ignition temperature for the droplet with a rapid heating process thus shortened the duration of droplet heating. For combustible fuel such as diesel, the QS prediction is more accurate when the droplet heating duration is shortened. In the case of flammable fuel (flash point lower than 37.5 °C) such as ethanol, the calculation error is higher although the droplet heating duration is considerably lower than diesel. This is due to the other simplified consideration of classical QS model that assumes liquid fuel to only evaporates once the droplet temperature reaches its boiling point [79]. Ethanol has a weaker intermolecular force which is the hydrogen bond and easily evaporates even in room temperature. Given the very low flash point (16.60 °C), more ethanol liquid evaporates in actual condition compared to the underpredicted evaporation rate of classical QS model. Nevertheless, experimental results clearly show that the accuracy of QS model highly dependent on the droplet heating effect for fuel tested in the present study.

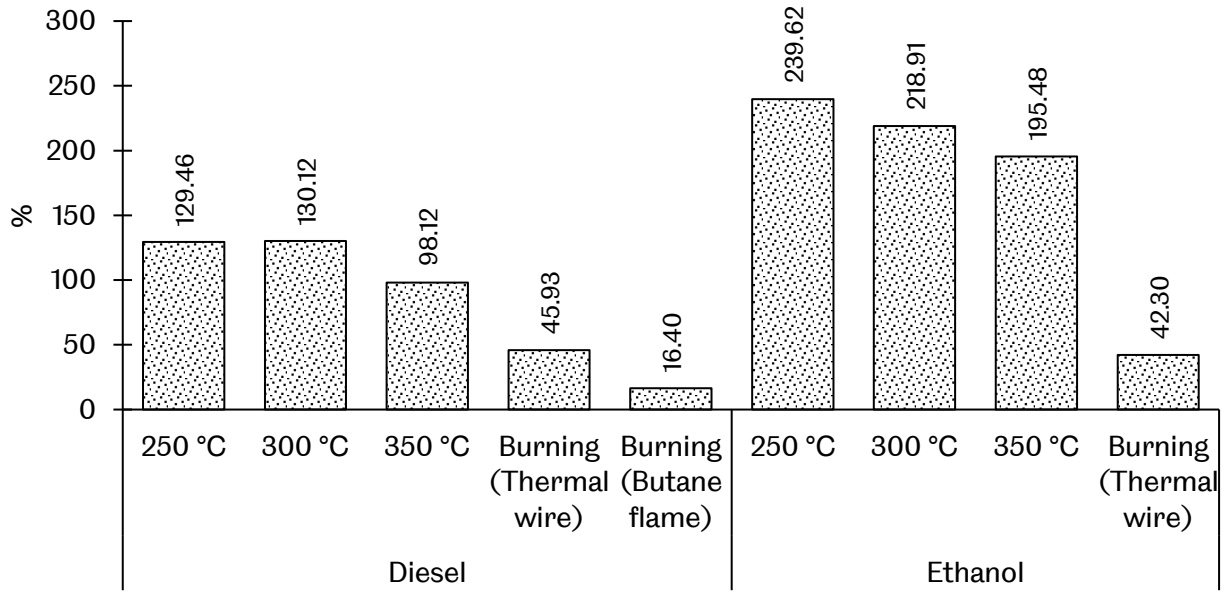

Fig. 4.5 Discrepancies of evaporation rate between experimental and QS model

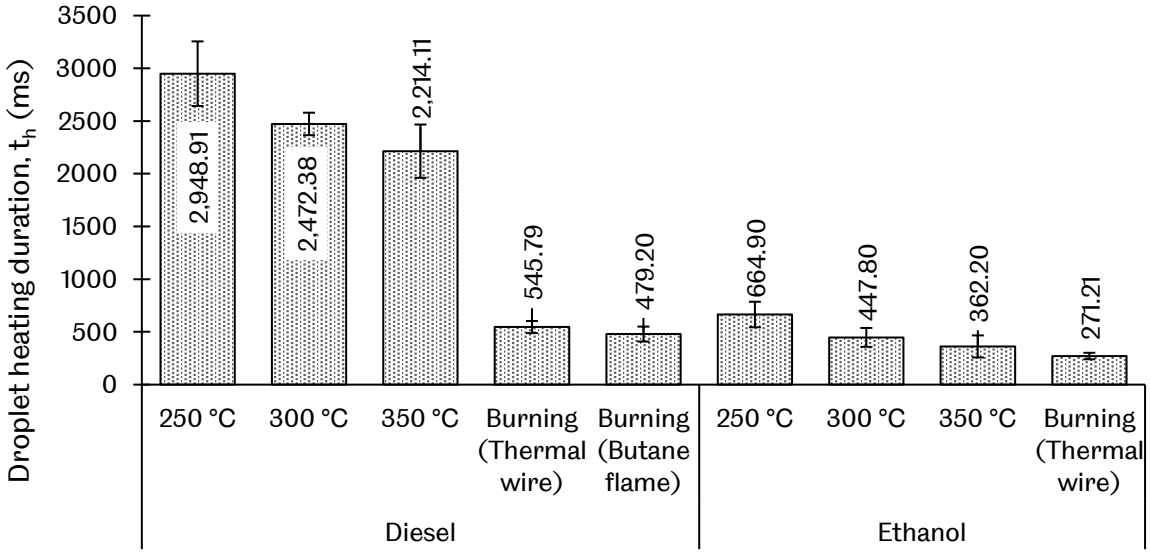

Fig. 4.6 Lifetime of droplet heating phase

Fig. 4.7 shows the instantaneous evaporation rate of burning diesel and ethanol droplet. The fluctuation of instantaneous evaporation rate during the heating phase of thermal wire-ignited diesel droplet shown in Fig. 4.7 (a) is more profound compared to others. However, once the droplet heating phase transitioned to a steady phase, the evaporation continues with steadier rate towards extinction. This provides a longer reliable measurement of steady evaporation rate since the evaporation is diffusion-controlled throughout its lifetime. In addition, it provides a more precise measurement of droplet evaporation rate without the interference of external influences; shown by high repetitive measurement in Fig. 4.2.

Instantaneous evaporation of diesel with butane flame ignition shown in Fig. 4.7 (b) has short droplet heating duration before transitioned to a steady evaporation rate. However, the transition to disruptive phase is earlier making the burning rate measurement unreliable for up to half of its lifetime. On the other hand, the instantaneous evaporation rate of ethanol shown in Fig. 4.7 (c) has a steadier distribution with obvious underprediction of QS model. Overall, the instantaneous evaporation rate of diesel lands closely to the classical QS prediction if the effect of droplet heating and fuel vapour accumulation are not taken into account [10, 11].

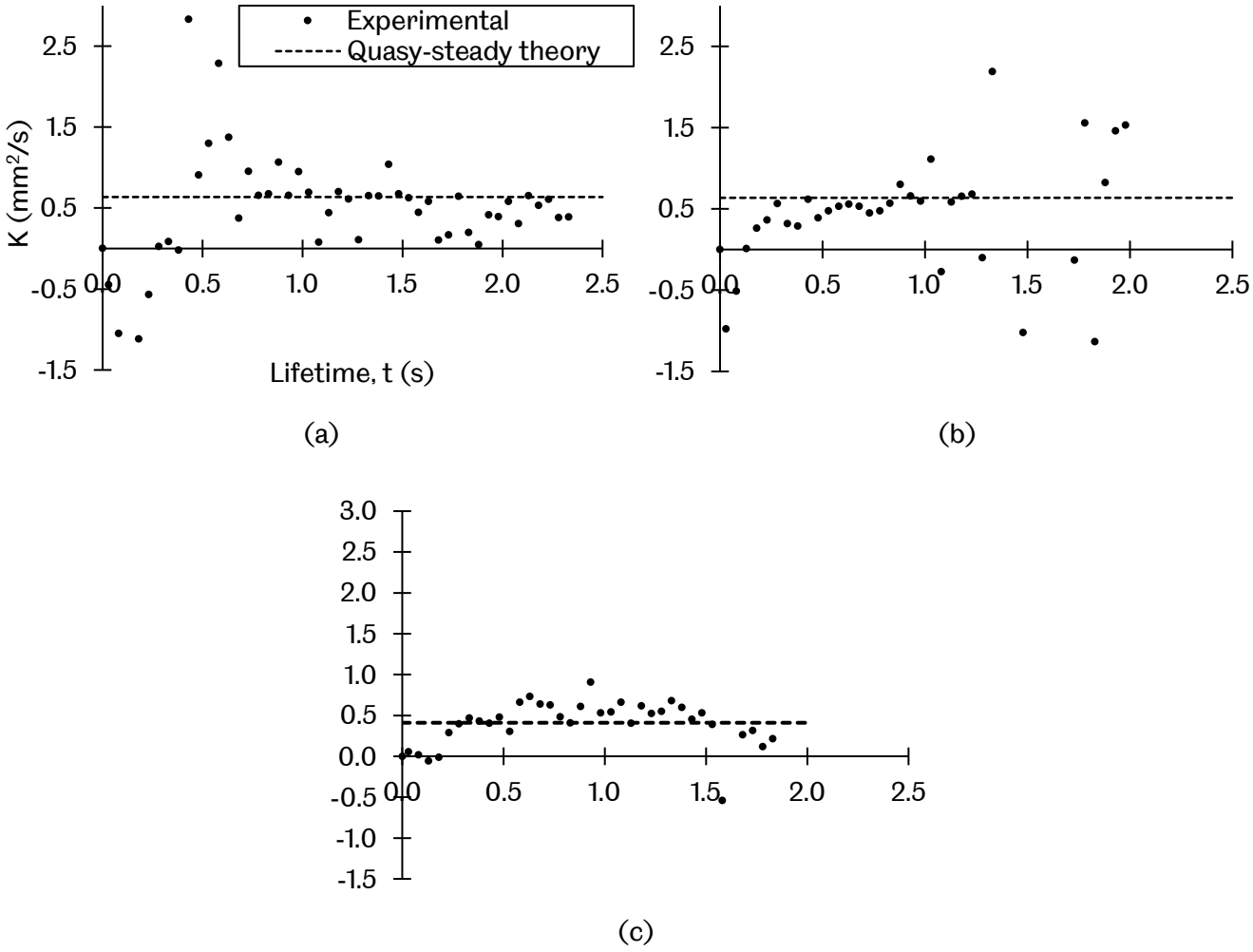

Fig. 4.7 Instantaneous evaporation rate of (a) diesel with thermal wire ignition, (b) diesel with butane flame ignition and (c) ethanol with thermal wire ignition

4.5 Flame Formation of Isolated Fuel Droplet Combustion

The length of flame that forms in the direction of buoyancy is measured and compared with the QS model for both thermal wire and butane flame ignition of diesel; shown in Fig. 4.8 (a)

and (b) respectively. In the present study, the flame formation of ethanol is not possible to be quantitatively measured due to unclear visible flame produced during ethanol combustion [77]. Upon ignition, QS model predicts larger flame formation with the assumption of negligible droplet heating effect [31]. The flame would form as if the droplet surface to have reached the boiling point upon ignition thus having a denser fuel vapour with a larger flame front. In actual observation, flame formation gradually enlarges upon ignition due to droplet heating; limiting the fuel evaporation [12].

The experimental measurement is in accordance to fuel vapour accumulation theory [88], showing considerably large flame front towards the end of the droplet lifetime. During the early combustion process, fuel vapour consumption rate (by the flame) is less than the evaporation, making the excess of unburned vapour to accumulate in the area between the droplet surface and the flame region [12]. This pushes the flame front further away from the droplet surface. Towards the end of the droplet lifetime, the vapour consumption rate is higher than the evaporation making the fuel stand-off ratio (FSR) increases towards infinity as shown in Fig. 4.9. QS model predicts constant FSR throughout droplet lifetime with steady evaporation rate and the flame shrinks in relation to the droplet diameter as the combustion progresses shown in Fig. 4.8 [32, 89].

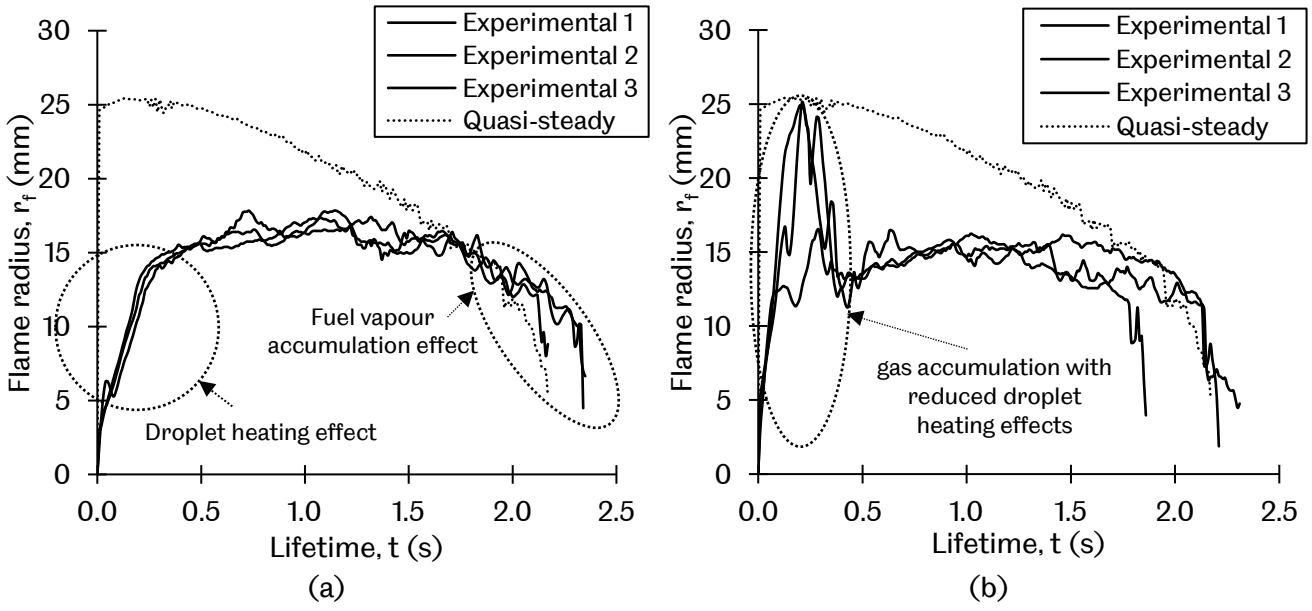

Fig. 4.8 Quantitative measurement of the flame length of (a) diesel with thermal wire ignition and (b) diesel with butane flame ignition

For diesel droplet with butane flame ignition, gas accumulated during ignition elevated the flame length briefly for 0.41 second before reduced sharply afterward. On top of

accumulated gas, the flame length is large due to the shortened droplet heating period, providing denser fuel vapour to be consumed by the flame. The sharp reduction in the flame length shown in Fig. 4.8 (b) indicates the transition phase of unburned butane gas and high droplet surface temperature spike upon ignition to a diffusion-controlled evaporation. The diesel vapour accumulation effect is still present a with shorter period due to the shorter time of diffusion-controlled evaporation. With both quantitative measurement done on the flame formation and droplet surface regression, it is evidenced that there is a trace of unburned butane gas accumulation upon ignition due to highly elevated flame formation without any drastic increase in the evaporation rate shown by D^2 regression in Fig. 4.3 and instantaneous evaporation rate in Fig. 4.7 (b). Overall, shown in Fig. 4.9, the FSR of both ignition methods is similar to each other during the diffusion-controlled evaporation period with slight differences towards the flame extinction.

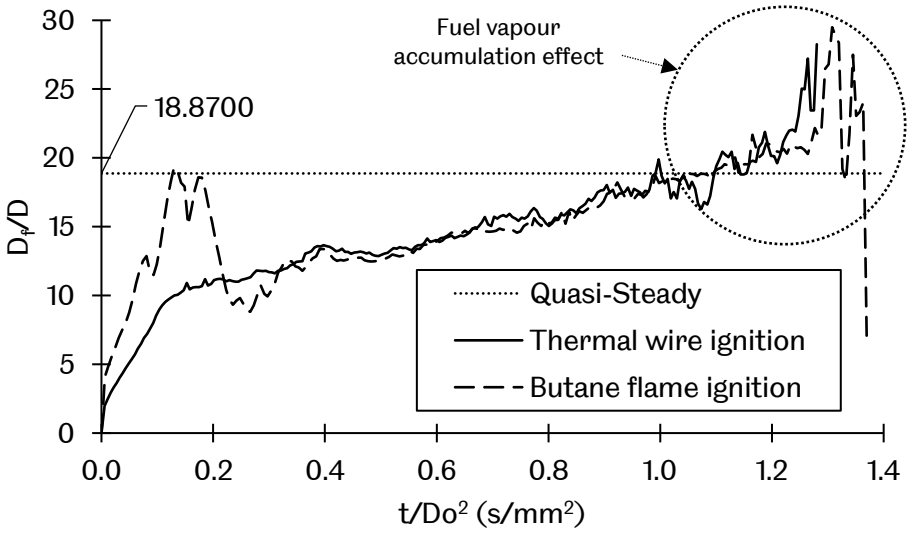

Fig. 4.9 Flame stand-off ratio of burning diesel droplet

4.6 Visualisation of Liquid-phase and Flame Formation

The effect of droplet heating and fuel vapour accumulation is further examined by the visualisation of liquid-phase and flame formation. Fig. 4.10 compares the droplet heating phase between thermal wire ignition (Fig. 4.10-a) and butane flame ignition (Fig. 4.10-b). During droplet heating period, thermal wire ignited diesel mildly distorted due to the slow heating effect and transitioned to a steady surface regression phase at 502 ms. During this period, droplet undergoes expansion under elevated temperature with a temperature

gradient along the surface to the core of the droplet. Because of the differences in local temperature throughout the droplet, the thermal expansion rate differs locally thus pushes the liquid surface at a different rate around the droplet [18]. Combining with droplet internal flows induced by buoyancy [50], the surface appears to be continuously distorted with the movement of bulged surface around the droplet. Distortion continuous until the droplet surface reached boiling temperature with a minimal temperature gradient across the droplet and proceeds to steady surface regression.

In Fig. 4.10 (a), the flame formation upon ignition is slightly blue in colour for a very short period of time due to well-mixed fuel vapour with the oxidiser prior to ignition [72]. The flame front continues to expand with orange-coloured diffusion flame to a steady flame length once the droplet heating effect has ended. The increase in flame length is linear during droplet heating, showing a complete fuel droplet diffusion-controlled evaporation and began to maintain in size once the steady evaporation phase is reached. The occurrence of small puffing slightly disrupted the flame shape throughout the steady evaporation phase due to the temperature gradient across the droplet that still exists [13] which locally elevated the temperature spot within the droplet with the help of internal circulation.

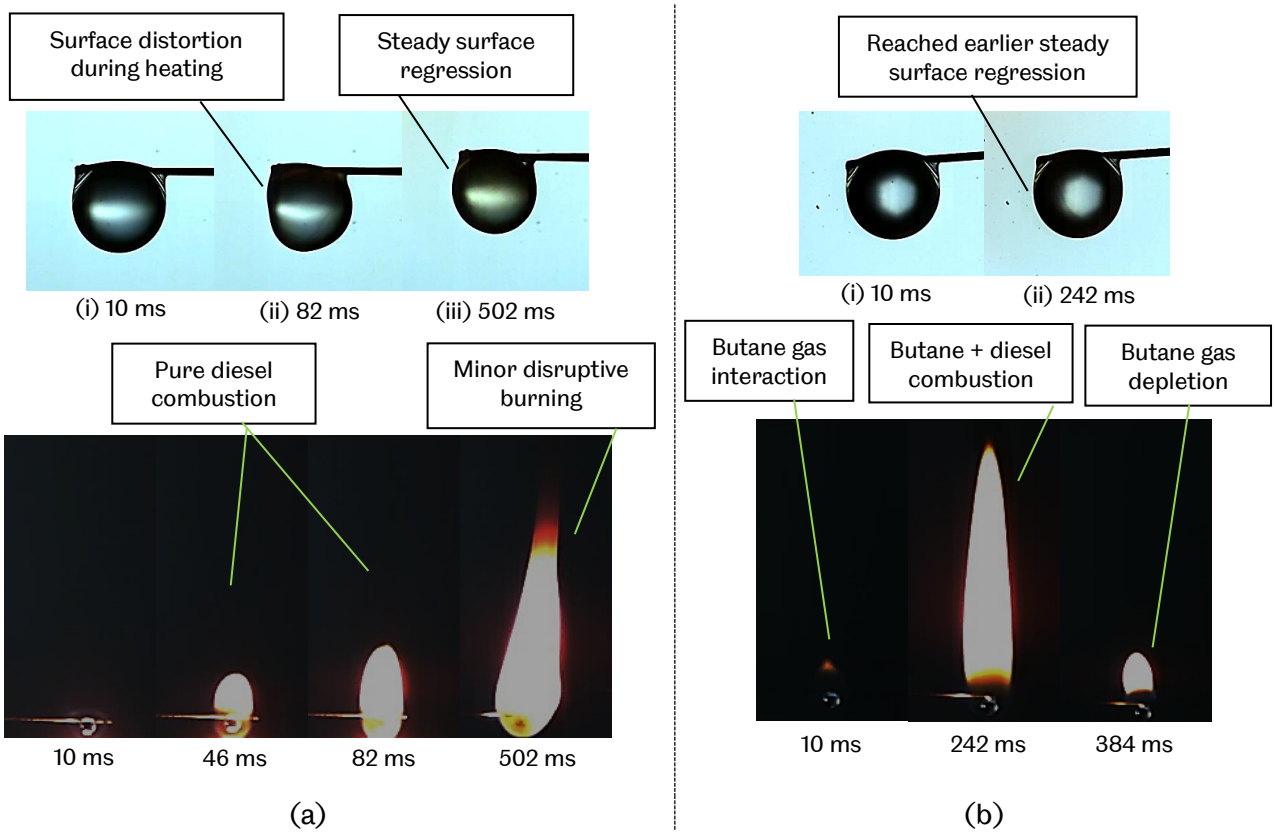

Fig. 4.10 Visualisation of diesel droplet liquid-phase and flame formation during droplet heating with (a) thermal wire ignition and (b) butane flame ignition

Diesel droplet ignited by the butane flame undergoes more rapid droplet heating process due to the higher ignition temperature exerted by the butane flame. Shortly upon ignition, the flame length increased significantly before sharply reduced to a smaller flame length shown in Fig. 4.10 (b) at 384 ms. The flame length then began to increase linearly before reaching a steady flame length similar to heating wire ignited droplet. The spike in flame length is the effect of the increased amount of volatile gas and vapour. This was attributed to the accumulation of unburned butane gas released by the butane lighter during ignition. Once the accumulated butane gas depleted, the flame length reduced to a smaller size and the combustion proceeds with diffusion-controlled evaporation of the diesel droplet. The onset of steady evaporation (PII) occurred during the combined consumption of butane gas and diesel fuel vapour and is shown by the droplet and flame formation at 242 ms in Fig. 4.10 (b).

Fig. 4.11 shows the disruptive phase of burning diesel droplet that further demonstrates self-contamination effect of diesel soot. Fig. 4.11 (a) shows typical puffing of diesel droplet and Fig. 4.11 (b) shows a typical process of sub-droplet ejection. In both cases, a trace of soot particles is observed to contaminate the droplet with butane flame ignited droplet having a higher concentration of contamination. The addition of butane gas around the droplet prolonged the droplet lifetime which in turn increases the residence time of fuel vapour. This in turn increases the sooting propensity [59] that would eventually pushes some of the combustion soot towards the surface of the droplet due to the thermophoretic force from the flame [28]. Fig. 4.11 (b) shows a darkened colour of the fuel droplet indicating the high amount of self-contamination.

The presence of soot particle on the droplet surface initiated heterogeneous bubble nucleation and eventually ruptured the surface as the mean of escape [97]. In the thermal heating wire ignition method, a smaller bubble nucleated inside the droplet and escaped through the surface by puffing. Puffing of fuel vapour occurred multiple times during steady and disruptive phase towards the end of droplet lifetime thus explains the fluctuation within the regression of D^2 shown in Fig. 4.2 and 4.3. On the other hand, a higher amount of soot presence in the droplet with butane flame ignition initiated multiple nucleation of the bubble in higher quantity compared to diesel droplet ignited with thermal heating wire. These bubbles tend to merge and forms a larger bubble that ruptured the surface with higher intensities, ejecting the vapour together with a smaller sized sub-droplet. Evaporation of ejected sub-droplets is then consumed by the flame, increasing the flame size due to the effect of gas-phase interaction between groups of burning fuel droplet. This explains the

fluctuation of flame size measured in Fig. 4.9 with butane flame ignited droplet having a higher magnitude of fluctuation in the regression of FSR. It is worth mentioning that the droplet ignited with thermal wire do ejects multiple sub-droplet during disruptive phase but was later in time with lower intensities compared to diesel droplet ignited with butane flame.

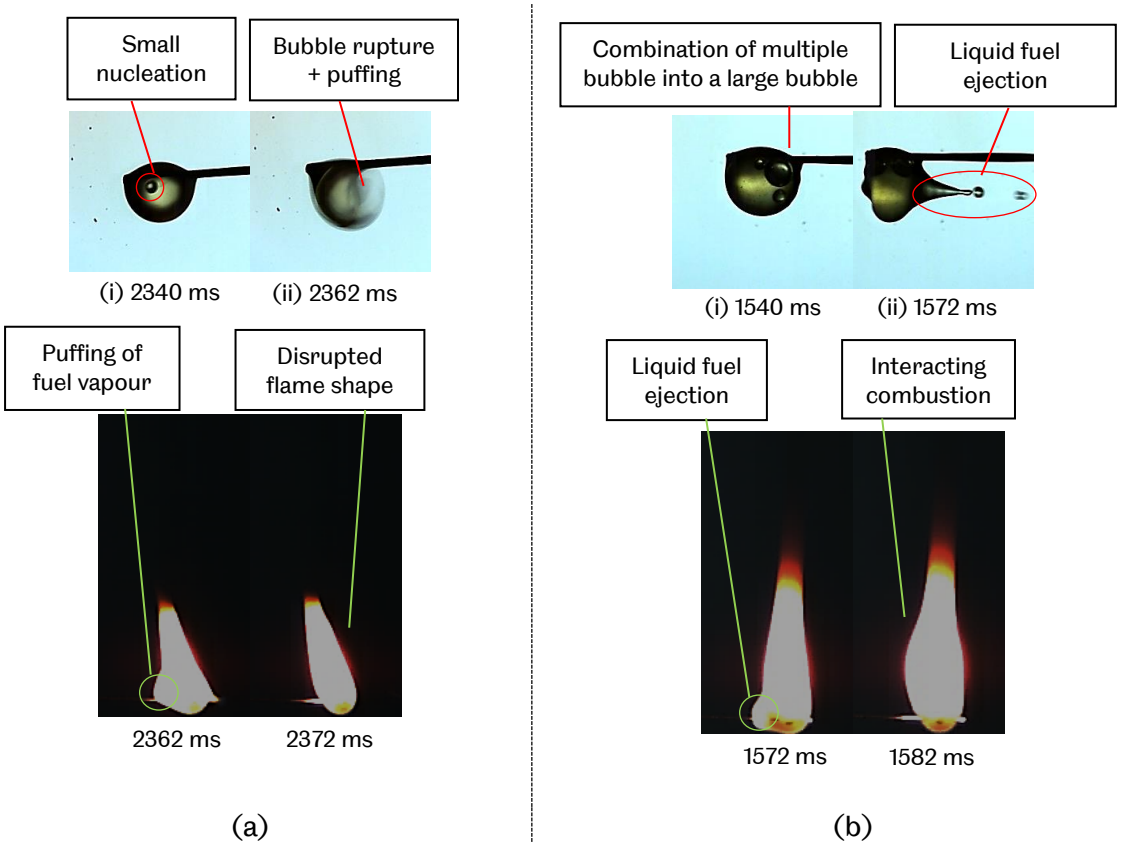

Fig. 4.11 Visualisation of diesel droplet liquid-phase and flame formation during typical (a) puffing and (b) sub-droplet ejection

The scattered measurements of instantaneous evaporation rate shown in Fig. 4.7 is well associated with the visualisation of liquid-phase and flame formation done in present work. The scattered instantaneous evaporation rate during early droplet lifetime in Fig. 4.7 (a) is due to the slow droplet heating process that distorts the droplet surface for a longer time before transitioned to a steady surface regression. On the other hand, scattering of instantaneous evaporation rate towards the end of droplet lifetime in Fig. 4.7 (b) is because of fuel vapour accumulation effects with a prolonged residence time of fuel vapour that would eventually contaminates the droplet with higher amount soot. This promotes multiple heterogeneous nucleation of vapour bubble to form and merge that would eventually ruptures the surface of the droplet with higher intensities.

4.7 Summary

The prediction of classical QS model is reliable to be applied on combustible fuel (diesel in the present study) when the periods of droplet heating and the effect of fuel vapour accumulation are minimum. This is clearly demonstrated by the reduction of discrepancies between the QS model and experimental results as the droplet heating duration reduces. Also, longer duration of steady droplet surface regression is produced for a reliable measurement of evaporation rate when the effect of fuel vapour accumulation reduces. Although flammable fuel (ethanol in present study) has minimum droplet heating and fuel vapour accumulation effects, the evaporation rates highly deviated from the QS prediction due to the tendency of ethanol to evaporate below its boiling point with a very low flash point; contradicting the model prediction that consider the evaporation of fuel starts when the droplet reaches its boiling point.

From the results presented in this chapter, the effects of transient liquid-phase combustion are determined by quantitatively measuring the droplet surface regression specifically during the early period of droplet lifetime. A longer period of unsteady surface regression indicates a higher effect of droplet heating thus further deviates the evaporation rate from the prediction of the classical QS model. On the other hand, the effects of transient gas-phase combustion are determined by quantitatively measuring the flame formation throughout the entire lifetime of the evaporating fuel droplet. The increasing trend of FSR towards infinity at the end of droplet lifetime indicates the effect of fuel vapour accumulation. With sufficient pieces of evidence demonstrated through quantitative measurement, liquid phase and flame visualisation, the transient behaviours of burning isolated neat fuel droplet are clearly explained in this chapter.

Chapter 5

Evaporation and Burning of Emulsion Fuel Droplet

5.1 Introduction

This chapter investigates the evaporation and combustion behaviour of emulsion fuel droplet. Tests were done on various conditions of emulsion fuel including water-in-diesel (WD), ethanol-in-diesel (ED), diesel-in-water (DW), diesel-in-ethanol (DE), diesel-water (WDns) and diesel-ethanol (EDns) mixture without any surfactant added. Analyses were done by quantitatively measuring the evolution of droplet diameter and flame formation. In addition, visualisations on the liquid-phase were done to observe their dynamic changes during evaporation process. The ambient temperature was varied from 423 K to a diffusion-controlled flame temperature in order to evaluate their respective changes.

The experimental tests were designed to clearly evaluate their differences in mixture stability, combustion behaviour, disruptive effect, phase separation process and their tendency to microexplode. Results obtained from this chapter would provide a new and clear insight on the evaporation behaviour of an emulsion fuel in normal atmospheric pressure and ambient condition. Water and ethanol are selected to be studied due to their common use in actual combustor. Comparisons are made to provide a clear description of disruptive mechanisms during the burning of water and ethanol emulsion. With the results provided in the present work, such behaviour could be expected at the basic level upon fuel selection between combustible (ethanol) and incombustible (water) as alternative source of component with low boiling point in emulsion fuels.

5.2 Combustion Characteristics of Water-in-oil Emulsion

The initial condition of emulsion droplet of ethanol-in-diesel (ED) and water-in-diesel (WD) is shown in Fig. 5.1. Pressure applied to the emulsion during droplet generation via syringe slightly aggregated the dispersed additives within the droplet. Furthermore, ethanol tends to diffuse towards the surface of the droplet upon suspension due to its tendency to evaporate

at room temperature. Due to their fast-diffusive properties, the translation of heating wire below the droplet was initiated as soon as the droplet was suspended to minimise the aggregation of dispersed phase and early evaporation of additives. It is observed that with any pressure applied to the emulsion in order to generate the droplet would slightly aggregates the liquid in dispersed phase. With high magnification and clear visualisation made in the present work; such condition is observed. The WD emulsion appeared to be opaque after the mixing process with milky white in colour. Therefore, internal visualisation of the droplet was not possible within half of their lifetime.

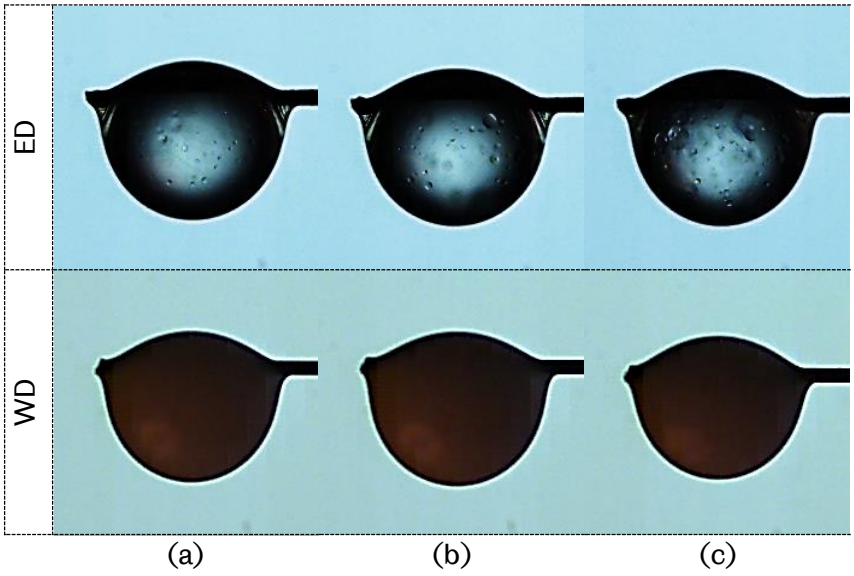

Fig. 5.1 Initial visualisation on emulsion droplet liquid-phase of ethanol-in-diesel and water-in-diesel in (a) 10% additive, (b) 20% additive and (c) 30% additive

5.2.1 Regression of Squared Droplet Diameter, D^2

Fig. 5.2 shows the measurements on D^2 regression of ED and WD emulsion in three additive volume composition with three elevated ambient temperature from 250 °C to diffusion-flame controlled temperature. In both ethanol and water emulsion, the dispersed liquid of additives diffused towards the surface of the droplet during the early lifetime of the evaporating droplet due to their lower boiling point which have the tendency to evaporate first. The evaporation follows the characteristics of batch distillation, where the evaporation proceeds with a preferential evaporation [76]. The component with a lower boiling point would evaporate first and followed by the evaporation of less volatile component [3, 7, 19]; which is diesel for both case in the present work. The preferential evaporation behaviours are clearly shown by each regression in Fig. 5.2, with high disruptive burning and steeper surface

regression upon ignition and began to decline to a steadier surface regression towards the end of droplet lifetime.

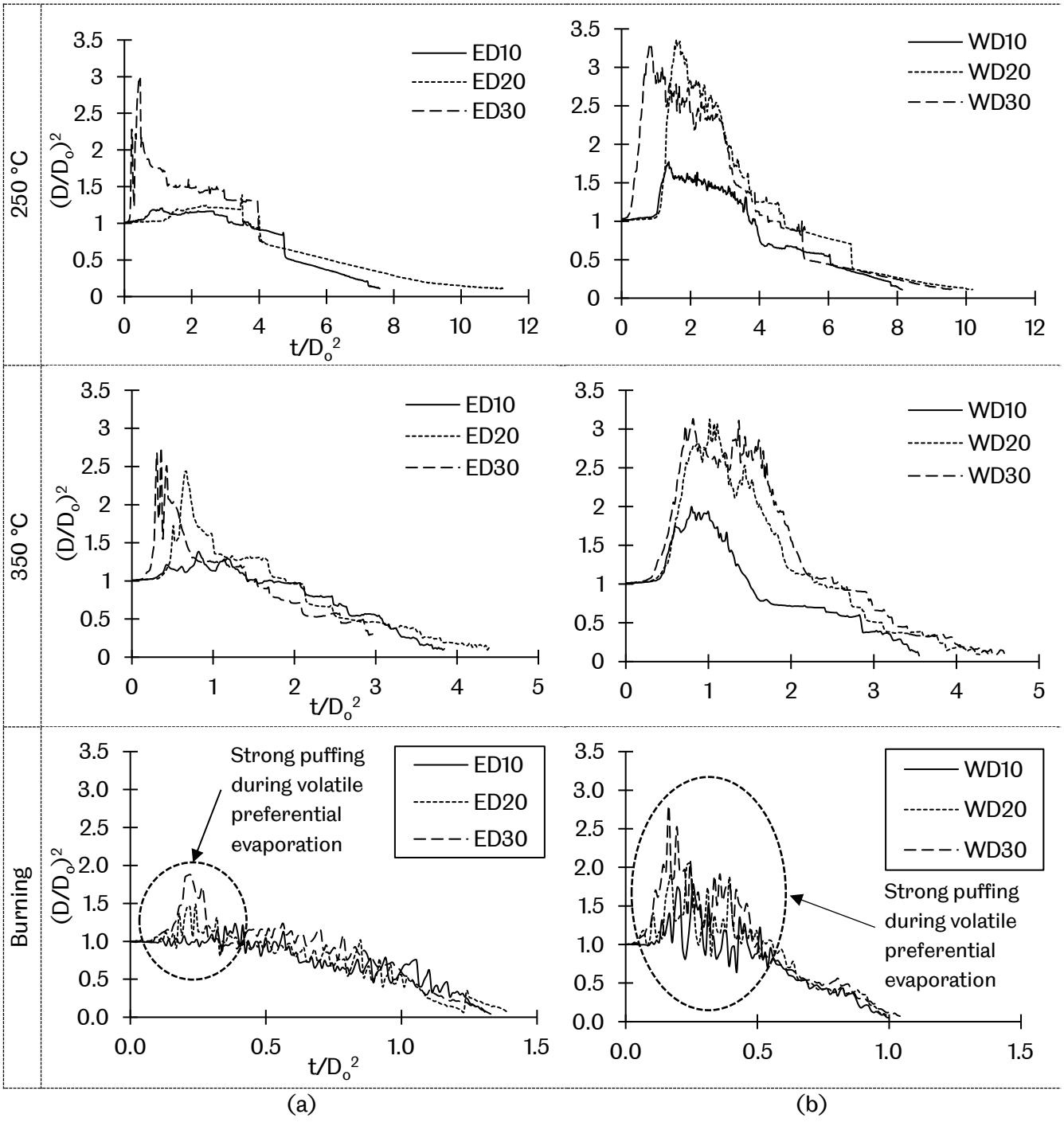

Fig. 5.2 D^2 regressions of emulsion droplet subjected to 250 °C, 350 °C and diffusion flame for (a) Ethanol-in-diesel and (b) water-in-diesel

The volatile evaporation phase is not necessarily longer when the composition of lower boiling point component is higher in volume. This is due to the occurrences of more rapid puffing and sub-droplet ejection during volatile evaporation phase. However, emulsion with

high ethanol and water additive shows high peak in D^2 regression. With high content of a more volatile component, more bubble nucleation had merged to form a larger bubble shortly before rupturing the surface of the droplet [36]. This in turn expanded the droplet to a larger size. Puffing from a larger bubble produced stronger pushing force upon surface rupture, ejecting higher volume of sub-droplet outward. Under these reasons, the composition of more volatile component depleted with similarly short amount of time regardless of their high initial volume in emulsion composition. Results obtained from the present work shows the duration of preferential evaporation in emulsion fuel is more temperature rather than volumetric dependant. The volatile component tends to evaporate in rapid manner as soon as the droplet temperature has reached its boiling point, diffusing most of its component to be released outward [129]. Volatile component that is readily dispersed near the droplet surface evaporates to a vapour phase with minimum distortion of the droplet surface whilst volatile component that is dispersed within the droplet nucleated to a bubble of vapour and ruptured the surface of the droplet as a means of escaping; highly distorting the surface [10, 126].

Slow evaporation process has impact on the droplet expansion. In lower ambient temperature, the disruptive surface regression occupies shorter portion of its lifetime and began to proceed with steady evaporation earlier. With lower ambient temperature around the droplet, the nucleated bubble expanded with longer time available for the bubble to merge into a larger bubble before being superheated and rupturing the droplet surface. With a slow increase in the droplet temperature and steadier temperature gradient across the droplet, more volatile component nucleated into a bubble and released via strong puffing less frequently during the early lifetime of droplet evaporation. Measurement of the dimensionless D^2 shows that the droplet expansion is larger in lower ambient temperature with a peak of 2.97 for ED and 3.3 for WD in 250 °C relative ambient temperature. The lifetime portion of disruptive surface regressions are longer during droplet burning, indicating continuous release of nucleated vapour throughout the droplet lifetime. Buoyancy induces internal flow within the droplet, transporting the liquid from the high surface temperature toward the centre of the droplet [76]. Because of the rapid heating, several high temperature spots are present inside the droplet and nucleates the volatile component around it locally. As a result, the vapour bubbles continuously emerged in different spot within the droplet until the volatile component nearly depleted [129] which in turn stabilised the droplet surface. Under these circumstances, high combustion temperature is preferable for emulsion fuel to enhance mixing due to their prolonged disruptive behaviour.

5.2.2 Evaporation and Burning Rate of Water-in-oil Emulsion Fuel Droplet

Average evaporation and burning rate constants of water-in-oil emulsion droplet subjected to elevated ambient temperature were measured and shown in Fig. 5.3. Measurement of the average evaporation rate considers the average from the scattering measurements of droplet squared diameter that includes heating phase, steady evaporation and disruptive phase. As demonstrated in Fig. 5.2, the droplet surface regressed disruptively throughout the entire droplet lifetime, making the precise measurement of steady evaporation phase impossible to be determined [66]. Nevertheless, the measurement of average evaporation rate serves as a relative measurement for a burning rate constant that fulfils D^2-law and would provide a meaningful insight to the evaporation behaviours of an emulsion fuel droplet.

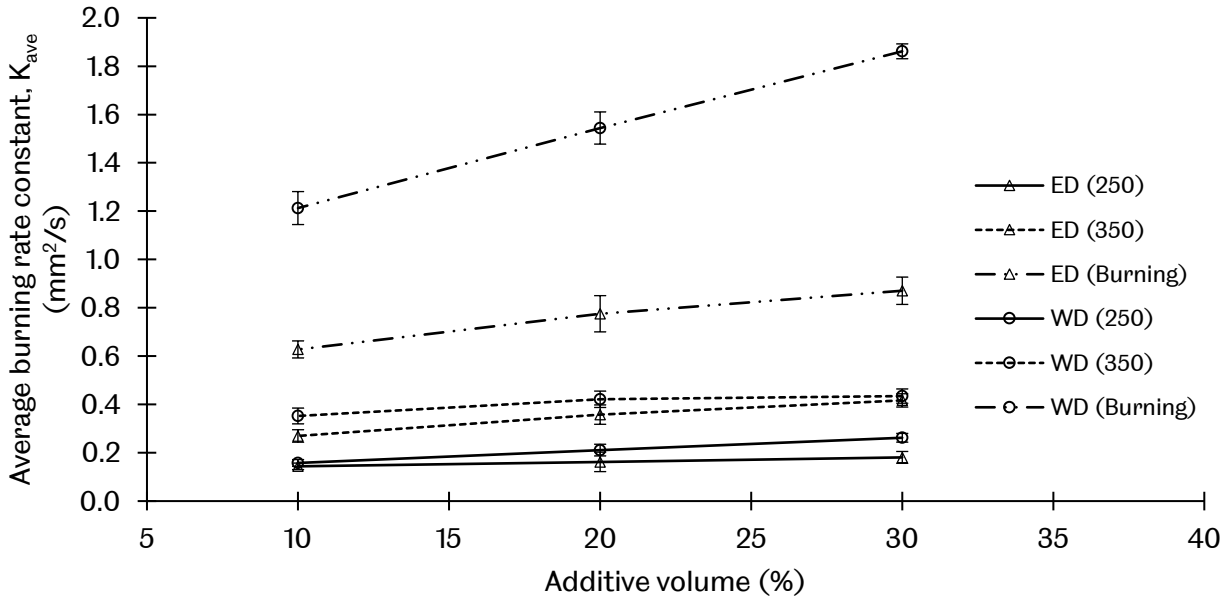

Fig. 5.3 Average evaporation and burning rate constant of water-in-oil emulsion droplet

In the evaporation mode, both emulsion fuels evaporated in similar fashion with little differences in the value of evaporation rate. The increase of additives slightly increased the evaporation rate for both emulsions due to the lowering of the droplet's boiling point. Evaporation rate of ethanol is more sensitive to temperature increase compared to water emulsion [35]. Shown in Fig. 5.4, the increase of evaporation rates from 250 °C to 350 °C

heating is high with 87.35%, 120.46% and 130.66% for ED10, ED20 and ED30 respectively. For water emulsion, the increase of evaporation rate when the ambient temperature was increased by 100 °C is 12.33%, 9.97% and 10.31% for WD10, WD20 and WD30 respectively. Such differences are due to the lower boiling (78 °C) and flash point (16.6 °C) of ethanol compared to water, making ethanol emulsion to be more sensitive to the temperature increase thus evaporates more rapidly. By analysing the fluctuation pattern of D^2, it shows that the ethanol tends to diffuse towards the surface of the droplet whilst water tend to be dispersed inside the droplet, diffusing slowly towards the surface. Major mechanics of preferential evaporation in water emulsion are through puffing shown by a more violent distortion of the surface regression shown in Fig. 5.2 (b). This explains the unchanged value of the evaporation rate increment between different water loadings as the ambient temperature was increased for water emulsion. The water trapped inside the droplet nucleated into vapour bubbles and released a strong puffing when the temperature exceeded its boiling point [104] rather than steadily evaporated on the surface like the ethanol, making the average evaporation rate remains unchanged.

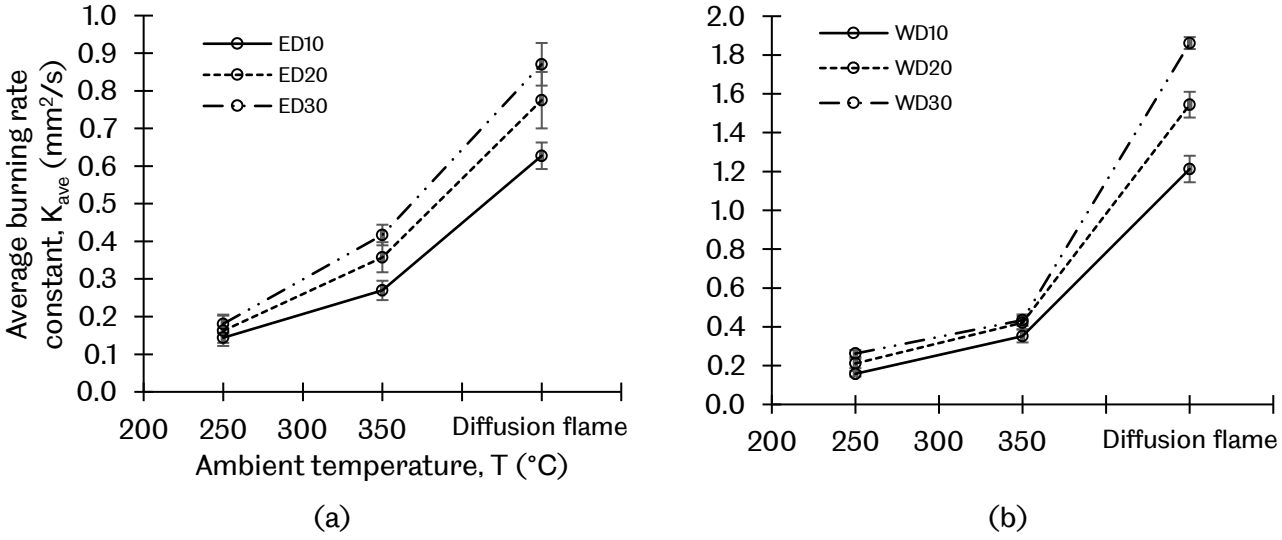

Fig. 5.4 Average burning rate comparison of increased additive loading and ambient temperature between (a) ED and (b) WD

In the burning mode, water emulsion has a higher burning rate increase when the water volume is increased. During combustion, water emulsion ejected a high amount of sub-droplet as it burns; different from low temperature evaporation mode which only involved puffing. Although both ethanol and water emulsion undergo several sub-droplet ejections during combustion, water emulsion has a higher ejection rate together with a larger-sized

sub-droplet. Because of a higher volumetric loss of the water emulsion through sub-droplet ejections, the measurement of average burning rate appeared to be higher than the ethanol emulsion. Droplet with a higher volume of water undergoes stronger and more frequent ejection of sub-droplet resulting increased value of the burning rate [36].

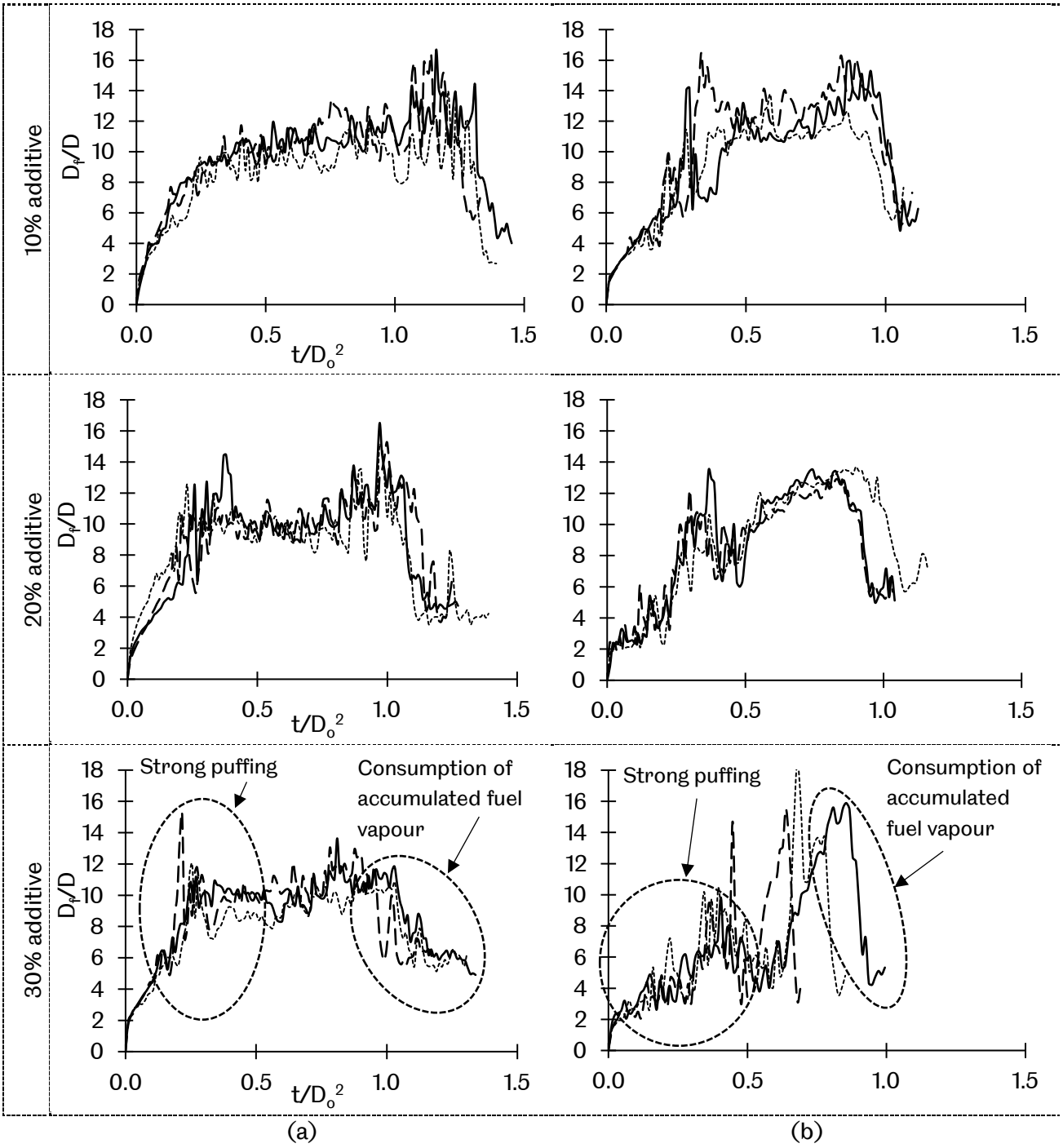

Fig. 5.5 Flame stand-off ratio of burning droplet with various volumetric loading of (a) ethanol emulsion and (b) water emulsion

5.2.3 Flame formation of Water-in-Oil Emulsion Fuel Droplet

Fig. 5 5 show the repetitive measurements on the flame stand-off ratio of the ethanol and water emulsion in 10%, 20% and 30% volumetric loadings of additive. Results shows high repeatability of the FSR measurement despite of high disruptive burning of both fuels. In both cases, the FSR continues to increase upon ignition to a peak before sharply reduced towards the end of the droplet lifetime. This indicates that the effect of the fuel vapour accumulation is still present [32, 88, 89] because diesel is used as the base fuel. However, the evaporated vapour is consumed by the flame earlier compared to the neat diesel shown in Fig. 5.6. The rate of vapour consumption is higher in smaller formation of flame [32]. The flame area of the burning emulsion fuel was smaller than the flame of the burning neat fuel, making the rate of vapour consumption higher. Also, high volatility of emulsion fuel restricts the amount of vapour to be accumulated due to a faster vapour consumption rate [81]. This is demonstrated by the regression of the FSR in Fig. 5.6. When the additive volume is low (10%), the effect of fuel vapour accumulation lasted longer in both case of ethanol and water emulsion. The decline in the FSR were earlier as the additive loading were higher.

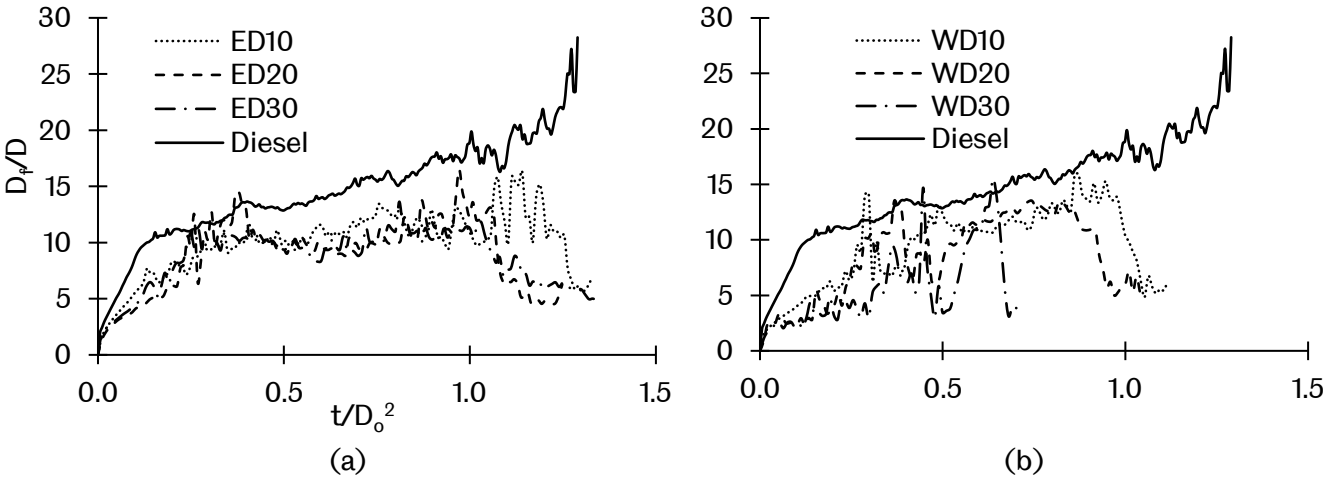

Fig. 5.6 Comparison of flame stand-off ratio between neat diesel and emulsion fuel droplet (a) ED and (b) WD

The FSR of the water emulsion climbed slowly during the early stage of the combustion and the rate of increase is even slower in higher additive loadings. On the other hand, the FSR of the ethanol emulsion regressed in the opposite manner as the additive loadings were increased. These differences are shown by the formation of flame in Fig. 5.7. For both emulsion fuels, the occurrences of puffing and sub-droplet ejection disrupted the flame

shape, especially during the early lifetime of the droplet. During this phase, most of ethanol and water evaporated first in a preferential evaporation either by gas diffusion or puffing shown by the fluctuation of D^2 during the early phase of combustion in Fig. 5.2. Ejection of sub-droplet and puffing effects the formation of flame during this period, with the ethanol emulsion flame grew larger in a stronger puffing whilst water emulsion flame shrunk in a stronger puffing. The ejection of the ethanol-diesel fuel vapour and sub-droplet enlarged the flame due to the sudden burst of additional fuel vapour, with ethanol as a flammable fuel. On the other hand, a burst of water vapour from the water emulsion partly extinguished the flame due to the incombustible properties of water [35]. Under these reasons, the flame enlarged as the ethanol loadings were higher which provided more easily consumed vapour due to its lower flash point whilst the evaporation of higher loading of water cooled the temperature surrounding the droplet thus shrinking the flame size.

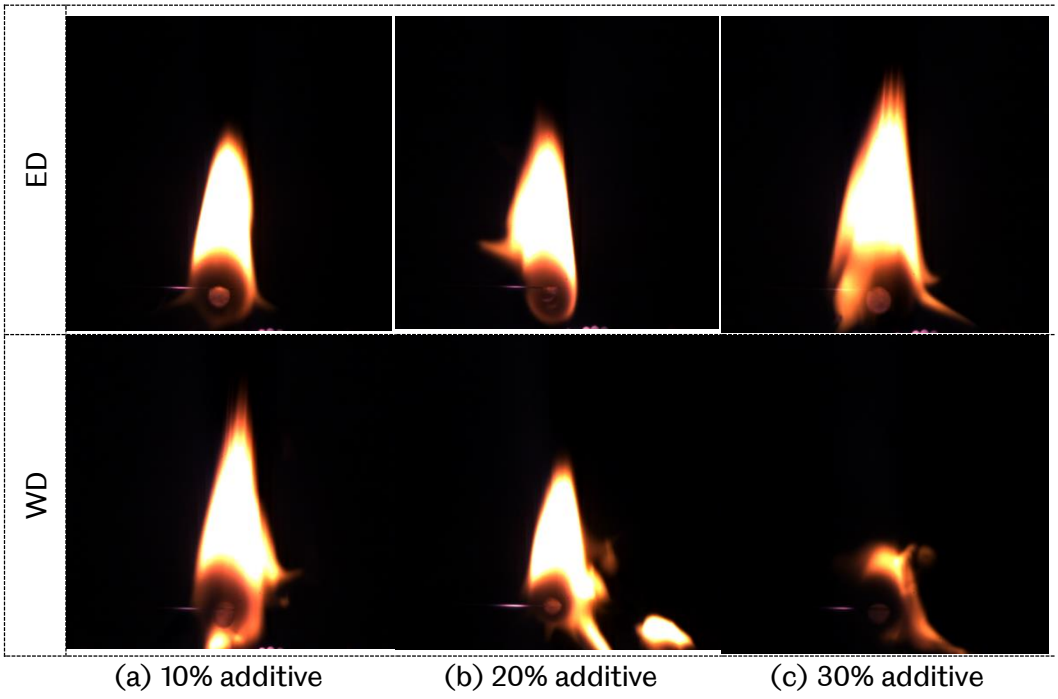

Fig. 5.7 Flame formation during preferential evaporation of volatile fuel component

5.2.4 Liquid-phase Visualisation on Water-in-oil Emulsion Fuel Droplet

Liquid-phase visualisations were done to examine the disruptive behaviours of the emulsion fuel droplet during combustion. With high temporal (20 000 frame per second) and spatial (130 pixel/mm) resolution, the mechanics of puffing, bubble breakup and sub-droplet ejections were observed and quantitatively measured. Fig. 5.8 shows typical puffing and sub-droplet ejection mechanics during the disruptive evaporation of the emulsion fuel (both

ethanol and water emulsion) which includes bubble breakups that leads to a recoiling motion, pinching of protruded liquid ligaments, repelling motion and ligament breakup. During the preferential evaporation, the droplet surface is heated to the boiling point of less volatile component; which is diesel in present study. This elevates the temperature exerted to the more volatile component inside the droplet beyond its boiling point [10, 126]. The volatile component evaporated into a vapour by the means of homogeneous nucleation inside the droplet and forms a vapour bubble that expands and merges with each other by time [7]. This process repeatedly occurred during the preferential evaporation and began to reduce in frequency and magnitude when the volatile component in the droplet is almost fully evaporated. Phase transition from the preferential evaporation of volatile component to less-volatile component can be approximated by examining the D^2 regression of the burning emulsion droplet shown in Fig. 5.2 with ethanol lasted by 0.36 and water by 0.52 of normalised droplet lifetime t/D_o^2.

Referring to the first row of Fig. 5.8, vapour is released through the rupturing of droplet surface once the pressure inside the bubble is higher than the surface tension of the droplet [66]. Release of vapour through the droplet surface created a low-pressure spot that pulls liquid towards the region. The internal pressure and velocity of the flowing fluid rushes toward this spot thus pushing the ruptured surface outward [126]. In the present study, this process which is also known as *recoiling* is visually confirmed by monitoring the movement of the unmerged vapour bubble. Once the larger bubble ruptured the surface of the droplet, the unmerged smaller bubble moved towards the periphery of the ruptured hole indicating a flow of the liquid to the bottom hole of the rupture. Shortly afterwards, the ruptured hole closes and the flowing liquid pushes the bottom part outwards and protrudes a ligament from the ruptured surface [130]. The strength of the push depends on the bubble size formed shortly before the surface rupture. Breakup of a larger bubble packed a stronger push of flowing liquid and protruded longer ligaments outward. Two parameters determined the shape and stability of the ligament evolution. Viscosity stabilised the evolution while surface tension inhibits the stretching of ligament and at the same time reduce the neck radius along the circumference to pinch-off the sub-droplet [100].

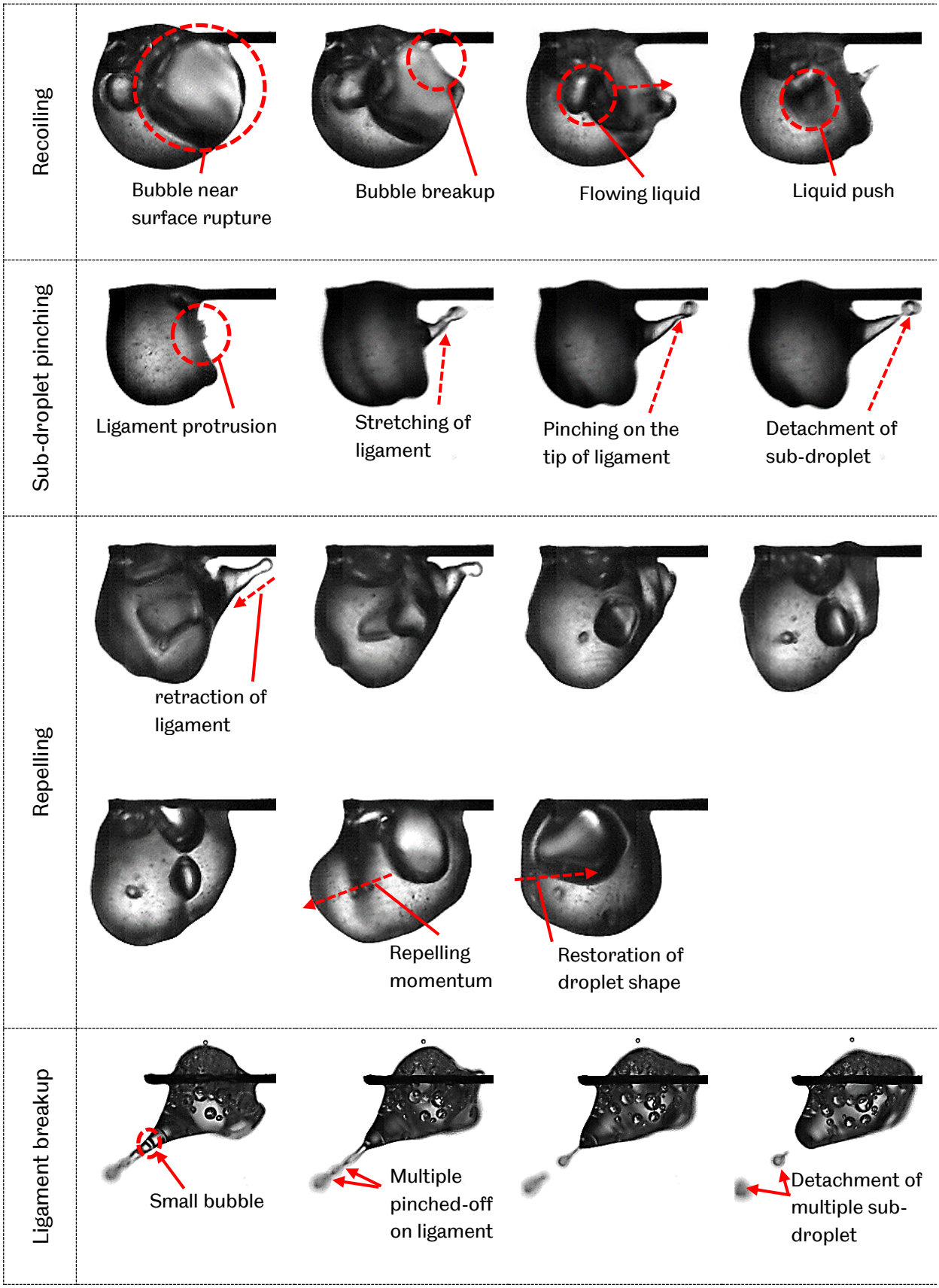

Fig. 5.8 Disruptive droplet evaporation process of emulsion fuel droplet

The detachment process of a sub-droplet is shown by the second row of Fig. 5.8. The ligament protruded to a certain length based on the strength of the push during bubble

rupture process. At critical length, the surrounding pressure pinched a section of the ligament once the internal pressure of the ligament is lower than the atmospheric pressure [131]. This detaches the sub-droplet with size depending on the width of the ligament during critical length of the ligament protrusion. Initial trajectory of the ejected sub-droplet is in-line with the direction of the ligament protrusion [36]. However, as the ejected sub-droplet instantly exposed to the heat generated by the flame, the trajectory changed due to the effect of buoyancy and floated upward while rapidly evaporating. The droplet recovers to its initial shape of ellipsoidal shortly after the ligament retracted. Retraction of the ligament is due to the pulling force of the surface tension which inhibit further protrusion of the ligament outward. The momentum of the pulling slightly moved the droplet in the opposite direction of the ligament protrusion before returning to its original shape. This process is known as the repelling motion [131].

Another mechanics of sub-droplet ejection were through multi-breakup of protruded ligament shown in the last row of Fig. 5.8. This type of sub-droplet ejection occurred when there is a formation of a vapour bubble within the protruded liquid ligament. The presence of these bubbles destabilised and weakened the ligament with the exertion of higher concentration of atmospheric pressure. As a result, the ligament broke into several sub-droplets with a minimum repelling motion. This process typically occurred in a higher loading of a volatile component which is observed to have higher number of bubble nucleation emerged within the droplet. The ejected sub-droplets resulted from multiple ligament breakup were observed to be smaller in size and slower in speed.

Fig. 5.9 shows the additional disruptive mechanics during a volatile preferential evaporation; unique to the water-in-diesel (WD) emulsion. As mentioned in the previous section, dispersed water droplet within the droplet tend to circulate within the centre rather than rapidly diffused towards the surface of the droplet. As a result, higher amount of vapour bubble with stronger pressure ruptured the surface of the droplet. This further destabilised the motion of the droplet that lead to a higher loss of liquid mass during burning process. The first row of Fig 5.9 shows the burst of the dispersed water bubble formed within the droplet. Emulsifier formed a protective layer between the dispersed water and base fuel, preventing a complete coalescence of water droplet within the droplet [84]. As a result, the pressure from the burst of superheated water vapour within the droplet was insufficient to completely break the droplet via microexplosion due to the smaller-sized bubble nucleation of dispersed water droplet. This process is similar to microexplosion mechanics explained by Rao et al. [100] but with lower intensities which only affecting one side rather than the whole droplet.

Vapour bursting through the surface pushed a sheet of liquid around the hole that formed to a shape of a half-cup. Small sub-droplets detached from the liquid sheet shortly after the burst and rapidly evaporated as they projected outward.

Another sub-droplet ejection process of water emulsion droplet is the *motion detachment* shown in the last row of Fig. 5.9. This ejection process contributes a major loss of liquid mass during the disruptive evaporation due to their larger size of ejected sub-droplets. Multiple protrusion of the ligaments caused the droplet to rotate in high speed due to the multiple repelling motion as well as the effect of buoyancy. As a result, larger portion of the ligament is detached from the parent droplet caused by the centrifugal force exerted by the rotating droplet. Both sub-droplet ejection process in Fig. 5.9 occurred multiple times in addition to the recoiling motion shown in Fig. 5.8 during the combustion of the WD. Under this reason, the WD has higher rate of mass loss compared to ED which further explains its higher burning rate compared in Fig. 5.3.

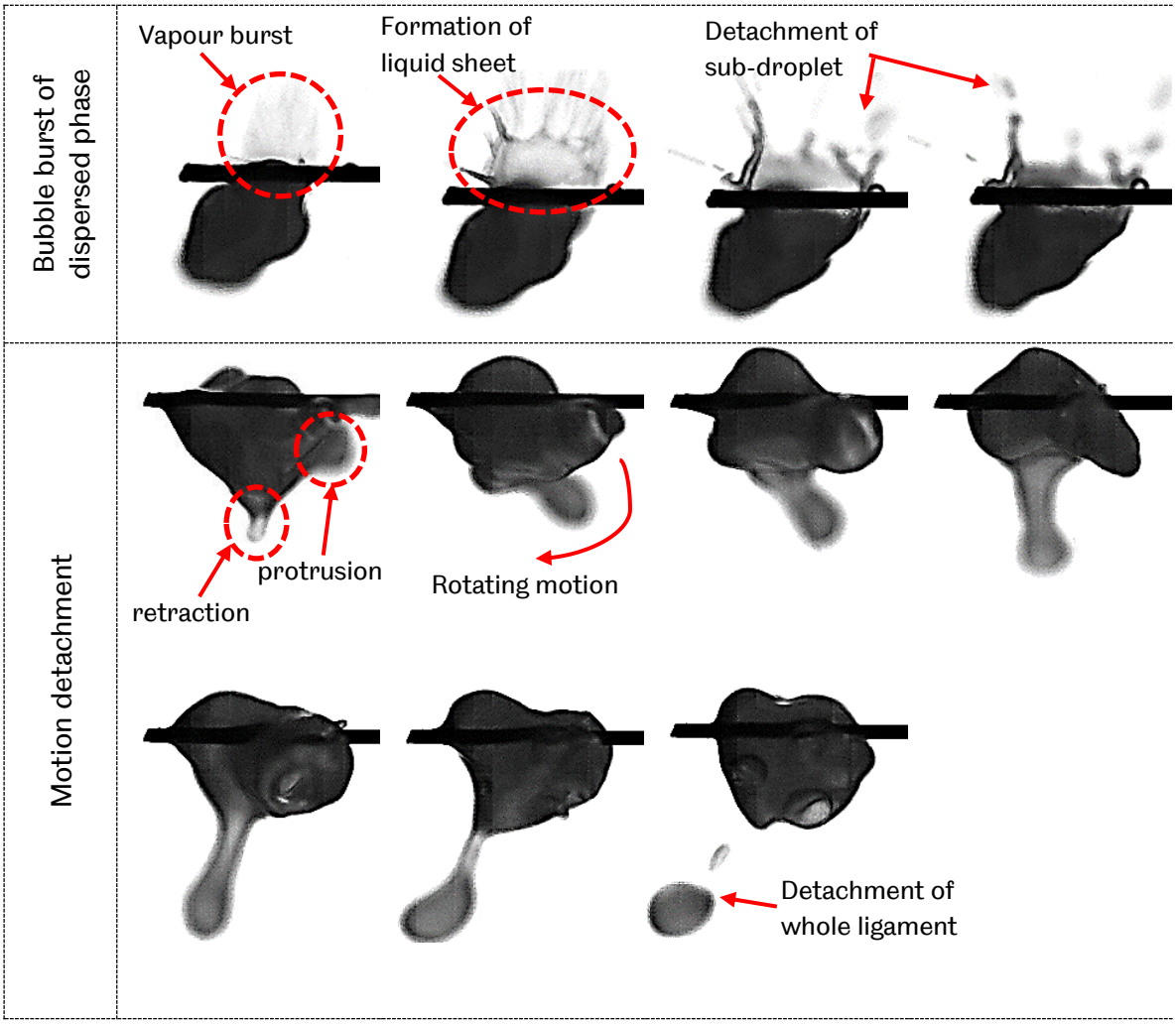

Fig. 5.9 Disruptive droplet evaporation process unique to water emulsion

Measurements were done on the disruptive process during the disruptive burning of the emulsion fuel droplet. These measurements focus on the physical change of the droplet liquid-phase during the volatile preferential evaporation. During this phase, the droplet still contains most of the volatile component inside the droplet which in turn highly disrupting the evolution of the liquid droplet. Once the evaporation phase transitioned beyond the volatile preferential evaporation, the disruptive mechanism changed inconsistently due to the depletion of volatile component and unreliable to be measured within the disruptive burning of a multicomponent fuel droplet since the droplet would be made up of mostly less volatile component with just a little trace of the trapped volatile component. Measurements were made within 0.36 and 0.52 normalised lifetime of the water-in-oil ethanol and water emulsion respectively with a satisfactory repeatability between the measurements. It is worth mentioning that it is not possible to precisely count the number of bubble nucleation, protruded ligaments and sub-droplet ejections in the present work as the visualisations were done in two-dimensional. Any occurrences towards and away from the imaging axis would be undetectable. Furthermore, the occurrences of disruptive process have low repeatability because of the complex mechanics of the internal circulation, radiative heat transfer from the unstable flame and random positioning of dispersed phase within the droplet.

Fig. 5.10 shows the measurement done on the bubble diameter near surface rupture, protruded ligament length near the tip breakup and ejected sub-droplet diameters during the volatile preferential evaporation phase. Bubble diameter near the surface rupture increased when the ethanol loading was increased to 20% by volume and decreased as the ethanol loading increased to 30%. As the ethanol loading increased, the homogeneous nucleation of ethanol into a bubble increased in number. The multiple bubble tends to merge with each other forming a larger bubble prior to the surface rupture of the droplet. This process is shown in Fig. 5.11. With more vapour bubble nucleated in higher loading, larger bubbles were formed as a result from the merging of multiple bubbles. However, as the ethanol loading was increased to 30%, multiple bubbles ruptured the surface of the droplet before completely merge with each other. This resulted smaller bubble diameter upon surface rupture with lower liquid ejection strength. As a result, the lengths of protruded ligament were shorter with a smaller sub-droplet being released as the surrounding pressure pinched the ligament. Bubble diameter, ligament length and sub-droplet diameter correlated between each other indicating the dependency of the liquid push upon surface rupture on the final size of the nucleated vapour bubble [100]. Furthermore, higher occurrences of the multiple ligament breakup shown by the last row in Fig. 5.8 were observed during the

disruptive evaporation of ED30. High amount of smaller bubble scattered within the droplet and contained within the protruded ligament as the liquid were pushed outward. This in turn shortened the ligament length and eventually breaks the ligament into multiple smaller sub-droplets.

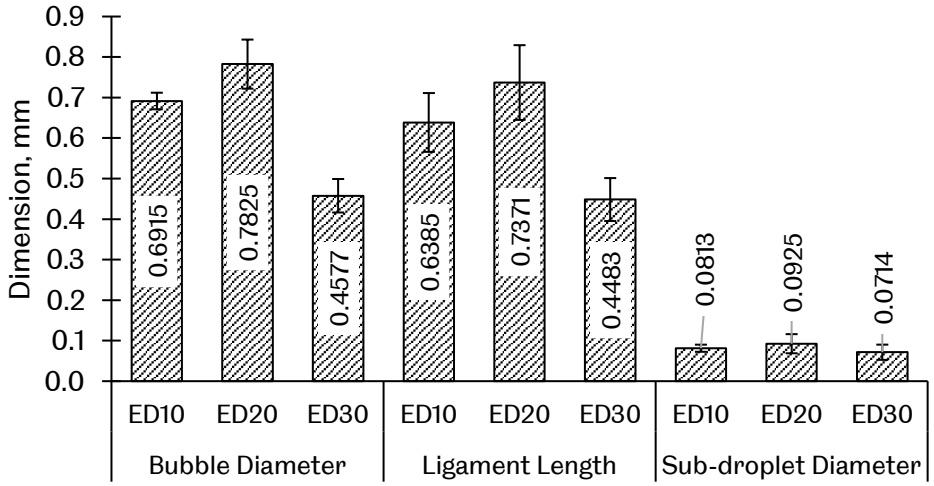

Fig. 5.10 Physical measurement on disruptive mechanics during volatile preferential evaporation of ethanol emulsion

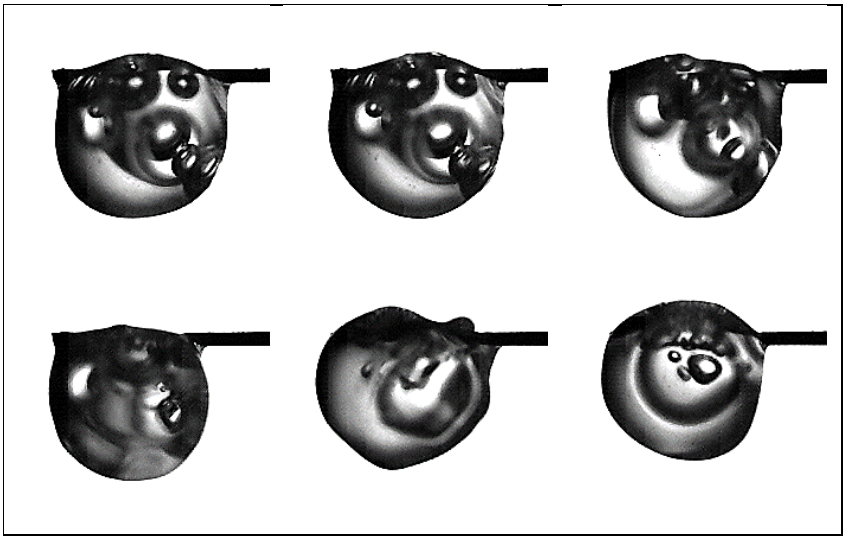

Fig. 5.11 Merging of nucleated vapour bubble during combustion of ED20

Similar measurements were done during the volatile preferential evaporation of the water emulsion. However, the measurement of bubble diameter near the surface rupture is not possible due to the droplet being opaque in appearance. The droplet only turned transparent when the volatile preferential evaporation has ended indicating the depletion of dispersed water phase within the droplet [41, 112]. The size of the ejected sub-droplets was

categorised from three ejection processes namely during; burst of dispersed phase, ligament pinched-off and motion breakup shown in Fig. 5.12.

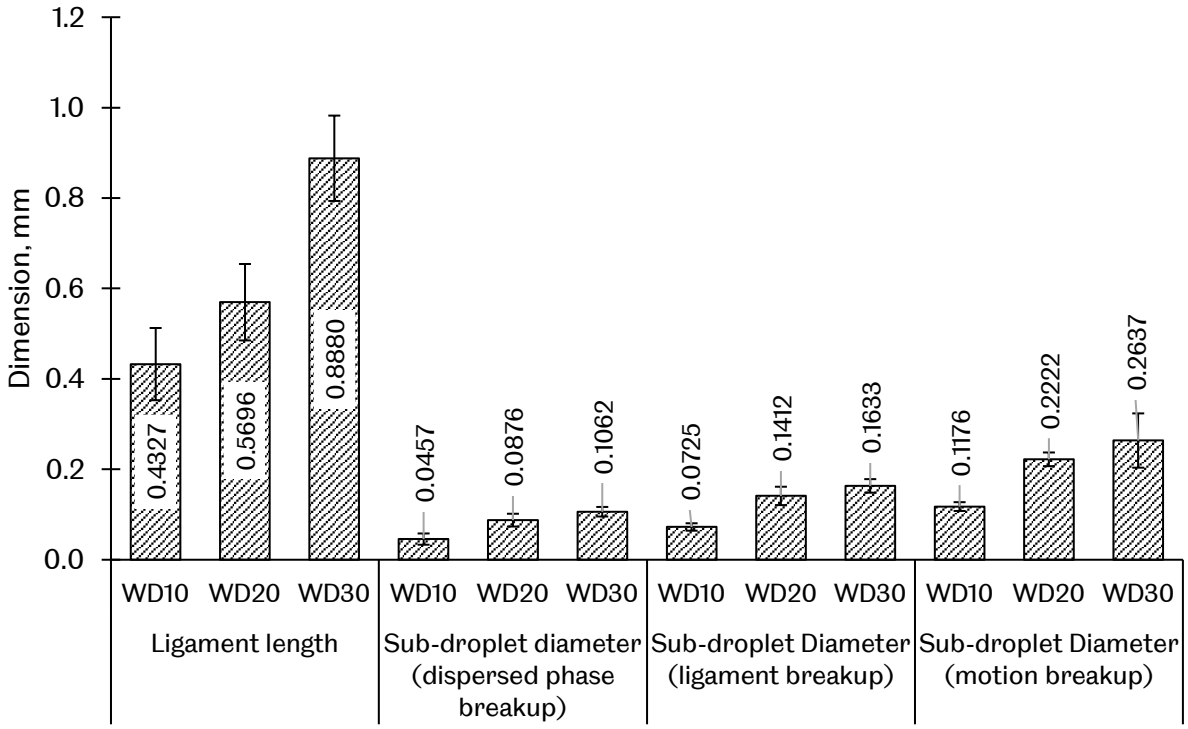

Fig. 5.12 Physical measurement on disruptive mechanics during volatile preferential evaporation of water emulsion

The ligament length of the water emulsion increased as the water loading increased. Higher amount of water possibly nucleated a larger-sized vapour bubble prior to droplet surface rupture. As a result, a stronger push of the liquid developed a longer ligament in the process. Compared to the ethanol emulsion which has shortened the ligament length in 30% loading, the increase in the ligament length of the water emulsion is substantial as the water loading was increased to 30%. Such difference contributed to their differences in the surface tension. Water has a higher surface tension compared to diesel and ethanol which inhibit the breakup of multiple ligament as it protruded outward and observed to be more stabilised when the water loading was increased. Furthermore, high surface tension of the water inhibits the stretching of the ligament [100], resulting shorter length of the ligament protrusion compared to the ethanol in each respective additive loading. Because of the tendency of water to coalescence inside the droplet, there were no observable bubble formed within the ligament, ensuring a single breakup on the ligament tip. All size of ejected sub-droplet in three breakup mode of water emulsion closely related with the water loading. Low loading with smaller dispersed phase of water inside the droplet has a weaker bubble

burst that would eventually eject smaller size sub-droplet. Shorter ligament length ejected smaller sub-droplet with minimal disruptive motion to the droplet. As a result, the centrifugal force exerted by the motion is lower and detached smaller size droplet during the motion breakup. As the waster loading increased, the size of ejected sub-droplet increased, and this process is similar to each breakup mode and protrusion of ligament.

Overall, the ethanol emulsion is easier to undergo breakup process due to its lower surface tension compared to diesel and water [35]. Having higher loading of ethanol would break the droplet into a much smaller size during the disruptive evaporation and the effect is opposite for water emulsion due to a higher surface tension of water compared to diesel and ethanol. As long as the disruptive evaporation does not undergo a microexplosion process, the physical behaviour of the droplet liquid-phase would behave similarly to the visualisations and measurements discussed in this section.

5.3 Phase separation in emulsion droplet

In the present work, separation of the continuous phase within the emulsion droplet were observed and associated with the oil-in-water emulsion fuel for both ethanol and water emulsion. Also, tests were done on the emulsion droplet without any surfactant added to clearly see the effect of phase separation that could potentially leads to a microexplosion. The analysis focuses on three phenomena mainly; the stability of the mixture to maintain evenly distributed droplets of the dispersed or continuous phase during combustion, the tendency of volatile component to coalescence and the main cause of emulsion droplet to microexplode. In this section, tests were done on 10%, 20% and 30% volume loading of additive. Because of their similar evaporation behaviour in each loading, only the result of 10% loading is presented in this section to summarise the phenomena of phase separation and microexplosion.

5.3.1 Phase Separation in Ethanol Emulsion

Prior to ignition, a slight phase separation is observed within the droplet shown in Fig. 5.13. Because of the ethanol had the tendency to evaporate in room temperature, the ethanol is observed to slowly coalescence even without being subjected to elevated ambient temperature. Since ethanol assumes the continuous phase within the droplet for diesel-in-ethanol emulsion (DE), the coalescence of ethanol was rapid due to the absence of protective

layer between them, completely separating diesel and ethanol aided by natural convection. For ethanol mixture without surfactant added (EDns), ethanol diffuses outward during evaporation prior to ignition and eventually coalescence near the surface of the droplet. In both cases, it was observed that ethanol coalescence on the surface of the droplet, especially when the ambient temperature was elevated during ignition process. For this reason, both diesel-ethanol mixture demonstrated in this section considered to be unstable and visualisations were done to specifically observe their effect to the disruptive evaporation.

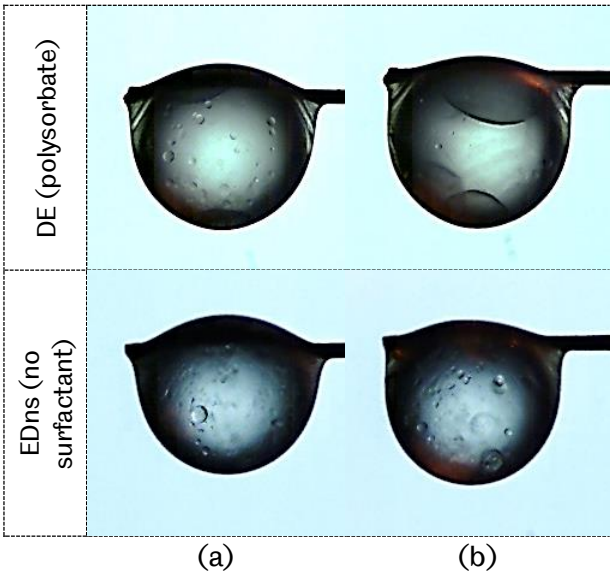

Fig. 5.13 Diesel-in-ethanol and diesel-ethanol mixture without surfactant added showing (a) initial condition and (b) phase separation

Quantitative measurements were done to the regression of the droplet surface for both DE and EDns shown in Fig. 5.14; in various ambient temperature. The ethanol evaporated first during the early lifetime of the droplet because of its lower boiling point. Different to ethanol-in-diesel (ED) discussed in the previous section, the ethanol in both mixtures presented here were readily coagulated on the surface of the droplet. As a result, the ethanol evaporated or ejected rapidly without any hindrance either from the protective layer of surfactant or the continuous phase of the diesel. This in turn depleted the ethanol component within a very short amount of time. The transitions of the volatile preferential evaporation to a steady surface regression were earlier, and the surface of the droplet continue to regress with minimum disruptive effect. Steady regression indicates the absence of the volatile component within the droplet and at the same time diminished the benefit of improved mixing provided by an emulsion fuel due to absence of secondary atomisation and droplet breakup.

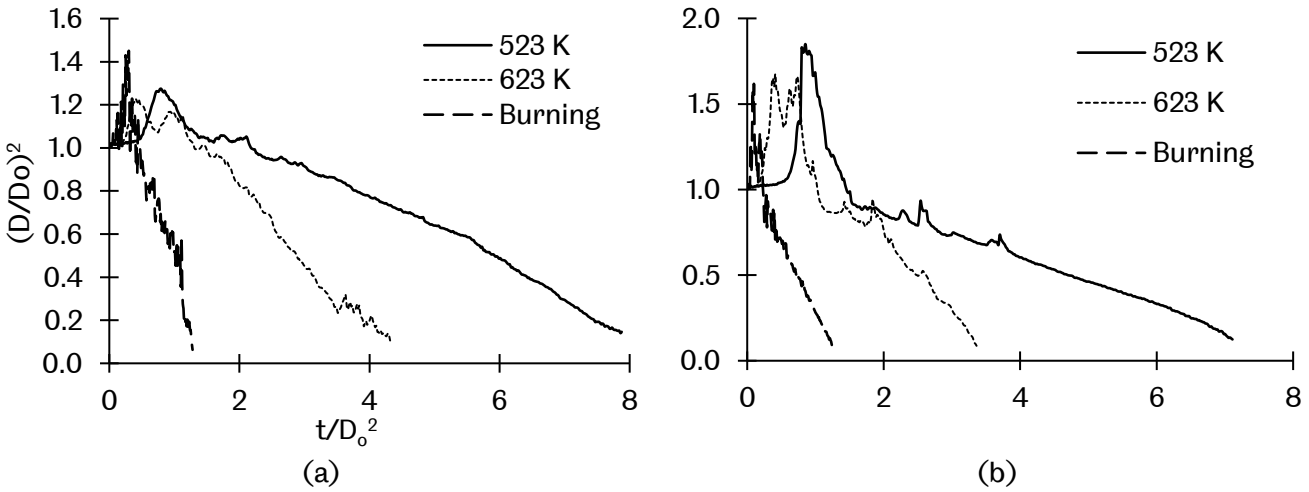

Fig. 5.14 D^2 regressions of (a) DE and (b) EDns

From the surface regressions shown in Fig. 5.14, there were only one strong puffing occurred before transitioned to the steady evaporation phase. To determine the cause of such behaviour, visualisations on the liquid-phase during droplet evaporation were made, shown in Fig. 5.15. As mentioned earlier, the ethanol rapidly aggregated near the surface of the droplet. Once the heating process commenced, the heat subjected to the surface of the droplet elevated the ethanol temperature above its boiling point thus nucleated the ethanol into a vapour bubble near the surface of the droplet. Because of the complete coalescence of ethanol due to phase separation, the entire ethanol composition nucleated into a bubble of vapour and released through puffing during the surface rupture. Observation on the liquid-phase shortly after the puffing shows no trace of ethanol in phase separation further justify the complete ejection of ethanol from the diesel-ethanol mixture. No microexplosions were observed due to the absence of ethanol component for the entire lifetime of the steady evaporation phase. With only single component of fuel continued to evaporate, no vapour bubble nucleated, and the superheat limit of the volatile component was not achieved. Similar behaviour was observed in both case of DE and EDns, confirming the rapid liquid-diffusion and coalescence of ethanol component theorised in present work.

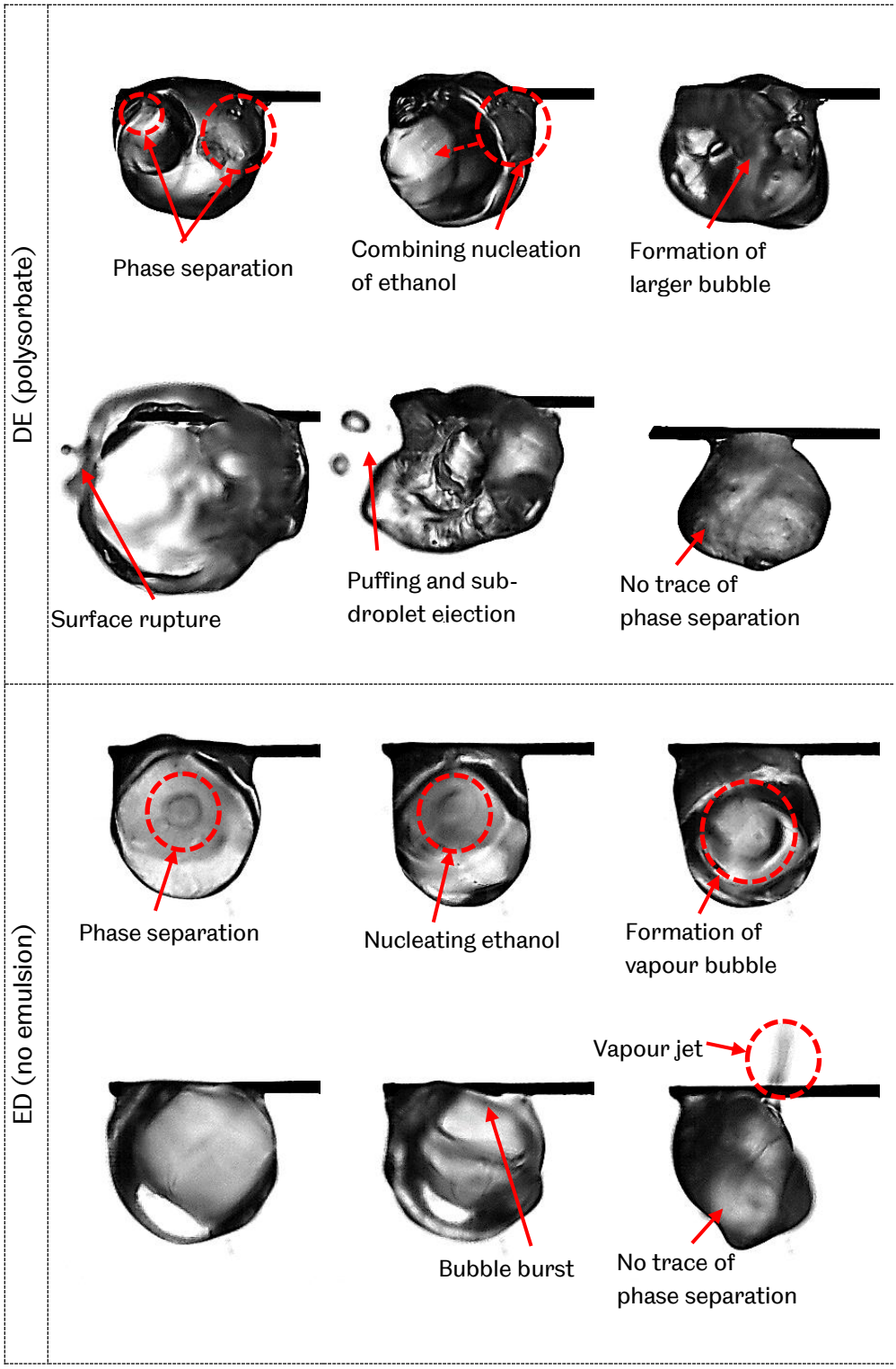

Fig. 5.15 Ejections of separated ethanol droplet

5.3.2 Phase Separation in Water Emulsion

Visualisation on the liquid-phase of diesel-in-water (DW) and diesel-water emulsion with no surfactant (WDns) were done and the initial and phase separated condition are shown in Fig. 5.16. Water component in the WDns separated earlier compared to the DW due to the

immiscibility of water and diesel [105]. The phase separation was observed almost instantly after the droplet was suspended. On the other hand, phase separation occurred in DW immediately after the droplet was subjected to a heat from the thermal wire. The holding strength of emulsion diminished when the droplet temperature increased [41, 112]. Also, the phase separated rapidly under similar reason as the DE; with water as the continuous phase within the droplet, there were no protective layer of surfactant to inhibit the coalescence of water. As soon as the droplet temperature was increased, the water component was shown to have completely separated from the diesel. Under these reasons, both water emulsion experimented in this section were unstable and have a high potential to microexplode.

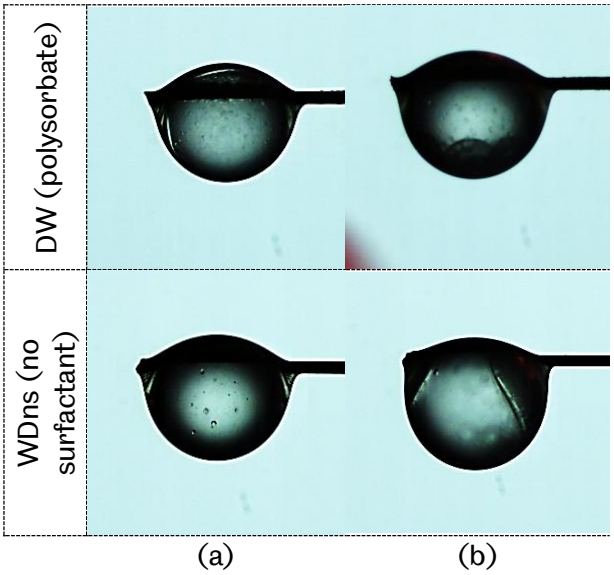

Fig. 5.16 Diesel-in-water and diesel-water mixture without surfactant added showing (a) initial condition and (b) phase separation

The regressions of squared droplet diameter of unstable water emulsion were quantitatively measured and depicted in Fig. 5.17. The droplet in both cases microexploded when exposed to a high ambient temperature shown by in the regression of D^2. Microexplosion occurred earlier with higher temperature indicating its temperature-dependant process [33, 40]. With rapid increase in the droplet temperature, the superheat limit of water is reached earlier thus rupturing the surface with a complete breakup of the entire droplet. Because there was a delay in the phase separation of water in DW, the onset of microexplosion was later when compared to the WDns. On the other hand, the WDns undergoes several puffing shortly before undergoes a complete droplet breakup. As shown by Fig. 5.16 (b), the water is readily coalescence near the surface of the droplet during the early lifetime of droplet evaporation. As a result, early nucleation of vapour produced a bubble that

could easily escaped through the surface without breaking the entire droplet. However, the disruptive behaviour is shown to be different from the EDns. Water component was not completely evaporated or ejected through puffing but undergoes a complete breakup of droplet shortly afterwards.

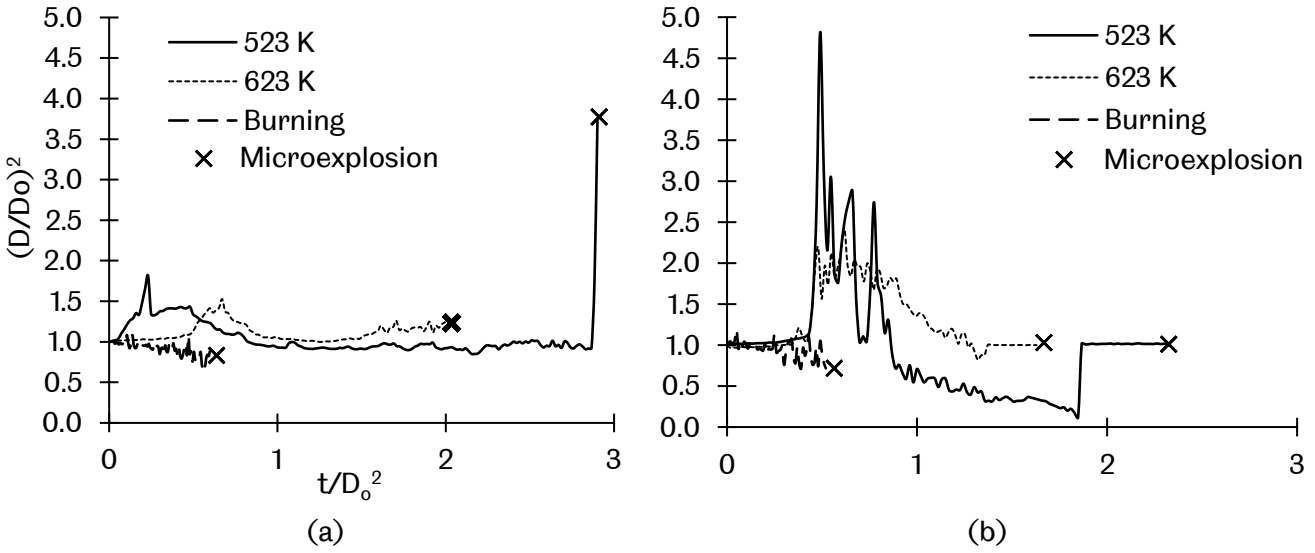

Fig. 5.17 D^2 regressions of (a) DW and (b) WDns

The liquid-phase visualisation was done on the DW and WDns to closely observe the microexplosion processes of the water emulsion droplet. Shown in Fig. 5.18, the coagulated water droplet diffused inward with the aid of the internal circulation and located near the centre of the droplet [73]. The positioning is confirmed by observing the expansion of vapour bubble in both cases. During the bubble expansion, the entire droplet expanded in all direction indicating the position of the coagulated water inside the droplet to be located near the core of the droplet. The droplet expanded to a shape of half-cup consists of liquid sheet during the combustion of the DW and the droplet breaks to a fairly large sub-droplet upon surface rupture. In the case of WDns, the vapour burst was observed to be stronger and breaks the entire droplet in all direction, pushing the sheet of liquid fuel outward that eventually breaks into smaller sub-droplets. This difference indicates the role of surfactant to form a protective layer within the droplet [138]. Surface tension of the DW is higher due to the addition of surfactant and prevented the droplet to break into smaller droplets compared to the WDns. Liquid-phase observation done in the present work brought a new insight to the microexplosion process; where the position of coagulated water plays a role in the droplet breakup. Coalescence of a volatile component near the surface would nucleate into a vapour bubble and released by a puffing process whilst coalescence of volatile component in the core

of the droplet would break the entire droplet in all direction and considered to be one of the criteria for a microexplosion to occur.

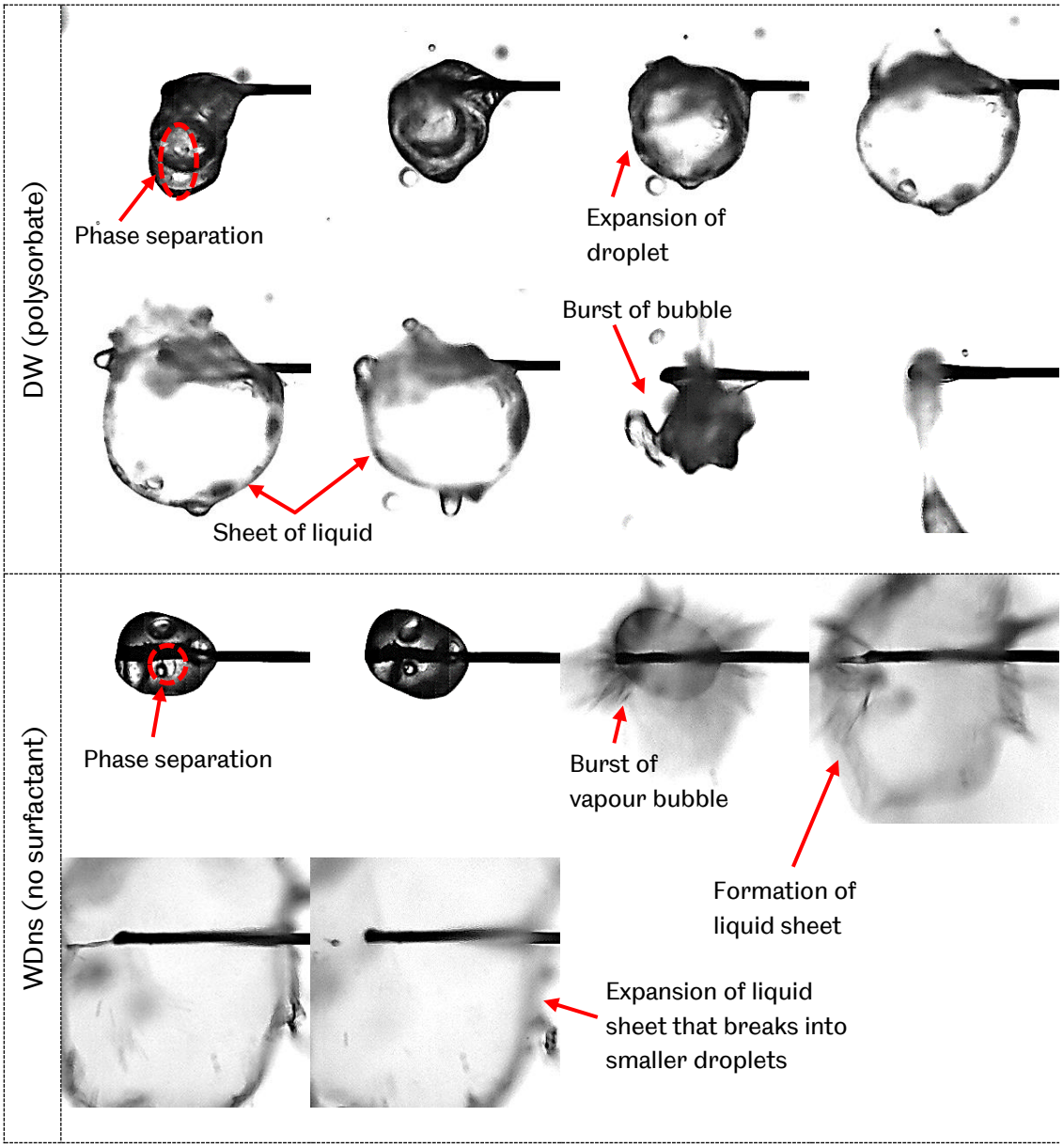

Fig. 5.18 Microexplosion processes of burning DW and WDns

The unstable water emulsion was subjected to ambient temperature below the superheat limit of water (543K [112]) to further confirm the theory made by various researchers [1, 29, 33, 37-39, 41] on the certainty of droplet to microexplode upon reaching the superheat limit of the more volatile component in emulsion droplet. The test was done to see whether the droplet would still microexplode if subjected to an ambient temperature below the superheat limit of water. The regression of D^2 when the unstable water emulsion droplet was subjected to a steady ambient temperature of 423 K is shown in Fig. 5.19. In both

unstable mixture of the DW and WDns, no microexplosion occurred despite having a complete phase separation of water within the droplet. Some puffing was observed as a mean of vapour to escape from the droplet core. Hence, comparisons made in present work confirms that the lower boiling point component need to reach its superheat limit in order for microexplosion to occur.

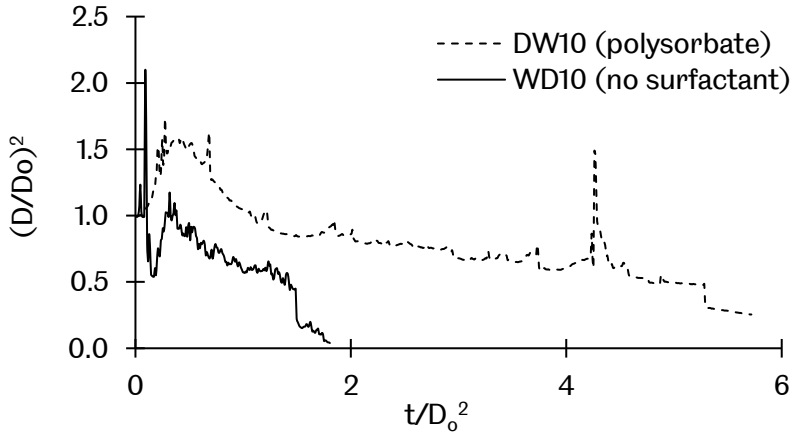

Fig. 5.19 D2 regression of DW10 and WDns10 subjected to 423 K ambient temperature.

5.4 Summary

Several key findings are highlighted in this chapter. From the experimental results, it is found that the water-in-oil emulsion is more stable compared to oil-in-water emulsion; based on two reasons. Firstly, the surfactant added to the emulsion forms a protective layer on the boundary between dispersed and continuous phase thus prevents early separation of phase during the droplet evaporation. The dispersed component of the water-in-oil emulsion are separated between each other by the continuous phase and the protective layer of the surfactant, ensuring minimum coalescence of the more volatile component during the evaporation process. With minimum phase separation occurs inside the droplet, the evaporation proceeds with disruptive evaporation until the end of droplet lifetime. Continuous occurrences of puffing and sub-droplet ejection in water-in-oil emulsion provides improved mixing through a secondary atomisation processes thus highly preferable in the application of an emulsion fuel.

Secondly, the more volatile component in the emulsion fuel have the tendency to diffuse towards the surface of the droplet during the early lifetime of the droplet. As a result, high volume of the component resides and coalescence on the surface. Since the volatile

component assumes the continuous phase in the oil-in-water emulsion, they coalescences rapidly and a complete phase separation occurs at the early lifetime of droplet. Most volatile component is released in a strong puffing which in turn completely evaporated from the droplet. With the aid of internal circulation, some volatile component moves towards the centre of the droplet and explodes violently as the temperature reaches its superheat limit. As a result, no puffing or sub-droplet ejection occurs once the volatile component is completely depleted which in turn diminished the benefit of emulsion droplet to improve mixing during combustion. On the other hand, microexplosion of water emulsion occurs early with high amount of water vapour being ejected and extinguish the flame upon a complete breakup.

Major finding in this chapter focuses on the characteristics of the emulsion fuel droplet to microexplode. With sufficient evidences provided by the quantitative measurement and liquid-phase visualisation conducted in the present work, the cause of emulsion fuel droplet to microexplode is determined. It is found that there are three conditions required for the onset of microexplosion. Firstly, the temperature of the component with a lower boiling point need to reach its superheat limit temperature. In present work, the diesel-in-water droplet undergoes a microexplosion each time a temperature above the superheat limit of water is subjected to the droplet. When the ambient temperature is lowered below its superheat limit, microexplosion does not occur. Secondly, the droplet would only microexplodes when there is a phase separation of component with a lower boiling point in the droplet. It is demonstrated in the present work that the onset of microexplosion was delayed when a complete separation phase of volatile component was delayed. Finally, a microexplosion would only occur when the water coalescence is located in the core of the droplet. It is clearly shown in the present work that the coalescence of the more volatile component near the surface does not induce a microexplosion. The dispersed droplet would only undergo strong puffing and released through the surface as shown by tests done on the diesel-in-ethanol. For the diesel-in-water and diesel-water mixture without any surfactant added, the dispersed water is found to be located near the core of the droplet thus breaking the droplet in a strong burst once the superheat limit of water is reached. Under these reasons, microexplosion would only occur once all three conditions are fulfilled; reaching the superheat limit temperature, a complete phase separation and when the dispersed phase located near the core of the droplet.

Chapter 6

Soot Contamination Effect on the Combustion Behaviour of Isolated Diesel Droplet

6.1 Introduction

This chapter analyses the quantitative measurement and the liquid-phase visualisation made during the combustion of the diesel droplet contaminated with soot particles. Imaging on the droplet liquid-phase and flame formation was synchronised to simultaneously observe the combustion behaviour. The analysis focuses on the effect of soot contamination to the burning rate, surface regression, combustion phases and flame formation during the lifetime of the burning diesel droplet.

Two contamination conditions were simulated in the present work. Firstly, the contamination was made by igniting the imaged diesel droplet with another diesel droplet positioned below it. The soot contained in the hot combustion gas from the contaminating droplet would flow upward due to the effect of buoyancy and contacts the imaged droplet [97]. This process assumes spontaneous contamination of soot during a non-turbulent fuel spray that would eventually collides with soot particles contained inside an actual cylinder [53]. Secondly, soot particles were evenly distributed inside the droplet by properly mixing the collected soot with diesel. Surfactant was not added into the mixture to avoid any change to the fuel properties [84]. This process assumes a spontaneous contamination of soot during turbulent mixing, with a possibility of soot particle to penetrate the surface towards the core of the droplet [158].

The findings of this chapter would provide an insight into the possibility of soot contaminating the fuel droplet in spray during an actual combustion process. Furthermore, the effect to the combustion behaviour is evaluated in detail by analysing the relation between the surface regression, flame formation and disruptive behaviour of contaminated droplet.

6.2 Combustion Characteristics and Liquid-phase Visualisation of Single Isolated Diesel Droplet with Surface Contaminated by Soot Particles

Investigations on the effect of soot contaminating a diesel droplet were done to simulate the continuous process during the combustion of diesel in actual engine cylinder. The soot produced within the hot combustion gas would have the potential to contaminate the diesel droplet being sprayed into the cylinder. Also, some soot would still be trapped inside a cylinder in each combustion cycle that would attach to the fuel droplet sprayed towards it [54]. To properly investigate this phenomenon, the flame from a diesel droplet was used to ignite the imaged diesel droplet. At the same time, the soot propagating upward from the flame would contaminate the diesel droplet positioned above it. To ensure soot to contaminate the imaged droplet, the flame edge was adjusted so that it was 1 mm away from the imaged droplet. Thermal heating wire was used to ignite the lower droplet for steady and neat ignition process. As soon as there was an observable formation of flame on the imaged droplet, the contaminating droplet was removed

6.2.1 Visualisation on the Contamination Process

The contamination process of soot particles was imaged and presented by the sequences shown in Fig. 6.1. As soon as the contaminating diesel droplet was ignited, soot formed within the hot combustion gas flowed upward due to the buoyancy effect. The soot particles were quenched immediately after in contact with the surface of the imaged droplet shown in Fig. 6.1 (b). The quenched soot particles agglomerated and resided on the surface of the droplet. As more soot being quenched, the agglomerated soot particles enveloped the surface of the droplet and formed a thin layer of a shell-like structure on the surface of the droplet. Repetitive visualisation on the imaged droplet has shown similar contamination mechanics, and a formation of a shell-like agglomerated soot particles that always reside on the surface of the droplet without penetrating towards the core. It is found that this would be the primary mechanism of soot contamination on any fuel droplet and the area covered by the shell depended on the amount of the contaminating soot particles quenched on the surface of the droplet [97].

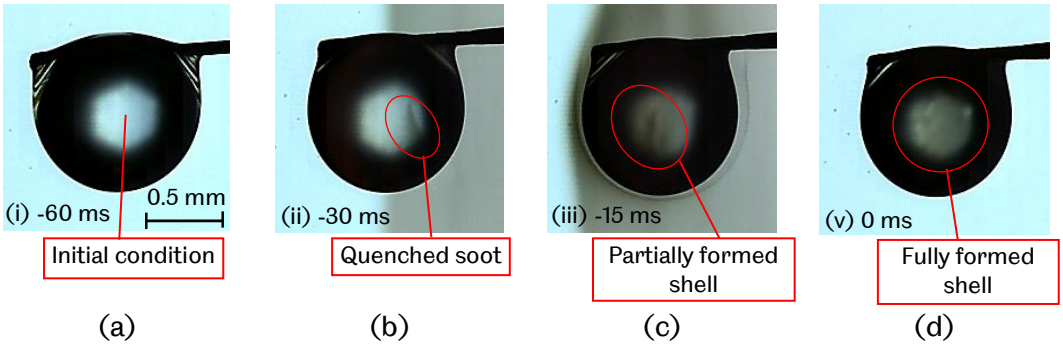

Fig. 6.1 Soot contamination process shown by sequence of (a) intial condition, (b) quenching and agglomeration of soot particles, (c) early formation of soot shell and (d) fully formed shell of agglomerated soot particles [97].

6.2.2 Initial Condition of Contaminated Droplet

The test was repeated more than 50 times due to the differences of the contamination densities between each repetitive measurement. Fig. 6.2 shows a typical contamination of the imaged droplets. The soot particles contaminated the surface of the droplet in various concentration, from light with a few uncovered surface areas of droplet to heavy with the droplet surface being completely covered by the shell of agglomerated soot. Random contamination process conducted in the present work would simulate the contamination process during actual fuel spray, limited to the contamination during vertical ignition process.

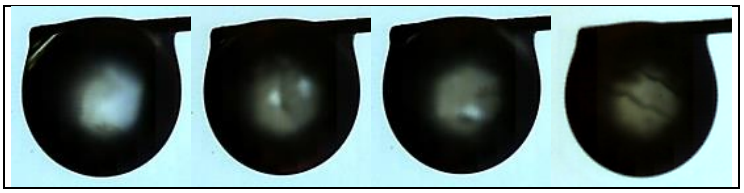

Fig. 6.2 Typical soot contamination from light to heavy surface coverage [97].

6.2.3 Evolution of Droplet Squared Diameter (D^2) and Flame Stand-off Ratio, FSR (D_f/D) of SCD Droplet

Quantitative measurements were done on the regression of droplet diameter represented as normalised squared droplet diameter and the flame stand-off ratio for both neat and surface-contaminated diesel (SCD) droplet shown in Fig. 6.3. High repeatability is shown in the regression of both D^2 and FSR. Further describing on the D^2 and FSR regression of SCD droplet, the contamination density was found to have negligible effect on the gradient during

the steady burning phase (PII). However, higher contamination density does increase the magnitude of the disruptive effect throughout the combustion. The SCD droplet undergoes a stronger puffing and surface distortion during the steady evaporation phase thus fluctuated the D^2 regression even more. There was no observable sub-droplet ejection occurred during steady burning phase thus explains the similarities of the burning rate between each sample regardless of their contamination densities. Once the combustion transitioned into the disruptive phase (PIII), their D^2 regressions deviated from each other with a steeper regression of denser contaminated droplet, indicating a higher amount of liquid mass loss.

There is a brief uncertainty in the measurement of the FSR between 0.15 and 0.18 s/mm^2 for the neat diesel and 0.07 to 0.1 s/mm^2 for the SCD droplet. During these period, slight elevation of the flame formation was observed and identified to be the interaction effect of the imaged droplet with their respective ignition media. Higher overshoot shown by the FSR of SCD during this period is because of the effect of accumulated fuel vapour provided by the contaminating droplet used to ignite the SCD droplet. As previously discussed in Chapter 4, ignition of a droplet with another combustible fuel or gas would have a brief moment of increased flame height due to the increase amount of fuel vapour accumulated between the droplet and the flame zone. Although the combustion characteristics of neat diesel were already discussed in Chapter 4, it is represented in this chapter for the sake of comparing it with the SCD droplet.

Most works on a droplet suspended with particles done by various researchers [18, 152, 185] used a low frame rate between 30 to 5200 fps in visualising the evolution of the droplet diameter which in turn would make the measurement on the regressing surface of the droplet to appear with less disruptive behaviour. In the present work, a higher frame rate of 10,000 with a spatial resolution of 130 pixel/mm was conducted to precisely track the disruptive regression of the droplet surface during the combustion processes.

Shown in Fig. 6.3 (a), the lifetime of the SCD droplet is shortened compared to the neat diesel due to its frequent sub-droplet ejections during the disruptive phase (PIII). Most of the heat gained from the flame absorbed by the soot shell formed on the surface of the droplet because of its high energy absorbance [71, 158], inhibiting the heat transfer towards the centre of the droplet thus reduced the expansion rate of the SCD droplet in heating phase (PI). As a result, the SCD droplet was observed to slightly expanded later at normalised lifetime of 0.4 s/mm^2. When the core temperature elevated at slower rate, lower amount of fuel vapour escaped through the surface thus reduces the surface distortion during the heating phase. Furthermore, the shell of agglomerated soot particles formed a protective

layer around the droplet, changes the surface tension and at the same time observed to be able to maintain the ellipsoidal shape of the droplet despite of being rapidly heated during droplet heating process.

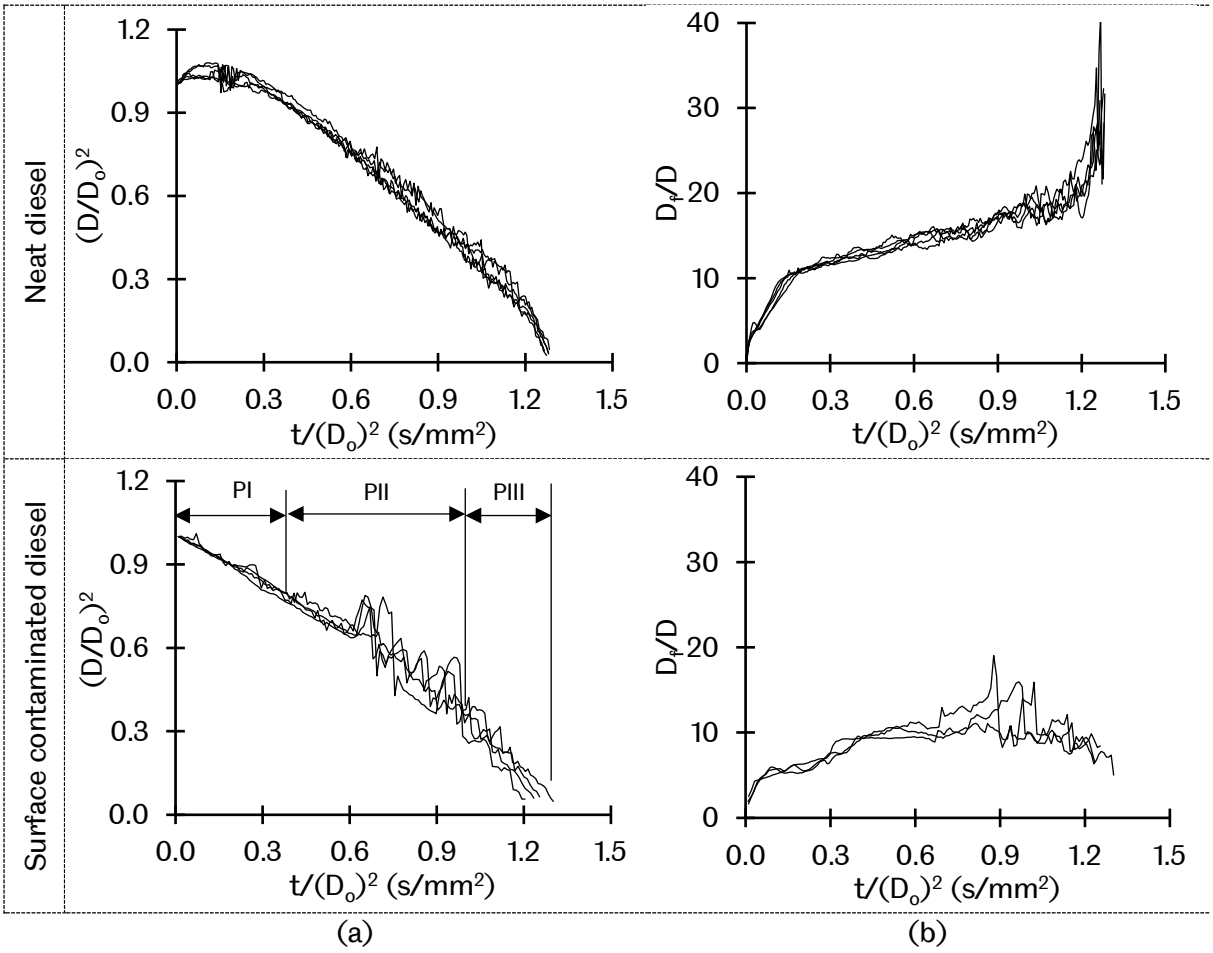

Fig. 6.3 Normalised regression of neat diesel and surface-contaminated diesel droplet on (a) D^2 and (b) FSR [97].

The FSR of SCD droplet is found to be declined as the combustion progressed shown in Fig. 6.3 (b). Early formation of the agglomerated soot shell on the surface of the droplet promotes faster agglomeration rate of soot particles during self-contamination process as the combustion progressed. Formation of soot shell around the droplet supressed the evaporation rate as a result of slower mass diffusion of liquid from the core to the surface of the droplet [97, 147, 148]. This in turn contracted the formation of flame due to the lowering of fuel vapour consumption with a minimum effect of fuel vapour accumulation. Ejection of the sub-droplet in the disruptive phase is known to increase the flame size due to the effect of gas-phase interaction. This process is observed and measured to have elevated the flame size during the combustion of neat diesel. Although burning SCD droplet shown more active sub-droplet ejection during the disruptive phase, the FSR continues to decline. Hence, clear

visualisation of the dynamics inside and on the surface of the droplet is needed to identify their differences.

6.2.4 Burning Rate Constant and Lifetime of Combustion Phases

In the case of SCD droplet, the regression of D^2 is still linear during Phase II despite having some fluctuation due to the more active puffing of fuel vapour through the surface of the droplet. This enables the measurement on the burning rate to be possible. Measurement of the burning rate shown in Fig. 6.4 indicates that the burning rate of SCD droplet declined similarly despite having different densities of soot contamination during the ignition process. Denser contamination of soot particles on SCD droplet does not further reduce the burning rate during PII and this is shown by relatively small deviation between each repetitive measurement done on the SCD droplet. Comparing to the neat diesel, it is found that even the slightest contamination of soot particles on the surface of the droplet reduces the burning rate by 17%. Formation of soot shell on the surface of the droplet prior to ignition inhibited the liquid diffusion of fuel from the interior to the surface of the droplet thus suppressing the evaporation process. However, the magnitude of disruptive behaviours is more profound with higher fluctuation of D^2 shown in Fig. 6.3 (a). The soot shell hinders the release of nucleated fuel vapour which in turn shortly expands the droplet before being release through the surface. Large differences were observed between the combustion characteristics of nanofluid and SCD droplet conducted in the present work. Small amount of energetic nanoparticles suspended in a base fuel (nanofluid) improves the burning rate [43, 152] whereas even the slightest contamination of soot on the surface of the droplet would be detrimental to the burning rate.

Imaging techniques applied in the present work with high repeatability provides a reliable identification of combustion phases in the regressions of D^2 with distinct changes from one phase to another during the combustion of neat diesel and SCD droplet. Contamination of soot deviated the regression of steady evaporation from D^2-law and prolongs the duration of droplet heating (PI) and disruptive phase (PIII) shown in Fig. 6.4. The reliable measurement of the burning rate of SCD droplet is shortened to 57.92% of its lifetime from 72.21% in neat diesel. Soot shell absorbed high amount of radiation from the flame during the combustion. As a result, heterogeneous nucleation is promoted inside the droplet due to high temperature spot around the soot shell on the surface. The soot shell creates an obstruction for the nucleated vapour bubble to escape through the surface. Nucleated

vapour trapped inside the droplet would require a higher pressure to be released through the thicker soot shell thus further disoriented the droplet surface. The surface of the droplet is then ruptured with stronger gush of vapour, ejecting a sub-droplet and soot particles outward which destabilises the surface regression with higher loss of mass thus transitioned the combustion to Phase III earlier. SCD droplet is measured to have longer disruptive burning (PIII) with 12.7% of its total lifetime.

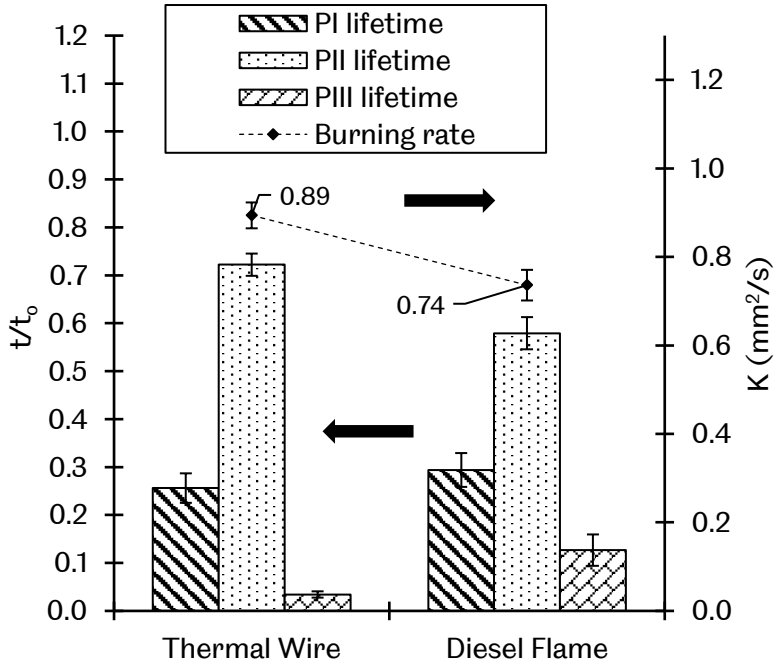

Fig. 6.4 Quantitative measurement on the burning rate and lifetime of combustion phases of neat diesel and SCD droplet [97].

Examination on the regression of D^2 in SCD droplet shows that the duration of lifetimes in each combustion phase does not affected by the variations of soot contamination degrees on the droplet surface prior to ignition. The lifetime of each phase measured in Fig. 6.4 has a deviation of less than 4% between each repetitive measurement despite having different condition of initial soot contamination. Typical findings on nanofluid droplet combustion suggests earlier destabilisation of combustion with longer duration of disruptive phase when the concentration of precursors or nanoparticles is increased beyond its critical loading [43, 148, 152]. However, findings obtained from the present work are distinctly different from nanofluid combustion due to its differences in the condition of particle laden. It is found that soot contamination on the surface of the droplet promotes rapid particle agglomeration and the effect to the droplet evaporation and stability is detrimental regardless of any contamination density.

6.2.5 Liquid-Phase Visualisation

Liquid-phase visualisations were done to monitor the dynamics of particle during the combustion process as well as obtaining a clearer view inside the droplet. Although such approach were done in various work on the droplet with a particle suspension [18, 43, 148, 152, 185, 186], the disruptive dynamics of particle were not closely associated with the regression of the D^2 and FSR. For instance, the puffing and liquid ejection are more active in the combustion of the SCD droplet in the present work but the FSR was measured to decline as the combustion transitioned to PIII. Although the effect of vapour accumulation is definitely reduced due to suppressed evaporation, there should be a slight enhancement to the flame formation due to the gas-phase interaction between the parent and ejected droplet as observed in the neat fuel. For this reason, a closer visualisation was done to observe the dynamics of the droplet and soot particles that would made the combustion of the SCD droplet behave differently from the neat diesel.

Evaporation of the SCD droplet during Phase I shows only a slight surface distortion. During this period, the soot shell resided on the surface of the droplet absorbed most of the radiation from the flame, locally heats the surface of the droplet. Elevation of the temperature to its boiling point evaporates the liquid fuel near the surface of the droplet. Because of there were no obstruction to the evaporating liquid near the surface, the evaporation proceeds with steadier manner. However, this slows the heating process towards the core of the droplet. As a result, liquid mass diffusion from the core to the surface of the droplet is retarded due to a slow heating process resulting suppressed evaporation. Less amount of vapour tries to escape through which in turn stabilises the surface of the droplet. The absence of a homogeneous bubble nucleation inside the droplet shown in Fig. 6.5 (i) minimised the droplet expansion during the heating period.

As the combustion progressed to Phase II, the shell began to be densely packed due to the reduced droplet size. The core temperature of the droplet would eventually increase towards its boiling point during this phase indicated by the steady regression of D^2. Escaping vapour through puffing ejected some of the agglomerated soot particles shown in Fig 6.5 (ii) without any protrusion of liquid ligaments. Multiple occurrences of puffing eventually fragmented the dense shell shown Fig. 6.5 (iii).

Segregation of the densely packed shell of agglomerated soot particles locally heats the liquid near the surface of the droplet. As the droplet continues to reduce in size, more fuel vapour that was trapped inside the shell tries to escape through the surface. Tougher

obstruction subjected by the soot shell caused the vapour to be released by a higher vapour pressure thus pushes out the vapour together with a fragment of the shell outward, clearly shown in Fig 6.5 (iv). Flame enveloping the droplet ignited the released particles and fuel vapour thus initiated an explosion outside the droplet shown in Fig. 6.5 (v). This explosion fluctuates the flame size in Phase III and the effect is clearly shown by the regression of the FSR in Fig. 6.3 (b). The measurement on the flame height shows that the explosion does not enhance the flame size upon interaction. Similar occurrences of non-interaction flame formation were observed in each repetition of flame visualisation. On top of reduced effect of fuel vapour accumulation, the ejected soot particle exploded without enhancing the flame formation through gas-phase interaction resulting continuous decline of the FSR towards the flame extinction. With such large differences in the dynamic of liquid-phase observed between the neat diesel and SCD droplet, the cause of declining FSR is identified.

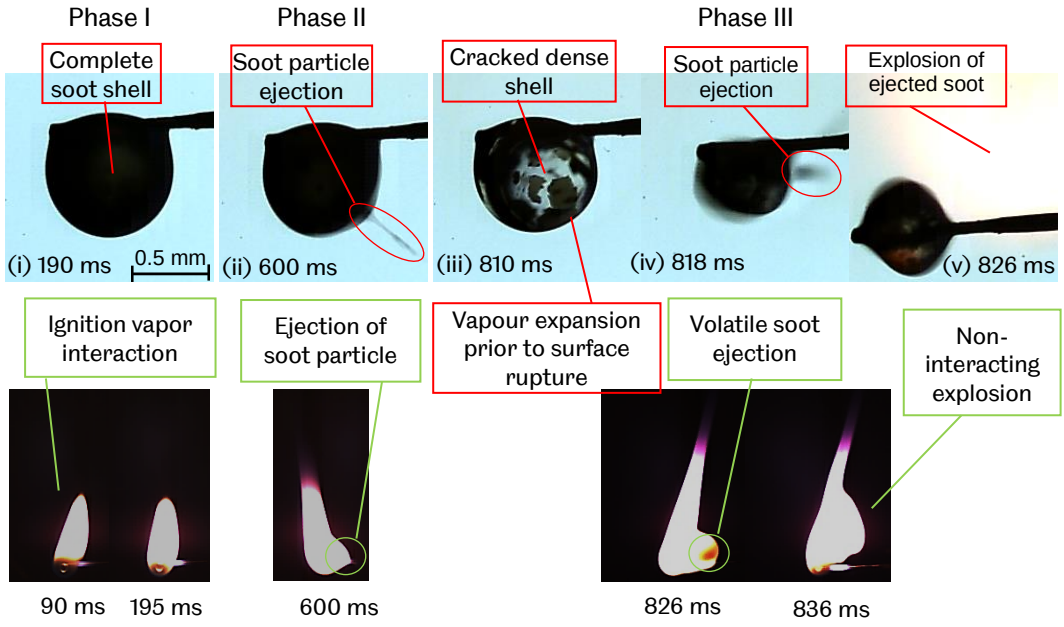

Fig. 6.5 Liquid-phase and flame visualisation during Ignition, swelling, boiling and disruptive phases of surface-contaminated diesel droplet [97].

6.3 Combustion Characteristics and Liquid-phase Visualisation of Single Isolated Diesel Droplet with Volume Contaminated by Soot Particles

Experimentations were done on the diesel droplet suspended with soot particles. The soot particles were thoroughly mixed with a diesel with increasing amount of particle loading by mass. This experiment was conducted to simulate the contamination process inside the

cylinder. There is a possibility of soot to penetrate the surface of the droplet during turbulent mixing. Also, this test was conducted to specifically compare the differences between surface soot contamination, energetic nanofluid and volume soot contamination effect. The loading was increased from 0.05% to 0.5% of loading by mass in 0.1% increment. 0.05% mass loading was tested for the sake of visualising the liquid-phase as well as to increase the precision of burning rate measurement in low particle loadings.

6.3.1 Initial Condition of Volume-Contaminated Diesel (VCD) Droplet

Fig. 6.6 shows the initial condition of the VCD droplet prior to ignition. With very low density of 1.84 g/cm^3 [158], the amount of soot contained in the droplet was high even with 0.05% mass loading. The VCD droplet is fairly transparent by up to 0.1% particle loading shown in Fig. 6.6 (b). Higher loading of particle turned the droplet to opaque in appearance, making visualisation inside the droplet to be impossible. The soot particles suspended inside the base fuel is observed to be evenly distributed even without any surfactant added. To prevent early agglomeration of soot particle due to a gravitational settling described by Gan and Liao as one of the factor of particle agglomeration inside a fuel droplet [107], the ignition was made as soon as the droplet was suspended on the fibre.

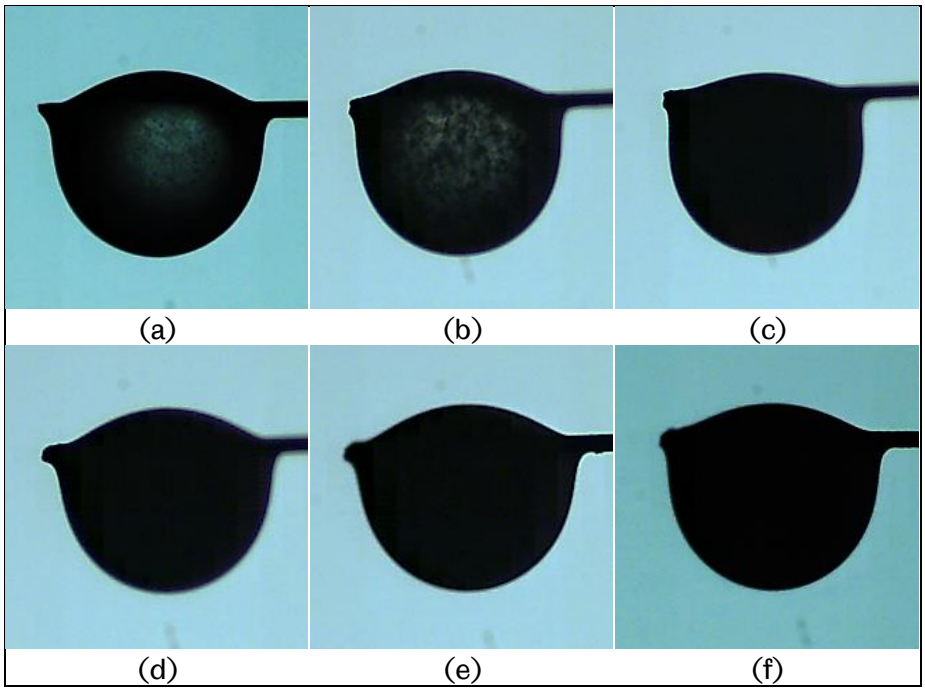

Fig. 6.6 Initial condition of VCD prior to ignition with mass loading of (a) 0.05%, (b) 0.1%, (c) 0.2%, (d) 0.3%, (e) 0.4% and (f) 0.5%

6.3.2 Evolution of Droplet Squared Diameter (D^2) of VCD Droplet

Measurements on the evolution of droplet diameter were made on VCD droplet with up to 0.5% soot particle mass loading and is presented in Fig. 6.7. Measurement of the D^2 shows good repeatability in each sample thus making the analyses done in the present work to be considered reliable. In low mass loading of 0.05%, the regression is steady with a minor puffing recorded throughout the lifetime of the droplet. The droplet undergoes less expansion during heating phase compared to the neat diesel. This is due to its prolonged droplet heating during the early lifetime of the droplet. When the loading increased to 0.1%, the regression of the D^2 fluctuates rapidly in Phase II and the magnitude of distortion is at the highest in 0.2% loading. This is believed to have occurred due to the multiple heterogeneous nucleation of vapour bubble emerged within the droplet. As a result, more puffing process occurred, and the effect is the highest when the particle loading increased to 0.2%. However, when the loading increased to 0.3%, the frequency and magnitude of fluctuation on D^2 regression began to reduce and observed to be steadier when the loading was further increased. On the other hand, the period of droplet heating has shown to be increased by a longer curve of D^2 regression during the early lifetime as the particle loading increased indicating higher amount of heat from the combustion being absorbed by the soot particles rather than heating the liquid fuel. Hence, closer visualisation on liquid-phase is needed to determine the cause of such change in combustion behaviour.

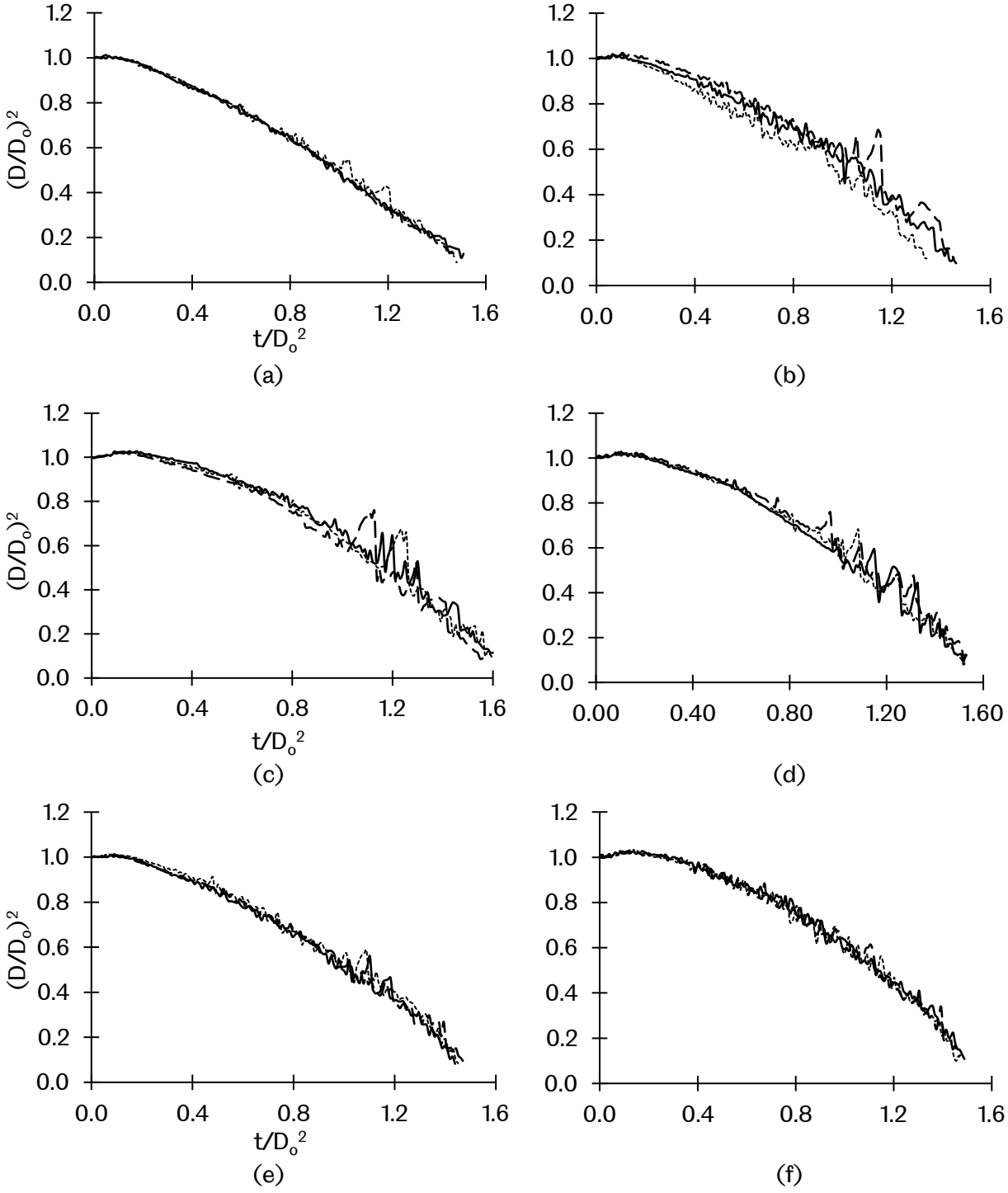

Fig. 6.7 Repetitive measurement on D2 regression of VCD droplet with soot particle mass loading of (a) 0.05%, (b) 0.1%, (c) 0.2%, (d) 0.3%, (e) 0.4% and (f) 0.5%

6.3.3 Dynamics of Soot particle inside VCD Droplet during combustion

To further understand such change in the combustion behaviour, the dynamics of particle within the droplet need to be identified. Fig. 6.8 shows sequential visualisation on the VCD droplet with 0.05% mass loading. This loading was selected to be demonstrated here due to

its transparent droplet appearance, making the observation on the particle dynamics inside the droplet to be possible. Upon ignition, the particle inside the droplet starts to move with the aid of internal circulation induced by buoyancy. Some of the particle began to agglomerate shown at t = 200.3 ms. The segregated particles near the surface of the droplet is shown to be oxidised in the early lifetime of droplet combustion shown by the darker combustion gas at 513.5 ms.

As the combustion progressed, the soot particle is shown to have agglomerated and formed a shell on the surface of the droplet at t = 788 ms. It is shown that the suspended soot was unable to be oxidised once they had agglomerated. Movement of the soot shell from t = 788 ms to t = 797.1 ms indicates that the shell is certainly located near the surface, which moves in relation with the rotation of the liquid surface. The tendency of the soot to move towards the surface of the droplet is due to its composition which made up of mostly hydrophobic element [156], that would move to area with less liquid being subjected to its surface area. As the droplet continues to evaporate and shrunk in size at t = 1049.9 ms, the shell is shown to have fully enveloped the droplet thus creating a barrier that obstructs any escaping fuel vapour through the surface.

Nucleation of the liquid fuel into a bubble of vapour within the shell is shown at t = 1079.6 ms. The bubble expands and moved towards the surface with the thinnest shell before the surface rupture shown by the more transparent area on the surface of the droplet during t = 1532.6 ms. Once the surface of the droplet ruptured during bubble breakup, a ligament of liquid fuel protruded outward thus ejects a sub-droplet outside. After the flame has extinct, residue of soot particle was left on the fibre indicating an incomplete ejection and oxidation of soot particles suspended inside the droplet during combustion process.

The dynamics of the VCD droplet combustion shown by the sequential images in Fig. 6.8 are found to be similar in each sample. However, the dynamics of soot particles inside the droplet with 0.2% and beyond cannot be observed due to their opaque appearances. Nevertheless, the occurrences of puffing and sub-droplet ejection were observed in each sample and can be identified by the fluctuation in the regression of the D^2 and FSR.

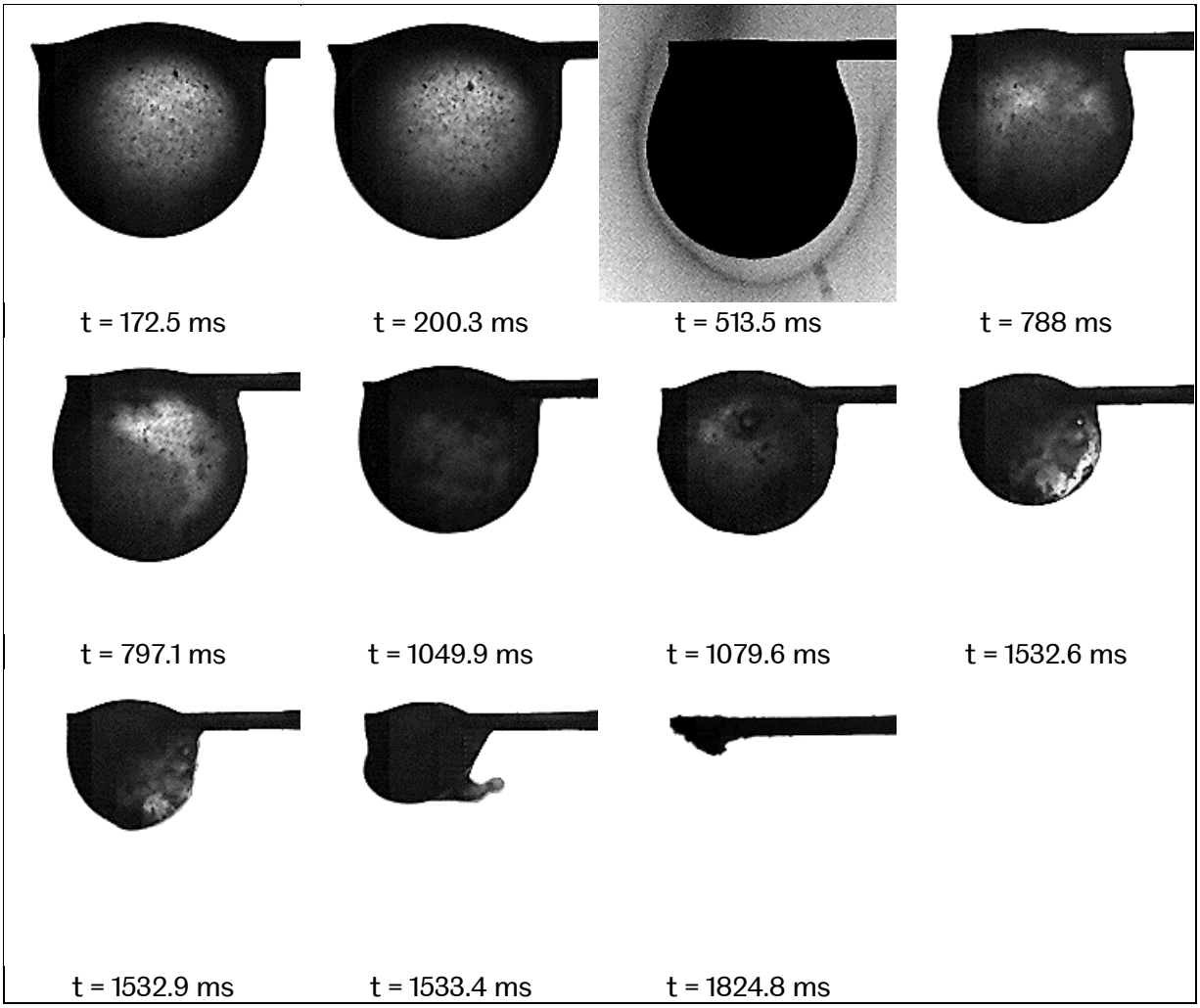

Fig. 6.8 Burning behaviour of VCD droplet with 0.05% particle loading

6.3.4 Burning Rate and Lifetime of Combustion Phases of VCD Droplet

The burning rates of the VCD droplets were measured and compared with the neat diesel shown in Fig. 6.9. Volume contamination of soot particle is found to have significantly reduce the burning rate of neat diesel in all mass loading. The burning rate reduced sharply in low particle loading of 0.05%, began to slightly increase to a peak in 0.2% particle loading and continue to reduce when the loading is increased further. From the observation made on the liquid-phase dynamics, it is known that the soot contained inside the droplet undergoes rapid agglomeration process. The agglomerated soot particles form a shell that resides on the surface of the droplet early in the lifetime of the burning VCD droplet. Due to the similar location of agglomerated soot shell to a surface-contaminated diesel droplet discussed in Section 6.2, the reduction in burning rate of the VCD droplet is well understood. The shell inhibits the liquid diffusion from the core towards the surface of the droplet which in turn supressed the evaporation rate [148].

The mass loading of soot is found to be critical at 0.2% which recorded to have the highest burning rate among other loading of the VCD droplet. As shown by the liquid-phase dynamics in Fig. 6.8, VCD droplet could undergo strong puffing and sub-droplet ejections during combustion. From the regression of the D^2 shown in Fig. 6.7(c), the fluctuation is more severe during the combustion of the VCD with 0.2% soot mass loading. This indicates the occurrences of a more rapid puffing and sub-droplet ejections which in turn making the 0.2% VCD droplet to have higher mass loss of liquid fuel through a vapour nucleation process especially during PII. Higher soot mass loadings formed a sturdier shell of agglomerated soot, obstructing any fuel vapour to be ejected through the surface. In addition, more heat is absorbed by thicker shell enveloping the droplet thus slowing the heating process within the core of the droplet. As a result, the evaporation only occurs near the formation of shell with minimal internal bubble nucleation and the evaporation progresses with less disruption that would have potentially be caused by the expansion of a nucleated vapour bubble within the core of the droplet.

Fig. 6.9 Burning rate of neat diesel and VCD droplet in various particle loadings.

Fig. 6.10 shows the lifetime of the combustion phases between the neat diesel and VCD droplet with 0.1% to 0.5% particle loadings. The bar graph shown during Phase I indicates the increase duration of droplet heating process when the soot particle loading is increased. According to Kittelson [167], the absorbance of visible light of soot is high compared to the scattering due high carbon content of the particle. Hence, the soot tends to act as a heat sink which absorb most of the heat from the flame during early combustion process. Once the temperature of the soot shell reaches the boiling point of diesel, it acts as a heat source that

starts to heat the liquid droplet toward its boiling point. This process delayed the onset of liquid heating thus prolongs its duration.

Steady burning phase of the VCD droplet is shortened to a similar duration between each loading. However, the disruptive burning behaviour during critical loading of 0.2% resulted higher deviation between repetitive measurement. It is shown that as long as there is a soot contaminating the droplet, the steady combustion shortens regardless of any particle loading, similar to the SCD droplet. In the VCD droplet combustion, the contamination only affected the duration of droplet heating (PI) and disruptive phase (PIII) when the particle mass loading is different. Longer duration of PIII is shown by the bar chart in Fig. 6.10 in low particle loading. This is caused by the occurrences of sub-droplet ejections of the VCD droplet with mass loading up to 0.2%. The soot shell in 0.1% is thinner which allows more puffing of fuel vapour and sub-droplet ejection to occur thus transitioned PII combustion to PIII earlier. With minimum mass loss of liquid fuel on the VCD droplets that has soot mass loading higher than 0.2%, their duration of disruptive phase is equivalently low.

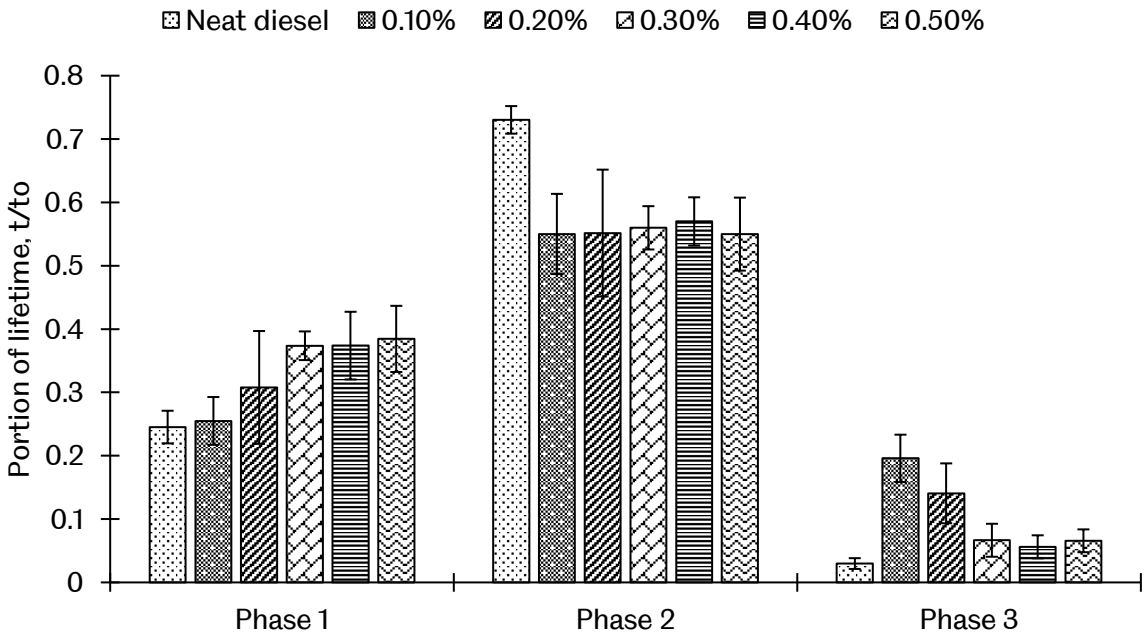

Fig. 6.10 Lifetime of combustion phases in various particle loadings of VCD

6.3.5 Liquid and Particle Ejections During Disruptive Burning

To further demonstrate the differences in disruptive burning between low and high particle loadings, sequential images of the liquid and particle ejections are presented in Fig. 6.11 and Fig. 6.12 respectively. For particle loading below critical value (0.2%), typical sub-droplet

ejection process is shown in Fig. 6.11. The combustion flame was unable to oxidise the soot particles once they are completely aggomerated thus turning the droplet into opaque in appearance when the droplet reduced to a smaller size. The sub-droplet ejection process is similar during any type of droplet combustion, which involves protrusion of liquid ligament that eventually detaches the sub-droplet upon being pinched by the surrounding pressure. Ejected sub-droplet of the VCD droplet contains soot particle inside it indicated by the colour of flame in the image at t = 1353.8 ms. The bright orange-coloured flame indicates the oxidation of soot contained inside the ejected sub-droplet. Similar ejection process occurred multiple times within the disruptive phase, further explaining the cause of the liquid mass loss that prolongs the duration of PIII.

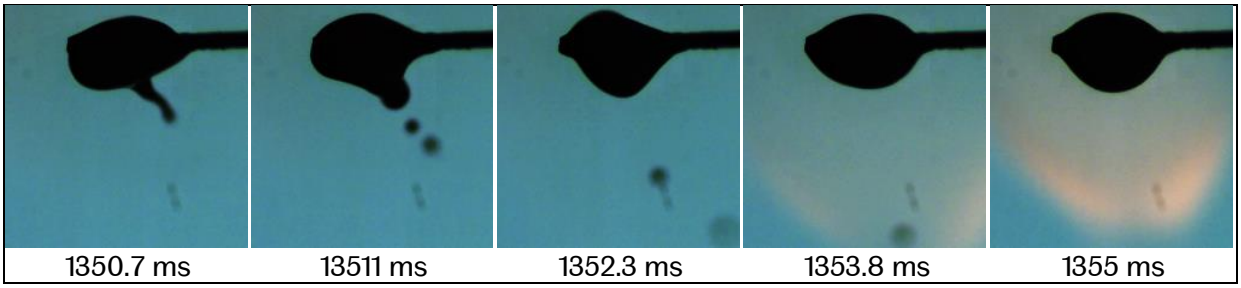

Fig. 6.11 Ejection of volatile mixture consisting liquid fuel and soot particles during the combustion of VCD droplet with 0.2% soot loading

Typical disruptive burning process of a VCD droplet with a particle loading above the critical loading is shown in Fig. 6.12. During this phase, the agglomerated soot particle is observed to be ejected through the surface of the droplet. Although the puffing intensities are lower, the soot particles contained inside the droplet is more densely packed. Slight puffing during the combustion would ejects low amount of volatile vapour together with a chunk of agglomerated soot particles outward. The certainty of the ejected matter to be a soot particle is shown in the image at t = 1457 ms, with a smouldering particle once it is transported to the flame region. Ejection of particle mildly distorts the surface of the droplet thus explains the lower intensities of fluctuation recorded in the D^2 regression of VCD droplet with loadings beyond critical of 0.2%.

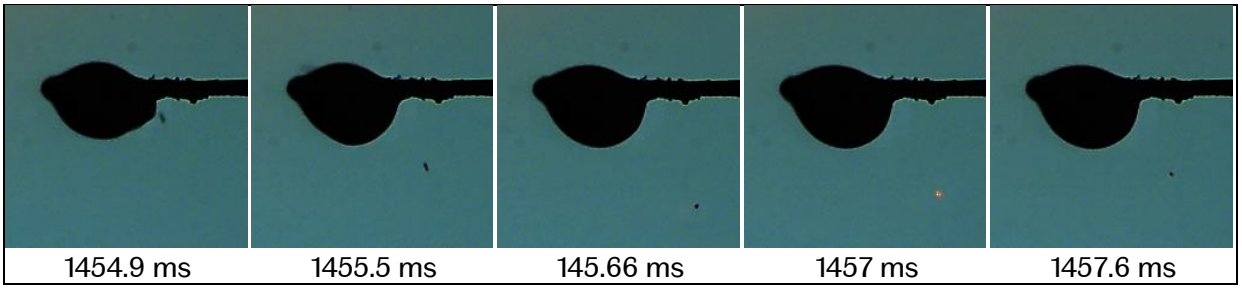

Fig. 6.12 Ejection of agglomerated soot particles during the combustion of VCD droplet with 0.3% soot loading

6.3.6 Flame Formation of VCD Droplet Combustion

Fig. 6.13 shows the comparison of the FSR between the neat diesel and VCD droplet with soot mass loading between 0.1% to 0.5%. Reduced burning rate of the VCD droplet in all loadings lowered the FSR throughout the entire droplet lifetime. Some vapour accumulation effect are present shown by the slight increase of the FSR during PII. Similar to the SCD droplet combustion, the FSR is found to be declined towards the end of droplet lifetime. Slight elevation of the FSR during sub-droplet ejection is shown for the VCD droplet with soot mass loading below critical of 0.2% indicating the gas-phase interaction between the flame of ejected sub-droplet and parent droplet. Regressions of the FSR for mass loading beyond critical are observed to have sharply decline due to non-interacting combustion between smouldering soot particle and enveloped flame of the parent droplet. With synchronised visualisation of droplet liquid-phase and flame formation conducted in present work, the decline of the burning rate and FSR is fully identified.

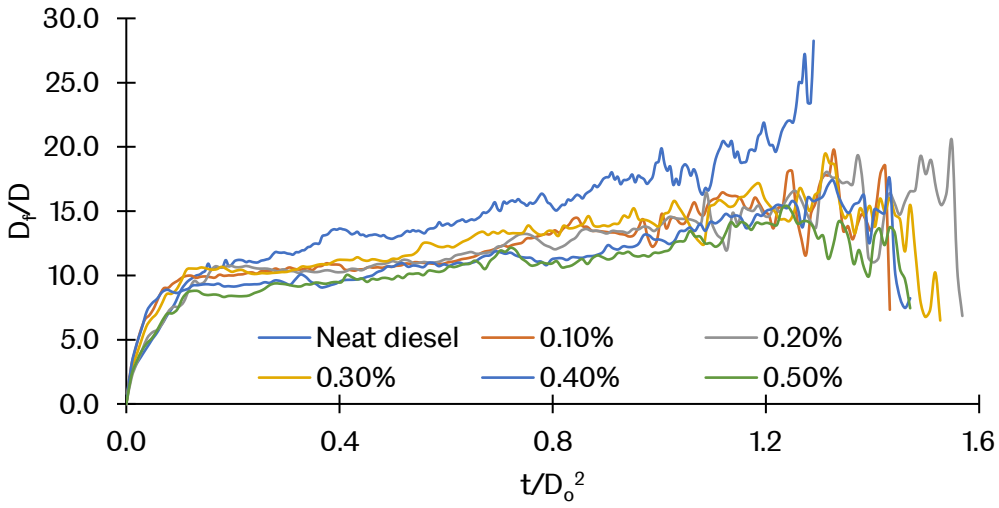

Fig. 6.13 Flame stand-off ratio comparison between neat diesel and VCD droplet

6.4 Summary

There are several key findings on the combustion behaviour of contaminated diesel droplet; worth to be mentioned in this chapter. Firstly, the contamination of soot particle on a fuel droplet during continuous combustion process is possible due to its fast reaction demonstrated in this chapter. As soon as the soot contained in the hot combustion gas contacts the surface of the droplet, it is quenched and form a shell of agglomerated soot particles that resides near the surface of the droplet. The shell of agglomerated soot particles enveloped the droplet and forms a barrier which inhibits the liquid diffusion from the core towards the surface of the droplet resulting suppressed evaporation. When the shell exists on the droplet surface prior to ignition, the burning rate of diesel is found to be reduced significantly. Higher density of surface contamination does not further reduce the burning rate but increases the magnitude of fluctuation in the regression of D^2. The formation of shell obstructs the nucleated fuel vapour to be released through the surface of the droplet thus highly distorts the surface of the droplet.

Secondly, it is found that soot has high tendency to agglomerate and forms a thin layer of shell that resides on the surface of the droplet. Having its component made up of mostly hydrophobic element, soot particles tend to move towards the surface of the droplet. The contamination retards the droplet heating process, as most of the combustion heat produced by the flame is absorbed by the agglomerated soot shell formed on the surface of the droplet. It is demonstrated that any contamination of soot either initially quenched on the surface or being evenly distributed within the droplet would significantly reduce the burning rate and highly distorts the surface of the droplet during combustion process. The slight enhancement of the burning rate in critical loading of 0.2% is due to the increased rate of liquid mass loss via multiple puffing of nucleated fuel vapour within the droplet.

With sufficient evidence between the regression of the D^2 and FSR, the transient behaviour of burning SCD and VCD droplet is identified. Morover, closer visualisation on the liquid-phase has provided further explaination on the main cause of change in combustion behaviour between combustion phases.

Chapter 7

Multi-Droplet Combustion Arranged in Horizontal Arrays

7.1 Introduction

Experimentations on the simultaneous combustion of multiple fuel droplet were done to evaluate the transient characteristics within the lifetime of evaporating droplets. Two and three droplets were simultaneously ignited and arranged horizontally. The diameter of the droplets was ensured to be equivalent prior to ignition to prevent inconsistent transient effect to occur during the combustion of each droplet such as increased sooting propensities, variable vapour accumulation effect and unequal size of flame formation.

In the combustion of closely packed fuel droplets, the oxygen depletion between the flame causes the flame to merge into one enveloped flame with a larger flame size. This in turn decreases the vaporisation rate, lower the temperature gradient within the group of flame thus prolong the combustion lifetime [170, 25]. In addition, formation of primary soot particle and precursor are within the area between the flame front and the droplet surface [77]. With a certain inter-droplet distance, the formed soot particle around the droplet would have the possibility to continuously contact and contaminated the nearby droplet. It is determined in Chapter 6 that contamination of soot on the droplet surface would reduce the burning rate and promotes instabilities in a burning droplet. Under these reasons, a closer evaluation on the change in the burning rate, surface stabilities and lifetime of a fuel droplet need to be done to determine and differentiate between the effect of oxygen starvation, fuel vapour accumulation and soot contamination. Hence, a diesel fuel with high sooting propensity and non-sooting ethanol were selected to be experimented in this chapter to compare the additional effect of soot contamination during a multi-droplet combustion.

The results from this chapter would provide a comprehensive analysis on the combustion behaviour of fuel droplets during multi-droplet combustion subjected to two prevalent effects namely; oxygen starvation and soot contamination. Furthermore, the results from the present work would provide a new insight on the effect of soot contamination to the transient behaviour during the combustion of closely packed fuel droplets.

7.2 Initial Condition of Multi-droplet Arrangement Prior to Ignition

Experimentations on the multi-droplet combustion were done on two and three droplets arranged in a horizontal array. Figure 7.1 shows the typical arrangement of three droplets prior to ignition. Droplet sizes were ensured to be 1 $\pm$ 0.05 mm before the ignition was made. The multi-droplet distance, L is the distance between the droplet centres of adjacent droplet. In three droplet arrangements, the distances were change symmetrically between right and left droplet in accordance to the centre droplet.

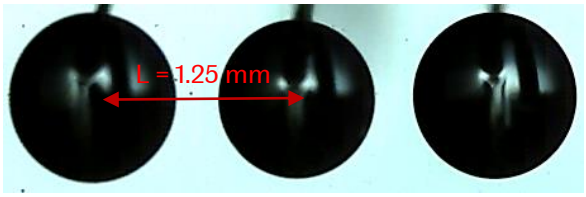

Fig. 7.1 Initial condition of three diesel droplet arranged in horizontal array.

7.3 Evolution of Squared Droplet Diameter During Multi-Droplet Combustion

Fig. 7.2 shows the normalised regression of D^2 in each normalised inter-droplet distance, L/D_o during multi-droplet combustion of diesel. In the combustion of two diesel droplet in array shown in Fig. 7.2 (a), a close inter-droplet distance of 1.25 and 1.50 shows a significant fluctuation of D^2 during the disruptive burning phase. The regression began to be steadier when L/D_o increased between 2.00 and 3.50 and started to fluctuate again in 4.00 and beyond. Closer examination on the D^2 shows that the regression of the inter-droplet distance between 2.00 and 3.50 transitioned to PII earlier and believed to be caused by rapid process of droplet heating. However, the magnitude of fluctuation in D^2 during PIII is shown to be reduced in proportion to the increase of L/Do. This indicates that a closer inter-droplet distance has earlier occurrences with higher strength of puffing and sub-droplet ejection. Normalised regression of D^2 from the combustion of three diesel droplets in array is shown in Fig. 7.2 (b). Compared with the two burning droplets in array, the D^2 fluctuation of close L/D_o distance (1.25) shows stronger with earlier onset of puffing and sub-droplet ejections. Changes of the gradient in D^2 is shown to be proportionally non-linear when L/D^o is increased with significant change in gradient during close multi-droplet proximity between $1.25 < L/Do < 3.50$.

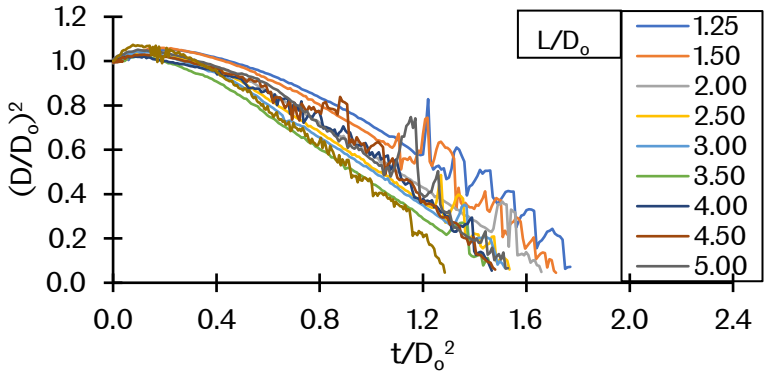

(a)

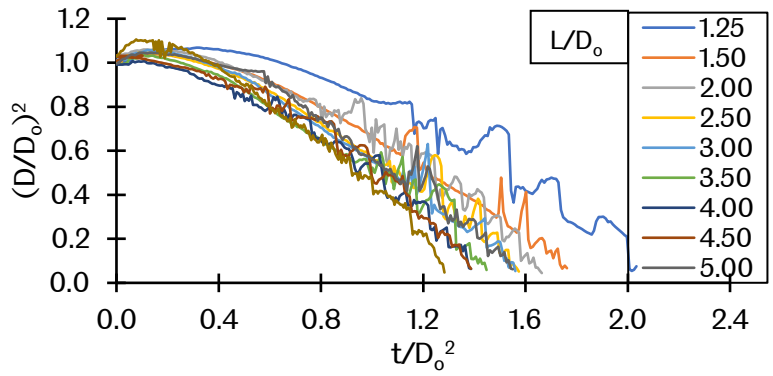

(b)

Fig. 7.2 Normalised regression of D^2 of each normalised inter-droplet distance, L/D_o during multi-droplet combustion of (a) two diesel droplets in array and (b) three diesel droplets in array

Figure 7.3 shows the normalised regression of D^2 in each normalised inter-droplet distance, L/D_o during multi-droplet combustion of ethanol. Shown in Fig. 7.3 (a), changes of D^2 gradient during two interacting droplets is linearly proportional to the change of inter-droplet distance between 1.25 < L/Do < 2.50. However, gas-phase interactions do not have any effect on the disruptive burning of ethanol. Fluctuations of D^2 are very low and comparably similar between each inter-droplet distance. Furthermore, the fluctuation of D^2 in PIII remains unchanged even with increased gas-phase interactions during the combustion of three ethanol droplets shown in Fig. 7.3 (b).

With similar trend of change in D^2 gradient observed between two and three arranged droplets in both fuels, it is certain that the centre droplet in a three droplet arrays have higher effect of oxygen starvation compared to two droplet arrays. These observations are in accordance with the findings discussed by Miyasaka and Law [82] who states that the gas-phase interference to the middle droplet is more severe compared to the side droplet during the combustion of three droplet in array. In two interacting droplets, each droplet having half of the droplet area exposed to the ambient air. This allows more oxidiser to be diffused towards the reaction zone thus enhances the combustion process. Also, the gas-phase

interaction area between droplets only affecting on one side of the droplet, thus influencing the combustion to behave proportionally linear with the change of inter-droplet distance.

Droplet interactions during the diesel droplet combustion significantly affected the stability of regressing droplet during PIII but has no effect on the ethanol. It is believed that the soot particles contained in the hot combustion gas would have contaminate the neighbouring droplet, contributing to the increased occurrences of puffing and sub-droplet ejections. According to Randolph and Law [52], incomplete soot oxidation is observed in strong interacting conditions of closely spaced droplets. This in turn would increase the possibility of interacting droplets to contaminate each other within a certain effective inter-droplet distance due to a higher soot emission during the combustion. The possibility of contamination is in agreeable relevance with the effects imposed during PIII. Presence of soot particles on the droplet surface would result multiple occurrences of heterogeneous nucleation of vapour bubble inside the droplet thus fluctuates the regression of D^2 upon a surface rupture. On the other hand, the contamination mechanics does not occur during multi-droplet combustion of ethanol due to its non-sooting properties when burns in atmospheric pressure [26, 27, 124, 140]; thus explains the unchanged disruptive burning of ethanol in any inter-droplet distances.

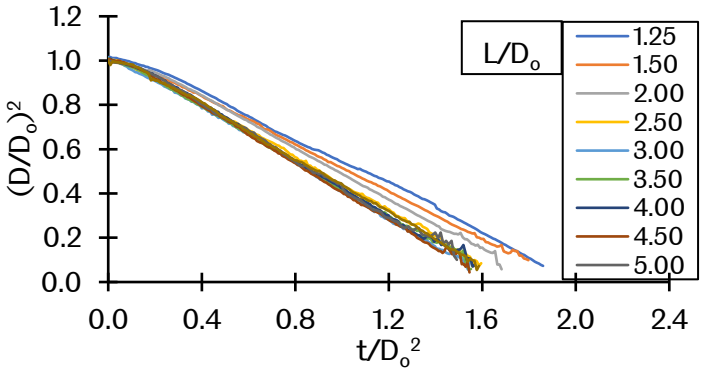

(a)

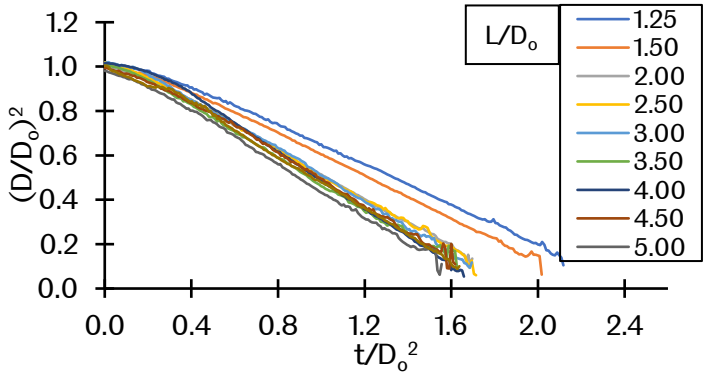

(b)

Fig. 7.3 Normalised regression of D^2 of each normalised inter-droplet distance, L/D_o during multi-droplet combustion of (a) two ethanol droplets and (b) three ethanol droplets

7.4 Visualisation of Soot Contamination During the Combustion of Interacting Diesel Droplets

Liquid-phase visualisations were done on the imaged droplet during interacting multi-droplet combustions to observe the contamination process and effects. Fig. 7.4 shows the liquid-phase of the imaged diesel and ethanol droplet during multi-droplet combustion with inter-droplet distances varied from the closest (L/Do = 1.25), the furthest (L/Do = 5.00) to infinity (isolated single droplet). Images from three interacting droplet combustion were presented in the figure for clearer provisions of the contamination effects. The soot contaminating the droplet is observed to be denser when the inter-droplet distance of diesel is closer. Very little amount of soot particle is observed to be present in the isolated droplet due to self-contamination effect. In the ethanol droplet, there is no observable soot contained in the droplet during PIII shown in the figure; and the condition is similar in each inter-droplet distance.

The onset of the disruptive burning is due to the breakup of bubble emerged from the heterogeneous nucleation induced by the presence of solid soot particle on the surface of the droplet. Closer inter-droplet distance experienced much earlier bubble rupture shown by the images in the second row of Fig. 7.4. This promotes early fluctuation of D^2 regression during the normalised lifetime of 0.50, 0.69, 0.74 and 0.78 in case A, B, C and D respectively. Larger size of bubble near surface rupture is shown in case A due to the mergence of high number of vapour bubbles. The size of bubble near surface rupture in puffing process is observed to be smaller as the inter-droplet distance are further away. As a result, the bubble breakup fluctuates the regression of D^2 with lower magnitude when the interactions between the droplet reduces. In the case of ethanol droplet, multiple smaller bubble was observed to have form within the droplet shortly before transitioned to PIII. Due to the tendency of ethanol to evaporate at room temperature, a region of stratified fuel vapour is formed with the surrounding air. During ignition, the igniter added an additional energy source to the rich stratified mixture of fuel vapour and oxidiser which in turn rapidly accelerates fuel pyrolysis, forming some soot in the process [124].

Shortly after the breakup of nucleated bubble, puffing of fuel vapour follows. Closely packed diesel droplets (L/Do = 1.25) ejects some amount of soot during puffing, indicating higher amount of soot contained within the droplet through continuous contamination process from the neighbouring droplets. Less contaminated droplet in higher inter-droplet distance ejects mostly fuel vapour during the puffing process shown by the third-row images

in Fig. 7.4. The bubble ruptures and puffing processes repeatedly occurred during Phase II before transitioned to Phase III which explains the continuous fluctuation of D^2 regression shown in the Fig. 7.2. On the other hand, puffing of ethanol is slightly different compared to the diesel droplet. Forces from the liquid push upon surface rupture able to completely ejects the soot contained inside the droplet with ease due to low surface tension of ethanol thus cleanses the droplet. This process was observed to be occurring once in every interacting condition of ethanol droplet and determined to be the main cause of slight elevation in the D^2 during the onset of PIII.

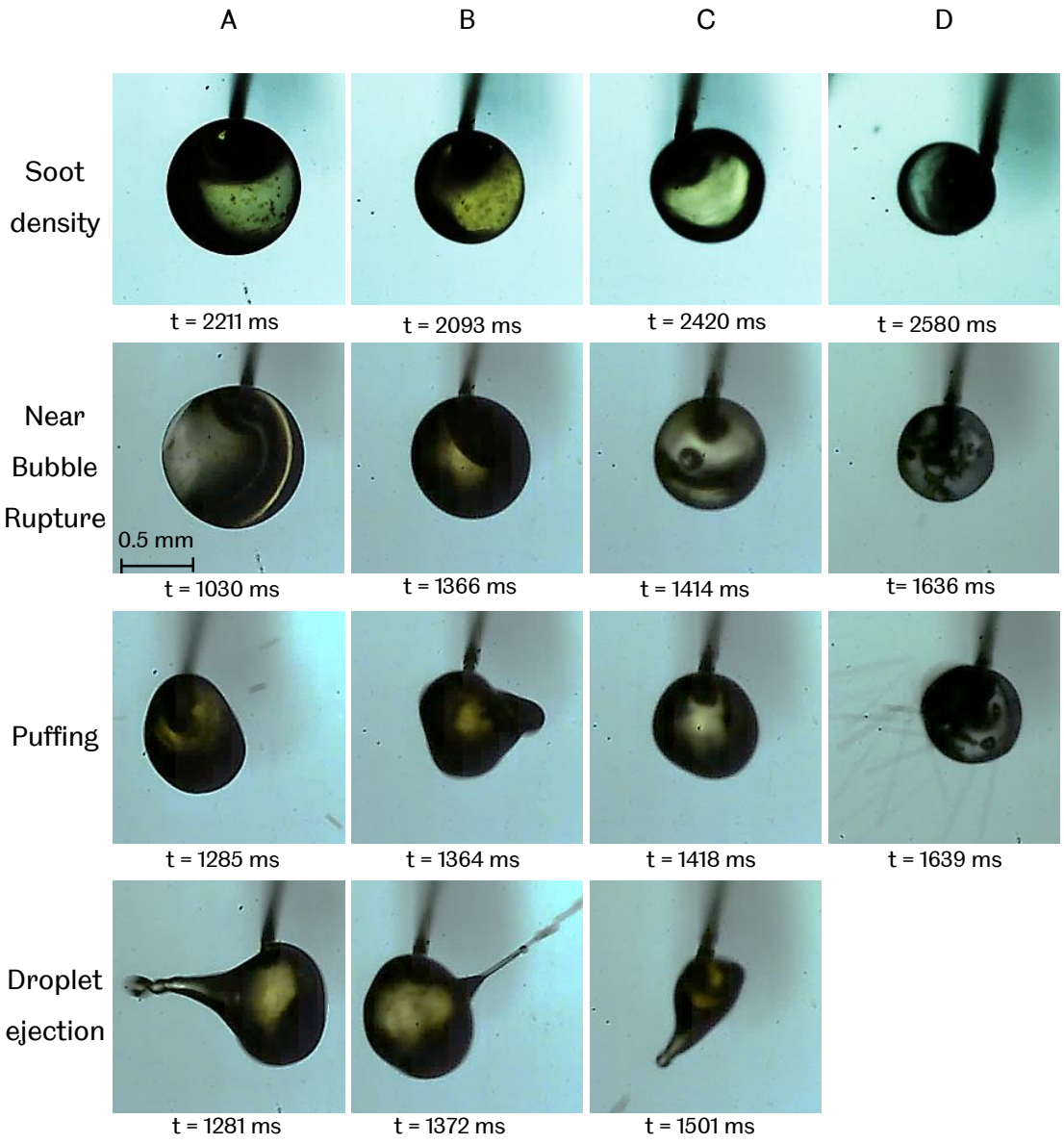

Fig. 7.4 Liquid-phase visualisation on multi-droplet combustion; (a) diesel with L/D_o = 1.25, (b) diesel with L/D_o = 5.00, (c) diesel with L/D_o = ∞ and (d) ethanol with L/D_o = 1.25

The combustion progresses with increasing amount of soot from the neighbouring droplet quenched on the surface of the imaged droplet. As a result, liquid diffusion from the core to the surface of the droplet reduces at increasing rate. Higher amount of soot particles induced multiple heterogeneous nucleation of vapour bubble that would eventually rupture the surface of the droplet with a stronger liquid push that ejects small sized sub-droplets from the parent droplet. Sudden loss of mass transitioned the combustion phase from PII to PIII with the regression of D^2 being deviated from the steady surface regression stated by D^2-law. The disruptive burning process is similar to the isolated fuel droplet contaminated by soot discussed in chapter 6 and well published by Rasid and Zhang [97]. However, the effect of soot contamination in interacting combustion of multiple droplet to the disruptive burning is less effective compared to the work done in previous chapter due to their difference in contamination rate and process. Horizontal arrangements of multiple interacting droplets do not contaminate nearby droplet heavily as most of the soot particles within the hot combustion gas moves upward. Only some portion of soot produced during fuel pyrolysis are continuously contaminating the droplet when the rich fuel region within the flame contacted the surface of nearby droplet. Furthermore, the arranged multi-droplet was in neat condition prior to ignition. Nevertheless, the disruptive effect observed in the regression of D^2 is well associated with the liquid-phase dynamics presented in present work.

7.5 Burning Rate and Lifetime of Multi-Droplet Combustion

Quantitative measurements were done on the burning rate and lifetime of the multi-droplet combustion of diesel and ethanol droplet to identify the critical distance of a strong gas-phase interaction during the combustion. Fig. 7.5 shows the burning rate and burning rate reduction during the combustion of two interacting droplet in comparison with single isolated neat diesel and ethanol droplet. The burning rate is shown to increase in two sections of linear line with slight difference in gradient for both fuel droplet when the inter-droplet distance is increased. It is shown that the first linear section of the ethanol is shorter; extending to $L/D_o = 2$ compared to the diesel which extended to $L/D_o = 3.50$.

The transition of a critical gas-phase interaction is further evaluated by examining the change in the total droplet lifetime shown in Fig. 7.6 (a) for the combustion of two interacting droplets. It is well established that the lifetime of droplet increases when there is an interaction of gas-phase during the combustion of closely packed droplets [21] and the effect is significant with strongly interacting droplets [108]. It is shown that the total lifetime of the

diesel and ethanol droplet reduces steeply until L/D_o = 3.50 and L/D_o = 2.00 respectively. The sudden change in the lifetime reduction shows the same critical inter-droplet distance with the measurement of the burning rate thus confirming this finding.

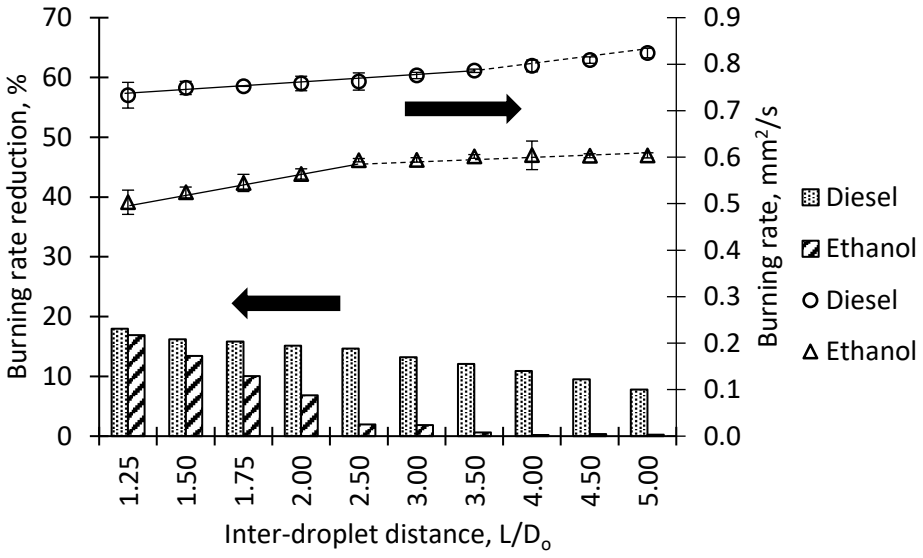

Fig.7.5 Burning rate and burning rate reduction of two interacting diesel and ethanol droplet.

The sudden change of gradient is assumed to be the transition from a strong towards weak gas-phase interaction. In strongly interacting droplet, the droplet burns in one large enveloping flame with significantly large flame size [21, 23, 24]. Starvation of oxidiser causes the flame to enlarge, seeking available oxidiser in larger area further away from the droplet [72]. When the position of the flame edge is further away from the surface of the droplet, the radiative heat transfer from the flame towards the surface of the droplet is lower and the rate of radiative heat loss from the flame to the surrounding is higher [28, 59]. As a result, the heat needed for droplet heating reduces which in turn supressing the evaporation rate. Beyond the critical distance of strong gas-phase interaction, the droplet burns with an individual flame with a smaller flame size. The deviation of D^2 regression from D^2-law is still present beyond this point but with lower rate. Additionally, the gas-phase interaction of two burning ethanol droplet is measured to be relatively short and completely burns with equivalent burning rate of its isolated counterpart when $L/D_o > 2.00$.

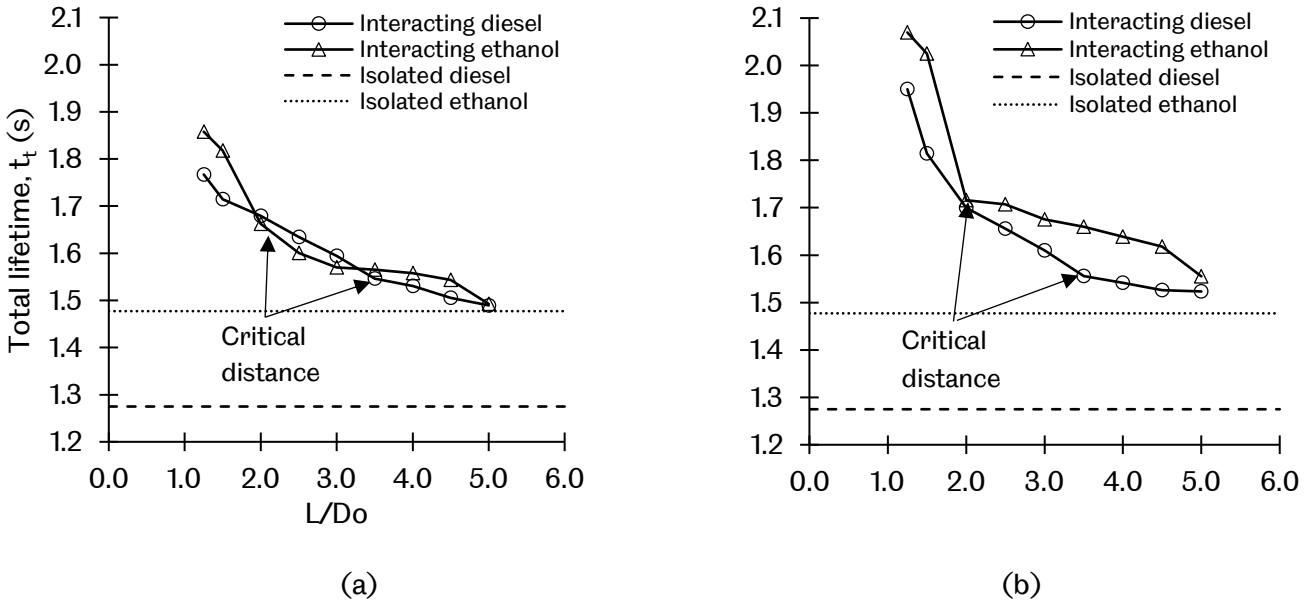

Fig. 7.6 Total lifetime of multi-droplet combustion with (a) two interacting droplets and (b) three interacting droplets

To further analyse the critical distance of strongly interacting droplet, measurements of the burning rate and burning rate reduction were made on the combustion of three interacting diesel and ethanol droplet; and it is shown in Fig. 7.7. The transition from a strong to weak gas-phase interaction is clearer for the ethanol droplet, with the same critical distance of $L/D_o = 2.00$. However, the critical transition is not clear for the diesel droplet. This is believed to be cause by the complex transient evaporation process of diesel, which have an additional interferences of prolonged droplet heating and high rate of the fuel vapour accumulation effect. From the scattering of the burning rate reduction, it is observed that the critical gas-phase interaction is within the range of $2.50 < L/D_o < 3.50$. On the other hand, the gas-phase interaction of the ethanol is further beyond $L/D_o > 5.00$ in three droplet combustion. This indicates the role of the fuel vapour accumulation effect. More evaporated fuel from neighbouring droplet interferes with the reaction zone of the droplet positioned in the centre, thus increases the fuel vapour accumulated within the flame reaction zone [108].

From the measurement done on the burning rate, it is determined that the inter-droplet distance of critical gas-phase interaction of fuel remains the same regardless of interacting droplet numbers. However, higher number of interacting droplets in multi-droplet combustion increases the effective distance due to a higher amount of fuel accumulated in the reaction zone in addition of further starvation of oxidiser. Under this reason, it is confirmed that the volatility of fuel plays an important role during the simultaneous combustion of multiple droplets. Lower volatility fuel such as diesel would increase the

effective distance of the critical gas-phase interaction as well as the gas-phase interaction as a whole due to a higher effect of the fuel vapour accumulation within the area between the droplet surface and the flame zone [88].

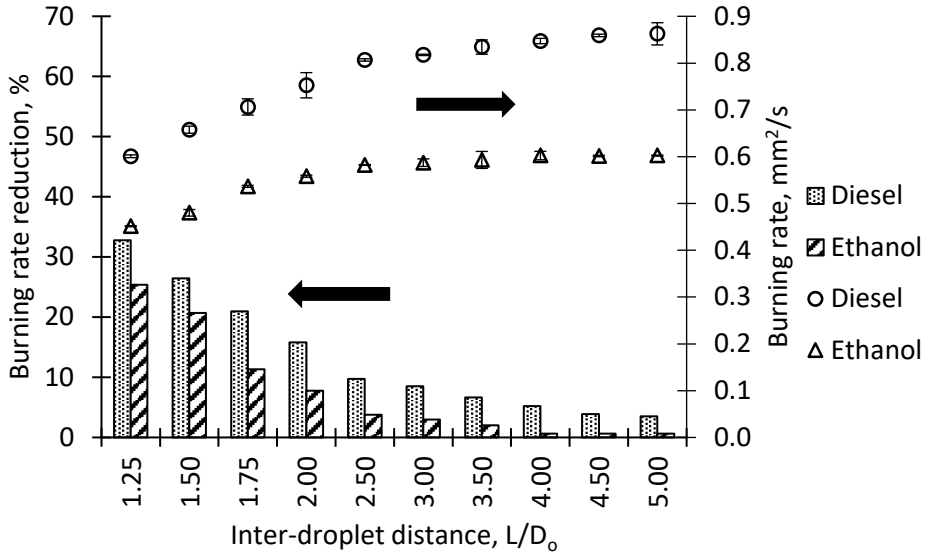

Fig. 7.7 Burning rate and burning rate reduction of three interacting diesel and ethanol droplet.

7.6 Combustion Phases of Interacting Multi-droplet Combustion

Flame formation in a cluster of droplets is larger, and because of that the droplet heating duration becomes longer due to the radiative heat loss of a larger flame formation [170]. Under this reason the droplet heating (PI) is found to be longer when the separation distance between the droplet reduces and the effect is similar during the combustion of two and three droplet in array shown in Fig. 7.8 (a) and 7.8 (b) respectively. However, the duration of droplet heating is observed to be reduced towards the critical gas-phase interaction distance and raises again beyond the critical point. This effect if more prevalent during the combustion of two interacting droplets. Within optimum range of separation distance, the effect of buoyancy would enhance the burning rate of the interacting droplets. It is known that too close proximity of droplet reduces the evaporation due to a higher decline in radiative and conductive heat transfer even though the effect of buoyancy is improved. When the distance is too far apart, the effect of natural convection is minimum [56]. Furthermore, Miyasaka and Law [82] stated that buoyancy is enhanced during interaction of two burning droplet with better interior motion which in turn enhances the heat transfer within the droplet hence shortened the heating period.

For the result obtained in the present work, the optimum distance of improved buoyancy is found to be the same as the critical gas-phase interaction. Within the critical distance of gas-phase interaction determined in the present work, the flame began to separate, caused by the effect of buoyancy flowing in between the flame zone of each droplet. In addition, the droplet is heated by the flame of neighbouring droplet due to the closer separated edge of flame. Under this reason, the shortened duration of droplet heating is well explained. However, the enhanced effect of droplet heating only effects the combustion of three droplet mildly especially on the diesel droplets. With the more revealing effect on ethanol, it is believed that the buoyancy effect is diminished by the effect of fuel vapour accumulation. During interaction of droplets, cooling effect is expected due to the duplication of heat sink and evaporation of more fuel vapour that cools the surrounding gas phase [108]. Diesel has lower volatility with high tendency of evaporated vapour to accumulate around the droplet resulting higher cooling effect to the droplet thus prolonged the droplet heating phase.

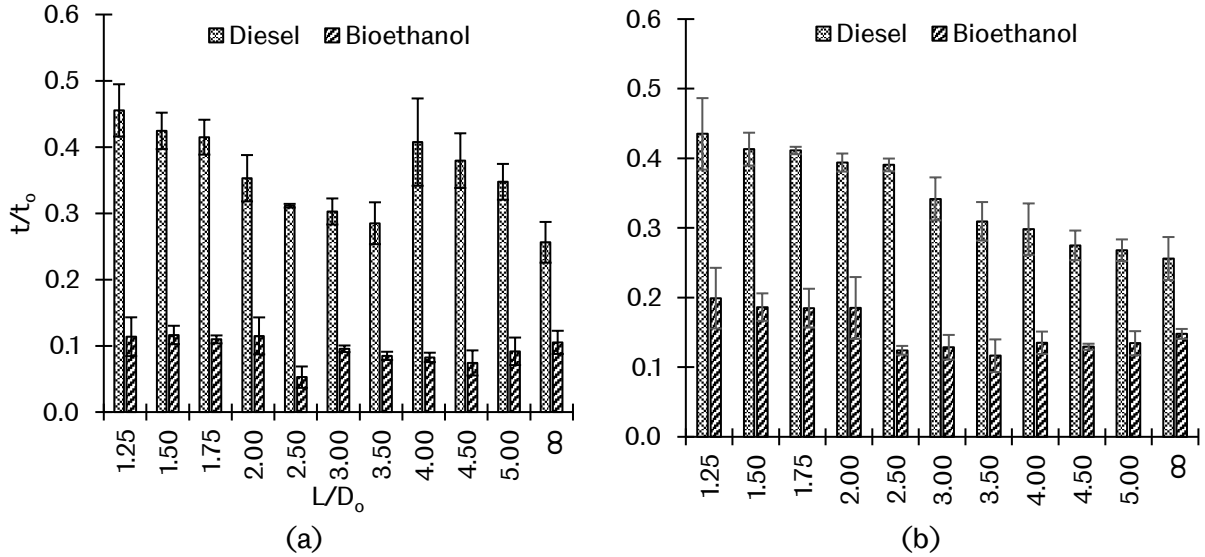

Fig. 7.8 Lifetime of droplet heating (PI) in the combustion of (a) two interacting droplets and (b) three interacting droplets

Flame images of interacting droplet was visualised to further identify the critical inter-droplet distance of the gas-phase interaction. Fig. 7.9 shows the flame formation of diesel burning in two (first row) and three (second row) droplets in horizontal array. In both case, it is shown that the droplets burns in merged flame that envelopes all burning droplet. In critical distance of 3.50 determined by the examination on the burning rate and total lifetime of diesel droplet, the flame starts to separate and a faint line of flame separation is observed.

Increasing the inter-droplet distance beyonf the critical distance would further separate the flame and shown by L/D_o = 5.00 in the figure. During critical distance, the distance of neigbouring flame edge is minimum, with natural convection separating the flame together with increased amount of oxidiser. Combination of both increased supply of the oxidiser and heat from the neighbouring droplet would heat the droplet rapidly, thus explains the optimum droplet heating distance described in Fig. 7.8.

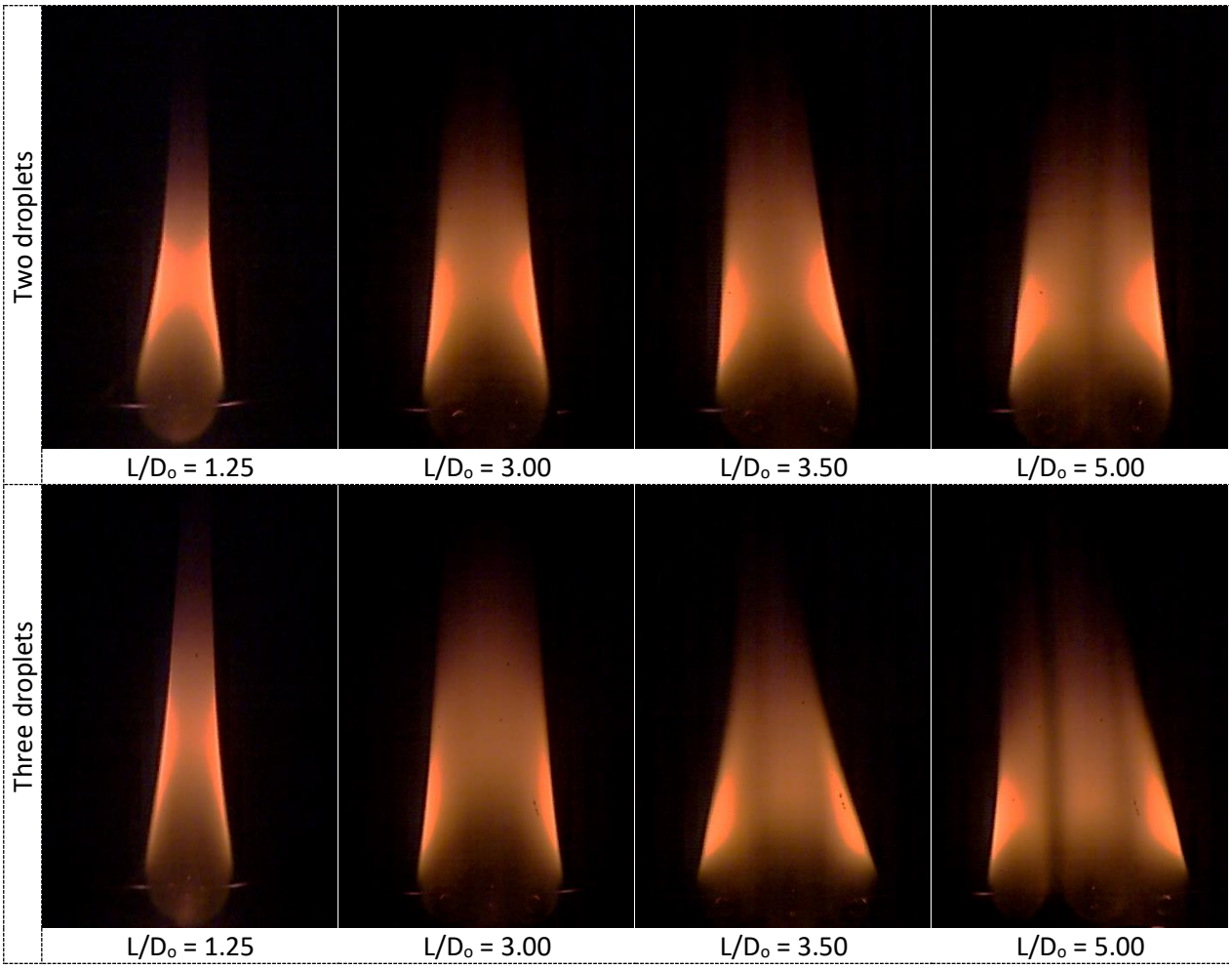

Fig. 7.9 Flame formation of interacting diesel droplet

Fig. 7.10 shows the disruptive phase (PIII) during the combustion of multiple fuel droplet in various inter-droplet distance. Closer inter-droplet distance increases the lifetime of the disruptive phase during the combustion of diesel droplet in both two and three simultaneous burning of droplet shown in Fig. 7.10 (a) and Fig. 7.10 (b) respectively. These behaviours are expected due to a higher effect of fuel vapour accumulation. The accumulation effect increases the residence time of fuel vapour [184] thus increasing the sooting propensity of the combustion [109] that would eventually contaminates the droplet. In

addition, findings from the liquid-phase visualisation done in present work shows that there is definitely a continuous process of soot produced by the neighbouring droplet to contaminate the surface of the imaged droplet. The contamination disrupted the liquid surface significantly with earlier onset of PIII. Higher mass loss of droplet due to frequent sub-droplet ejection deviated the surface regression from D^2-law thus prolonged the disruptive phase.

On the other hand, the duration of disruptive phase in multiple combustion of ethanol is observed to be fairly unaffected by the change of the inter-droplet distance. It is known that the effect of fuel vapour accumulation is still present shown by the increase of effective distance of gas-phase interaction in Fig. 7.7 beyond L/D_o = 5. However, there were no significant contamination of soot observed during the combustion of ethanol except during the rapid pyrolysis upon ignition. Under this comparison, it is determined that the effect of soot contamination is significant to the reduction of burning rate (reduced liquid diffusion) as well as prolonged disruptive burning during the combustion of fuel with high sooting propensities. Although the exact portion of detrimental effect from the soot contamination is unable to be quantified in the present work, it is certain that the effect plays a significant role in the reduction of the burning rate and promotes instabilities during the combustion of closely packed fuel droplet.

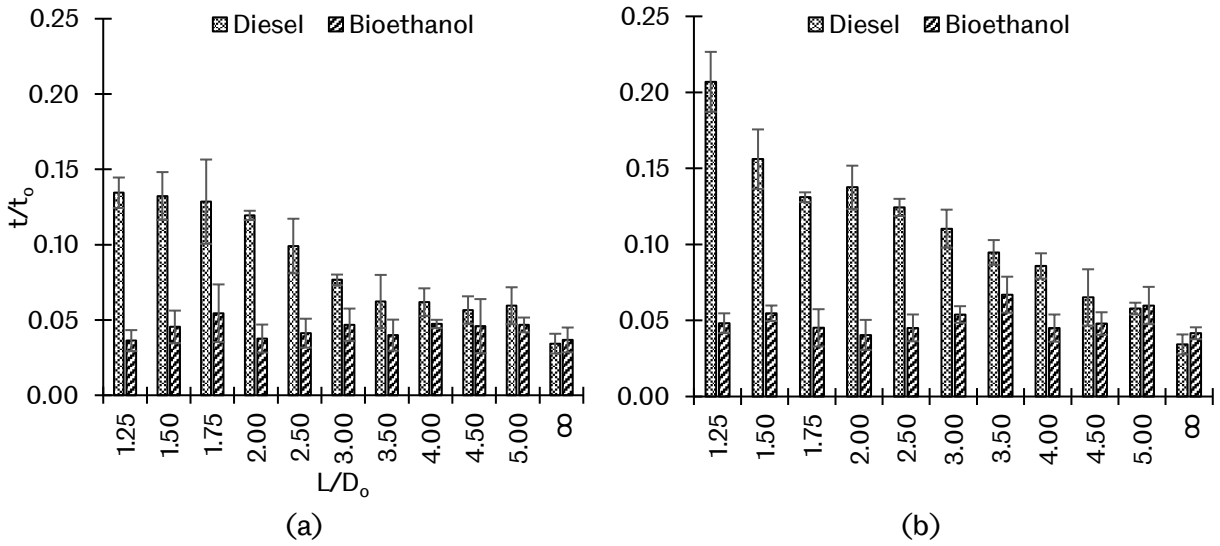

Fig. 7.10 Lifetime of disruptive phase (PIII) in the combustion of (a) two interacting droplets and (b) three interacting droplets

7.7 Summary

The evaluation made on the combustion of closely packed fuel droplets in this chapter provided several unique findings within the scope of a multi-droplet combustion. It is found that there is a specific critical inter-droplet distance of strong gas-phase interaction which would form one large enveloping flame around burning droplets. Within this critical distance, the burning rate is significantly reduced due to the enhanced heat loss from the enlarged flame caused by the starvation of oxygen. Also, it is found that the effective inter-droplet distance for optimised droplet heating falls within the critical gas-phase interaction distance. The droplet heating is shorter when the separation distance approaches the critical value for both tested fuels and increased beyond this distance. This is explained by the enhanced effect of oxygen diffusion by the buoyancy and additional droplet heating by the edge of neighbouring flame. Once the droplet is separated further, the additional heat provided by the neighbouring droplet reduces thus increases the droplet heating period.

The critical distance of gas-phase interaction does not affect the lifetime of the disruptive phase shown by the proportionally linear relation between the lifetime of disruptive phase and inter-droplet distance. It is determined that the duration of disruptive phase is highly dependent on the soot contamination process. Larger flame increases the residence time of accumulated vapour thus increases the sooting propensities. The soot formed within the hot combustion gas would eventually pushed towards the surface of the droplet during self-contamination process. Furthermore, more soot particles from the side droplet is observed to contaminate the imaged droplet when the inter-droplet distance is closer. The effect is clearly shown by the fluctuation in the regression of D^2; with high magnitude and earlier onset of disruptive burning when the inter-droplet distance was reduced. On the other hand, the duration of disruptive burning of non-sooting ethanol remains fairly unchanged in each inter-droplet distance, further demonstrates the significant effect of soot contamination to the combustion stability.

Chapter 8

Conclusions and Future Works

8.1 Conclusions

The work presented in this thesis mainly focuses on the transient and unsteady condition during the evaporation of fuel droplet. The type of fuel selected in this work is based on their practical use in the combustion of fuel spray. In chapter 4, the experimentation was designed so that it highlights any significant transient combustion behaviour that causes the discrepancies between the predicted model and actual combustion characteristics of evaporating fuel droplet. Experimentation continues to explore the causes of disruptive effects that occurred during the combustion of multicomponent droplet which are not possible to be predicted by a quasi-steady model, specifically on emulsion fuel droplet presented in Chapter 5. Chapter 6 further explores the combustion characteristics of fuel droplet with a possibility of being contaminated by soot during mixing in actual combustion process. Finally, Chapter 7 further simulates the combustion of fuel droplet that burns in group. Although the combustion process is more complex during the combustion of closely packed fuel droplets, analyses done in the present work focuses on categorising the main cause of transient burning behaviour throughout the lifetime of the fuel droplet.

The effect of droplet heating can be clearly evaluated by measuring the droplet surface regression. During transient droplet heating, longer duration taken for a fuel droplet to reach its boiling point would prolong its effect. It is demonstrated that a fuel with high boiling point would extend the period of droplet heating. This effect is further explained by soot contamination effect. Soot resides within the droplet or on the surface of the droplet absorbs most of the heat transferred to the droplet during the early lifetime of droplet. This in turn delayed the droplet heating towards its boiling point. Furthermore, interaction between multi-droplet combustion pushes the flame away from the droplet even further. This in turn in increases the rate of heat loss from the flame that would otherwise used for droplet heating. With all effects demonstrated in the present work, the main cause of prolonged droplet heating is determined to be the effect of delayed temperature increase towards the

boiling point of fuel. Longer period of droplet heating deviates the experimental and predicted result even further.

On the other hand, fuel vapour accumulation can be clearly evaluated by measuring the flame stand-of ratio of a burning droplet. The effect of fuel vapour accumulation is highly depended on the evaporation rate and volatility of fuel. It is found that although the evaporation rate of emulsion fuels is higher than a neat diesel, their volatility is much higher. This in turn increases the vapour consumption rate thus diminishes the vapour accumulation effect. Contamination of soot is found to have suppressed the evaporation rate. Although the volatility of contaminated diesel remained fairly low, the evaporation rate reduced significantly. This in turn lowers the fuel accumulation effect due to a reduced evaporation rate. During multi-droplet combustion, the evaporation rate of combined droplets is much higher which in turn increases the fuel vapour accumulation effect.

Optical setups were made to suit the testing requirements. In order to observe clear droplet dynamics for the identification of transient burning behaviour, the images of droplet liquid-phase were taken with high spatial resolution of 130 pixel/mm and temporal resolution between 10,000 to 20,000 fps depending on the test conditions. Furthermore, simplified experimental setup done in present work produced high repeatability of quantitative measurements which enables the identification of combustion phases that can be related to the disruptive behaviour of droplet liquid-phase. It is found that the fuel types and imaging setups done were sufficient to reach the objectives in the present work. Significant findings from each chapter of this thesis are highlighted in the next sub-section.

8.1.1 Evaporation Behaviour of Isolated Neat Fuel Droplet

1. The transient effect of droplet heating is identified to be the non-linear regression of squared droplet diameter, D^2 during early lifetime of droplet evaporation. During this period, the droplet undergoes thermal expansion and at the same time gradually increase its evaporation rate. Once the D^2 regression assumes linear regression, the droplet heating period ends. This transient period is clearly shown by the curve in the D^2 regression upon droplet ignition. In short, the identification of droplet heating effect can be made by evaluating the regression of D^2; generally categorised as the *transient liquid-phase effect.*

2. The effect of droplet heating is significant, and it is crucial to be considered during numerical prediction of evaporating fuel droplet. Longer period of droplet heating further increase the discrepancies between the experimental results and numerical prediction. Furthermore, the classical quasi-steady model implemented in the present work has very low accuracy when the evaporating temperatures are low due to the its underprediction of heat transfer rate within the fuel droplet.

3. The duration of droplet heating highly depended on the volatility of fuel. For droplet with low boiling point, the regression of droplet surface assumes linear faster even though the droplet heating still progressing. As long as the surface layer is heated to a boiling at high rate, the subsequent heating of droplet interior required less heating for evaporation thus satisfies the requirement of D^2-law.

4. Increasing trends of flame stand-off ratio, FSR indicates the increased amount of vapour accumulated between the flame and the surface of the droplet. During this period, the rate of evaporated vapour is higher than the rate of vapour being consumed by the flame which in turn pushes the flame edge away from the surface of the droplet. High vapour accumulation effect is determined during the end of droplet lifetime, with FSR approaching infinity indicating there is still vapour being consumed although the droplet has been fully evaporated. Identifications of fuel vapour accumulation effect were made by evaluating the regression of FSR. Hence, the transient effect of fuel vapour accumulation is generally recognised as the *transient gas-phase effect*.

5. Fuel vapour accumulation effect prolongs the residence time of accumulated vapour surrounding the droplet which in turn increases the sooting propensity during combustion of fuel droplet. Thermophoretic force induced by the heat from the flame would eventually pushes the denser formation of soot towards the droplet surface, causing the droplet to be contaminated by the soot through self-contamination process.

6. Strong fuel vapour accumulation effect causes the droplet surface to regress disruptively due to the more frequent and stronger puffing. The duration of steady surface regression was found to be shortened and transitioned to the disruptive burning earlier throughout the lifetime of evaporating droplet.

8.1.2 Evaporation and Burning of Emulsion Fuel Droplet

1. Evaporation behaviours of emulsion droplet is well demonstrated in present work. It is found that the component with a lower boiling point evaporates first through a process termed as *preferential evaporation*. The volatile component has tendency to diffuse towards the surface of the droplet during early lifetime of the evaporating droplet. The surface regresses with the evaporation of less volatile component once the volatile component is almost completely evaporated.

2. Dispersed liquid of the more volatile component that is trapped inside the droplet homogeneously nucleates into a vapour bubble when it is heated beyond its boiling point. The bubble expands and eventually ruptured the surface of the droplet as a mean of escape. Higher additive loading of the more volatile component promotes higher number of bubbles to be nucleated inside the droplet and merges into a larger sized bubble before bursting through the surface. However, the bubble breakup process is highly dependent on the surface tension of the emulsion. Ethanol has lower surface tension compared to diesel and water. As a result, the droplet surface undergoes multiple bubble breakup in smaller sizes during the combustion of emulsion fuel with high ethanol volume.

3. Sub-droplet ejection processes were determined by observing the sequential images during the disruptive burning. It is observed that the bubble breakup creates a low-pressure region which draws the liquid fuel towards the bottom of the periphery. The push from the flowing liquid protruded a ligament outward with a length proportional to the bubble size near surface rupture. The end of the protruded ligament was then pinched by the surrounding pressure once the ambient pressure exceeds the internal pressure of the ligament. This process detaches a sub-droplet projecting in the direction of the protruded ligament. High surface tension of water emulsion protruded a shorter ligament with a larger size of the ejected sub-droplet.

4. Surface distortion of the water emulsion was found to be more violent than the ethanol emulsion. As a result, two additional processes of liquid ejections were observed. The strength of surfactant to hold the dispersed water inside the droplet is stronger than ethanol. As a result, the nucleated vapour inside the droplet needed higher pressure to

burst through the surface, which was observed to be released by a gush of vapour jet, pushing the side of the ruptured area to a sheet of liquid that eventually detaches multiple sub-droplet. Furthermore, because of the violent distortion caused by a strong repelling motion, the droplet surface rotates in relation to the core of the droplet. As a result, the whole protruded ligament detaches into a larger sized sub-droplet with the aid of centrifugal force.

5. Ethanol within the dispersed (ethanol-in-diesel) and continuous phase (diesel-in-Ethanol) diffuses rapidly towards the droplet surface due to its low flash point and weaker holding strength of the surfactant. As a result, no microexplosion occurred during the combustion of the ethanol emulsion by up to 30% of volume loading. The ethanol component is observed to reside near the surface of the droplet and easily ejected from the emulsion droplet through puffing.

6. The microexplosion of the emulsion droplet was determined to be caused by three factors. Firstly, the droplet temperature needs to reach the superheat limit of the lower boiling point component. Secondly, there must be a complete phase separation between the components within the emulsion fuel. Thirdly, the position of the dispersed liquid must be near the centre of the droplet upon reaching the superheat limit. Microexplosion only occurs once these three conditions are met.

8.1.3 Soot Contamination Effect on the Combustion Behaviour of Isolated Diesel Droplet

1. The process of soot contaminating a fuel droplet is observed in present work. As soon as the soot particles contained in the hot combustion gas contacted the surface of the droplet, it is quenched on the surface of the droplet. The quenched particles immediately form a shell of agglomerated particles that enveloped the droplet.

2. The presence of the soot shell on the surface of the droplet forms a barrier which inhibits the liquid diffusion from the core towards the surface of the droplet resulting suppressed evaporation. The effect of reduced evaporation rate was quantitatively measured by evaluating the slope of D^2 regression.

3. When the soot contaminates the droplet during the early lifetime of combustion, the burning rate is found to be reduced significantly. Higher density of surface contamination does not further reduce the burning rate but increases the magnitude of fluctuation in the regression of D^2. Denser shell of soot creates tougher barrier that obstructs the release of the nucleated vapour bubble inside the droplet. Hence, higher force of recoiling occurs which highly distorts the surface of the droplet.

4. The effect of fuel vapour accumulation reduces when the droplet is contaminated by a soot particle which in turn suppresses the evaporation. This is evaluated by the declines of the FSR towards the end of the droplet lifetime. In addition, the ejected matters during the disruptive burning phase contains mostly agglomerated soot particles. Explosion of the ejected mixture outside the droplet was observed to have no gas-phase interaction with the parent droplet resulting continuous decline of the FSR towards the end of the droplet lifetime.

5. The critical loading of volume-contaminated diesel (VCD) droplet is found to be at 0.2%. The slight increase in the burning rate was observed to be caused by the more frequent puffing processes during the steady burning phase. This indicates higher amount of liquid evaporation by the means of vapour nucleation and liquid-gas diffusion on the surface of the droplet. The shell formed on the surface is thin enough to allow the nucleated vapour bubble to escape through the surface. Higher loading of the soot particles retarded the heat transfer process toward the core of the droplet. As a result, no vapour bubble was observed to have nucleated within the droplet. Hence, the evaporation rate is reduced with only liquid-gas diffusion process occurred on the surface of the droplet.

6. As long as there is a soot particle contaminating the fuel droplet, the burning rate is found to have significantly reduced. The differences of burning rate between the surface-contaminated diesel (SCD) and the VCD droplet experimented in this study is determined to be affected by their differences in particle agglomeration rate. Soot particles on the SCD has completely agglomerated into a shell upon ignition. The soot contained within the VCD droplet only began to agglomerate once the droplet ignites. Higher particle loadings have more rapid particle agglomeration rate which explains the declining burning rate of VCD in higher loadings. Overall, as soon as the soot particle

completely agglomerated to a soot shell, the evaporation of contaminated fuel droplet is suppressed.

8.1.4 Combustion of Multiple Droplets Arranged in a Horizontal Array

1. There is a critical distance of strong gas-phase interaction during the combustion of multiple fuel droplets. The distance is highly dependent on the volatility of fuel; with longer inter-droplet distance of the critical reaction between lower volatility fuel droplets. Within this critical distance, the arranged droplets burn in one large enveloped flame. The burning rate of droplets positioned within this critical distance is found to be significantly reduced due to the enhanced heat loss from the flame.

2. Fuel Droplets that burns closely to each other have significant increase during the heating period due to the reduced heat being transferred to the surface of the droplet. However, the droplet heating period is measured to reduce gradually when the inter-droplet distance approaches the critical distance of respective fuel droplet. More oxidiser is able to diffuse towards the reaction zone due to enhanced buoyancy. Slight separation of flame within the critical distance further improves droplet heating by the heat being transferred from the flame of neighbouring droplets. Inter-droplet distance beyond the critical reaction distance prolongs the droplet heating. Although the effect of buoyancy is enhanced, the heat transfer from the neighbouring flame reduces as it separated further away from the droplet.

3. Visualisation on liquid-phase of a grouped fuel droplet combustion demonstrates that there is a soot contamination process throughout the lifetime of the droplet. It is found that the contamination was denser when the inter-droplet distance was shorter. More soot is shown to be quenched on the surface of three droplets in array; confirming that the soot particles were originated from the neighbouring droplets. Furthermore, the regression of the D^2 during the combustion of three diesel droplets shows higher fluctuation compared to the two droplets in array; further confirming this observation.

4. The lifetime of the disruptive phase is found to be unaffected by the critical distance of the gas-phase interaction. However, it is highly affected by the contamination of soot from the neighbouring droplets. The lifetime of the disruptive phase is found to increase

proportionally linear with the reduction of the inter-droplet distance. Higher amount of soot contamination would promote more heterogeneous nucleation of vapour bubble inside the droplet. This in turn would increase the occurrences of puffing and sub-droplet ejections. Hence, the steady burning is measured to be transitioned to the disruptive burning earlier due to the sudden loss of the liquid mass during the sub-droplet ejection process.

5. The effect of soot contamination to the lifetime of the disruptive burning was further evaluated by comparing the diesel interaction with the multiple combustion of ethanol droplets. It is shown that the lifetime of disruptive phases during the combustion of multiple ethanol droplets were unaffected in any inter-droplet distance. Hence, it is confirmed that the critical distance of gas-phase interaction highly effects the lifetime of droplet heating and the soot contamination density highly effects the lifetime of the disruptive phase during the combustion of interacting multiple fuel droplets.

8.2 Future works

The results presented in this thesis raises more research questions on the combustion behaviour of fuel droplets; worth investigating in near future. The following suggestions could satisfy the research gap highlighted in present work;

8.2.1 Acoustic effect on droplet evaporation

This study would provide further insight into the effect of acoustics and vibration on the evaporation process of droplets. Study would include the effect of acoustics to the droplet surface distortion. Theoretically, distorted droplet surface would expose larger surface area of liquid to the ambient. The effect of increased surface exposure to the evaporation rate would be beneficial in understanding the evaporation characteristics of liquid droplet. Furthermore, the effect of heat and mass transfer to the acoustically agitated liquid could be further explore in this study.

8.2.2 Three-Dimensional Visualisation on the Liquid-phase of the Droplet

Visualisation on the liquid-phase in three-dimensional images would provide additional info to the evaporating liquid droplet. This technique would provide precise quantitative measurement on the number of nucleated vapour bubble inside the droplet, the frequency of sub-droplet ejections and the volume of protruded ligaments during disruptive burning. Furthermore, the position of bubble nucleation could be tracked and reconstructed to further understand the dynamics of disruptive process within the droplet. Also, the strength of sub-droplet ejection could be determined with more precise measurement on the ejection speed of sub-droplets.

8.2.3 Selective Enhancement on Flame Formation of Burning Droplet

With this technique, the composition of soot, premixed flame and diffusion flame can be precisely measured. This would provide further information on the effect of soot contamination on the droplet. In addition, the effect of oxygen starvation can be evaluated by the flame formation of interacting droplet. Also, the effect of ignition temperature to the early formation of flame can be evaluated quantitatively.

8.2.4 Numerical Study on the Effect of Transient Burning Using Modified QS Model

A modified model of QS could be established using the experimental data provided by present work. Implementing the transient burning condition within the model would increase the modelling accuracy. The completion of this modelling would provide the opportunity to predict more complex combustion behaviour of fuel droplet such as multi-droplet combustion, particle interferences, and secondary atomisation characteristics.

8.2.5 Particle Image Velocimetry to Visualise the Dynamics of Particle During Combustion

This study would provide better insight into the dynamics of particles inside the droplet as well as the liquid flow of droplet during combustion. The effect of natural convection during the combustion of fuel droplet in normal gravity and atmospheric pressure to the internal

circulation can be determine. In addition, the agglomeration rate of particles can be precisely quantified and its effect to the evaporation behaviour could be evaluated.

Appendices

Appendix A

Sample calculation using classical quasi-steady model on neat diesel droplet

By neglecting the heat transferred to the interior of the droplet, the Spalding transfer number is;

$$B = \frac{\Delta h_c/v + c_{pg}(T_a - T_s)}{q_{i-l} + h_{fg}}$$

$$B = \frac{\left(\frac{44800}{14.6}\right) + 1.81(298 - 443)}{0 + 250} = 11.22$$

Assuming the droplet evaporates when its surface has reached the boiling point, the flame temperature is;

$$T_f = T_s + \frac{q_{i-l} + h_{fg}}{c_{pg}(1 + v)}(vB - 1)$$

$$T_f = \frac{0 + 250}{1.81(1 + 14.6)}[(14.6)(11.22) - 1] + 443 = 1884.53\ K$$

By dividing the flame height with the droplet diameter, the flame stand-off ratio is;

$$\frac{r_f}{2r_s} = \frac{ln(1 + B)}{ln[(v + 1)/v]}$$

$$\frac{r_f}{2r_s} = \frac{\ln\,(1 + 11.22)}{\ln\left[\frac{(14.6 + 1)}{14.6}\right](2)} = 18.87$$

Based on the calculated flame temperature, calculating the average gas-phase temperature is;

$$\bar{T} = \frac{T_{boil} + T_\infty}{2}$$

$$\bar{T} = \frac{443 + 1884.53}{2} = 1163.77$$

Based on average gas-phase temperature, the gas-phase specific heat is;

$C_{pg} = 3.791 \frac{kJ}{kg.K}$ (referring to Table B. 2 of Turns [79])

By considering the thermal conductivity of liquid fuel and ambient air, the gas-phase thermal conductivity is;

$k_g = 0.4k_F\bar{T} + 0.6k_\infty\bar{T}$

$k_F = 0.06137 \frac{W}{m.K}$ (referring to Table B. 3 of Turns [79])

$k_\infty = 0.1268 \frac{W}{m.K}$ (referring to Table C. 1 of Turns [79])

$k_g = 0.4(0.06137) + 0.6(0.1268) = 0.1 \frac{W}{m.K}$

By considering the parameters in gas-phase, the burning rate of diesel fuel droplet is;

$K = \frac{8k_g}{\rho_l c_{pg}} ln(B + 1)$

$K = \frac{8(0.1)}{830(3791)} \ln(11.22 + 1) = 0.6364 \text{ mm}^2/\text{s}$

References

[1] C. H. Wang, K. L. Pan, W. C. Huang, H. C. Wen, J. Y. Yang, and C. K. Law, "Effects of fuel properties on the burning characteristics of collision-merged alkane/water droplets," *Exp. Therm. Fluid Sci.*, vol. 32, no. 5, pp. 1049–1058, 2008.

[2] J. Huang and T. Lee, "Comparison of Single-Droplet Combustion Characteristics between Biodiesel and Diesel," *10th Int. Conf. Liq. At. Spray Syst.*, 2006.

[3] C. H. Wang, K. H. Shy, and L. C. Lieu, "An experimental investigation on the ignition delay of fuel droplets," *Combust. Sci. Technol.*, vol. 118, no. 1–3, pp. 63–78, 1996.

[4] M. Zhu, Y. Ma, and D. Zhang, "Effect of a homogeneous combustion catalyst on combustion characteristics of single droplets of diesel and biodiesel," *Proc. Combust. Inst.*, vol. 34, no. 1, pp. 1537–1544, 2013.

[5] S. G. Orlovskaya, V. V Kalinchak, M. S. Shkoropado, F. F. Karimova, and O. Y. Vergun, "Investigation Of The Burning Of Paraffin Droplets," *Ukr. J. Phys.*, vol. 59, no. 4, pp. 396–400, 2014.

[6] T. Saitoh, S. Ishiguro, and T. Niioka, "An experimental study of droplet ignition characteristics near the ignitable limit," *Combust. Flame*, vol. 48, no. C, pp. 27–32, 1982.

[7] A. Faik, "The Investigation Of Droplet Combustion Characteristics Of Biodiesel – Diesel Blends Using High Speed Camera," *12th Int. Conf. Heat Transf. Fluid Mech. Thermodyn.*, vol. 12, no. 1, pp. 8–10, 2016.

[8] G. A. . Godsave, "Burning of Fuel Droplets," *Symp. Combust.*, vol. 4, pp. 818–830, 1953.

[9] D. B. Spalding, "The Combustion of Liquid Fuels," *Proceeding Combust. Inst.*, vol. 4, pp. 847–864, 1953.

[10] G. Strotos, M. Gavaises, A. Theodorakakos, and G. Bergeles, "Numerical investigation of the evaporation of two-component droplets," vol. 90, pp. 1492–1507, 2011.

[11] C. K. Law, S. H. Chung, and N. Srinivasan, "Gas-Phase Quasi-Steadiness and Fuel Vapor Accumulation Effects in Droplet Burning," *Combust. Flame*, vol. 198, pp. 173–198, 1980.

[12] Y. C. Liu, Y. Xu, M. C. Hicks, and C. T. Avedisian, "Comprehensive study of initial diameter effects and other observations on convection-free droplet combustion in the standard atmosphere for n-heptane, n-octane, and n-decane," *Combust. Flame*, vol. 171, pp. 27–41, 2016.

[13] W. A. Sirignano and C. K. Law, "Unsteady Droplet Combustion and Droplet Heating-II: Conduction Limit," *Combust. Flame*, vol. 28, pp. 175–186, 1977.

[14] S. K. Aggarwal and M. Mawid, "Fuel vapor accumulation effect on the combustion characteristics of multicomponent fuel droplets," *Chem. Eng. Commun.*, vol. 157, pp. 35–51, 1997.

[15] M. Zhu, Z. Zhang, Y. L. Chan, S. Yani, and D. Zhang, "An Experimental Investigation into the

Ignition and Combustion Characteristics of Single Droplets of Biochar Slurry Fuels," *Energy Procedia*, vol. 75, pp. 180–185, 2015.

[16] F. E. Alam, Y. C. Liu, C. T. Avedisian, F. L. Dryer, and T. I. Farouk, "n-Butanol droplet combustion: Numerical modeling and reduced gravity experiments," *Proc. Combust. Inst.*, vol. 35, no. 2, pp. 1693–1700, 2015.

[17] P. Prakash, V. Raghavan, and P. S. Mehta, "Analysis of Multimode Burning Characteristics of Isolated Droplets of Biodiesel–Diesel Blends," *J. Energy Resour. Technol.*, vol. 135, no. 2, p. 024501, 2013.

[18] M. Ikegami *et al.*, "Distinctive combustion stages of single heavy oil droplet under microgravity," *Fuel*, vol. 82, pp. 293–304, 2003.

[19] W. A. Sirignano, "Fuel droplet vaporization and spray combustion theory," *Prog. Energy Combust. Sci.*, vol. 9, no. 4, pp. 291–322, 1983.

[20] K. Okai *et al.*, "Pressure effects on combustion of methanol and methanol/dodecanol single droplets and droplet pairs in microgravity," *Combust. Flame*, vol. 121, no. 3, pp. 501–512, 2000.

[21] J. J. Sangiovanni and M. Labowsky, "Burning times of linear fuel droplet arrays: A comparison of experiment and theory," *Combust. Flame*, vol. 47, no. C, pp. 15–30, 1982.

[22] M. Mikami, H. Oyagi, N. Kojima, M. Kikuchi, Y. Wakashima, and S. Yoda, "Microgravity experiments on flame spread along fuel-droplet arrays using a new droplet-generation technique," *Combust. Flame*, vol. 141, no. 3, pp. 241–252, 2005.

[23] H. Oyagi, H. Shigeno, M. Mikami, and N. Kojima, "Flame-spread probability and local interactive effects in randomly arranged fuel-droplet arrays in microgravity," *Combust. Flame*, vol. 156, no. 4, pp. 763–770, 2009.

[24] M. Mikami, H. Oyagi, N. Kojima, Y. Wakashima, M. Kikuchi, and S. Yoda, "Microgravity experiments on flame spread along fuel-droplet arrays at high temperatures," *Combust. Flame*, vol. 146, no. 3, pp. 391–406, 2006.

[25] P. M. Struk, D. L. Dietrich, M. Ikegami, and G. Xu, "Interacting droplet combustion under conditions of extinction," *Proc. Combust. Inst.*, vol. 29, no. 1, pp. 609–615, 2002.

[26] A. Yozgatligil, S. H. Park, M. Y. Choi, A. Kazakov, and F. L. Dryer, "Burning and sooting behavior of ethanol droplet combustion under microgravity conditions," *Combust. Sci. Technol.*, vol. 176, no. 11, pp. 1985–1999, 2004.

[27] S. H. Park, "Investigation of Sooting Behavior and Soot Nanostructures of Ethanol Droplet Flames in Microgravity," Drexel University, 2007.

[28] S. Nakaya, D. Segawa, T. Kadota, Y. Nagashima, and T. Furuta, "Combustion behaviors of isolated n-decane and ethanol droplets in carbon dioxide-rich ambience under microgravity," *Proc. Combust. Inst.*, vol. 33, no. 2, pp. 2031–2038, 2011.

[29] C. Y. Chao, H. W. Tsai, K. L. Pan, and C. W. Hsieh, "On the microexplosion mechanisms of burning droplets blended with biodiesel and alcohol," *Combust. Flame*, vol. 205, pp. 397–406, 2019.

[30] N. Al-esawi, M. Al Qubeissi, R. Whitaker, and S. S. Sazhin, “Blended E85 – Diesel Fuel Droplet Heating and Evaporation,” *Energy Fuels*, vol. 33, pp. 2477–2488, 2019.

[31] N. Shaygan and S. Prakash, “Droplet Ignition and Combustion Liquid-Phase Heating,” *Combust. Flame*, vol. 102, pp. 1–10, 1995.

[32] I. Awasthi, D. N. Pope, and G. Gogos, “Effects of the ambient temperature and initial diameter in droplet combustion,” *Combust. Flame*, vol. 161, pp. 1883–1899, 2014.

[33] M. Tsue, H. Yamasaki, T. Kadota, and D. Segawa, “Effect Of Gravity On Onset Of Microexplosion For An Oil-In-Water Emulsion Droplet,” *Symp. Combust.*, vol. 27, pp. 2587–2593, 1998.

[34] H. Watanabe, Y. Suzuki, T. Harada, and Y. Matsushita, “An experimental investigation of the breakup characteristics of secondary atomization of emulsified fuel droplet,” vol. 35, pp. 806–813, 2010.

[35] Z. Wang, S. Wu, Y. Huang, S. Huang, S. Shi, and X. Cheng, “Experimental investigation on spray , evaporation and combustion characteristics of ethanol-diesel , water-emulsi fi ed diesel and neat diesel fuels,” *Fuel*, vol. 231, no. May, pp. 438–448, 2018.

[36] A. M. D. Faik and Y. Zhang, “Multicomponent fuel droplet combustion investigation using magnified high speed backlighting and shadowgraph imaging,” *Fuel*, vol. 221, no. December 2017, pp. 89–109, 2018.

[37] C. H. Wang, S. Y. Fu, L. J. Kung, and C. K. Law, “Combustion and microexplosion of collision-merged methanol/alkane droplets,” *Proc. Combust. Inst.*, vol. 30, no. 2, pp. 1965–1972, 2005.

[38] C. H. Wang, K. L. Pan, G. J. Ueng, L. J. Kung, and J. Y. Yang, “Burning behaviors of collision-merged water / diesel , methanol / diesel , and water + methanol / diesel droplets,” vol. 106, pp. 204–211, 2013.

[39] K. L. Pan and M. C. Chiu, “Droplet combustion of blended fuels with alcohol and biodiesel/diesel in microgravity condition,” *Fuel*, vol. 113, pp. 757–765, 2013.

[40] T. Kadota and H. Yamasaki, “Recent advances in the combustion of water fuel emulsion,” *Prog. Energy Combust. Sci.*, vol. 28, no. 5, pp. 385–404, 2002.

[41] T. Kadota, H. Tanaka, and D. Segawa, “Microexplosion of an emulsion droplet during Leidenfrost burning,” vol. 31, pp. 2125–2131, 2007.

[42] S. Tanvir and L. Qiao, “Droplet burning rate enhancement of ethanol with the addition of graphite nanoparticles: Influence of radiation absorption,” *Combust. Flame*, vol. 166, pp. 34–44, 2016.

[43] I. Javed, S. W. Baek, and K. Waheed, “Autoignition and combustion characteristics of kerosene droplets with dilute concentrations of aluminum nanoparticles at elevated temperatures,” *Combust. Flame*, vol. 162, no. 3, pp. 774–787, 2015.

[44] P. M. Guerieri, R. J. Jacob, J. B. DeLisio, M. C. Rehwoldt, and M. R. Zachariah, “Stabilized microparticle aggregates of oxygen-containing nanoparticles in kerosene for enhanced droplet combustion,” *Combust. Flame*, vol. 187, pp. 77–86, 2018.

[45] W. J. Gerken, A. V Thomas, N. Koratkar, and M. A. Oehlschlaeger, “International Journal of Heat and Mass Transfer Nanofluid pendant droplet evaporation : Experiments and modeling,” *Int. J. Heat Mass Transf.*, vol. 74, pp. 263–268, 2014.

[46] P. K. Ojha, R. Maji, and S. Karmakar, “Effect of crystallinity on droplet regression and disruptive burning characteristics of nanofuel droplets containing amorphous and crystalline boron nanoparticles,” *Combust. Flame*, vol. 188, pp. 412–427, 2018.

[47] B. Rohani and C. Bae, “Morphology and nano-structure of soot in diesel spray and in engine exhaust,” *Fuel*, vol. 203, pp. 47–56, 2017.

[48] J. O. Müller, D. S. Su, R. E. Jentoft, U. Wild, and R. Schlögl, “Diesel engine exhaust emission: Oxidative behavior and microstructure of black smoke soot particulate,” *Environ. Sci. Technol.*, vol. 40, no. 4, pp. 1231–1236, 2006.

[49] F. Tao, V. I. Golovitchev, and J. Chomiak, “A phenomenological model for the prediction of soot formation in diesel spray combustion,” *Combust. Flame*, vol. 136, no. 3, pp. 270–282, 2004.

[50] C. T. Avedisian, “Recent Advances in Soot Formation from Spherical Droplet Flames at Atmospheric Pressure,” *J. Propuls. Power*, vol. 16, no. 4, pp. 628–635, 2008.

[51] T. Kadota and H. Hiroyasu, “Soot concentration measurement in a fuel droplet flame via laser light scattering,” *Combust. Flame*, vol. 55, no. 2, pp. 195–201, 1984.

[52] A. L. Randolph and C. K. Law, “Influence of physical mechanisms on soot formation and destruction in droplet burning,” *Combust. Flame*, vol. 64, no. 3, pp. 267–284, 1986.

[53] B. D. Shaw and F. A. Williams, “Theory of influence of a low-volatility, soluble impurity on spherically-symmetric combustion of fuel droplets,” *Int. J. Heat Mass Transf.*, vol. 33, no. 2, pp. 301–317, 1990.

[54] D. Kittelson and M. Kraft, “Particle Formation and Models in Internal Combustion Engines,” no. 142, 2014.

[55] S. Mosbach *et al.*, “Towards a detailed soot model for internal combustion engines,” *Combust. Flame*, vol. 156, no. 6, pp. 1156–1165, 2009.

[56] T. Y. Xiong, C. K. Law, and K. Miyasaka, “Behavior of the Basic ModelInteractive vaporisation and combustion of Binary Sroplet Systems,” *Symp. Combust. Combust. Inst.*, vol. 20, pp. 1781–1787, 1984.

[57] M. Labowsky and D. E. Rosner, “Evaporation-Combustion of Fuels,” in *Advances in Chemistry*, 1978, p. 166.

[58] N. A. Chigier and C. G. McCreath, “Combustion of droplets in sprays,” *Acta Astronaut.*, vol. 1, no. 5–6, pp. 687–710, 1974.

[59] S. L. Manzello, M. Y. Choi, A. Kazakov, F. L. Dryer, R. Dobashi, and T. Hirano, “The burning of large n-heptane droplets in microgravity,” *Proc. Combust. Inst.*, vol. 28, no. 1, pp. 1079–1086, 2000.

[60] G. S. Jackson, C. T. Avedisian, and J. C. Yang, “Observations of soot during droplet combustion at low gravity: heptane and heptane/monochloroalkane mixtures,” *Int. J. Heat Mass Transf.*, vol. 35,

no. 8, pp. 2017–2033, 1992.

[61] F. El Mahallawy and S. D. El Habik, *Fundamentals and Technology of Combustion*. Elsevier Science, 2002.

[62] K. Schmidt-Rohr, "Why Combustions Are Always Exothermic, Yielding about 418 kJ per Mole of O2," *J. Chem. Educ.*, vol. 92, no. 12, pp. 2094–2099, 2015.

[63] W. W. Pulkrabek, *Engineering Fundamentals of the Internal Combustion Engine*. Prentice Hall, 1997.

[64] C. K. Law, *Combustion physics*. Cambridge University Press, 2006.

[65] K. . Ragland and K. M. Bryden, *Combustion Engineering*, 2nd Editio. CRC Press, 2011.

[66] A. M. D. Faik, "Quantitative Investigation of the Multicomponent Fuel Droplet Combustion Using High Speed Imaging and Digital Image Processing," University of Sheffield, 2017.

[67] C. L. Cummins, *Diesel's engine, Volume One from Conception to 1918*. Carnot Press/Graphic Arts Center, 1993.

[68] J. Barker, P. Richard, C. Snape, and W. Meredith, "Diesel Injector Deposits - An Issue That Has Evolved with Engine Technology," *SAE Tech. Pap. Ser.*, vol. 1, 2011.

[69] M. Arai, "Physics behind Diesel Sprays," *ICLASS 2012, 12th Trienn. Int. Conf. Liq. At. Spray Syst. Heidelberg, Ger. Sept. 2-6, 2012 Phys.*, pp. 1–18, 2012.

[70] A. H. Lefebvre, *Atomization and Sprays*. Hemisphere Publishing Corporation, 1989.

[71] J. B. Heywood, *Internal Combustion Engine Fundamentals*. New York: McGraw-Hill, 1988.

[72] A. Umemura, "Interactive droplet vaporization and combustion: Approach from asymptotics," *Prog. Energy Combust. Sci.*, vol. 20, no. 4, pp. 325–372, 1994.

[73] X. Ma, F. Zhang, K. Han, B. Yang, and G. Song, "Evaporation characteristics of acetone-butanol-ethanol and diesel blends droplets at high ambient temperatures," *Fuel*, vol. 160, pp. 43–49, 2015.

[74] A. J. Marchese, T. L. Vaughn, K. Kroenlein, and F. L. Dryer, "Ignition delay of fatty acid methyl ester fuel droplets: Microgravity experiments and detailed numerical modeling," *Proc. Combust. Inst.*, vol. 33, no. 2, pp. 2021–2030, 2011.

[75] S. Ulzama and E. Specht, "An analytical study of droplet combustion under microgravity: Quasi-steady transient approach," *Proc. Combust. Inst.*, vol. 31 II, no. 2, pp. 2301–2308, 2007.

[76] C. K. Law, C. H. Lee, and N. Srinivasan, "Combustion Characteristics of Water-in-Oil Emulsion Droplets," *Combust. Flame*, vol. 37, pp. 125–143, 1980.

[77] M. Zhu, Y. Ma, Z. Zhang, Y. L. Chan, and D. Zhang, "Effect of oxygenates addition on the flame characteristics and soot formation during combustion of single droplets of a petroleum diesel in air," *Fuel*, vol. 150, pp. 88–95, 2015.

[78] G. Castanet and F. Lemoine, "Heat transfer within combusting droplets," *Proc. Combust. Inst.*, vol. 31 II, no. 2, pp. 2141–2148, 2007.

[79] S. R. Turns, *An Introduction to Combustion, Concepts and Applications*, 3rd Editio. Singapore:

McGraw Hill, 2012.

[80] C. T. Avedisian and B. J. Callahan, “Experimental study of nonane/hexanol mixture droplet combustion without natural or forced convection,” *Proc. Combust. Inst.*, vol. 28, no. 1, pp. 991–997, 2000.

[81] V. Deprédurand, G. Castanet, and F. Lemoine, “Heat and mass transfer in evaporating droplets in interaction: Influence of the fuel,” *Int. J. Heat Mass Transf.*, vol. 53, no. 17–18, pp. 3495–3502, 2010.

[82] K. Miyasaka and C. K. Law, “Combustion of Strongly-Interacting Linear Droplet Arrays,” *Symp. Combust.*, vol. 18, pp. 283–292, 1981.

[83] S. Prakash and W. Sirignano, “Theory of Convective Droplet Vaporization with Unsteady Heat Transfer in the Circulating Liquid Phase,” *Int. J. Heat Mass Transf.*, vol. 23, pp. 253–268, 1980.

[84] A. K. Yadav, K. Nandakumar, A. Srivastava, and A. Chowdhury, “Combustion of rocket-grade kerosene droplets loaded with graphene nanoplatelets—A search for reasons behind optimum mass loadings,” *Combust. Flame*, vol. 203, pp. 1–13, 2019.

[85] T. Ueda, O. Imamura, K. Okai, M. Tsue, M. Kono, and J. Sato, “Combustion behavior of single droplets for sooting and non-sooting fuels in direct current electric fields under microgravity,” *Proc. Combust. Inst.*, vol. 29, no. 2, pp. 2595–2601, 2002.

[86] Y. Ogami *et al.*, “Microgravity experiments of single droplet combustion in oscillatory flow at elevated pressure,” *Proc. Combust. Inst.*, vol. 32 II, pp. 2171–2178, 2009.

[87] H. P. Stout and E. Jones, “The ignition of gaseous explosive media by hot wires,” *Symp. Combust. Flame, Explos. Phenom.*, vol. 3, no. 1, pp. 329–336, 1949.

[88] H. Nagata, I. Kudo, K. Ito, S. Nakamura, and Y. Takeshita, “Interactive combustion of two-dimensionally arranged quasi-droplet clusters under microgravity,” *Combust. Flame*, vol. 129, no. 4, pp. 392–400, 2002.

[89] S. L. Manzello, S. H. Park, A. Yozgatligil, and M. Y. Choi, “Fuel-dependent effects on droplet burning and sooting behaviors in microgravity,” *Energy and Fuels*, vol. 23, no. 7, pp. 3586–3591, 2009.

[90] A. Muelas, P. Remacha, A. Martínez, A. Sobrino, and J. Ballester, “Droplet Combustion and Sooting Characteristics of Biodiesel , Heating Oil and their Mixtures,” *Combust. Flame*, vol. 203, no. April, pp. 18–21, 2017.

[91] G. M. Jang and N. Il Kim, “Surface tension , light absorbance , and e ff ective viscosity of single droplets of,” *Fuel*, vol. 240, no. August 2018, pp. 1–9, 2019.

[92] Z. Ni, K. Han, C. Zhao, H. Chen, and B. Pang, “Numerical simulation of droplet evaporation characteristics of multi- component acetone-butanol-ethanol and diesel blends under di ff erent environments,” vol. 230, no. December 2017, pp. 27–36, 2018.

[93] A. Lee and C. K. Law, “Gasification and shell characteristics in slurry droplet burning,” *Combust. Flame*, vol. 85, no. 1–2, pp. 77–93, 1991.

[94] J. Gong and F. You, “Disruptive Burning of Precursor/Solvent Droplets in Flame-Spray Synthesis of Nanoparticles,” *Am. Inst. Chem. Eng.*, vol. 60, no. 9, pp. 4553–4566, 2014.

[95] M. L. Botero, Y. Huang, D. L. Zhu, A. Molina, and C. K. Law, “Synergistic combustion of droplets of ethanol, diesel and biodiesel mixtures,” *Fuel*, vol. 94, pp. 342–347, 2012.

[96] D. M. Kim, S. W. Baek, and J. Yoon, “Ignition characteristics of kerosene droplets with the addition of aluminum nanoparticles at elevated temperature and pressure,” *Combust. Flame*, vol. 173, pp. 106–113, 2016.

[97] A. F. A. Rasid and Y. Zhang, “Combustion characteristics and liquid-phase visualisation of single isolated diesel droplet with surface contaminated by soot particles,” *Proc. Combust. Inst.*, vol. 37, no. 3, pp. 3401–3408, 2019.

[98] S. Nakaya, K. Fujishima, M. Tsue, M. Kono, and D. Segawa, “Effects of droplet diameter on instantaneous burning rate of isolated fuel droplets in argon-rich or carbon dioxide-rich ambiences under microgravity,” *Proc. Combust. Inst.*, vol. 34, no. 1, pp. 1601–1608, 2013.

[99] M. Tsue, T. Kadota, D. Segawa, and H. Yamasaki, “Statistical Analysis on Onset of Microexplosion for an Emulsion Droplet,” *Symp. Combust.*, vol. 26, pp. 1629–1635, 1996.

[100] D. C. K. Rao, S. Karmakar, and S. Basu, “Atomization characteristics and instabilities in the combustion of multi-component fuel droplets with high volatility differential,” *Sci. Rep.*, vol. 7, pp. 1–15, 2017.

[101] P. Antaki and F. A. Williams, “Observations on the combustion of boron slurry droplets in air,” *Combust. Flame*, vol. 67, no. 1, pp. 1–8, 1987.

[102] G. Xu, M. Ikegami, S. Honma, K. Ikeda, H. Nagaishi, and Y. Takeshita, *Burning droplets of heavy oil residual blended with diesel light oil: Characterization of burning steps*, vol. 174, no. 2. 2002.

[103] G. Xu, M. Ikegami, S. Honma, K. Ikeda, X. Ma, and H. Nagaishi, “Burning droplets of heavy oil residual blended with diesel light oil: Distinction of burning phases,” *Combust. Sci. Technol.*, vol. 175, no. 1, pp. 1–26, 2003.

[104] Y. Suzuki *et al.*, “Visualization of aggregation process of dispersed water droplets and the effect of aggregation on secondary atomization of emulsified fuel droplets,” *Proc. Combust. Inst.*, vol. 33, no. 2, pp. 2063–2070, 2011.

[105] H. Kim, J. Won, and S. W. Baek, “Evaporation of a single emulsion fuel droplet in elevated temperature and pressure conditions,” *Fuel*, vol. 226, no. March, pp. 172–180, 2018.

[106] M. Mohan, T. Megaritis, J. Xia, and L. Ganippa, “Experimental understanding on the dynamics of micro-explosion and puffing in ternary emulsion droplets,” *Fuel*, vol. 239, no. October 2018, pp. 1284–1292, 2019.

[107] Y. Gan and L. Qiao, “Combustion characteristics of fuel droplets with addition of nano and micron-sized aluminum particles,” *Combust. Flame*, vol. 158, no. 2, pp. 354–368, 2011.

[108] B. Y. Nishiyama, O. Moriue, and H. Kato, “Effects of Droplet Interaction on Spontaneous Ignition of Droplet Pair in Pressurized Air,” *Proc. Combust. Inst.*, vol. 34, pp. 1585–1592, 2013.

[109] S. H. Park and M. Y. Choi, “Formation of sootshell and attendant effects on droplet burning rate and radiative heat transfer in microgravity ethanol droplet flames,” *Energy and Fuels*, vol. 23, no. 9, pp. 4395–4403, 2009.

[110] A. Yozgatligil, S. H. Park, M. Y. Choi, A. Kazakov, and F. L. Dryer, “Influence of oxygen concentration on the sooting behavior of ethanol droplet flames in microgravity conditions,” *Proc. Combust. Inst.*, vol. 31 II, pp. 2165–2173, 2007.

[111] M. Mikami, H. Kato, and M. Kono, “The Interavtive Combustion of Two Droplet in Microgravity,” *Twenty-Fifth Symp. Combust. Combust. Inst.*, pp. 431–438, 1994.

[112] D. Segawa, H. Yamasaki, T. Kadota, H. Tanaka, H. Enomoto, and M. Tsue, “Water-coalescence in an oil-in-water emulsion droplet burning under microgravity,” *Proc. Combust. Inst.*, vol. 28, no. 1, pp. 985–990, 2000.

[113] Y. Zhang, R. Huang, Z. Wang, S. Xu, S. Huang, and Y. Ma, “Experimental study on puffing characteristics of biodiesel-butanol droplet,” *Fuel*, vol. 191, pp. 454–462, 2017.

[114] J. H. Bae and C. T. Avedisian, “Experimental study of the combustion dynamics of jet fuel droplets with additives in the absence of convection,” *Combust. Flame*, vol. 137, no. 1–2, pp. 148–162, 2004.

[115] S. R. Gollahalli and T. A. Brzustowski, “The effect of pressure on the flame structure in the wake of a burning hydrocarbon droplet,” *Symp. Combust.*, vol. 15, no. 1, pp. 409–417, 1975.

[116] S. Parag and V. Raghavan, “Experimental investigation of burning rates of pure ethanol and ethanol blended fuels,” *Combust. Flame*, vol. 156, no. 5, pp. 997–1005, 2009.

[117] P. Balakrishnan, T. Sundararajan, and R. Natarajan, *Combustion of a fuel droplet in a mixed convective environment*, vol. 163, no. 1–6. 2001.

[118] M. Das, A. Chakraborty, A. Datta, and A. K. Santra, “Experimental Studies on Burning Characteristics of Methanol, Diesel, and Sunflower Biodiesel Fuels,” *Combust. Sci. Technol.*, vol. 189, no. 2, pp. 213–230, 2017.

[119] S. Rajesh, V. Raghavan, U. S. P. Shet, and T. Sundararajan, “Analysis of quasi-steady combustion of Jatropha bio-diesel,” *Int. Commun. Heat Mass Transf.*, vol. 35, no. 9, pp. 1079–1083, 2008.

[120] J. B. R. Melissa, G. L. Vogt, and J. W. Michael, “Microgravity - A Teacher’s Guide With Activities in Science, Mathematics, and Technology.”

[121] C. Norberg, *Human Spaceflight and Exploration*. Berlin: Springer Berlin Heidelberg, 2013.

[122] S. Kumagai and H. Isoda, “Combustion of fuel droplets in a falling chamber,” *Symp. Combust.*, vol. 6, no. 1, pp. 726–731, 1957.

[123] A. Cuoci, A. Frassoldati, T. Faravelli, and E. Ranzi, “Numerical modeling of auto-ignition of isolated fuel droplets in microgravity,” *Proc. Combust. Inst.*, vol. 35, no. 2, pp. 1621–1627, 2015.

[124] F. L. D. B. D. Urban, K. Kroenlein, A. Kazakov, “Sooting Behavior of Ethanol Droplet Combustion at Elevated Pressures a Microgravity,” *Microgravity sci. technol*, vol. 3, pp. 12–18, 2004.

[125] C. K. Law and H. K. Law, “A d2-Law for Multicomponent Droplet Vaporization and Combustion,”

AIAA J., vol. 20, no. 4, pp. 522–527, 2008.

[126] D. Tanimoto and J. Shinjo, "Numerical simulation of secondary atomization of an emulsion fuel droplet due to pu ffi ng : Dynamics of wall interaction of a sessile droplet and comparison with a free droplet," *Fuel*, vol. 252, no. April, pp. 475–487, 2019.

[127] D. F. Lasheras JC, Fernandez-Pello AC, "On the disruptive burning of free droplets of alcohol/n-paraffin solutions and emulsions," *Symp. Combust.*, vol. 18, no. 1, pp. 293–305, 1981.

[128] R. B. Landis and A. F. Mills, "Effects of Internal Diffusional Resistance on the Vaporization of Binary Droplets," in *Fifth International Heat Transfer Conference*, 1974, p. 345.

[129] A. Hoxie, R. Schoo, and J. Braden, "Microexplosive combustion behavior of blended soybean oil and butanol droplets," *Fuel*, vol. 120, pp. 22–29, 2014.

[130] J. Shinjo, J. Xia, A. Megaritis, L. Ganippa, and R. Cracknell, "Modeling temperature distribution inside and emulsion droplet under convective heating: a key to predicting microexplosion and puffing," *At. Sprays*, vol. 26, pp. 551–83, 2016.

[131] A. Miglani, S. Basu, and R. Kumar, "Insight into instabilities in burning droplets," *Phys. Fluids*, vol. 26, no. 3, 2014.

[132] H. Watanabe and K. Okazaki, "Visualization of secondary atomization in emulsified-fuel spray flow by shadow imaging," vol. 34, pp. 1651–1658, 2013.

[133] J. Shinjo, J. Xia, L. C. Ganippa, and A. Megaritis, "Physics of puffing and microexplosion of emulsion fuel droplets," *Phys. fluids*, vol. 26, pp. 1–22, 2014.

[134] X. Zhang, T. Li, B. Wang, and Y. Wei, "Superheat limit and micro-explosion in droplets of hydrous ethanol-diesel emulsions at atmospheric pressure and diesel-like conditions," *Energy*, vol. 154, pp. 535–543, 2018.

[135] Z. Wang *et al.*, "Effects of water content on evaporation and combustion characteristics of water emulsified diesel spray," *Appl. Energy*, vol. 226, pp. 397–407, 2018.

[136] F. Harusawa, H. Nakajima, and M. Tanak, "The Hydrophile-Lipophile Balance of Mixed Nonionic Surfactants," *J. Soc. Cosmet. Chem.*, vol. 33, pp. 115–129, 1982.

[137] M. H. Grubenmann, *Formulation technology: emulsions, suspensions, solid forms*. Wiley-VCH, 2001.

[138] O. Moussa, D. Tarlet, P. Massoli, and J. Bellettre, "Parametric study of the micro-explosion occurrence of W/O emulsions," *Int. J. Therm. Sci.*, vol. 133, no. July, pp. 90–97, 2018.

[139] M. S. Iqbal *et al.*, "Ethanol production from waste materials," *J. Biochem. Technol.*, vol. 4, no. 1, pp. 285–288, 2012.

[140] A. Kazakov, J. Conley, and F. L. Dryer, "Detailed modeling of an isolated, ethanol droplet combustion under microgravity conditions," *Combust. Flame*, vol. 134, no. 4, pp. 301–314, 2003.

[141] Y. Xu, D. Meilin, I. Keresztes, D. Phillips, P. Pepiot, and C. Thomas Avedisian, "The droplet burning characteristics of algae-derived renewable diesel, conventional #2 diesel, and their mixtures," *ASME Int. Mech. Eng. Congr. Expo. Proc.*, vol. 6A-2015, pp. 295–305, 2015.

[142] M. Saravanan, A. Anbarasu, and B. M. Gnanasekaran, “Study of performance and emission characteristics of IC engines by using diesel-water emulsion,” *Int. J. Adv. Manuf. Technol.*, vol. 69, no. 9–12, pp. 2531–2544, 2013.

[143] S. U. S. Choi and J. A. Eastman, “Enhancing Thermal Conductivity Of Fluids With Nanoparticles,” in *ASME Int Mech Eng Congress Expo*, 1995, pp. 99–106.

[144] Y. Gan and L. Qiao, “Optical properties and radiation-enhanced evaporation of nanofluid fuels containing carbon-based nanostructures,” *Energy and Fuels*, vol. 26, no. 7, pp. 4224–4230, 2012.

[145] S. P. Jang and S. U. S. Choi, “Role of Brownian motion in the enhanced thermal conductivity of nanofluids,” *Appl. Phys. Lett.*, vol. 84, no. 4316, 2004.

[146] W. Yu and S. U. S. Choi, “The role of interfacial layers in the enhanced thermal conductivity of nanofluids : A renovated Hamilton – Crosser model,” *J. Nanoparticle Res.*, vol. 6, pp. 355–361, 2004.

[147] C. D. Rosebrock, T. Wriedt, and M. Lutz, “The Role of Microexplosions in Flame Spray Synthesis for Homogeneous Nanopowders from Low-Cost Metal Precursors,” *AIChE J.*, vol. 62, no. 2, pp. 381–391, 2016.

[148] H. Li, C. D. Rosebrock, N. Riefler, T. Wriedt, and L. Mädler, “Experimental investigation on microexplosion of single isolated burning droplets containing titanium tetraisopropoxide for nanoparticle production,” *Proc. Combust. Inst.*, vol. 36, no. 1, pp. 1011–1018, 2017.

[149] R. A. Yetter, G. A. Risha, and S. F. Son, “Metal particle combustion and nanotechnology,” *Proc. Combust. Inst.*, vol. 32 II, pp. 1819–1838, 2009.

[150] S. U. S. Choi, “Nanofluids: From Vision to Reality Through Research,” *J. Heat Transfer*, vol. 131, no. March 2009, pp. 033106, 1–9, 2019.

[151] C. Wu, T. J. Cho, J. Xu, D. Lee, B. Yang, and M. R. Zachariah, “Effect of nanoparticle clustering on the effective thermal conductivity of concentrated silica colloids,” *Phys. Rev. E*, vol. 81, no. 1, p. 011406, 2010.

[152] M. Ghamari and A. Ratner, “Combustion characteristics of colloidal droplets of jet fuel and carbon based nanoparticles,” *Fuel*, vol. 188, pp. 182–189, 2017.

[153] I. Javed, S. W. Baek, and K. Waheed, “Autoignition and combustion characteristics of heptane droplets with the addition of aluminium nanoparticles at elevated temperatures,” *Combust. Flame*, vol. 162, pp. 191–206, 2015.

[154] K. J. Rockne, G. L. Taghon, and D. S. Kosson, “Pore structure of soot deposits from several combustion sources,” *Chemosphere*, vol. 41, pp. 1125–1135, 2000.

[155] L. M. Pickett and D. L. Siebers, “Soot in diesel fuel jets: Effects of ambient temperature, ambient density, and injection pressure,” *Combust. Flame*, vol. 138, no. 1–2, pp. 114–135, 2004.

[156] J. C. Chow *et al.*, “The application of thermal methods for determining chemical composition of carbonaceous aerosols: A review,” *J. Environ. Sci. Heal. - Part A Toxic/Hazardous Subst. Environ. Eng.*, vol. 42, no. 11, pp. 1521–1541, 2007.

[157] K. T. and K. H., “Combustion Processes in Diesel Engines,” *Prog. Energy Combust. Sci.*, vol. 17, pp. 163–189, 1991.

[158] D. K. Srivastava, A. K. Agarwal, and T. Gupta, “Effect of Engine Load on Size and Number Distribution of Particulate Matter Emitted from a Direct Injection Compression Ignition Engine,” *Aerosol Air Qual. Res.*, vol. 11, pp. 915–920, 2011.

[159] D. R. Tree and K. I. Svensson, “Soot processes in compression ignition engines,” *Prog. Energy Combust. Sci.*, vol. 33, no. 3, pp. 272–309, 2007.

[160] M. Patel, C. Leonor, A. Ricardo, P. Scardi, and P. B. Aswath, “Morphology, structure and chemistry of extracted diesel soot—Part I: Transmission electron microscopy, Raman spectroscopy, X-ray photoelectron spectroscopy and synchrotron X-ray diffraction study,” *Tribiology Int.*, vol. 52, no. August, pp. 29–39, 2012.

[161] R. H. Hurt, G. P. Crawford, and H. S. Shim, “Equilibrium nanostructure of primary soot particles,” *Proc. Combust. Inst.*, vol. 28, no. 2, pp. 2539–2546, 2000.

[162] Z. Su, W. Zhou, and Y. Zhang, “New insight into the soot nanoparticles in a candle flame,” *Chem. Commun.*, vol. 47, no. 16, pp. 4700–4702, 2011.

[163] H. Omidvarborna, A. Kumar, and D. S. Kim, “Recent studies on soot modeling for diesel combustion,” *Renew. Sustain. Energy Rev.*, vol. 48, pp. 635–647, 2015.

[164] G. S. Jackson and C. T. Avedisian, “The Effect of Initial Diameter in Spherically Symmetric Droplet Combustion of Sooting Fuels,” *Proc. R. Soc. A Math. Phys. Eng. Sci.*, vol. 446, no. 1927, pp. 255–276, 2006.

[165] B. Knight and F. Williams, “Observations on the burning of porcelain,” *J. Franklin Inst.*, vol. 178, no. 3, p. 380, 2003.

[166] B. J. Alder, L. K. Tseng, N. M. Laurendeau, and J. P. Gore, “Effects of partial premixing on NOx emission indices of soot-containing flames,” *Combust. Sci. Technol.*, vol. 152, no. 1, pp. 167–178, 2000.

[167] D. B. Kittelson, “Engines and nanoparticles: A review,” *J. Aerosol Sci.*, vol. 29, no. 5, pp. 575–588, 1998.

[168] M. Marberry, A. K. Ray, and K. Leung, “Effect of Multiple Particle Interactions on Burning Droplets,” *Combust. Flame*, vol. 57, pp. 237–245, 1984.

[169] M. Labowsky, “The Interavtive Combustion of Two Droplet in Microgravity,” *Combust. Sci. Technol.*, vol. 22, pp. 217–226, 1980.

[170] Y. Yoshida *et al.*, “Flame-spread limit from interactive burning droplets in microgravity,” *Proc. Combust. Inst.*, vol. 37, no. 3, pp. 3409–3416, 2019.

[171] D. Splitter, M. Wissink, D. DelVescovo, and R. Reitz, “RCCI Engine Operation Towards 60% Thermal Efficiency,” *SAE Tech. Pap.*, vol. 1, pp. 1–279, 2013.

[172] J. E. Dec, E. . Bechtold, S. . Aceves, and R. . Bechtold, “The Potential of HCCI Combustion for High Efficiency and Low Emissions,” *Soc. Automot. Eng.*, vol. 1, p. 1923, 2002.

[173] R. Johansson, D. Blom, M. Karlsson, K. Ekholm, and P. Tunestal, “No Title,” *Soc. Automot. Eng.*, vol. 1, p. 789, 2008.

[174] K. Hiraya, K. Hasegawa, T. Urushihara, A. Iiyama, and T. Itoh, “A Study on Gasoline Fueled Compression Ignition Engine- A trial of Operation Region Expansion,” *SAE Pap.*, vol. 1, p. 416, 2002.

[175] S. Kook and C. Bae, “Combustion Control Using Two-Stage Diesel Fuel Injection in a Single-Cylinder PCCI Engine,” *SAE Pap.*, vol. 1, p. 938, 2004.

[176] T. Wilson, H. M. Xu, S. Richardson, M. D. Yap, and M. Wyszynski, “An Experimental Study of Flame Initiation and Development in an Optical HCCI Engine,” *SAE Tech. Pap.*, vol. 1, p. 2129, 2005.

[177] A. Alahmer, J. Yamin, A. Sakhrieh, and M. A. Hamdan, “Engine Performance using Emulsified Diesel Fuel,” *Energy Convers. Manag.*, vol. 51, pp. 1708–1713, 2010.

[178] A. Maiboom and X. Tauzia, “NOx and PM Emissions Reduction on an Automotive HSDI Diesel Engine with Water-in-Diesel Emulsion and EGR: An Experimental Study,” *Fuel*, vol. 90, pp. 3179–3192, 2011.

[179] M. E. A. Fahd, Y. Wenming, P. S. Lee, S. K. Chou, and C. R. Yap, “Experimental Investigation of the Performance and Emission Characteristics of Direct Injection Diesel Engine by Water Emulsion Diesel under Varying Engine Load Condition,” *Appl. Energy*, vol. 102, pp. 1042–1049, 2013.

[180] Leal-Calderon, F., V. Schmitt, and J. Bibette, *Emulsion Science Basic Principles*, 2nd editio. Springer, 2007.

[181] L. Cassiday, “Emulsions: Making Oil and Water Mix,” *The American Oil Chemists’ Society*, 2014.

[182] V. Califano, R. Calabria, and P. Massoli, “Experimental Evaluation of the Effect of Emulsion Stability on Micro-Explosion Phenomena for Water-in-Oil Emulsions,” *Fuel*, vol. 117, pp. 87–94, 2014.

[183] I. Langmuir, “The Evaporation Of Small Spheres.,” *Phys. Rev. A*, vol. 12, no. 5, pp. 368–370, 1918.

[184] H. Nomura, T. Murakoshi, Y. Suganuma, Y. Ujiie, N. Hashimoto, and H. Nishida, “Microgravity experiments of fuel droplet evaporation in sub- and supercritical environments,” *Proc. Combust. Inst.*, vol. 36, no. 2, pp. 2425–2432, 2017.

[185] F. Takahashi, F. L. Dryer, and F. A. Williams, “Combustion behavior of free boron slurry droplets,” *Symp. Combust. Combust. Inst.*, vol. 21, pp. 1983–1991, 1986.

[186] S. C. Wong and A. C. Lin, “Microexplosion mechanisms of aluminum/carbon slurry droplets,” *Combust. Flame*, vol. 89, no. 1, pp. 64–76, 1992.